ENGINEERING REPORT

ANALYTICAL INVESTIGATIONS OF THE BEHAVIOR AND FAILURE OF COMPOSITE MASONRY WALLS

A technical report submitted to the National Science Foundation
for NSF Research Award No. ECE-8410081, entitled
"Analytical and Experimental Evaluation of Composite Masonry Walls
Subjected to Gravity and Earthquake Loads"

by

Subhash C. Anand

and

Md. Ayubur Rahman

Department of Civil Engineering
Clemson University
Clemson, South Carolina 29634-0911

August, 1989

1 0 S - 8 9

DEPARTMENT OF
CIVIL ENGINEERING

CLEMSON
UNIVERSITY

l. a

ANALYTICAL INVESTIGATIONS OF THE BEHAVIOR AND FAILURE

OF COMPOSITE MASONRY WALLS*

by

Subhash C. Anand
and
Md. Ayubur Rahman

Department of Civil Engineering
Clemson University
Clemson, South Carolina   29634-0911

August, 1989

10S-89

ABSTRACT

Composite action in a masonry wall is obtained when two independent
wythes are connected together by metal ties and the cavity between the
two wythes is grouted. For the two wythes to act together under the
action of internal and/or external loads, it is important that the collar
joint is strong enough to resist the shearing stresses induced in it. A
quasi three-dimensional finite element model has previously been proposed
by researchers at Clemson University for predicting shear stresses in the
collar joint. This quasi three-dimensional model has previously been used
in the analysis of single story and multistory composite walls that are
subjected to only vertical loads. The behavior of composite masonry walls
which act as shear walls and are subjected to horizontal in-plane loads
is a subject, on the other hand, that has recieved little attention. This
research presents the results of analyses of composite walls subjected
to horizontal in-plane loads using the previously developed quasi three-
dimensional model. It is shown that the distribution of horizontal shear
stress in the collar joint is very similar to that of the vertical shear
stress due to vertical loads, indicating that the horizontal stiffness
which is smaller than the vertical stiffness of the wall has little in-
fluence on the shear stresses in the collar joint. Some additional re-
sults for two story composite masonry walls are also presented.

A computational procedure based on the principle of superposition
to estimate creep strains in composite masonry walls is developed. This
development is based on the assumption that creep vs. time relationship
in masonry can be uniquely defined by a specific creep (i.e., creep per

unit stress) vs. time curve. Experimentally obtained specific creep vs. time curves for various components of composite masonry walls subjected to uniaxial compressive loads are utilized to establish relationships between the components of creep strain increments and existing stresses. These relationships are used in conjunction with the principle of super-position to compute creep strains in composite masonry walls. In addition, the effects of creep strains on stress changes is also investigated. It is shown that although substantial additional strains occur in a composite wall due to creep, their effect on the corresponding stresses is minimal.

A procedure utilizing the initial strain approach to estimate stresses in the collar joint of composite walls due to differential temperatures on the inside and outside wythe faces in a wall is developed. It is shown that the shear stresses and strains in the collar joint do not undergo any substantial changes due to realistic temperature variations; however, it is observed that the normal stresses change significantly due to temperature variations.

Variable-node-number isoparametric elements are also developed in this research for an accurate prediction of stresses in composite masonry walls. The locations of optimal stress points, where the calculated stresses are more accurate, are also determined for one specific variable-node-number element which is used to model the collar joint-wythe interface.

In order to determine an accurate behavior at the interfaces of the brick and block wythes in composite masonry walls, an interface element is proposed in the collar joint. It is shown that the interfaces in a composite masonry wall act as perfectly bonded joints. A procedure for

accurate estimation of stresses at the interfaces of composite walls involving stress discontinuities is suggested.

In an effort to develop a cracking analysis procedure for composite masonry walls, an empirical Mohr-Coulomb type of failure criterion, based on a nonuniform state of stress in the joint, is proposed. This failure criterion is developed using a few experimentally available failure expressions that assume a uniform state of normal and shear stress in the joint. It is shown that the failure of any concrete block-mortar joint can be described by a single expression which is dependent on the values of elastic modulii of the concrete block and joint mortar.

Failure loads in composite masonry walls of various heights are determined using the failure criterion developed in this research. The failure loads estimated analytically are compared with those obtained by assuming uniform failure shear stress given in the literature. The above comparison indicates that the prediction of failure loads in composite walls using average shear stress not only overestimates the strength of walls but also produces very unrealistic results.

ACKNOWLEDGMENTS

TABLE OF CONTENTS

Table of Contents (Continued)

Table of Contents (Continued)

CHAPTER I

INTRODUCTION

Background

A composite masonry wall consists of a wythe of brick and another
wythe of concrete block. If the cavity (i.e., the collar joint) between
the two wythes remains hollow, then the structural properties of each
wythe are independent of each other. On the other hand, if the cavity
between the two wythes is parged or grouted, as shown in Figure 1.1, the
two wythes are bonded together and react as a single unit. The mechanical
properties of this complex structural assemblage are dependent upon the
constituents of the wall, i.e., concrete block, brick and grout.

In recent years, composite masonry construction has become extremely
popular to engineers and architects. Composite masonry structures si-
multaneously serve several functions of prime importance, such as, (1)
permitting overall economy of design, (2) permitting an unusual amount
of flexibility for the architect, (3) providing a complete, self-
sufficient structural system, (4) proving capability of supporting all
design loads, (5) providing acoustical insulation, (6) making building
fireproof and (7) creating weather resistant enclosures.

Brick is one of the oldest building materials known to man and until
the beginning of the twentieth century masonry, in its various forms, was
the principal building material. Since then, however, new building ma-
terials, such as structural steel, reinforced concrete, etc., have been
developed. Theories and progressive building codes were established for
these new materials. However, it was not until recent years that any

Block Wythe

Brick Wythe
Collar Joint
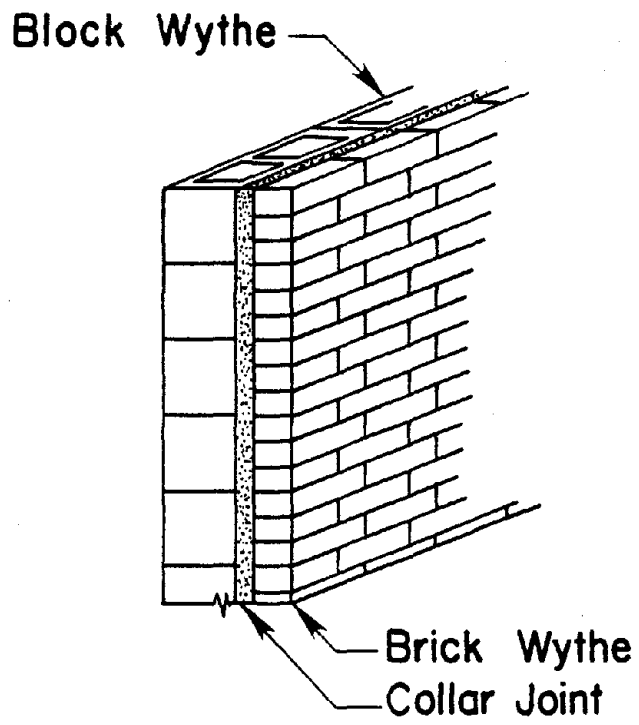
Figure 1.1 Composite Masonry Wall

progress had been made in the development of theory and design codes for structural masonry.

Because of the increased popularity of structural masonry, extensive theoretical and experimental research has been directed towards its development during the last three decades. The standards for the design and construction of brick masonry and concrete masonry have been developed from research performed on masonry consisting of only brick or concrete block. On the other hand, although a considerable portion of all non-residential masonry construction is composite, there exists no thorough design standard for structural members composed of both clay brick and concrete block masonry. Most standards (105,108) have included provisions for the design of such composite members, which are based on limited experimental data.

The interaction of the block wythe with the brick wythe in a composite masonry wall under internal stresses and external loads is a subject that needs special attention. As a result of this interaction, shearing stresses are created in the collar joint, and their magnitudes at the block-collar joint interface and brick-collar joint interface are important for predicting possible failure of the wall.

In composite construction, the floor slab usually rests on the interior (block) wythe of the composite wall as shown in Figure 1.2. The vertical and horizontal in-plane loads are transferred from the floor directly on the inner concrete block wythe. Some percentage of these loads is transferred to the outer brick wythe through shear stresses in the collar joint. Significant amounts of shear stresses develop as a result of the loads applied only on the block wythe. Shear stresses may also be caused due to moisture and thermal strains in a composite wall

(a) Horizontal loading

(b) Vertical loading
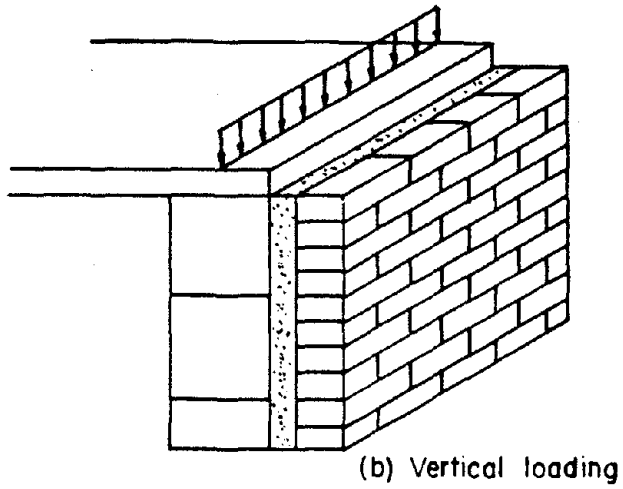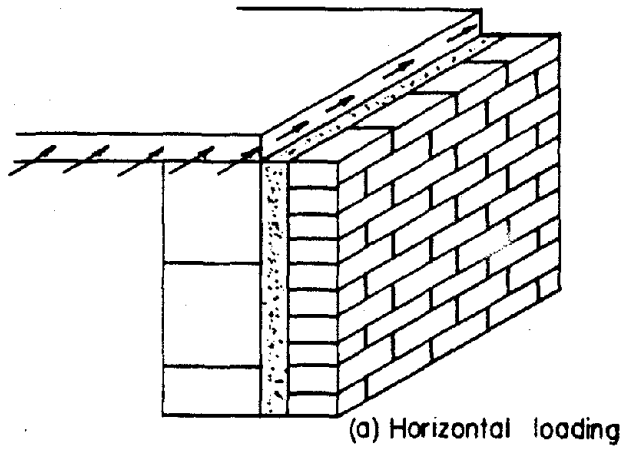
Figure 1.2 Loads on a Block Wythe

without necessarily any application of external loads. The temperature difference between the exterior brick wythe, which is exposed to a continuously changing weather, and the climatically controlled interior block wythe may cause large shear stresses in the collar joint. Similarly, the expansion of the brick wythe and contraction of the block wythe due to moisture variation in a composite wall could also cause considerable amount of shearing strains and stresses in the collar joint. The creep strains under sustained loads may also become important for consideration in the estimation of stresses in a composite wall where only the interior block wythe is subjected to external loads.

Determination of the correct magnitude of shear stresses in the collar joint due to external loads, creep, moisture and temperature is extremely important because the failure in composite masonry walls is essentially due to delamination of the wythes caused by the collar joint shear stresses. Previous investigators involved in analytical research in the area of composite masonry (3-8, 13-16, 19, 20) were primarily concerned with an understanding of the load transfer mechanism and overall behavior of the wall instead of an accurate prediction of the shear stresses in the collar joint. The experimental research (9, 26, 31, 65, 94) in this field focussed its attention only towards obtaining an average value of the collar joint shear stress. An extensive review of the literature by the writer revealed that no attempts had been made to develop a procedure for an accurate prediction of the collar joint shear stresses in composite masonry walls.

Researchers engaged in the theoretical investigations of the behavior of jointed rocks (38, 40-42) consider a joint of two dissimilar materials to be very weak in shear. Although the planes of weakness in composite

masonry walls are expected to exist along the block wythe-collar joint and brick wythe-collar joint interfaces, the shearing strength of these interfaces are, however, not known. Page (71), on the other hand, has modelled the mortar joints in single wythe brick masonry by using the joint element developed by Goodman et al. (42), which is based on the assumption that the mortar joints are planes of weakness. Unfortunately, there exists no evidence of any research that has been conducted previously or is being performed presently in composite masonry regarding the behavior of the interfaces, except the one being reported in this work.

In the past, researchers have modelled the interfaces in composite masonry walls assuming that the two dissimilar materials are perfectly bonded together and there exists no plane of weakness along an interface. The finite element model based on the above mentioned assumption could produce too high shear stresses in the collar joint at the block wythe-collar joint interface near the region of load application as the loads are applied only on the inner block wythe of the wall. This numerical problem arises due to the stress discontinuity at the top of the wall near the block wythe-collar joint interface which develop as a result of the applied loads. A similar situation was investigated by Whitcomb et al. (93) in the area of composite laminates using the finite element method. The investigators demonstrated the numerical problem in that research and suggested a procedure to overcome the difficulty. This suggested procedure can be utilized in the analysis of composite masonry walls to determine the magnitude of shearing stresses in the collar joint at the interface when the two dissimilar materials are considered perfectly bonded together. A review of the analytical research in the area of composite masonry walls indicates that the exact behavior of the block

wythe-collar joint or brick wythe-collar joint interface has not been determined as yet and a solution procedure for correct estimation of collar joint shear stresses at the interface has not been suggested.

Failure of composite masonry walls occurs either at the brick wythe-collar joint or block wythe-collar joint interface. Brown and Cousins (26) observed that the failure in their composite wall test specimens rarely occured on both interfaces. They also observed that the cracks in the collar joint spread very quickly and the failure of a specimen was abrupt. For analytical prediction of failure loads in composite masonry walls, which generally fail at the block wythe-collar joint interface, Mohr-Coulomb type of failure criterion must be available. Mohr-Coulomb failure criterion is defined by the shear bond strength and the coefficient of friction. Very limited information regarding this type of failure criterion for block wythe-mortar joint interfac, is available in the literature. Thus, for a material that is widely used in construction, sufficient information is not available for the development of an appropriate design and construction standard.

It is proposed herein to investigate the behavior of composite masonry walls subjected to vertical and horizontal in-plane loads. The effect of the creep strains and temperature variations on the collar joint shear stress are also studied. In addition, a procedure to determine the correct shear stress distribution in the collar joint at the interface is suggested. Improved failure criterion for the block-collar joint interface is proposed and a procedure to determine wall failure loads using the proposed failure criterion is described. Failure loads in composite masonry walls of various heights are determined following the

suggested procedure in which the failure plane is assumed to be at the interface between the block wythe and collar joint.

Previous Research

A considerable amount of theoretical and experimental research has been conducted in the past at Clemson University to determine the shear stress distribution and average failure shear stress in the collar joint of composite masonry walls. A quasi three-dimensional finite element model which was developed to overcome the shortcomings of the three-dimensional models was proposed by Anand and Young (19). The three-dimensional model requires a large amount of computer time and the results are difficult to evaluate due to the complexity of the model. The model proposed by Anand and Young incorporates some positive aspects of the three-dimensional models without the associated restrictions. The original work of Anand and Young contains an extensive and in-depth review of all the previous research dealing with composite masonry walls (19).

The original quasi three-dimensional model of Anand and Young was further improved by Anand and Stevens (13). The improved model can predict the complete state of stress in the collar joint under the assumption that the magnitude of the normal as well as shear stress components in the out-of-plane direction of the wall are negligible or zero.

As in the original model (19), out-of-plane displacements were not permitted in the improved model (13). These displacements may have significant effects on the stresses in a composite wall. It has further been shown by Anand et al. (16) that the quasi three-dimensional model cannot correctly reproduce stresses that are obtained by the use of a plane strain two-dimensional model. They have also suggested load factors to correlate the results of the two models.

In the above mentioned references, the variation of stresses in the collar joints of composite masonry walls due to only vertical loads on the block wythe was investigated. However, no attempts were made to develop a solution procedure using a two-dimensional finite element model to accurately predict the collar joint shear stresses at the interface.

Grimm amd Fowler (46) used an elementary mechanics of materials approach to determine shear stresses in the collar joint of a wall. Only a few additional theoretical and experimental studies have been undertaken by other researchers to investigate the behavior of collar joints in composite masonry walls (31, 74-76, 83, 94, 97, 98).

The previously developed quasi three-dimensional model was used by Anand and Gandhi (7) to examine the long term effects of creep and shrinkage in composite masonry walls. The method employed by these investigators is based on the assumption that the rate of creep is independent of the age at loading. An in-depth review of the previous research dealing with the determination of inter-laminar shear stresses due to creep strains in fibrous composites, which may be adopted for the study of the creep behavior in composite masonry, can be found in Reference (7).

The effects of creep in composite masonry was further studied by Anand and Dandawate (4, 5). They developed a numerical methodology based on the principle of superposition to predict the creep behavior in masonry walls which did not depend on the assumption made earlier by Anand and Gandhi (7). They also used the previously developed quasi three-dimensional finite element model to predict the creep behavior in composite masonry walls. They did not attempt to investigate the creep

behavior of composite walls by modelling the cross-section of a wall using two-dimensional plane strain finite elements.

The presence of large shear stresses in a collar joint due to the imposed loading, temperature changes, and or moisture and creep effects can cause failure of the wall. Anand and Stevens (15) were the first investigators who proposed cracking models for composite masonry walls. They defined cracking in their model based on a simple shear failure criterion. Their analyses modelled the existence of ladder type re-inforcement in the bed joints across the two wythes using a quasi three-dimensional model. The concept of shear friction was utilized to monitor the growth of shear cracks within the collar joint. An extensive review of the literature concerning crack modelling in the related fields of geology, reinforced concrete and masonry can be found in Reference (15).

In an effort to improve the results obtained in Reference (15), a two-dimensional finite element model for cracking analysis of composite walls was later proposed by Anand and Yalamanchili (17). This model was based on the double-node technique for which a simple shear failure criterion was utilized to define the onset and spread of cracking. Re-cently, Anand and Yalamanchili (18) expanded their two-dimensional cracking model into a quasi three-dimensional model that is capable of predicting cracking in composite walls subjected to vertical as well as horizontal loads. The double node technique was utilized once again and the onset of cracking was based on a simple shear stress criterion.

In all of the above mentioned analytical research, the failure in a composite masonry wall is assumed to initiate and propagate in the collar joint at the interface. In masonry construction, the failure at an interface can normally be defined by a Mohr-Coulomb type of failure

criterion. On the other hand, very little information is available in the literature on the behavior of block-mortar interfaces. Only Hamid et al. (48) and Hegemier et al. (50) have proposed a Mohr-Coulomb type of failure criteria for a block wythe-mortar joint interface. The magnitudes of the shear bond strength at an interface presented by them are the average values obtained by dividing the failure shear force by the total area of the interface. No consideration is given in their results for the fact that the actual shear stress distribution at the interface is not uniform.

Experimental research in composite masonry walls has been mainly directed towards obtaining average values for the collar joint shear strength. Brown and Cousins (26) performed a series of tests in which the failure shear stress was determined for 16 in x 16 in reinforced and unreinforced composite wall specimens with 3/8 inch collar joints. Failure shear stress for reinforced and unreinforced composite walls with 2 inch collar joints, on the other hand, was determined by McCarthy et al. (65).

Proposed Research

In the research presented in this work, the finite element method is used once again to investigate the behavior of composite masonry walls subjected to vertical and horizontal in-plane loads, and due to creep strains and temperature variations. A solution procedure using two-dimensional plane strain finite elements is proposed to compute correct stresses in the collar joints of composite masonry walls. An improved failure criterion for the block wythe-collar joint interface is proposed and a failure analysis procedure is presented. Failure loads in composite

masonry walls of various heights using the proposed failure criterion and method of analysis are determined.

The various phases of the research performed are summarized below. The effect of horizontal in-plane loads on the behavior of composite masonry walls is investigated. The previously developed, improved, quasi three-dimensional finite element model is used in this investigation.

The behavior of composite masonry walls subjected to creep strains and temperature variations is studied using the two-dimensional finite element models in which the cross section of a wall is analyzed by employing linear quadrilateral elements.

Three types of variable-node-number isoparametric serendipity elements are developed in an effort to estimate the collar joint shear stresses more accurately at the interface. The locations of the optimal stress points within the elements are also determined.

An interface element is developed to model the block wythe-collar joint interface in composite masonry walls. The constitutive relationships for the interface element are derived from the experimental results available in the literature. For a better understanding of the behavior of the interface in composite walls, the composite masonry wall specimens that were tested at Clemson University are investigated analytically.

A procedure is proposed to determine correct shear stresses in the interfaces of composite masonry walls using a two-dimensional finite element model. This procedure is considered especially useful when only the inner block wythe is loaded and the shear stresses in the block-collar joint interface near the region of load application are of interest.

An improved Mohr-Coulomb type failure criterion for the block wythe-collar joint (mortar) interface is developed. Empirical equations

are proposed for obtaining failure criteria for masonry once the material
properties for the masonry units and mortar are known. In Addition, a
finite element procedure for cracking analysis of composite masonry walls
in a two-dimensions is proposed. Failure loads in composite masonry walls
of various heights are determined using the failure criterion developed
in this research. The failure loads estimated analytically are compared
with those obtained by assuming uniform failure shear stress given in the
literature.

CHAPTER II

EFFECTS OF HORIZONTAL AND VERTICAL LOADS

ON COMPOSITE MASONRY WALLS

Composite masonry walls carry substantial loads in many practical applications. Figure 1.2 shows a floor slab which has been placed on the concrete block wythe of a composite wall. The slab can transfer horizontal as well as vertical loads to the block wythe some of which are then distributed through the collar joint to the brick wythe.

In all of the previously reported analytical and experimental research, only vertical loads acting on the block wythe have been considered. In many cases, however, the composite walls may be subjected to in-plane horizontal loads on one wythe due to wind and earthquakes. It is not obvious whether the shear stress distribution in the collar joint due to the vertical loads could also be assumed for the horizontal loads. The effects of the horizontal in-plane loads acting on the composite walls are studied in this chapter in which the previously developed quasi three-dimensional finite element model has been utilized. The results obtained from this analysis are compared with those due to the vertical loads. Although the development of the quasi three-dimensional model has previously been presented elsewhere (13, 19, 20), some important features of the model are given in the next section for completeness.

Description of the Quasi Three-Dimensional Model

Since the composite walls to be studied are subjected to the horizontal in-plane loads, these cannot be analyzed by considering only a cross section of the wall, as was possible when the loads were vertical

(13, 19, 20). Thus, either a complete three-dimensional finite element model must be utilized, which could be very complicated and time consuming, or a quasi three-dimensional model could be used.

In this development, a new "composite" element is created. In this new element, the brick and block wythes are each modelled as plane stress elements which are joined together by a collar joint shear element to form the composite element which has eight nodes (four for each wythe) as shown in Figure 2.1. As each node has two degrees of in-plane displacement freedom, the total degrees of freedom for the composite element are equal to sixteen. The shear stresses that act in the collar joint shear element are shown in Figure 2.2.

The stiffness matrix of the proposed composite element is formed by combining the stiffness matrices of the two wythe elements with the collar joint stiffness matrix. Detailed expressions for these matrices are derived in the following sections. It should be noted that the following assumptions have been made in this development: (1) All materials are considered as elastic, homogeneous and isotropic; (2) Displacements are assumed to vary linearly between nodes in an element; (3) Out-of-plane bending effects in the wall are ignored; and (4) The steel reinforcement in the collar joint as well as two wythes is neglected in the model.

Stiffness Matrix of a Wythe Element

Determination of stresses, strains and displacements in the wythes due to in-plane loads can be accomplished by a standard plane stress finite element analysis. The governing matrix equation relating forces and displacements in an element is given by

$$\{P\} = [k] \{U\} \tag{2.1}$$
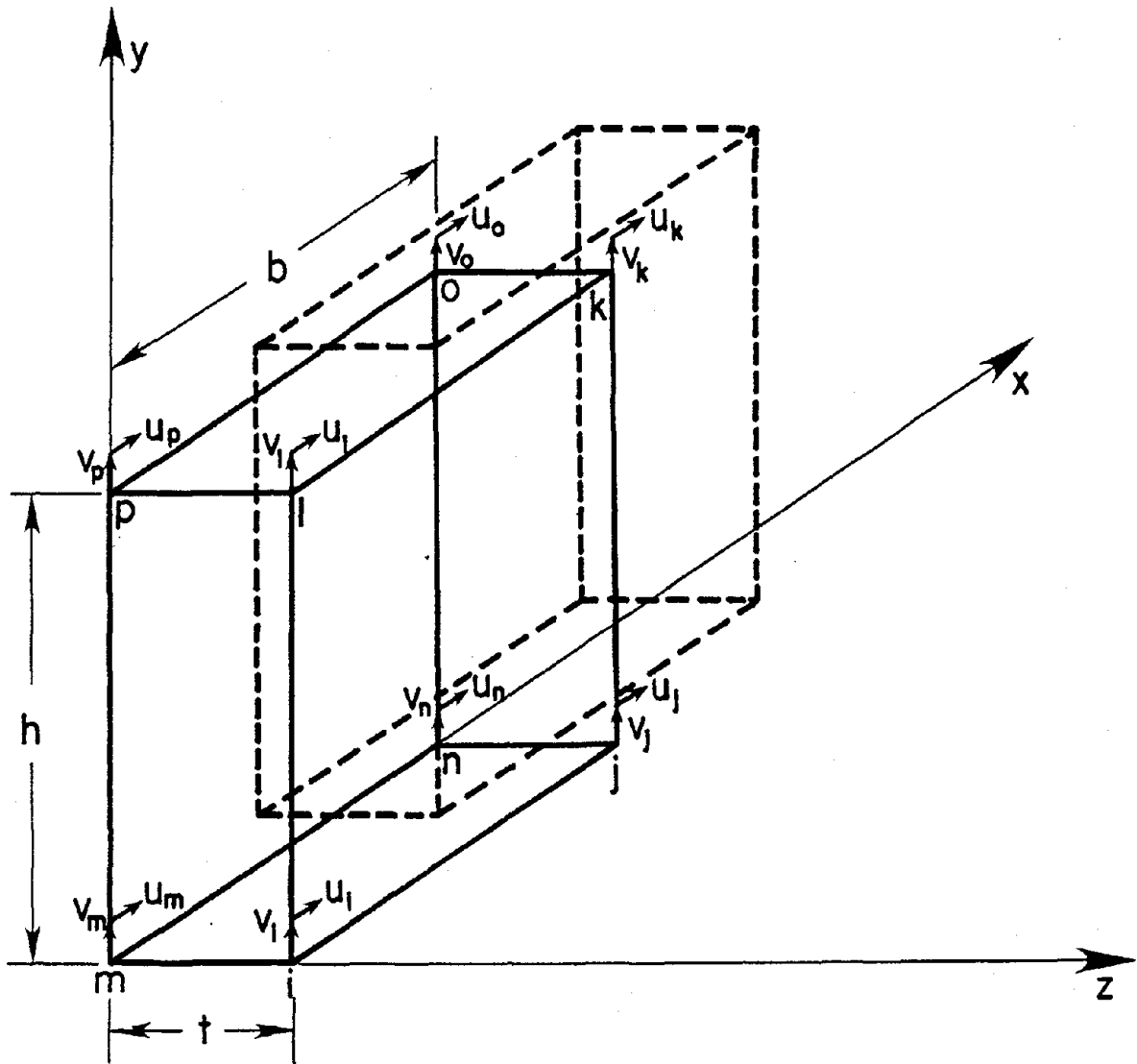
Figure 2.1 Nodal Displacements in an Element

Composite wall section

Inter-laminar
shear element

Inter-laminar
shear element

Top View

Side View

Front View
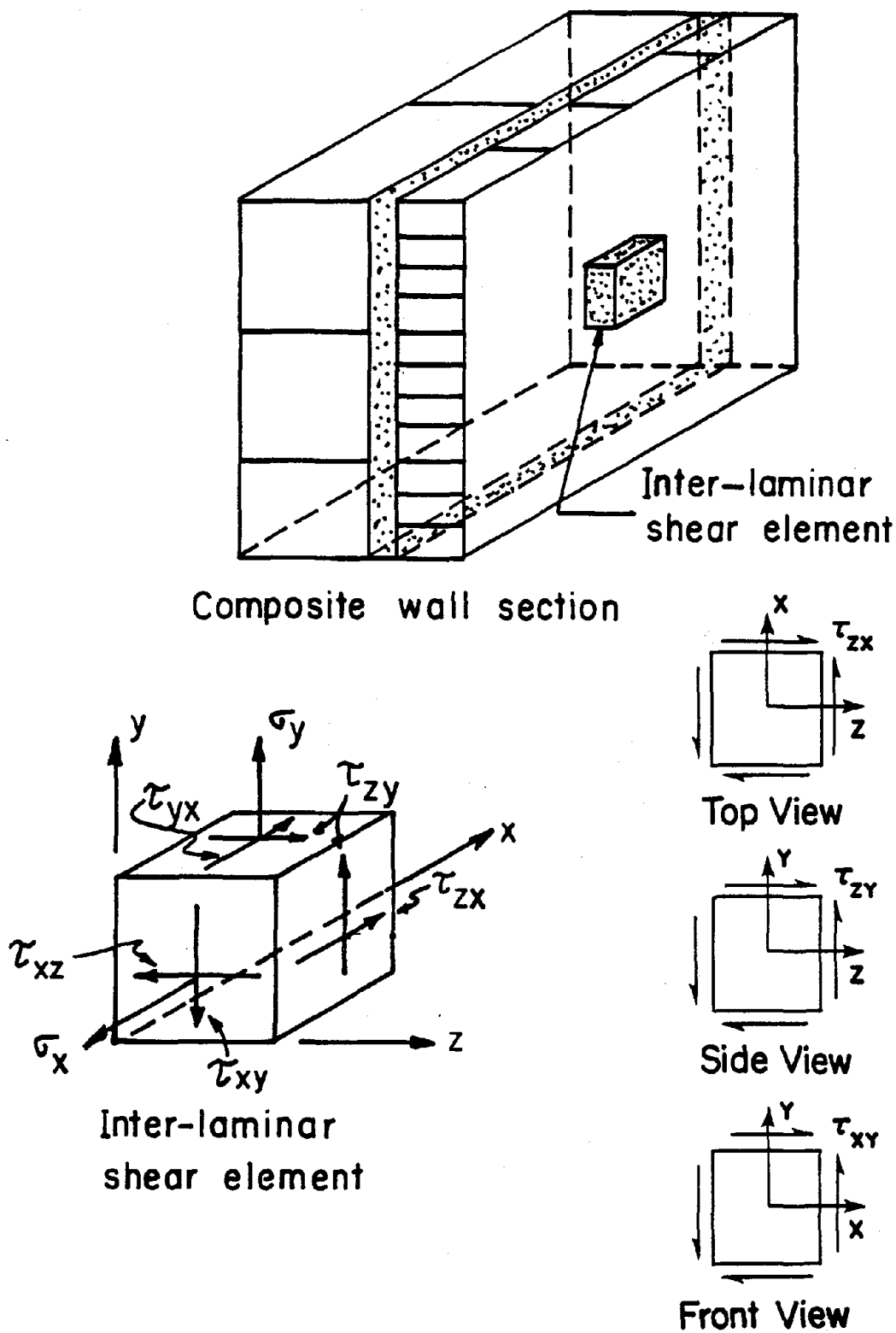
Figure 2.2   Shear Stresses in the Collar Joint

where {P} is a column matrix of force-components in the x and y directions at the nodes of an element, [k] is the in-plane stiffness matrix for an element, and {U} represents the corresponding displacement components at the nodes. A more detailed development of the in-plane stiffness matrix may be found in standard finite element texts. Quadrilateral elements, each consisting of four triangular elements, are utilized in subdividing the wythe faces into a finite element mesh. As each node has two degrees of freedom, Equation 2.1 yields an 8 x 8 stiffness matrix, [k], for each wythe element.

Stiffness Matrix of a Collar Joint Element

The collar joint element stiffness provides the interaction between the two plane stress elements representing the masonry wythes. Stiffness matrices for the front wythe, [k_f], and the back wythe, [k_b], can be developed using Equation 2.1. Shear deformation of the collar joint element is composed of displacements in the x and y directions only. Since these displacements vary linearly between the nodes of the wythe mesh , the stiffness properties of the collar joint element are also based on a linear displacement field in the x-y plane. Thus, the strain-displacement relations in the collar joint element may be written in terms of the nodal displacements as

$$\varepsilon_x = \partial u / \partial x = (u_j + u_k + u_n + u_o - u_i - u_l - u_m - u_p)/4b, \tag{2.2}$$

$$\varepsilon_y = \partial v / \partial y = (v_k + v_l + v_o + v_p - v_i - v_j - v_m - v_n)/4h, \tag{2.3}$$

$$\gamma_{xy} = \partial u / \partial y + \partial v / \partial x = (u_k + u_l + u_o + u_p - u_i - u_j - u_m - u_n)/4h$$
$$+ (v_j + v_k + v_n + v_o - v_i - v_l - v_m - v_p)/4b, \tag{2.4}$$

$$\gamma_{zx} = \partial u / \partial z + \partial w / \partial x^0 = (u_i + u_j + u_k + u_l - u_m - u_n - u_o - u_p)/4t \text{ and} \tag{2.5}$$

$$\gamma_{zy} = \partial v / \partial z + \partial w / \partial y^0 = (v_i + v_j + v_k + v_l - v_m - v_n - v_o - v_p)/4t \tag{2.6}$$

in which u and v are the displacements in the x and y direction, respectively, subscripts refer to the specific element nodes, and t, h, and b, are the thickness, height, and length, respectively, of the collar joint element shown in Figure 2.1. Note that displacement, w, in the z direction is not allowed in this model.

The shearing strains γ_{zx} and γ_{zy} in these equations are defined as the average relative displacement between the two wythes divided by the distance between the two wythes. Thus, the medium resisting shear across the two wythes may be considered as a shear segment connecting the centroids of the two elements facing each other. The shear strain, γ_{xy}, on the other hand, is defined by the sum of the quantities obtained by dividing the average relative y-displacements of the nodes on the two x-faces of the composite element by the length of the element in the x-direction and the average relative x-displacements of the nodes on the two y-faces by the height of the element. The two normal strains, ε_x and ε_y, can be defined similarly.

Equations 2.2 - 2.6 may be written in the matrix form as

$$\{\varepsilon\} = [B] \{U\}, \tag{2.7}$$

where

$$\{\varepsilon\} = \lfloor \varepsilon_x \ \varepsilon_y \ \gamma_{xy} \ \gamma_{zx} \ \gamma_{zy} \rfloor^T \tag{2.8}$$

and

$$[B] = \frac{1}{4} \begin{bmatrix}
\frac{-1}{b} & 0 & \frac{1}{b} & 0 & \frac{1}{b} & 0 & \frac{-1}{b} & 0 & \frac{-1}{b} & 0 & \frac{1}{b} & 0 & \frac{1}{b} & 0 & \frac{-1}{b} & 0 \\
0 & \frac{-1}{h} & 0 & \frac{-1}{h} & 0 & \frac{1}{h} & 0 & \frac{1}{h} & 0 & \frac{-1}{h} & 0 & \frac{-1}{h} & 0 & \frac{1}{h} & 0 & \frac{1}{h} \\
\frac{-1}{h} & \frac{-1}{b} & \frac{-1}{h} & \frac{1}{b} & \frac{1}{h} & \frac{1}{b} & \frac{1}{h} & \frac{-1}{b} & \frac{-1}{h} & \frac{-1}{b} & \frac{-1}{h} & \frac{1}{b} & \frac{1}{h} & \frac{1}{b} & \frac{1}{h} & \frac{-1}{b} \\
\frac{1}{t} & 0 & \frac{1}{t} & 0 & \frac{1}{t} & 0 & \frac{1}{t} & 0 & \frac{-1}{t} & 0 & \frac{-1}{t} & 0 & \frac{-1}{t} & 0 & \frac{-1}{t} & 0 \\
0 & \frac{1}{t} & 0 & \frac{1}{t} & 0 & \frac{1}{t} & 0 & \frac{1}{t} & 0 & \frac{-1}{t} & 0 & \frac{-1}{t} & 0 & \frac{-1}{t} & 0 & \frac{-1}{t}
\end{bmatrix}$$

$$\tag{2.9}$$

and $\{U\} = [u_i \ v_i \ u_j \ v_j \ldots u_p \ v_p]^T.$ (2.10)

The stress-strain relations, in this case, may be given by

$$
\begin{Bmatrix} \sigma_x \\ \sigma_y \\ \tau_{xy} \\ \tau_{zx} \\ \tau_{zy} \end{Bmatrix} = \frac{E}{1-\nu^2} \begin{bmatrix} 1 & \nu & 0 & 0 & 0 \\ \nu & 1 & 0 & 0 & 0 \\ 0 & 0 & \frac{1-\nu}{2} & 0 & 0 \\ 0 & 0 & 0 & \frac{1-\nu}{2} & 0 \\ 0 & 0 & 0 & 0 & \frac{1-\nu}{2} \end{bmatrix} \begin{Bmatrix} \epsilon_x \\ \epsilon_y \\ \gamma_{xy} \\ \gamma_{zx} \\ \gamma_{zy} \end{Bmatrix}
$$ (2.11)

which yields the material property matrix, $[D]$, as

$$
[D] = \frac{E}{1-\nu^2} \begin{bmatrix} 1 & \nu & 0 & 0 & 0 \\ \nu & 1 & 0 & 0 & 0 \\ 0 & 0 & \frac{1-\nu}{2} & 0 & 0 \\ 0 & 0 & 0 & \frac{1-\nu}{2} & 0 \\ 0 & 0 & 0 & 0 & \frac{1-\nu}{2} \end{bmatrix} .
$$ (2.12)

As in the case of the in-plane stiffness matrix for an element, the force-displacement relations for the collar joint shear element may be given by Equation 2.1, in which the element stiffness matrix $[k]$ is defined as

$$[k] = \int [B]^T [D][B]dV.$$ (2.13)

Carrying out the matrix multiplication above using Equations 2.9 and 2.12 leads to the collar joint shearing element stiffness matrix, $[k_{sh}]$.

Stiffness Matrix of a Composite Element

The superposition of the two 8 x 8 wythe element stiffness matrices and the 16 x 16 collar joint shear element stifness matrix results in a 16 x 16 composite element stiffness matrix, written symbolically as,

$$[k] = \int_{vol} [B]^T [D][B] dV.$$

$$= \left[\begin{bmatrix} [k_f] & [0] \\ 8x8 & 8x8 \\ [0] & [k_b] \\ 8x8 & 8x8 \end{bmatrix} + [k_{sh}] \\ 16 \times 16 \end{bmatrix} \right] \qquad (2.14)$$

in which $[k_f]$ and $[k_b]$ are the plane stress stiffness matrices of the front and back wythes, respectively; and $[k_{sh}]$ is the stiffness matrix of the collar joint.

Calculation of Displacements, Stresses and Strains

Using the stiffness matrix of a composite element given in Equation 2.14, the stiffness matrix for a finite element model of the total structure can be assembled by the standard methods leading to the equilibrium equations which are solved for the nodal point displacements. Normal and shearing strains in the wythe elements are obtained by using the standard strain-displacement relations of 2-D quadrilateral elements, whereas the corresponding strains in the collar joint elements are calculated by using Equations 2.2 - 2.6. The in-plane stresses in the wythe elements are calculated from the in-plane strains by using the standard plane stress constitutive relations. The normal and shearing stresses in the collar joint, on the other hand, are calculated from the corresponding strains using Equation 2.12.

Analysis of One Story Composite Masonry Walls

Two 10 ft. high walls, one 20 ft. long and the other 12 ft. long, are analyzed to investigate the influence of the longitudinal stiffness of the wall on the stresses and strains using the model described in the previous section. Each composite wall is made of an 8 in. thick wythe

of concrete block that is attached to a 4 in. thick wythe of clay brick through a 2 in. thick grouted collar joint. The effects of only the horizontal in-plane loads due to earthquakes are examined in this example.

To compute the horizontal earthquake load, it is assumed that the composite shear wall supports a vertical load on the block wythe which is transmitted to it from a 12 ft. wide and 14.5 in. thick concrete slab. A live load of 100 psf is added to the dead load of the slab to compute the total vertical load that acts on the block wythe. The horizontal in-plane load is obtained following the procedure outlined in ANSI A58.1-1982 (107). It is assumed that the structure is in an earthquake zone 2 and can be designed as a class II building. It is further assumed that the block wythe is reinforced whereas the collar joint and brick wythe are unreinforced. Performing the necessary calculations in ANSI for the above given vertical loads leads to a uniform horizontal load intensity on the block wythe of 1.0 k/ft. This load is shown in Figure 2.3 along with the finite element mesh which has been employed in this study.

It is not quite clear if the above mentioned horizontal loads which are generated due to the earthquake acceleration on the mass of the floor slab would act with a uniform intensity on the block wythe. The actual distribution of this load would depend upon the aspect ratio of the floor slab and the relative stiffness of the shear wall to the longitudinal wall. It could be surmised, however, that the center of the wall would resist much larger horizontal load. Accordingly, a load distribution that is parabolic in shape, and leads to the same total load, has also been assumed in these analyses. The maximum horizontal load intensity in this

1.57 k/ft

1.0 k/ft

A   B   C

10'

y

Center Line of Wall

D   D

x

A   B   C

10' or 6'
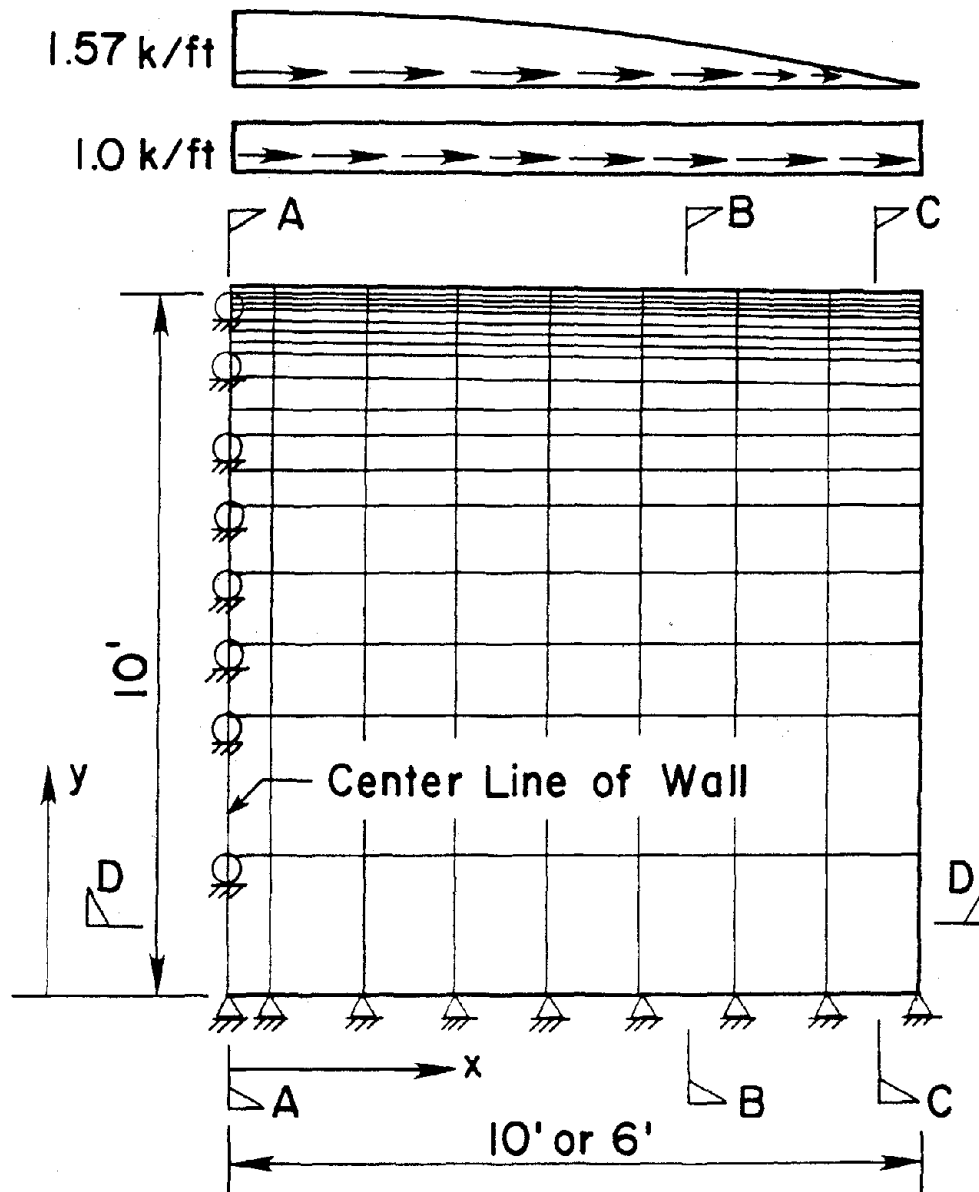
Number of Elements = 288

Number of Nodes   = 342

Band   Width   =   44

Figure 2.3   Finite Element Mesh of One Story Wall

case is equal to 1.57 k/ft., at the center of the wall. The load intensity
is zero at the ends.

As a wall with the horizontally applied loads can be assumed to be
in a state of antisymmetry about an axis through the midpoint along its
length, only half the length of the wallis considered in the analyses.
The wall is considered pinned at the base and the antisymmetric condition
can be modelled by providing horizontal rollers at the midpoint of the
wall. The finite element mesh consists of 280 quadrilateral elements and
342 nodal points which yield a half-bandwidth of 44 in the assembled
stiffness matrix. A relatively fine mesh is utilized near the top of the
wall as it is known from the previous experience that large stress changes
in the collar joint occur near the top of a wall. It is further assumed
that the materials of the composite wall behave linearly elastic. The
values of the elastic modulus and Poisson's ratio utilized in the analysis
are based on the formulas recommended by the Brick Institute of America
(108) and American Concrete Institute (105), and ultimate strengths of
the various material components measured in the laboratory. These cal-
culations may be found in Appendix A of Ref. (8) and lead to elastic
modulus values of 1040 ksi and 2000 ksi for the block and brick wythes,
and 1600 ksi for the collar joint, respectively. The corresponding values
for the Poisson's ratio are 0.25, 0.25, and 0.20 (8).

Results and Discussion

Because the strength of a collar joint is critical in the composite action
of a wall, shear stresses in the collar joint at three different lo-
cations, defined by Section A-A, B-B, and C-C in Figure 2.3, are presented
and discussed. In addition, the normal strains and normal stresses in
the brick wythe and block wythe, as well as in the collar joint, are

investigated along the length of the wall. The above mentioned stresses and strains are shown for the uniform as well as parabolic loads for the 20 ft. and 12 ft. walls.

Collar Joint Shear Stress τ_{xz}

The horizontal loads acting only on the block wythe are transferred to the brick wythe through the collar joint primarily in the top portion of the wall as in the case for the vertically applied loads (19). This load transfer produces horizontal shear stresses in the collar joint which are functions only of the x-displacements of the individual wythes as the proposed model does not have the capability to compute the out-of-plane displacements in the z-direction.

The shear stress distribution in the collar joint due to a uniformly distributed loads of 1 k/ft is shown in Figure 2.4. It can be noted that the shear stress is the same at all points along the length of the wall and it has a maximum value of 16 psi at the top which drops to zero within 10-12 inches. A similar phenomenon was observed in a composite wall subjected to vertical loads in an earlier investigation (19) which indicates that the shear stiffness of the collar joint is much more predominant than the total stiffness of wall in the load transfer mechanism between the two wythes. The difference between the vertical and horizontal stiffness in a composite wall is of relatively little significance. As the horizontal shear stress distribution is the same for both the 20 ft. and 12 ft. long walls, it can be surmized that the horizontal shear stress in the collar joint is independent of the wall length.

The horizontal shear stress in the collar joint due to a parabolic distribution of the horizontal earthquake load is shown in Figure 2.5. As the maximum load intensity is at section A-A near the center of the

All Sections
for 20' and 12' Walls

Uniform Load

Distance along Height of Wall, inches

120

100

80

60

40

20

0

-20

-10

0

Collar Joint Shear Stress, τ_{xz}
$(x\,10^3)$ ksi

Figure 2.4 τ_{xz} in the Collar Joint due to Uniform
Horizontal Load
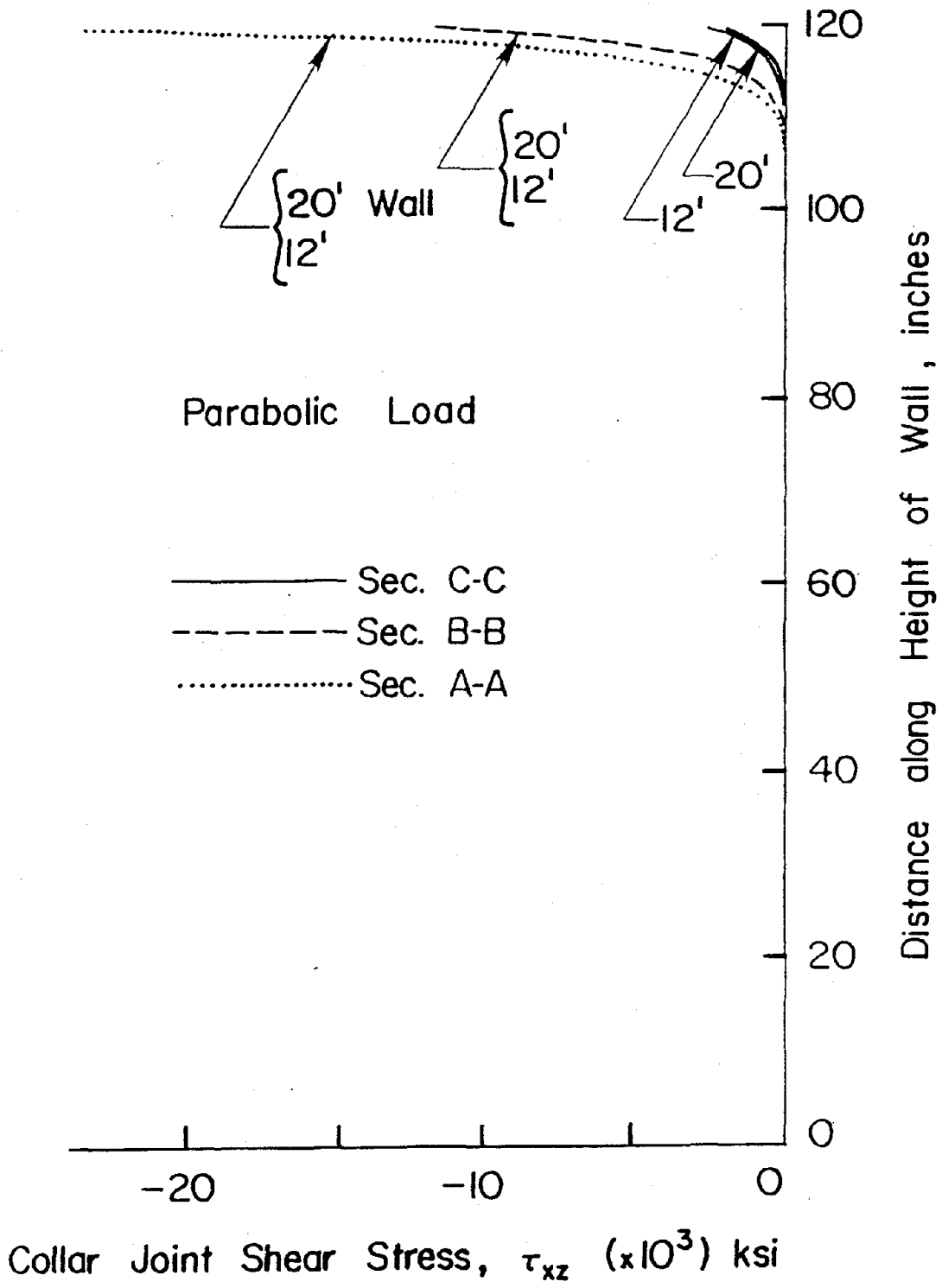
Figure 2.5 τ_{xz} in the Collar Joint due to Parabolic
Horizontal Load

wall, the maximum shear stress also occurs at this section with a value

of 25 psi. This magnitude is approximately 1.57 times larger than that

due to the uniform load. It is of interest to note that the ratio between

the maximum horizontal shear stress due to the parabolic load to that due

to uniform load is the same as the corresponding ratio between the loads

at any point along the length of the wall. This indicates once again that

the stiffness of the collar joint relative to the longitudinal stffness

of the total composite wall is of major importance in transferring the

load across the collar joint. As can be seen in Figure 2.5, the shear

stress magnitudes at Sections B-B and C-C are smaller than at Section A-A

in this case, and the values for the 20 ft. wall are almost identical to

those for the 12 ft. wall.

Collar joint Shear Stress τ_{yz}

The vertical shear stress, τ_{yz}, in the collar joint of a composite

wall is a function only of the relative vertical displacements between

the nodes of the two wythes as is obvious from the strains given in

Equation 2.6. Due to antisymmetric behavior of the wall about its center

line along the length, the maximum vertical displacements in a wall occur

near the wall end Section C-C and are zero at the center line Section A-A.

Thus, the vertical shear stresses are also largest at Section C-C and are

zero at Section A-A. As the vertical displacements in the two wythes

become equal at approximately 15 in. from the top at all sections, τ_{yz}

vanishes to zero at this height. It should be noted that, for a fixed

height of the wall, the vertical displacements of the wythes are larger

for a 12 ft. wall than for a 20 ft. wall, thus, leading to larger magni-

tudes of maximum τ_{yz} for a 12 ft. wall as can be seen in Figures 2.6 and
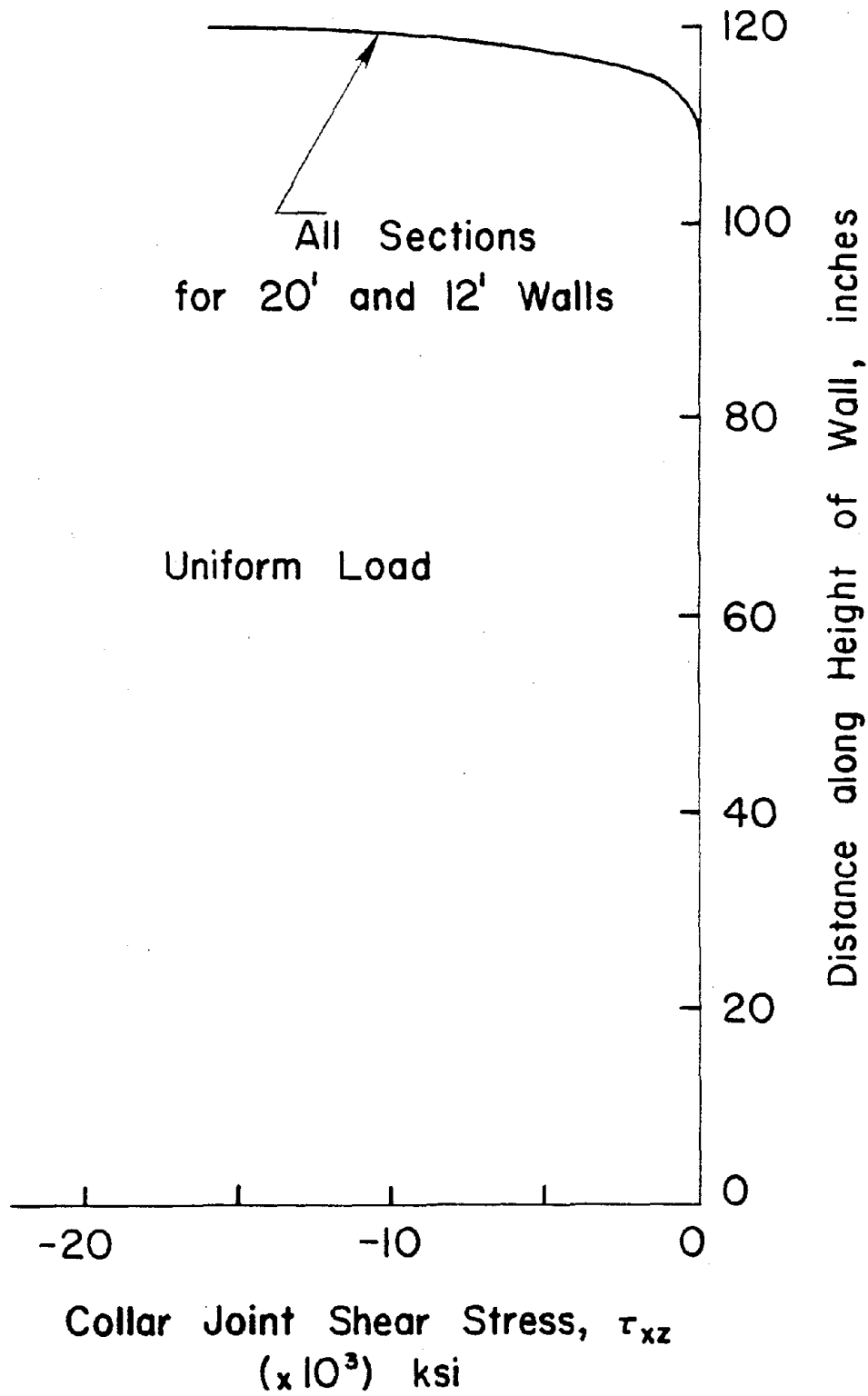
2.7.

Figure 2.6 τ_{yz} in the Collar Joint due to Uniform Horizontal Load
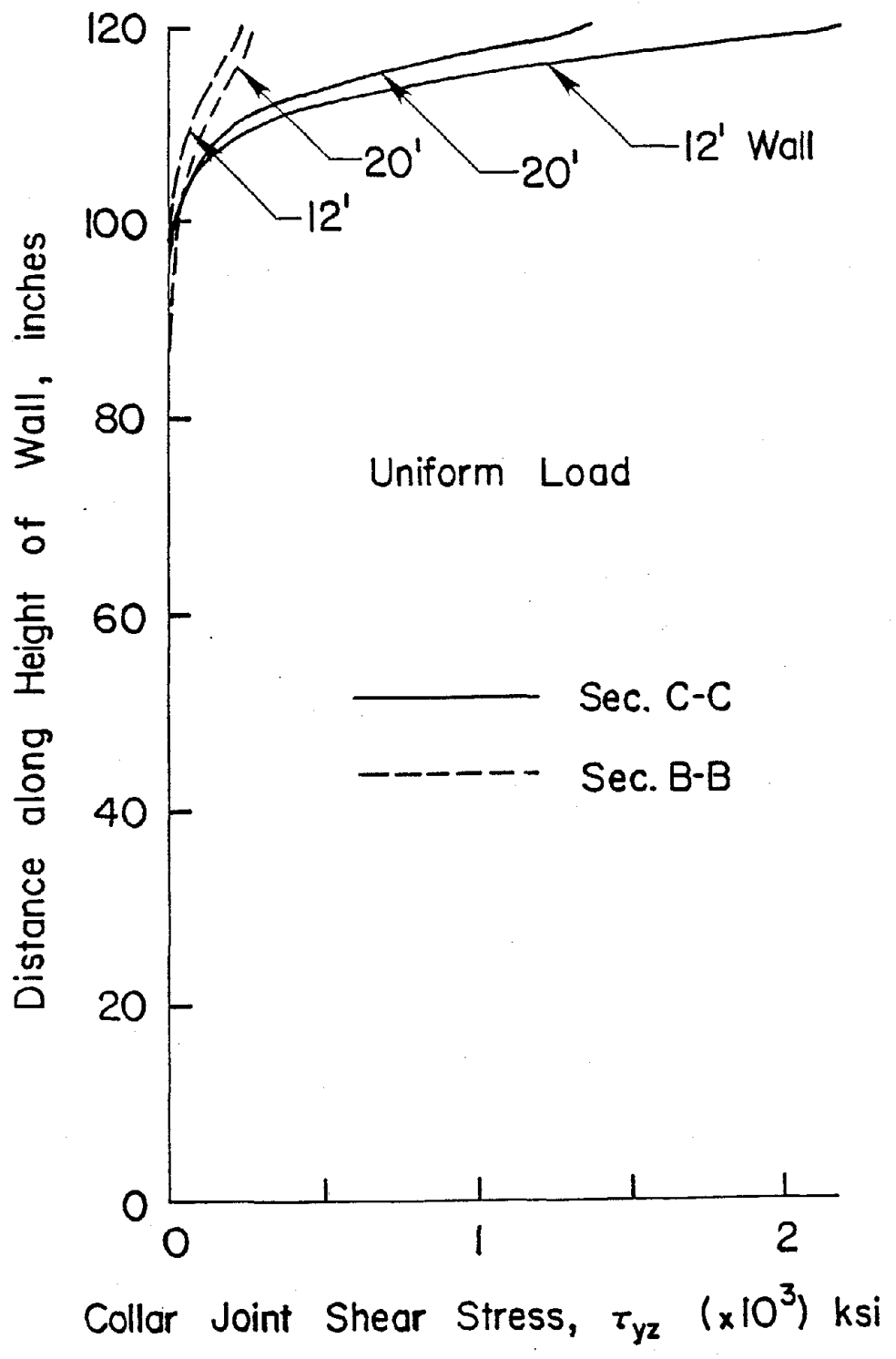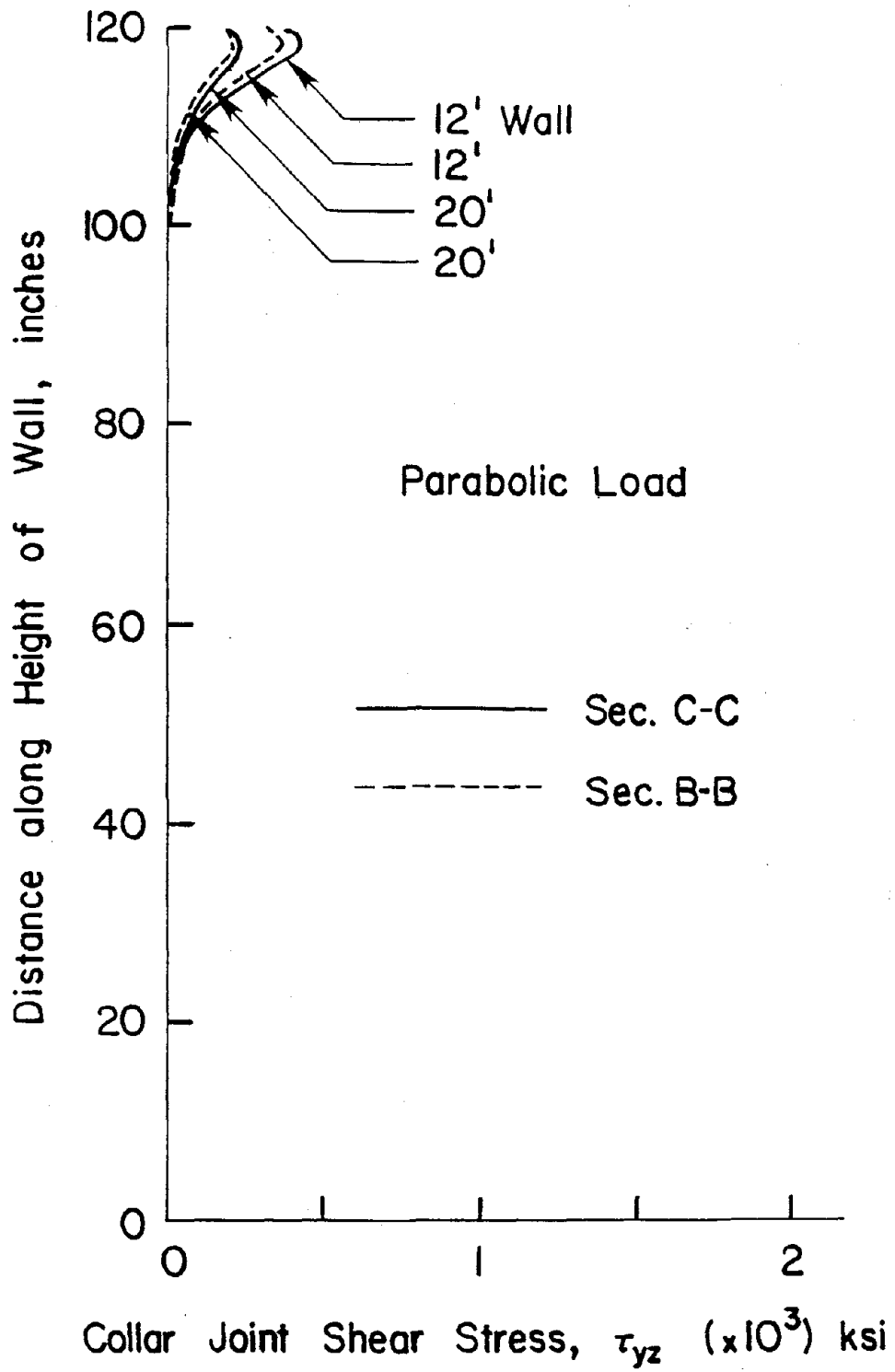
Figure 2.7 τ_{yz} in the Collar Joint due to Parabolic Horizontal Load

The maximum value of τ_{yz} for a uniformly loaded wall is equal to 2 psi for a 12 ft. wall and 1.5 psi for a 20 ft. wall at Section C-C as shown in Figure 2.6. The corresponding values for a parabolically loaded wall are 0.5 psi and 0.25 psi, respectively. The smaller values for the parabolic loading are due to the fact that the load intensities at Sections B-B and C-C are much smaller in this case. A comparison of τ_{yz} with τ_{xz} suggests that the maximum horizontal shear stress is approximately 8 times larger than the maximum vertical shear stress for the uniform load. For parabolic loading, however, the horizontal shear stress is much larger at the center line of the wall (Section A-A) where the vertical shear stress is zero.

Collar Joint Shear Stress τ_{xy}

The collar joint shear stress τ_{xy} for the uniform and parabolic loads is shown in Figures 2.8 and 2.9. Although at first glance, these distributions appear to be rather difficult to grasp, a little effort can lead to a better understanding of this shear stress variation if one notes that τ_{xy} in the collar joint is a function of the horizontal and vertical displacement gradients.

It can be anticipated that the value of the shear stress τ_{xy} at the top of the wall due to the uniform horizontal load would be the same at all sections. In addition, as the load is transferred uniformly to the support at the base, τ_{xy} should be uniform at this place along the length of the wall. These phenomena can be observed in Figure 2.8 for the 20 ft. and 12 ft. walls with an approximate magnitude of τ_{xy} as 7 psi. At Section A-A near the center of the 20 ft. wall, the shear stress increases from 7 psi at the top to approximately 11 psi at 2/3rd the height. This can be attributed to the fact that most of the acting horizontal load is
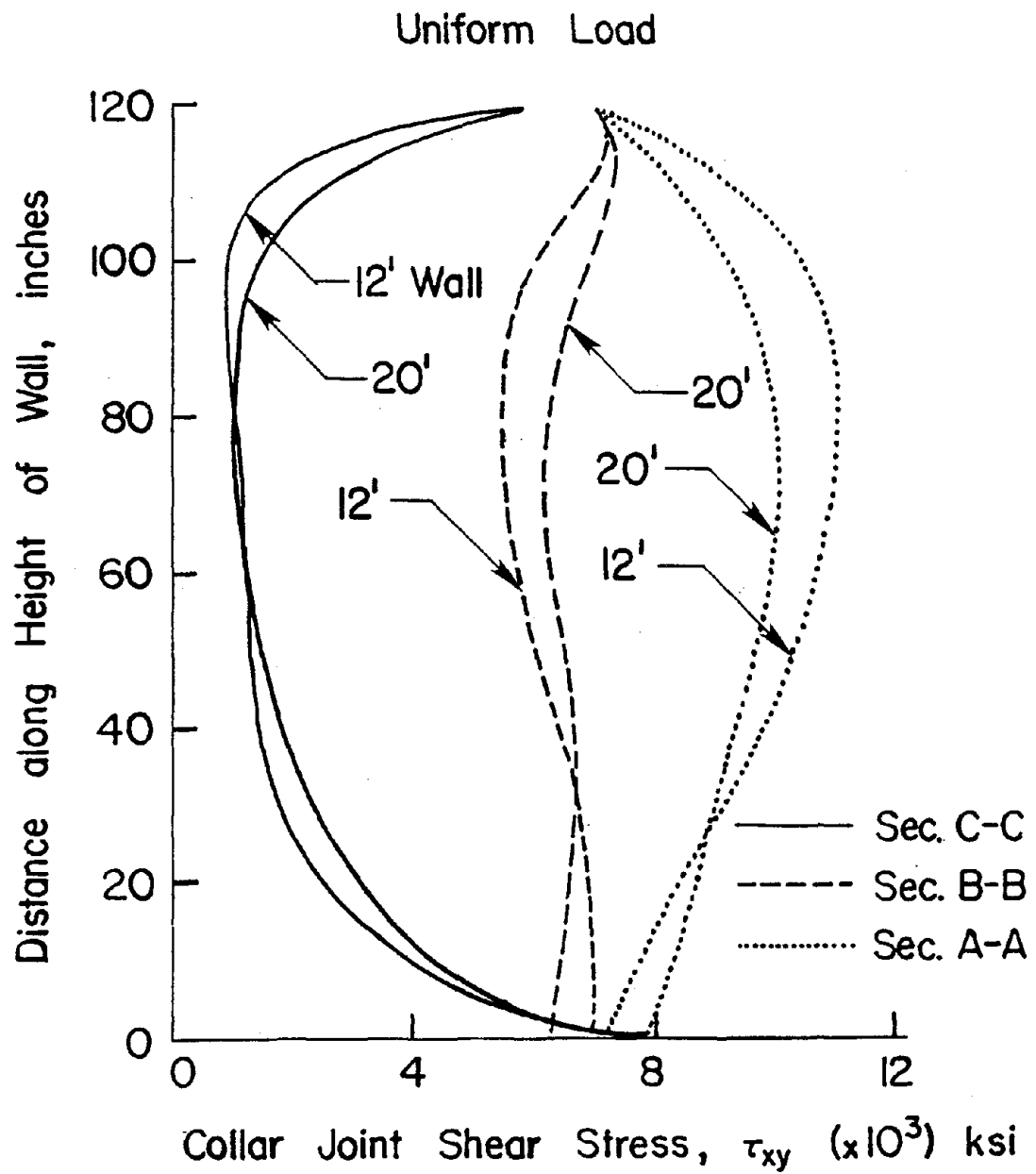
Figure 2.8 τ_{xy} in the Collar Joint due to Uniform
Horizontal Load
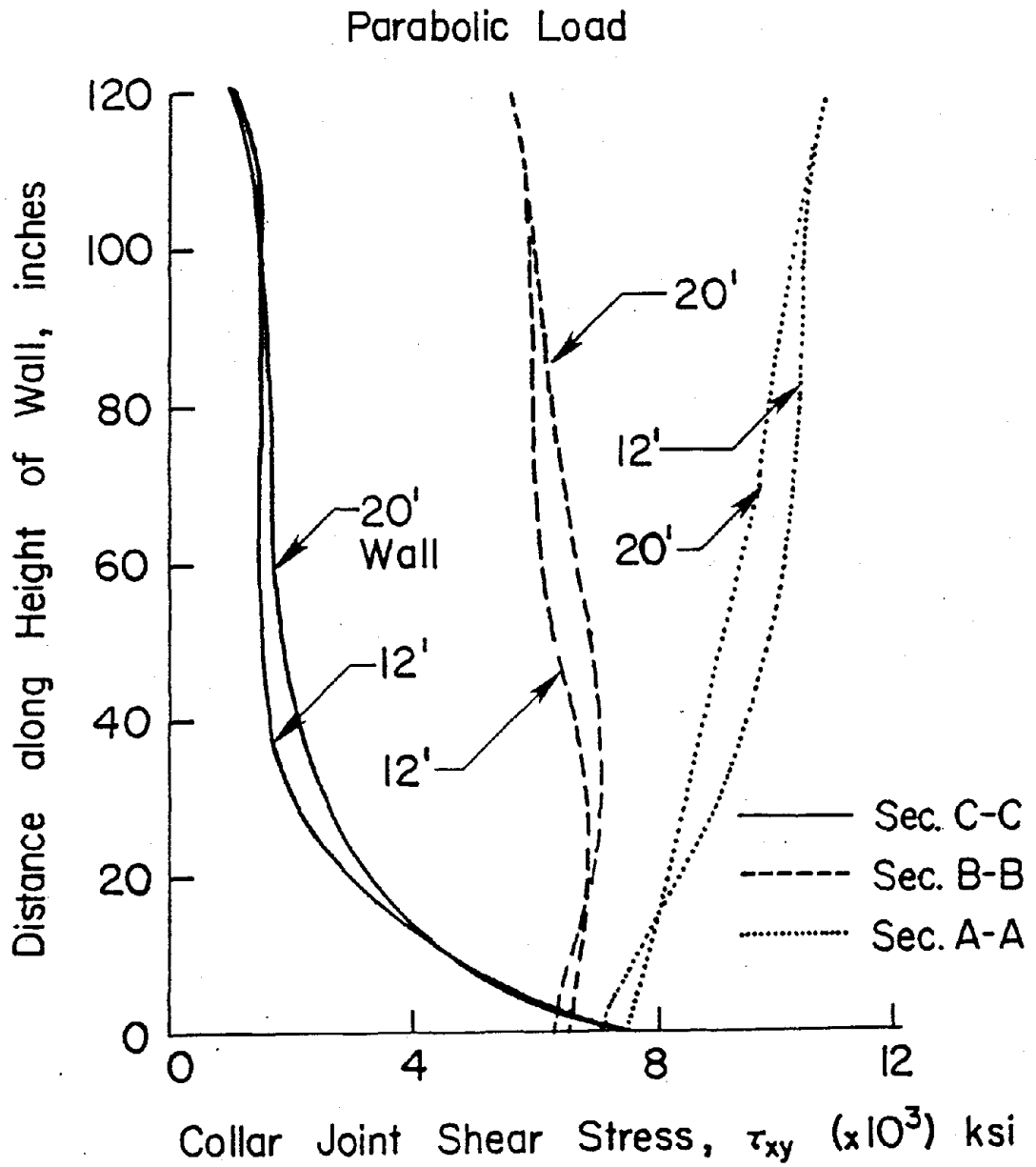
Figure 2.9 τ_{xy} in the Collar Joint due to Parabolic
Horizontal Load

transferred from the block wythe to the collar joint in the top 10 inches. At Section C-C near the end of the wall, on the other hand, the shear stress reduces with height as this section could be construed as the top or bottom vertical fibers of a vertical cantilever beam subjected to a uniformly distributed horizontal load applied at the free end. These fibers in a beam naturally must have zero shear stress. At the bottom of the wall, however, the shear stress increases again due to a uniform horizontal load transfer at this boundary. These phenomena are observed for both the 20 ft. and 12 ft. long walls.

In the case of the parabolic load distribution, the shear stress τ_{xy} at the top of the wall at various sections is a function of the intensity of the applied horizontal load. The maximum shear stress has a magnitude of 11 psi and it occurs at Section A-A as shown in Figure 2.9. τ_{xy} at the bottom of the wall, on the other hand, is approximately equal to 7 psi for all sections as was the case for the uniformly distributed horizontal load.

Vertical Normal Strains and Stresses in the Wall

The normal strains, ε_y, in the block wythe, brick wythe and collar joint at the bottom of the 20 ft. and 12 ft. walls are plotted in Figure 2.10. It can be seen in this figure that the normal strains in each component of the composite wall are equal. This is due to the fact that most of the load transfer from the block wythe to the brick wythe through the collar joint occurs in the top short distance of the wall. It is also for this reason that the shape of the load intensity does not have any effect on the strain distribution at the bottom of the wall, and the normal strains for the uniform and parabolic horizontal loads are the same.

Normal Strain, ϵ_y along Section D-D

Brick
Coll. Jt.
Block

Strain, ϵ_y ($\times 10^5$)

—————— 20' Wall

– – – – – 12' Wall

Brick
Coll. Jt.
Block

Normal

-120   -80   -40   0   40   80   120

Distance x from Center Line of Wall, inches
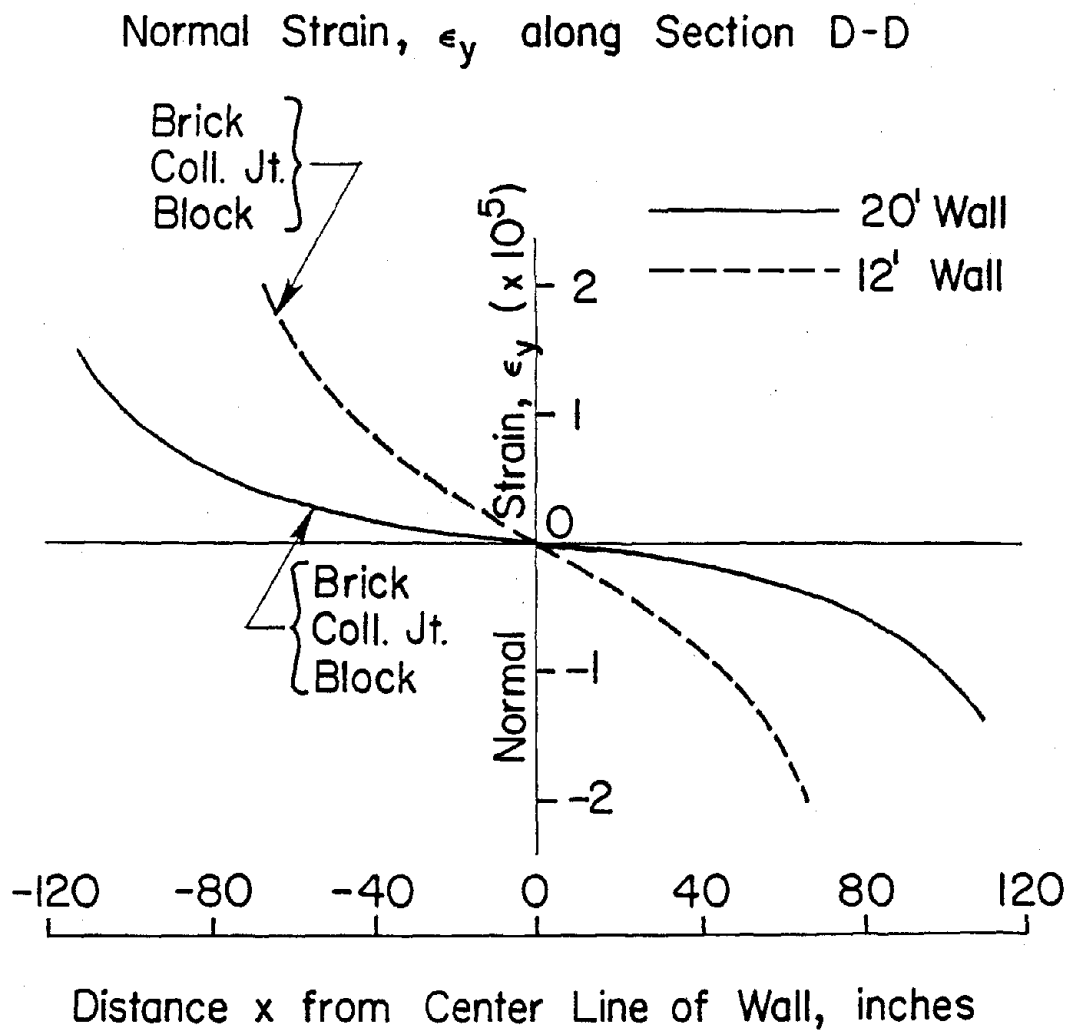
Figure 2.10 ϵ_y along the Length of the Wall

The resisting couples provided by a 12 ft. and a 20 ft. wall, individually must equal to the acting couple at the base of the wall due to the horizontal in-plane load. Since the intensity of loads in both the walls are the same, it is obvious that the stresses, and accordingly, strains, that are created in the 12 ft. wall must be larger than those in a 20 ft. wall. This can be seen in Figure 2.10 from which it is also evident that the strain variation along the length of the wall is not linear. This shape can be attributed to the large length to height ratio of the wall, making the wall behave like a very deep cantilever beam subjected to end loads.

Although the normal strains in the three components of the composite wall are the same, the corresponding stresses are different due to different moduli values. These normal stresses are shown in Figure 2.11 where the maximum value of 40 psi occurs in the brick wythe for a 12 ft. wall.

Conclusions

The results presented in the previous section for single story shear walls subjected to horizontal loads due to an earthquake, lead to the following conclusions:

1. The horizontal shear stress, τ_{xz}, in the collar joint is maximum at the top of the wall and reduces to zero within a distance of approximately 10 in.

2. The vertical shear stress, τ_{yz}, though much smaller than τ_{xz}, reduces to zero within the top 15-20 in.

3. The shear stress, τ_{xy}, in the collar joint varies approximately uniformly from top to bottom at the center line of the wall length and its magnitude is roughly equal to 2/3rd of the maximum horizontal shear stress, τ_{xz}, for a uniform load.

4. Vertical normal stresses are the largest at the base near the ends of the wall. The only shear stress present at these locations is τ_{xy}.

Figure 2.11 σ_y along the Length of the Wall

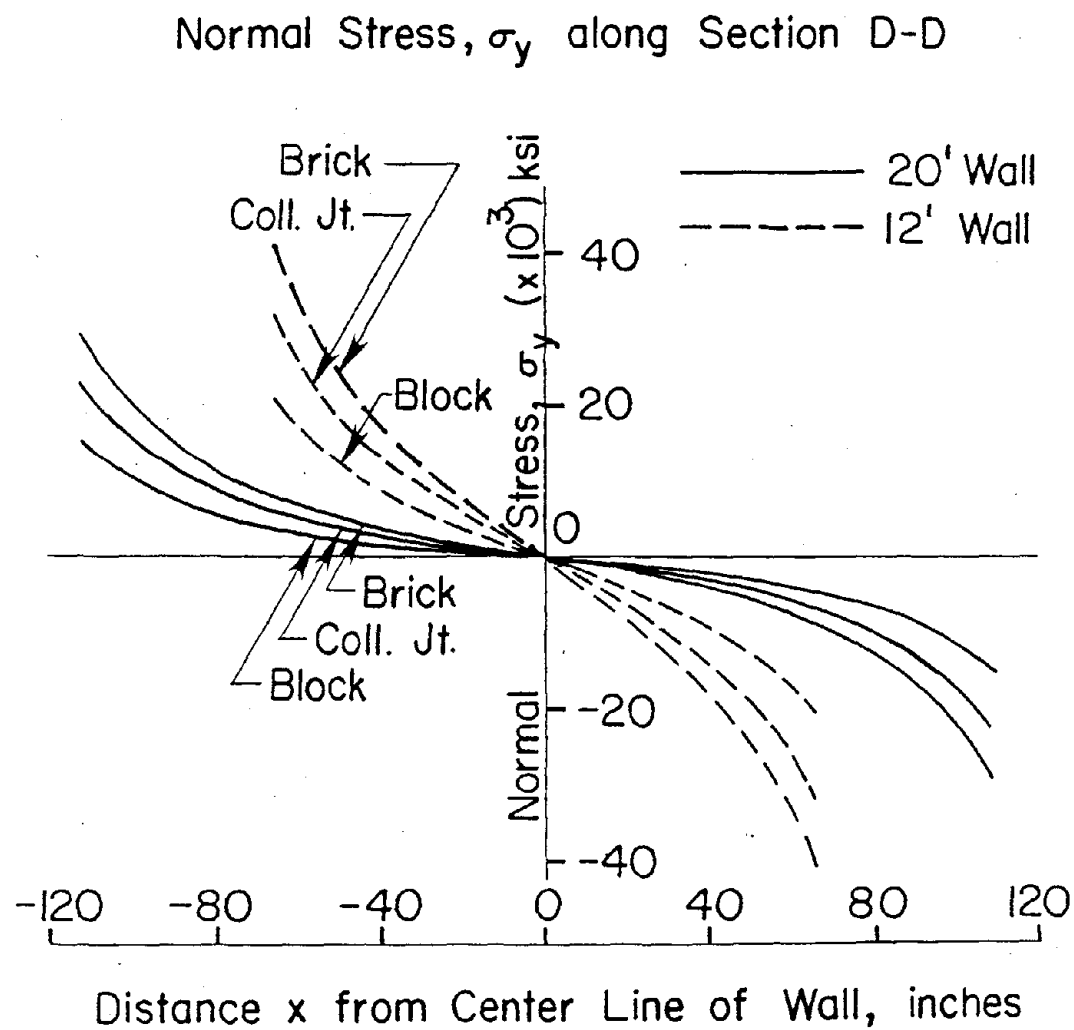5. The horizontal load transfer from the block to the brick occurs within a distance from the top of the wall which is shorter than the distance within which the vertical load transfer occurs. This phenomenon is also due to the smaller horizontal stiffness of the wall compared to its vertical stiffness.

6. Failure criteria based upon the presence of the three shear stresses in the collar joint at the top of the wall, and the normal stresses and shear stress τ_{xy} at the bottom of the wall, must be developed for a better prediction of the wall failure.

Analysis of a Two Story Composite Shear Wall

As a composite masonry wall could also be used as shear wall in a two-story structure, it is of interest to estimate shear stresses in the collar joint due to vertical (gravity) and horizontal (earthquake) loads. The composite shear wall, in this case, is assumed to be made of an 8 in. thick wythe of concrete block that is attached to a 4 in. thick brick wythe through a 2 in. thick grouted collar joint. The wall is 20 ft. high and is subjected to vertical and horizontal loads from the floor slab at 10 ft. and 20 ft. heights, repectively.

It is assumed that the composite wall is a 20 ft. long end-wall for a two-story covered area of the size 20 ft. x 60 ft. The 60 ft. long sides are provided with columns in the middle on which rest beams each 30 ft. long. The floor slabs at each level thus behave as 20 ft. x 30 ft. two-way slabs as far as the vertical loads are concerned, and one 20 ft. side of each slab rests on the concrete block wythe of the composite masonry wall. The vertical load at the roof level is based on a 5 in. concrete slab with 2 in. covering and no live loads whereas at the 10 ft. level, it is based on a 10 in. concrete slab, 2 inch floor finish and a live load of 100 psf. As the slab is supported on all four sides, the total load on the composite wall is calculated from the appropriate tributary area. This leads to the total vertical loads on the block wythe of 8 kips and 24.8 kips

at the roof and first floor levels, respectively. Assuming a parabolic distribution for the vertical loads yields the corresponding maximum load intensities at the center of the wall of 0.63 k/ft and 1.95 k/ft.

The horizontal earthquake loads that act on the composite masonry wall at each floor level are computed using the base shear formula given in ANSI A58.1-1982 (107). It is assumed in this calculation that the shear wall supports the horizontal load due to a tributary area of 20 ft x 30 ft. It is further assumed that the building is located in earthquake zone 3 and has an importance factor of one. Since the collar joint is unreinforced, even if the composite wall itself is reinforced, the value for the numerical coefficient, K, in the base shear formula is taken as four. Performing standard calculations for the base shear magnitude and dividing the total load for the two floors appropriately leads to horizontal loads of 50.5 kips and 42 kips at the roof and first floor levels, respectively. These loads further yield the corresponding uniform horizontal load intensities on the block wythe of 2.52 k/ft and 2.10 k/ft. As for a one story composite wall, a load distribution that is parabolic in shape has also been assumed in this analysis. The maximum horizontal load intensities at the center of the wall in this case are equal to 3.97 k/ft at the roof level and 3.30 k/ft at the first floor level and are zero at the ends.

As in the case of a single story wall, a wall with the horizontally applied loads can be assumed to be in a state of anti symmetry about an axis through the midpoint along its length, only half the length of the wall is considered in the analysis. The wall is considered pinned at the base and the antisymmetric condition can be modelled by providing horizontal rollers at the midpoint of the wall. Similarly, for the vertically

applied loads, only half the length of the wall with vertical rollers at the center line can be considered due to symmetry. These boundary conditions along with the finite element mesh used in the analysis are shown in Figure 2.12. It should be noted that the loads at each floor level are applied only on the block wythe. The finite element mesh consists of 768 quadrilateral elements and 882 nodal points leading to a half-bandwidth of 44 in the assembled stiffness matrix. A relatively fine mesh is utilized near the points of load application as it is known from the previous experience that large stress changes in the collar joint occur near these points. The values for the elastic modulus and Poisson's ratio utilized in the analysis are based upon the formulas recommended by the Brick Institute of America (108) and the American Concrete Institute (105), and ultimate strengths of the various material components measured in the laboratory. These calculations may be found in Appendix A of Reference (8) and lead to modulii values of 1040 ksi and 2000 ksi for the block and brick wythes, and 1600 ksi for the collar joint, respectively. The corresponding values for the Poisson's ratio are 0.25. 0.25 and 0.20.

Results and Discussion

Shear stresses in the collar joint at two different locations, defined by Sections A-A and C-C in Figure 2.12, are shown and discussed. In addition, the normal strains and normal stresses in the brick and block wythes, and collar joint are investigated along the length of the wall. The above mentioned stresses and strains are shown for a uniform as well as a parabolic horizontal load distribution at these sections. In addition, the shear stress distribution in the collar joint due to vertical loads is also presented.
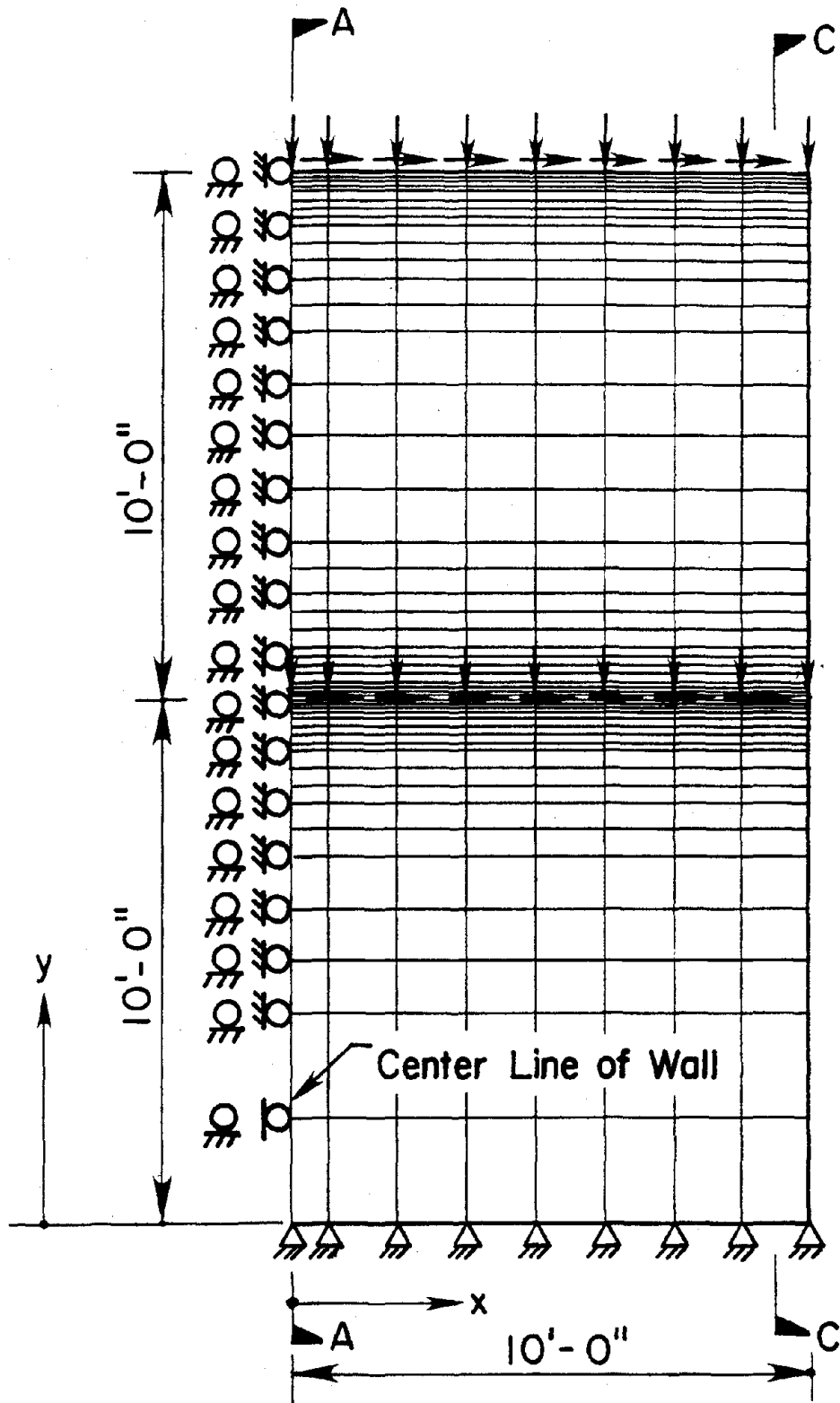
Figure 2.12   Finite Element Mesh of Two Story Wall

Collar Joint Shear Stress τ_{xz}

The horizontal shear stress distribution in the collar joint due to the uniformly distributed horizontal loads of 2.1 k/ft at the 2nd floor level and 2.52 k/ft at the roof level is shown in Figure 2.13. It can be noted that the shear stress magnitude near the roof level is very much higher compared to its value at the 2nd floor level (40 psi vs. 16 psi) although the load intensity at the roof is only slightly larger than at the 2nd floor level. This phenomenon can be attributed to the fact that the load in the block wythe at the 2nd floor level can be transferred to the brick wythe through the collar joint in a region both above and below the slab. On the other hand, the load at the roof level can be transferred to the brick wythe only below the roof slab. Since the stiffness of the collar joint at the 2nd floor level to resist the horizontal in-plane loads is double that at the roof level, smaller displacements, strains and stresses are caused at this level. The shear stresses in the collar joint drop to zero within a distance of 10-12 inches from the slab level, a phenomenon similar to the one observed in the analysis of a single story composite wall. This indicates that the shear stiffness of the collar joint is much more predominant than the total stiffness of the wall in the load transfer mechanism between the two wythes.

The horizontal shear stress distribution in the collar joint at the two levels due to a parabolic distribution of the horizontal loads is shown in Figure 2.14. As the maximum load intensity at each level is at Section A-A near the center of the wall, the maximum shear stresses also occur at this section with a value of 60 psi at the roof level and 25 psi at the 2nd floor level. These magnitudes are approximately 1.57 times larger than those due to the uniform load. It is of interest to note that
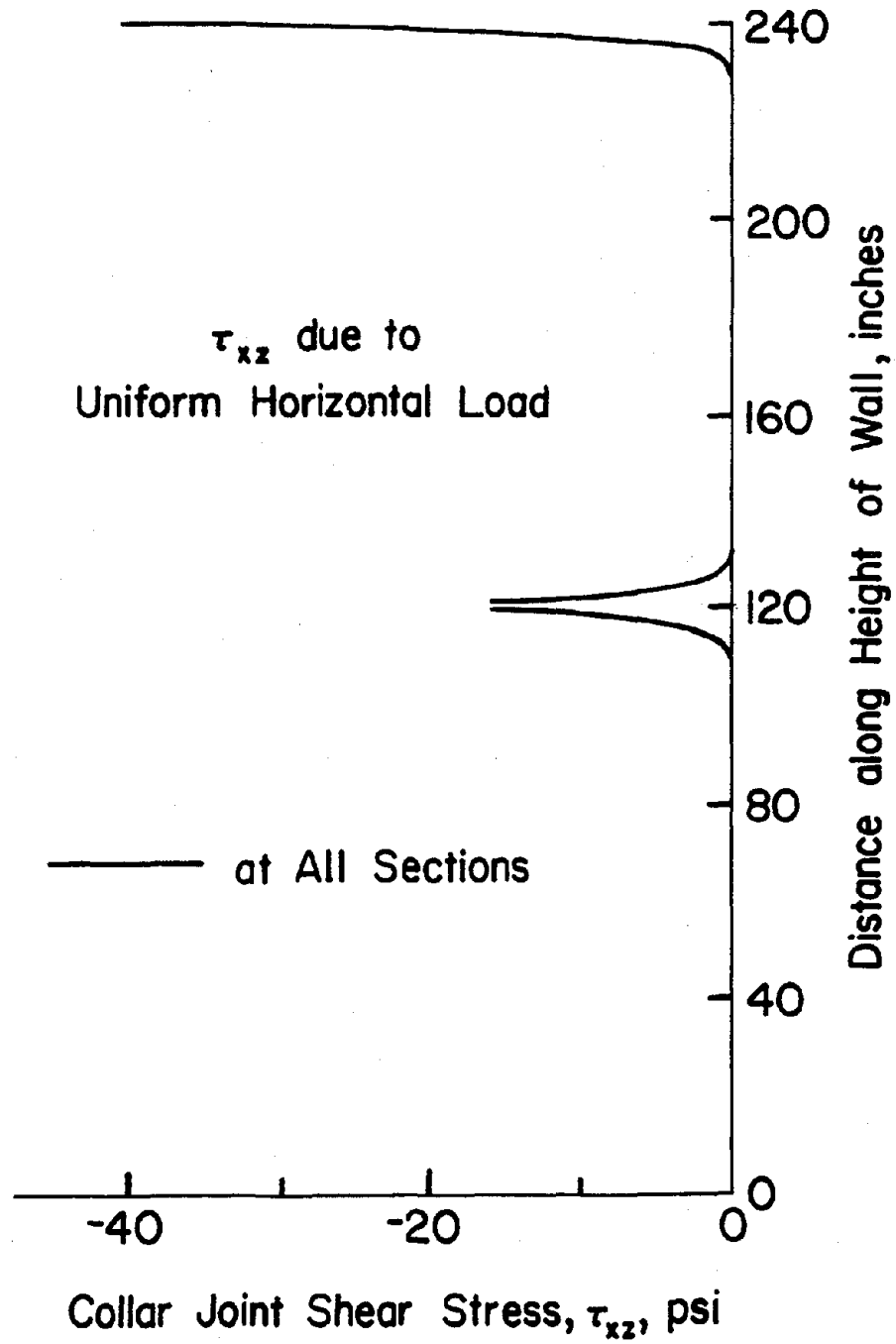
τ_{xz} due to
Uniform Horizontal Load

———— at All Sections

Distance along Height of Wall, inches

Collar Joint Shear Stress, τ_{xz}, psi

Figure 2.13 τ_{xz} in the Collar Joint due to Uniform
Horizontal Load

τ_{xz} due to
Parabolic Horizontal Load

───── at Sec. A–A
────── at Sec. C–C

Collar Joint Shear Stress, τ_{xz}, psi
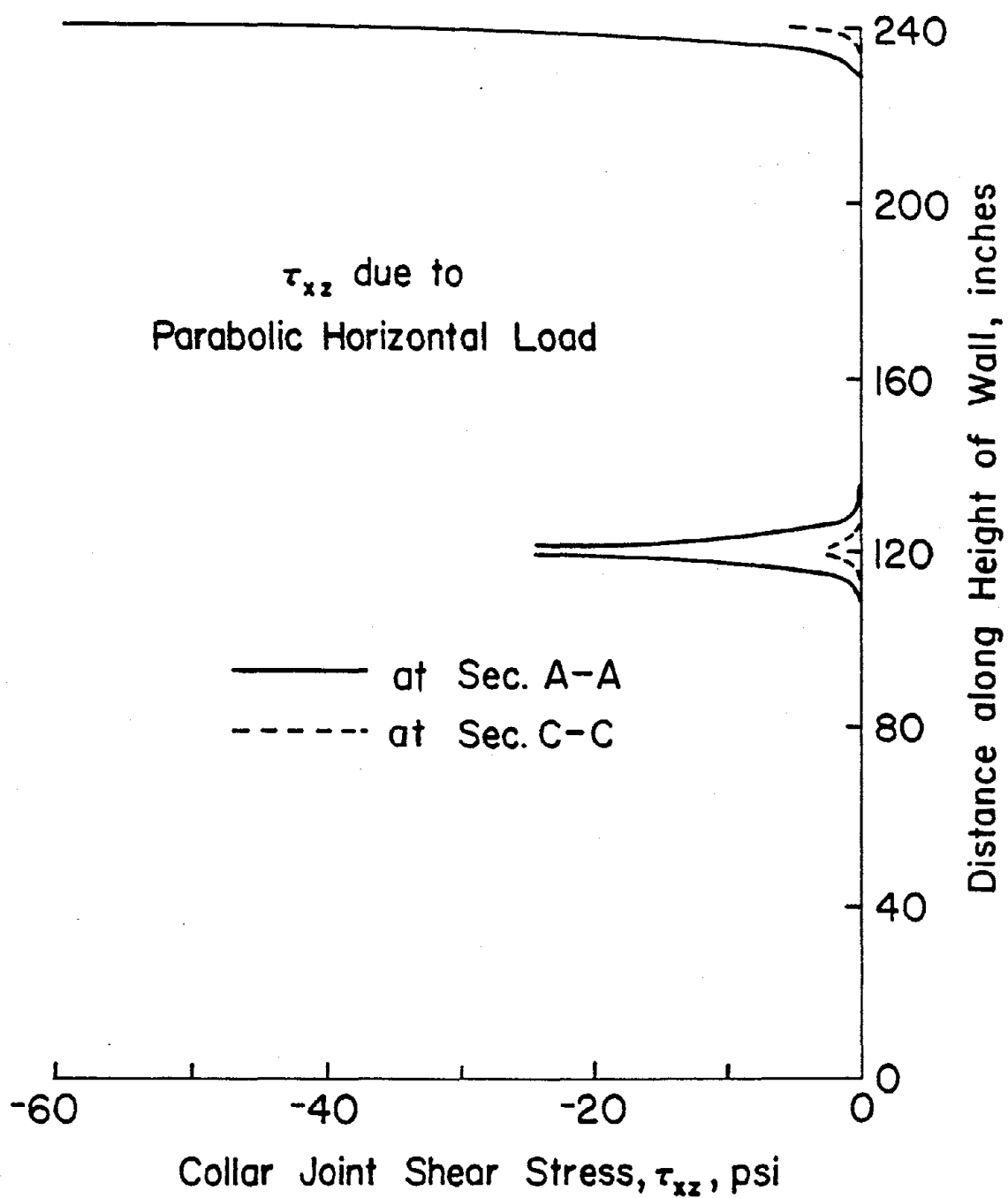
Distance along Height of Wall, inches

Figure 2.14 τ_{xz} in the Collar Joint due to Parabolic
Horizontal Load

the ratio between the maximum horizontal shear stress due to the parabolic load to that due to the uniform load at each level is the same as the corresponding ratio between the loads at any point along the length of the wall. This indicates once again that the stiffness of the collar joint in transferring the load across the collar joint is of major importance instead of the total longitudinal stiffness of the composite wall. It can be seen in Figure 2.14 that the shear stress magnitudes at Section C-C are much smaller than at Section A-A in this case. This is so because the horizontal load intensity varies parabolically at each floor level and has a much smaller magnitude at Section C-C.

It should be noted here that the vertical loads from the slab at each of the two levels act symmetrically with respect to the center line along the length of the wall and, thus, do not cause any horizontal shear stresses in the collar joint irrespective of the shape of the assumed load distribution.

Collar Joint Shear Stress τ_{yz}

The variation of the vertical shear stress due to the vertical slab loads, which are assumed to be distributed parabolically, is shown in Figure 2.15. The maximum values for this stress are 6.5 psi and 9.5 psi at the roof and 2nd floor levels, respectively. It can be noted, as in the case of the horizontal loads, that although the loads at the 2nd floor level are approximately three times larger than those at the roof level, the corresponding shear stresses are only one and one-half times larger. This phenomenon again can be attributed to the fact that the load transfer at the 2nd floor level occurs both above and below the slab whereas at the roof this transfer takes place only below the slab level.
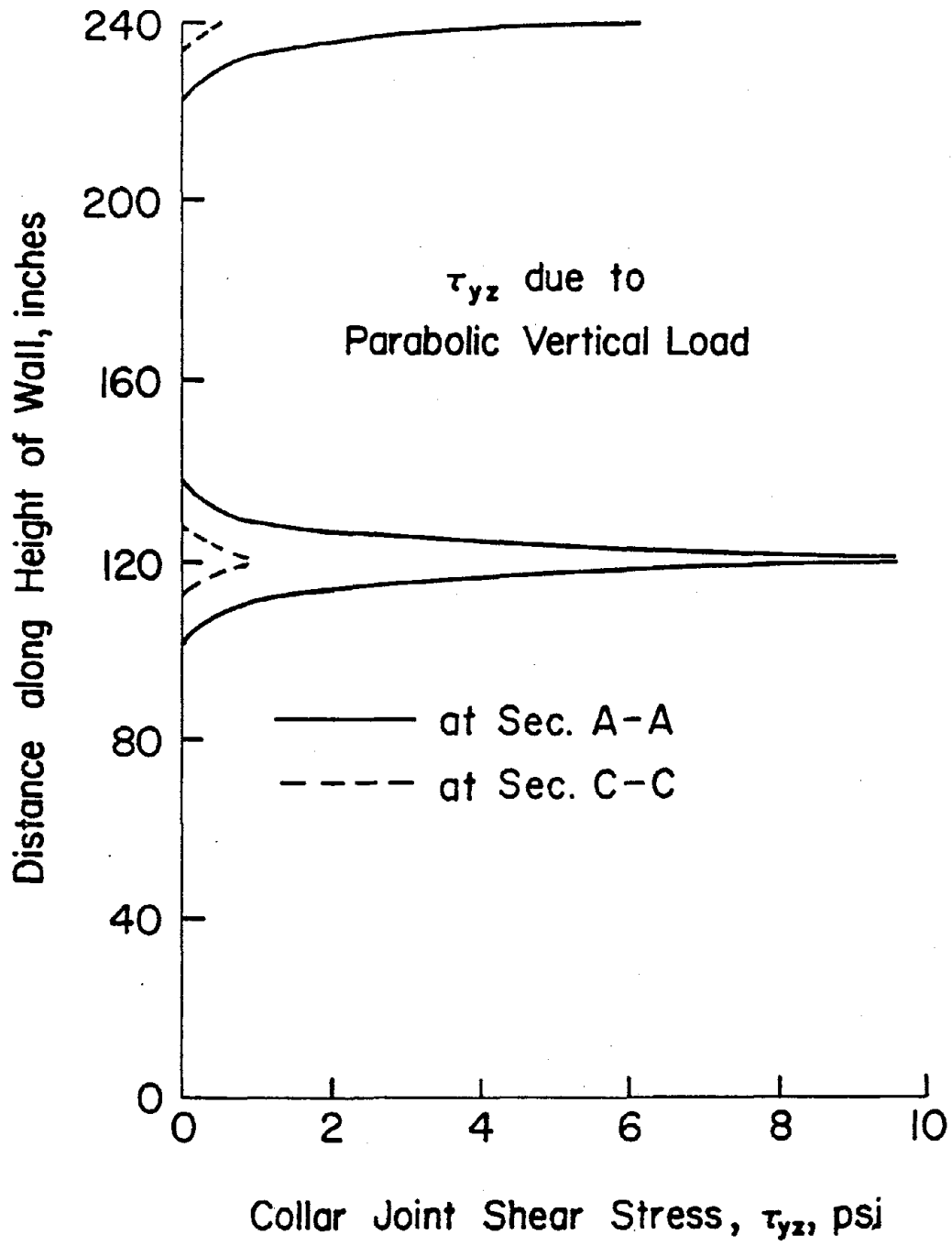
Figure 2.15 τ_{yz} in the Collar Joint due to Parabolic
Vertical load

If the maximum shear stress magnitudes in Figures 2.14 and 2.15 are normalized with respect to the corresponding maximum load intensities, some interesting results can be observed. The normalized horizontal shear stresses due to the earthquake loads are approximately 50% larger than the corresponding normalized vertical shear stresses. This is so because the wythe stiffness in the vertical direction is much larger than in the horizontal direction, which in turn reduces the vertical load transfer to the brick wythe. Hence, the shear stresses in the collar joint are smaller in this case.

Because of the antisymmetric behavior of the composite wall about its center line along the length when subjected to in-plane horizontal loads, the maximum vertical displacements occur near the wall end Section C-C and are zero at the center line Section A-A. Thus, the vertical shear stresses are the largest at Section C-C and are zero at Section A-A. As the vertical displacements in the two wythes become equal to each other at approximately 20 inches away from the slab, τ_{yz} vanishes at this height.

The vertical shear stress distribution in the collar joint due to the horizontal loads is shown in Figure 2.16. It is obvious in this figure that the maximum shear stress τ_{yz} occurs at the roof level. Its value for a uniform horizontal load assumption is equal to 3.7 psi at Section C-C. This stress reduces to 0.7 psi at this section if a parabolic load assumption is made. The smaller value for the parabolic load is due to the fact that the load intensity at this section is much smaller in this case. A comparison of τ_{yz} with τ_{xz} suggests that the maximum horizontal shear stress is approximately 11 times larger than the maximum vertical shear stress for the uniform horizontal load. For
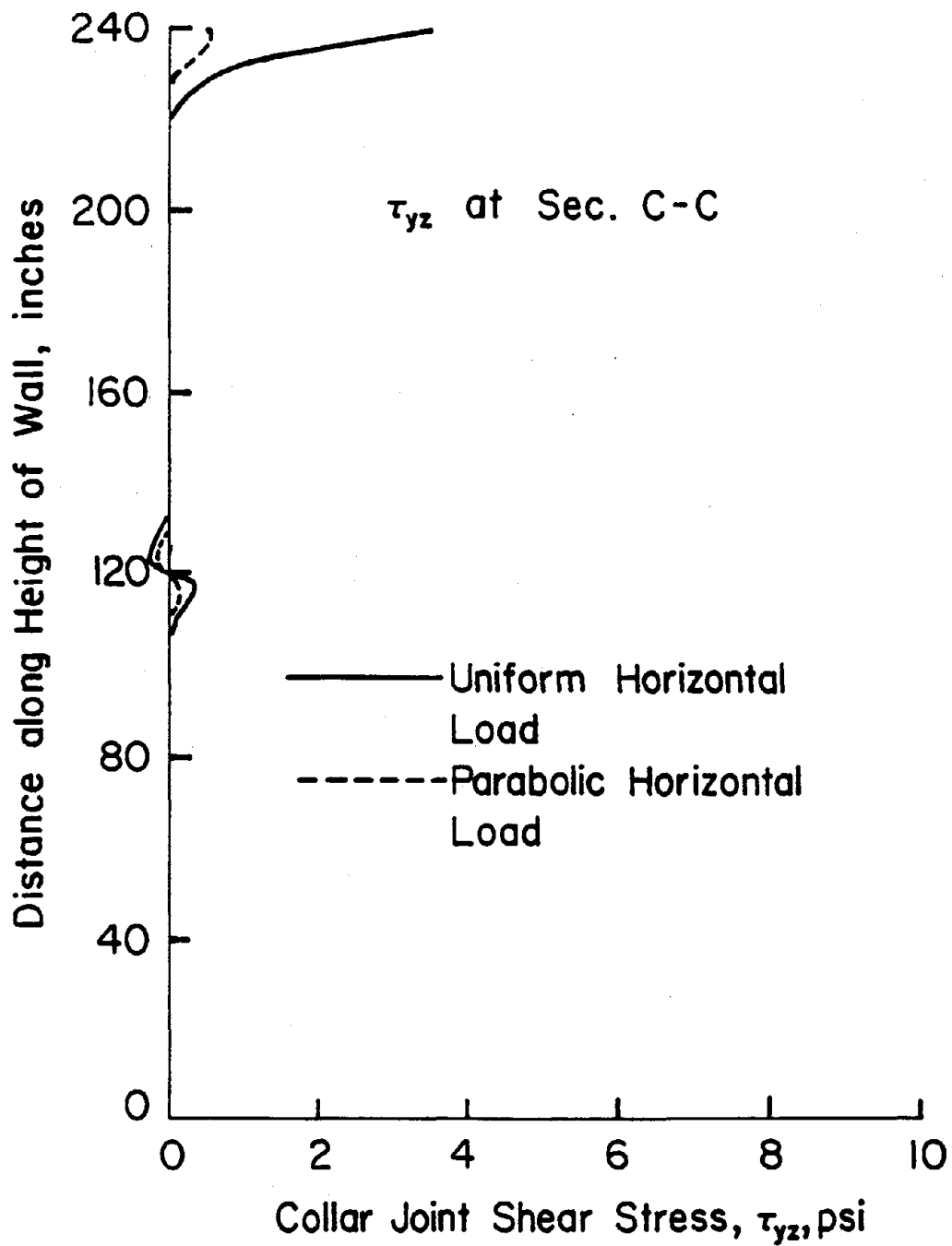
Figure 2.16 τ_{yz} in the Collar Joint due to Uniform and Parabolic Horizontal Loads

parabolic loading, however, the horizontal shear stress is much larger
at the center line of the wall (Section A-A) where the vertical shear
stress is zero.

Collar Joint Shear Stress τ_{xy}

The collar joint shear stress τ_{xy} for the uniform and parabolic hor-
izontal loads is shown in Figure 2.17. It can be seen that the value of
the shearing stress τ_{xy} at the top of the wall due to the uniform hori-
zontal load is the same at all points along its length. At Section A-A
near the center of the wall, τ_{xy} increases from 17 psi at the top to 30
psi just above the second floor level. This can be attributed to the fact
that Section A-A of the wall could be construed as the neutral axis of a
cantilever wall fixed at the base and subjected to a uniform horizontal
load at the roof level. Shear stress τ_{xy} at the neutral axis in a beam
is naturally maximum. Similarly, Section C-C could be regarded as the
top (or bottom) fiber in the cantilever wall where the shear stress is
zero. This can also be seen in Figure 2.17 where τ_{xy} at Section C-C just
above the second floor level is approximately zero. As additional hori-
zontal load intensity is applied at the second floor level, shear stress
τ_{xy} takes a sudden jump and its magnitude becomes equal to 45 psi and 12
psi just below the second floor level at Sections A-A and C-C, respec-
tively. The total horizontal in-plane load along the length of the wall
is transferred uniformly to the foundation and produces a uniform τ_{xy} of
32 psi in the collar joint at the wall base.

If the horizontal load is assumed to have a parabolic load distrib-
ution along the length of the wall, the shear stress τ_{xy} at the roof level
will be proportional to the load intensity at any point. This is the case
in Figure 2.17 where τ_{xy} is equal to 28 psi at Section A-A and 5 psi at
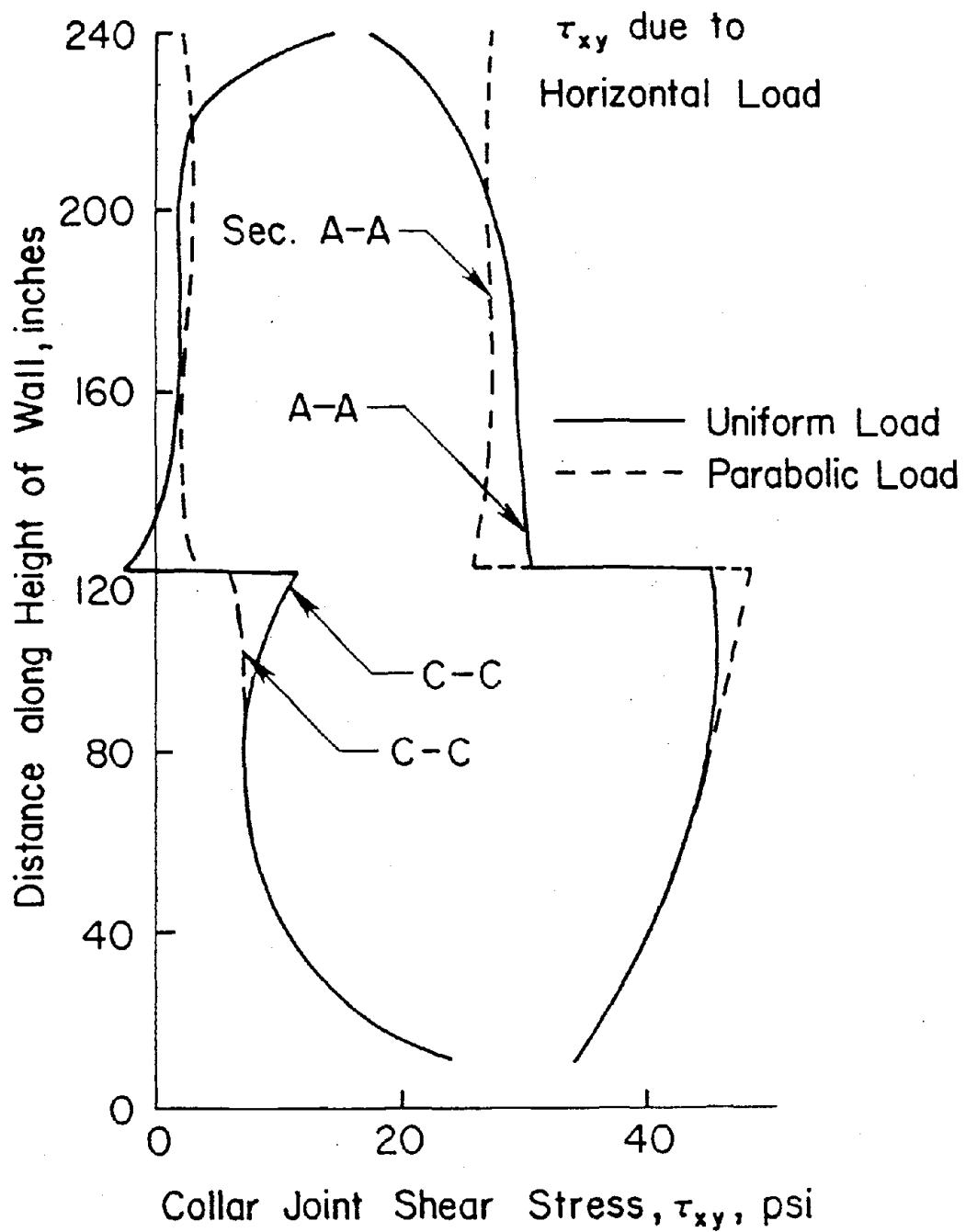
Figure 2.17 τ_{xy} in the Collar Joint due to Uniform and Parabolic Horizontal Loads

Section C-C. These values remain approximately constant up to just above the second floor level where an additional horizontal load with a parabolic distribution is applied. This produces a sudden increase of shear stress which becomes equal to 48 psi and 8 psi at Section A-A and Section C-C, respectively. As in the case of uniform load distribution, the magnitude of the collar joint shear stress τ_{xy} at the bottom of the wall becomes equal at all sections along its length. This magnitude is equal to 32 psi which is the same as for the uniform load. Although the shear stress τ_{xy} in the collar joint is not zero due to a non-uniform vertical load along the length of the wall, its magnitude is relatively small and can be neglected.

Vertical Normal Strains and Stresses at the Wall Base

The vertical normal strains and stresses are computed at the base of the wall due to the combined action of the vertical and horizontal loads. It is found that the normal strains in the block wythe are the same as those in the collar joint and brick wythe. This is due to the fact that most of the load transfer from the block wythe to the brick wythe through the collar joint occurs in the top short distance of the wall. It is also for this reason that the shape of the load intensity does not have any effect on the strain distribution at the wall base, and the normal strains for the uniform and parabolic horizontal loads are the same.

The normal stresses at the base in various materials of the composite wall are shown in Figure 2.18. The maximum stresses, on the compression side of the center line of the wall, in the brick wythe, collar joint, and block wythe are 210 psi, 170 psi and 105 psi, respectively. It is evident from this figure that the stress variation along the length of
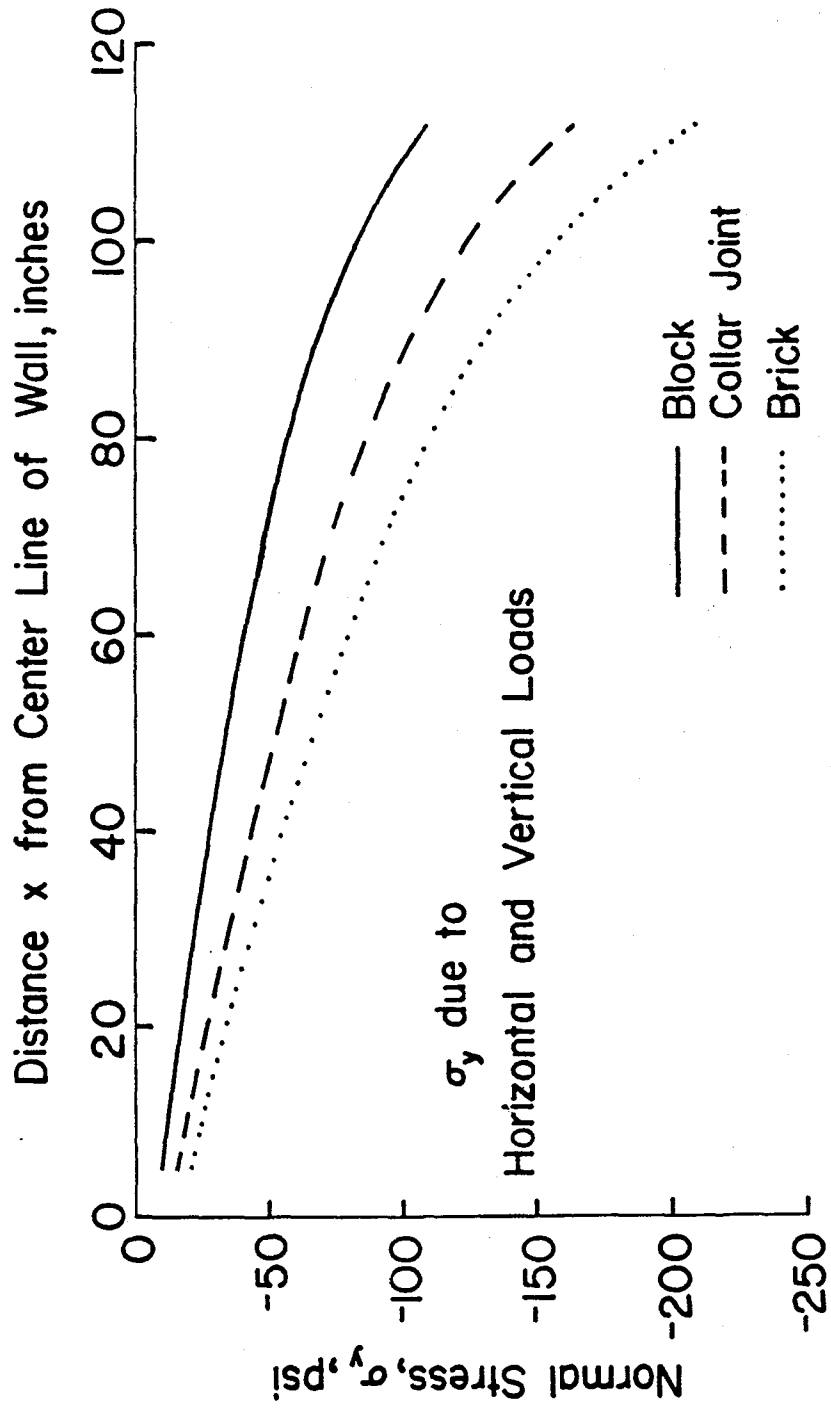
Figure 2.18 σ_y in the Collar Joint due to Horizontal and Vertical Loads

the wall is nonlinear. This shape can be attributed to the large length
to height ratio of the wall, making the wall behave like a very deep
cantilever beam.

Conclusions

The results presented in the previous section for a two story wall
subjected to horizontal and vertical loads, lead to the following con-
clusions:

1. The maximum horizontal shear stress τ_{xz} in the collar
   joint for a two-story wall subjected to horizontal loads
   (assuming a parabolic load distribution) occurs near the center
   line of the wall at the roof level. This shear stress reduces
   to zero at a distance of approximately 20 inches from the top
   of the wall. The horizontal shear stress at the second floor
   level, on the other hand, is much smaller.

2. The vertical shear stress, τ_{yz}, in the collar joint due to
   all loads is rather small. Its maximum value due to vertical
   loads occurs at the center line of the wall. The corresponding
   maximum vertical shear stress due to the horizontal loads is
   much smaller and it occurs at Section C-C where its value due
   to the vertical loads is small. This suggests that Section A-A
   at the center of the wall length is a more critical section.

3. The shear stress, τ_{xy}, in the collar joint is quite signi-
   ficant just below the second floor level. It appears, therefore
   that two locations, one at the roof level and the other just
   below the second floor level, are critical for the failure of a
   collar joint.

4. As the quasi three-dimensional model used in this research pre-
   dicts higher shear stresses in the collar joint (16), and does
   not take the out-of-plane displacements into account, the
   results presented are not accurate; however, the analysis
   provides sufficient information to understand qualitatively the
   behavior of the wall subjected to horizontal loading. a 3-D
   model must be developed for further investigation of the beha-
   vior of composite walls subjected to horizontal loads.

CHAPTER III

CREEP MODELLING IN COMPOSITE MASONRY UNDER PLANE STRAIN

If load is applied to a specimen, which first undergoes an instantaneous deformation and subsequently a further slow deformation with time without an increase in load, the specimen is said to creep. The phenomenon of creep has been investigated extensively in the last few years, both analytically and experimentally, for metals as well as for concrete (24, 28, 35, 36, 43, 49, 67). As a result of these investigations, various analytical techniques have been proposed in the literature for the prediction of creep (24, 35), and several expressions to estimate creep in concrete have become available. On the other hand, creep in masonry has primarily been estimated by performing laboratory tests on masonry wall specimens (91, 92). These tests have been the basis from which several design formulas for computation of creep have been proposed (59, 85, 91). It should be noted that the previously cited creep predictions in masonry specimens have not been utilized in any form to estimate the amount of load redistribution in composite masonry walls.

The purpose of this phase of the research is to extend the numerical technique proposed in Reference (6) to problems of creep in composite masonry walls which are in a state of plane strain. New relationships for components of incremental creep strains in terms of existing stresses at an instant, equivalent stress, and equivalent creep strain are developed for plane strain and are utilized in the incremental solution technique using the finite element method.. Creep behavior for the individual materials in a composite wall is derived from experimentally obtained

specific creep curves available in the literature (91, 92). It is shown that the proposed numerical technique can be used successfully to estimate stress and strain changes due to creep in the cross-section of a long composite wall. In particular, the effect of creep on load transfer from the loaded block wythe to the unloaded brick wythe is studied.

Various Methods for Predicting Creep

The amount of creep that occurs in a member depends on the intensity of the applied loads, the time of application of the load, temperature, humidity, volume to surface ratio and many other factors, especially cement content. Several strategies have been suggested for obtaining analytical solutions of problems involving creep, and the initial strain approach is used most widely in the creep analysis. Briefly, this method involves solving a problem for stresses and strains due to loads and calculation of initial creep strain increments from these results. These initial strains are then used to compute equivalent load increments from which incremental displacements, strains and stresses due to creep are calculated in the whole wall. As these incremental stresses could have appreciable magnitude and could affect the creep behavior, the problem should be treated as a case of variable stress. Some researchers (24, 35) have also suggested the prediction of creep under the influence of variable stress using history integrals. However, as a closed form solution to such integrals could be complicated, other methods have been suggested in the literature (24, 43). One of these methods, that can account for the effect of stress changes on subsequent creep, is based on the principle of superposition which is used in this study.

Principle of Superposition

It is assumed under this principle that each increment in stress produces a resulting deformation which continues for an indefinite length of time. Thus, creep-time curves are required for various ages at which stress changes occur. Gradual variation of stress can be treated as a series of small finite increments and a summation can be applied. For increasing stress and slightly decreasing stress, the principle of superposition is in good agreement with the experimental data; however, for complete unloading, the recovery is overestimated (35). Neverthe-less, this is not a serious handicap since complete unloading is normally not important in a practical situation. Bazant et al. (24) have shown that the prediction of creep by an application of the principle of superposition is in good agreement with the experimental results for concrete, provided (1) the material is linearly viscoelastic, (2) the magnitude of the applied stress is not larger than 40% of the material strength, i.e., the stress is within the service range, (3) the strains do not decrease with time, (4) the material undergoes no significant drying during creep, and (5) the stresses due to the applied loads do not change considerably at any instant of time.

The principle of superposition states that if a structure is sub-jected to various stresses at different times, then the response due to each stress is independent of the responses generated by any other stress (28, 36). This is explained below.

Suppose a structure is subjected to a stress σ_0 at time $t_0 = 0$, then the creep strain $\varepsilon_0^{cr}(t)$ due to this stress is given by

$$\varepsilon_0^{cr}(t) = \sigma_0 J(t, t_0) \tag{3.1}$$

where $J(t, t_0)$ is creep compliance defined as the creep strain per unit stress, also known as the virgin specific creep curve. The specific creep curve which predicts creep due to the stress σ_0 starts at time $t_0 = 0$ as shown in Figure 3.1(a). If the structure is then subjected to a stress increment $\Delta\sigma_1$ at time $t_1 > t_0$, the creep strain increment $\Delta\varepsilon_1{}^{cr}(t)$, due to $\Delta\sigma_1$ alone, at any time $t > t_1$ is given by

$$\Delta\varepsilon_1{}^{cr}(t) = \Delta\sigma_1 J(t, t_1), \tag{3.2}$$

in which $J(t, t_1)$ is the creep compliance or the virgin specific creep curve that starts at time t_1 as shown in Figure 3.1(b). Hence, the total creep strain at time $t > t_1$ is cumulative and is given by

$$\varepsilon^{cr}(t) = \varepsilon_0{}^{cr}(t) + \Delta\varepsilon_1{}^{cr}(t) \tag{3.3}$$

or

$$\varepsilon^{cr}(t) = \sigma_0 J(t, t_0) + \Delta\sigma_1 J(t, t_1) \tag{3.4}$$

as shown in Figure 3.1(c). If there are $(n-1)$ stress changes in n time intervals, the total creep strain $\varepsilon^{cr}(t)$ is, then, given by

$$\varepsilon^{cr}(t) = \varepsilon_0{}^{cr}(t) + \sum_{i=1}^{n-1}\Delta\varepsilon_i{}^{cr}(t) \tag{3.5}$$

or

$$\varepsilon^{cr}(t) = \sigma_0 J(t,t_0) + \sum_{i=1}^{n-1}\Delta\sigma_i J(t,t_i). \tag{3.6}$$

If the stress is a continuously changing function, then the total creep at any time t can also be written as

$$\varepsilon^{cr}(t) = \sigma_0 J(t, t_0) + \int J(t, \tau)(d\sigma/d\tau)\, d\tau, \tag{3.7}$$

in which τ defines the time when $d\sigma$ is applied on the structure. Equations 3.1 to 3.7 describe the principle of superposition to predict uniaxial creep strain due to a changing uniaxial stress. However, since the masonry walls under consideration are in a condition of plane strain and are, consequently, subjected to stresses in two directions, the above
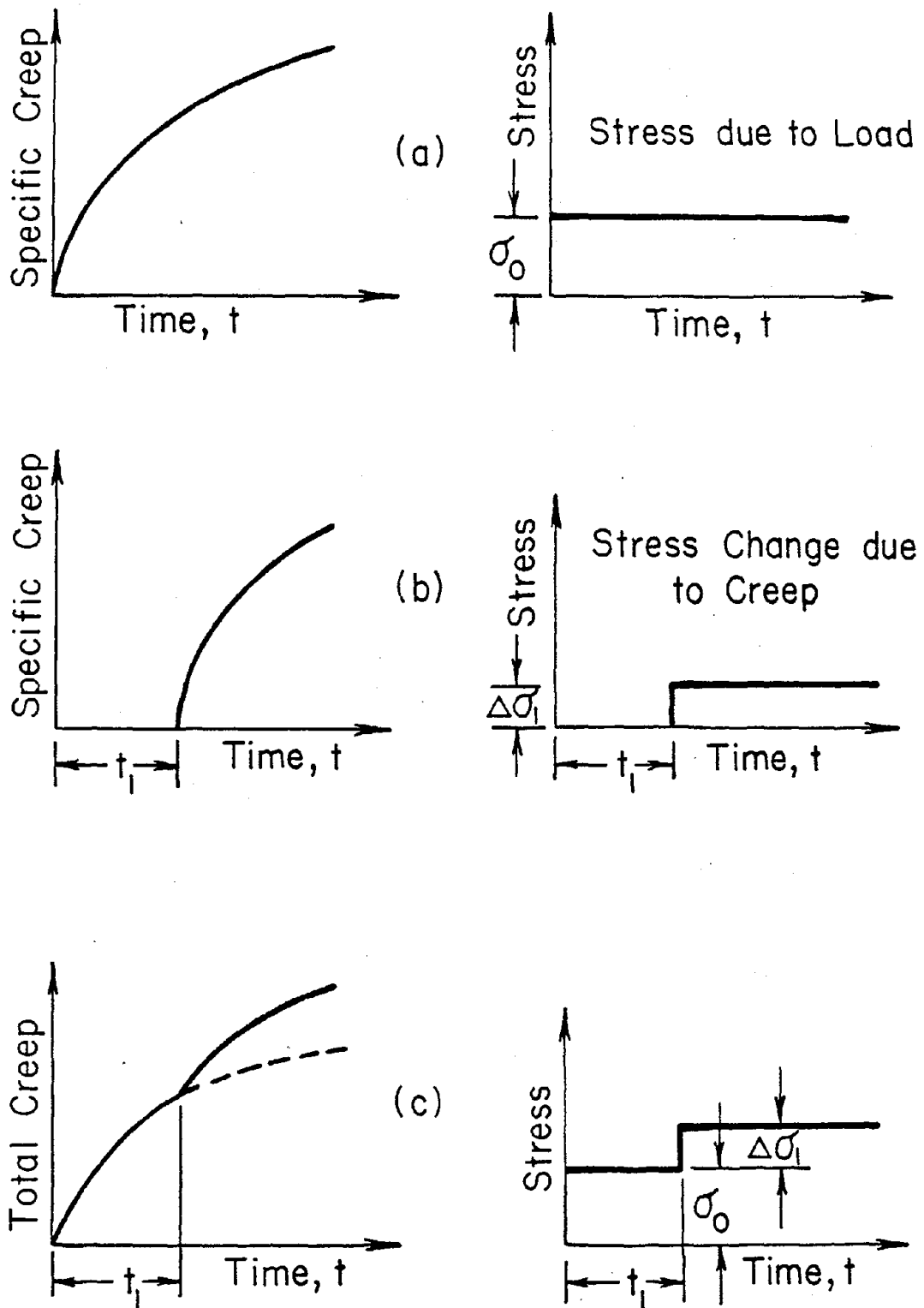
Figure 3.1 Principle of Superposition

equations must be modified. Incremental creep strain expressions for plane strain are developed in the following section.

Creep Laws for Multiaxial Stress

The creep strain components in multiaxial applications are determined from the flow rule, usually associated with a yield locus as in plasticity, using the concept of effective stress and effective strain (36). The effective stress $\bar{\sigma}$ and effective strain $\bar{\varepsilon}$ in terms of corresponding quantities in the three principal directions are defined as (56)

$$\bar{\sigma} = (1/\sqrt{2})(\sqrt{(\sigma_1-\sigma_2)^2 + (\sigma_2-\sigma_3)^2 + (\sigma_3-\sigma_1)^2}), \tag{3.8}$$

and

$$\bar{\varepsilon} = (\sqrt{2}/3)(\sqrt{(\varepsilon_1-\varepsilon_2)^2 + (\varepsilon_2-\varepsilon_3)^2 + (\varepsilon_3-\varepsilon_1)^2}). \tag{3.9}$$

For plane strain, $\varepsilon_3 = 0$, for which Equation 3.9 reduces to

$$\bar{\varepsilon} = (2/3)\sqrt{\varepsilon_1^2 + \varepsilon_2^2 - \varepsilon_1 \varepsilon_2}. \tag{3.10}$$

If $\Delta\varepsilon_x{}^{cr}$, $\Delta\varepsilon_y{}^{cr}$, and $\Delta\gamma_{xy}{}^{cr}$ are defined as the normal and shear incremental creep strain components in the x-y plane and $\Delta\bar{\varepsilon}^{cr}$ is the corresponding incremental equivalent creep strain, then the creep strain increments, $\Delta\varepsilon_{ij}{}^{cr}$, like the plastic strain increments, at any stress level may be given by (56)

$$\Delta\varepsilon_{ij}{}^{cr} = (3/2)(\Delta\bar{\varepsilon}^{cr}/\bar{\sigma})S_{ij} \tag{3.11}$$

in which $\Delta\bar{\varepsilon}^{cr}$ is the incremental equivalent creep strain and s_{ij} is the deviatoric stress tensor. Equation 3.11 is given explicitly for the plane strain condition below.

Using the standard definition of the deviatoric stress tensor s_{ij} (56), its elements can be expressed for plane strain in terms of the cartesian stresses σ_x, σ_y, σ_z, and τ_{xy} as

$$S_{ij} = \begin{bmatrix} (1/3)(2\sigma_x-\sigma_y-\sigma_z) & \tau_{xy} & 0 \\ \tau_{xy} & (1/3)(2\sigma_y-\sigma_x-\sigma_z) & 0 \\ 0 & 0 & (1/3)(2\sigma_z-\sigma_x-\sigma_y) \end{bmatrix} \quad (3.12)$$

The values of s_{xx}, s_{yy} and s_{xy} from Equation 3.12 can be substituted into Equation 3.11 to yield relations between incremental creep strains and existing stresses for the plane strain case as

$$\Delta\varepsilon_x^{cr} = (\Delta\bar{\varepsilon}^{cr}/2\bar{\sigma})(2\sigma_x-\sigma_y-\sigma_z),$$

$$\Delta\varepsilon_y^{cr} = (\Delta\bar{\varepsilon}^{cr}/2\bar{\sigma})(2\sigma_y-\sigma_x-\sigma_z) \text{ and} \quad (3.13)$$

$$\Delta\gamma_{xy}^{cr} = (3/2)(\Delta\bar{\varepsilon}^{cr}/\bar{\sigma})\tau_{xy}.$$

These incremental creep strains are the initial strains from which incremental loads are computed to calculate creep strains in composite masonry walls. $\Delta\bar{\varepsilon}^{cr}$ in the above expressions is obtained from the specific creep vs. time curves (8) which for the materials in a composite wall are shown in Figure 3.2. Details of the method to compute initial strains are given below.

Method of Analysis

Masonry walls subjected to in-plane loads lead to a condition of either plane stress or plane strain. A plane strain 2-dimensional finite element model could be used for the analysis of long composite masonry walls in order to understand the overall elastic behavior of these walls. As the procedure for a 2-dimensional finite element analysis is well known in the literature, no attempts are made here to give the details of such an analysis. Creep analysis using the principle of superposition, on the other hand, is not commonly known and is described in the following paragraphs. For further details of this method, the reader should consult References (6, 35).
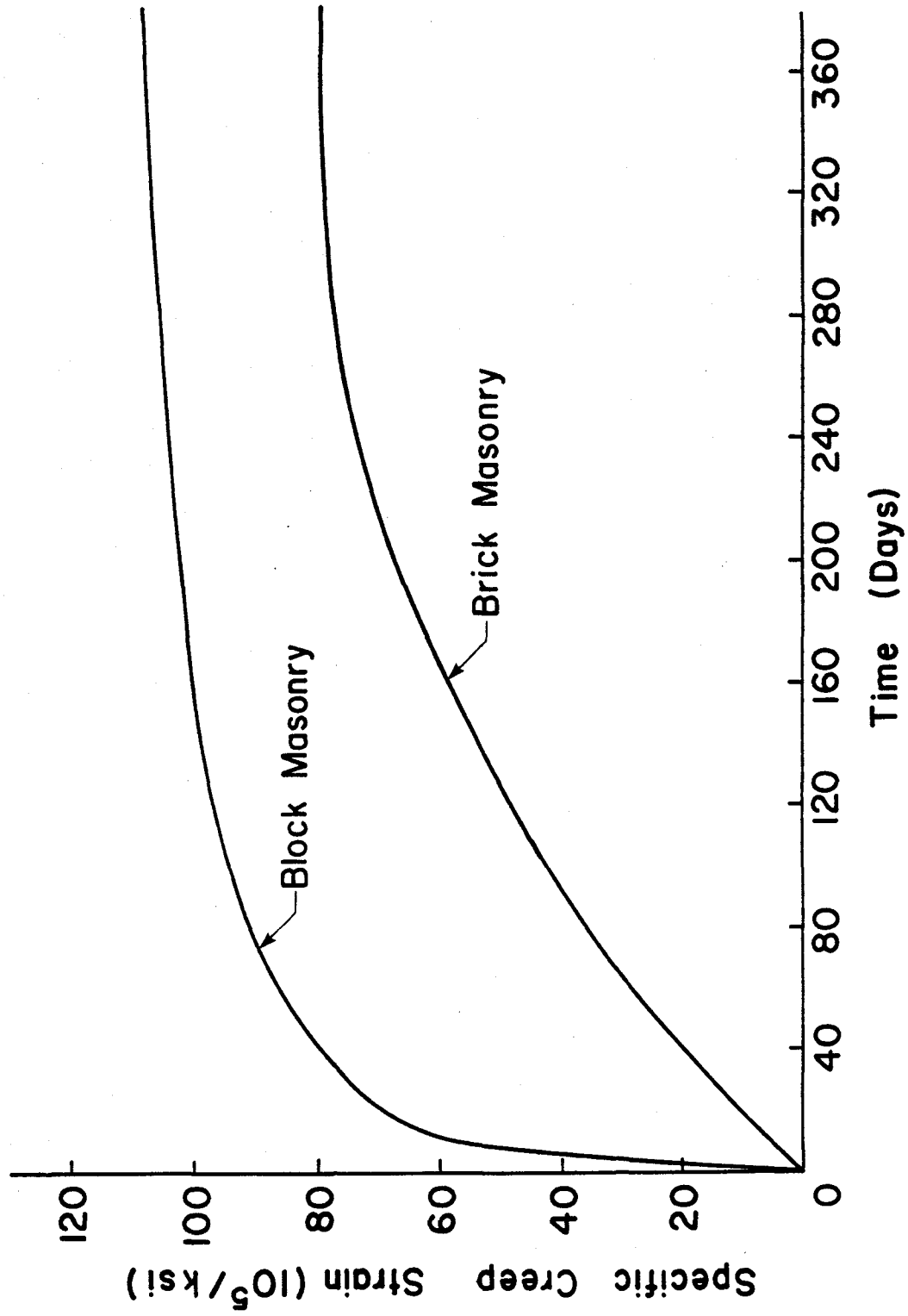
Figure 3.2 Specific Creep vs. Time for Brick and Block Masonry

Creep Analysis for Plane Strain Condition

The necessary steps for the initial strain approach used in conjunction with the principle of superposition are given below.

<u>Step 1.</u> It is assumed that the stresses σ_x, σ_y, σ_z and τ_{xy} due to the applied loads and the corresponding strains are known before the creep analysis is performed. The total time, t, for which the creep analysis is carried out is divided into small intervals, Δt. Specific creep curves shown in Figure 3.2 are assumed to be piecewise linear within these time intervals.

The equivalent stress $\bar{\sigma}_0$ at time $t = 0$ is calculated from the known stresses using Equation 3.8. Hence, the specific creep curve, which predicts creep strains due to this equivalent stress, starts at time $t = 0$ and is shown as curve A in Figure 3.3. Let ΔC_0 be the specific creep strain increment for a time interval Δt_1. The incremental eqivalent creep strain for Δt_1 is given by

$$\Delta \bar{\varepsilon}_0{}^{cr} = \Delta C_0 \ \bar{\sigma}_0 \tag{3.14}$$

where it is assumed that the equivalent stress σ_0 remains constant during this time step. The components of strain increments in different directions are calculated using Equations 3.13 for the plane strain condition. These strains are, therefore, considered as initial strains during the first time interval.

<u>Step 2.</u> Equivalent joint loads are calculated from these initial strains. A method to calculate these equivalent loads is described in Reference (7). Some important features of the method to calculate equivalent joint loads are also given in the next chapter. These loads are then applied on the structure which is solved to yield incremental displacements.
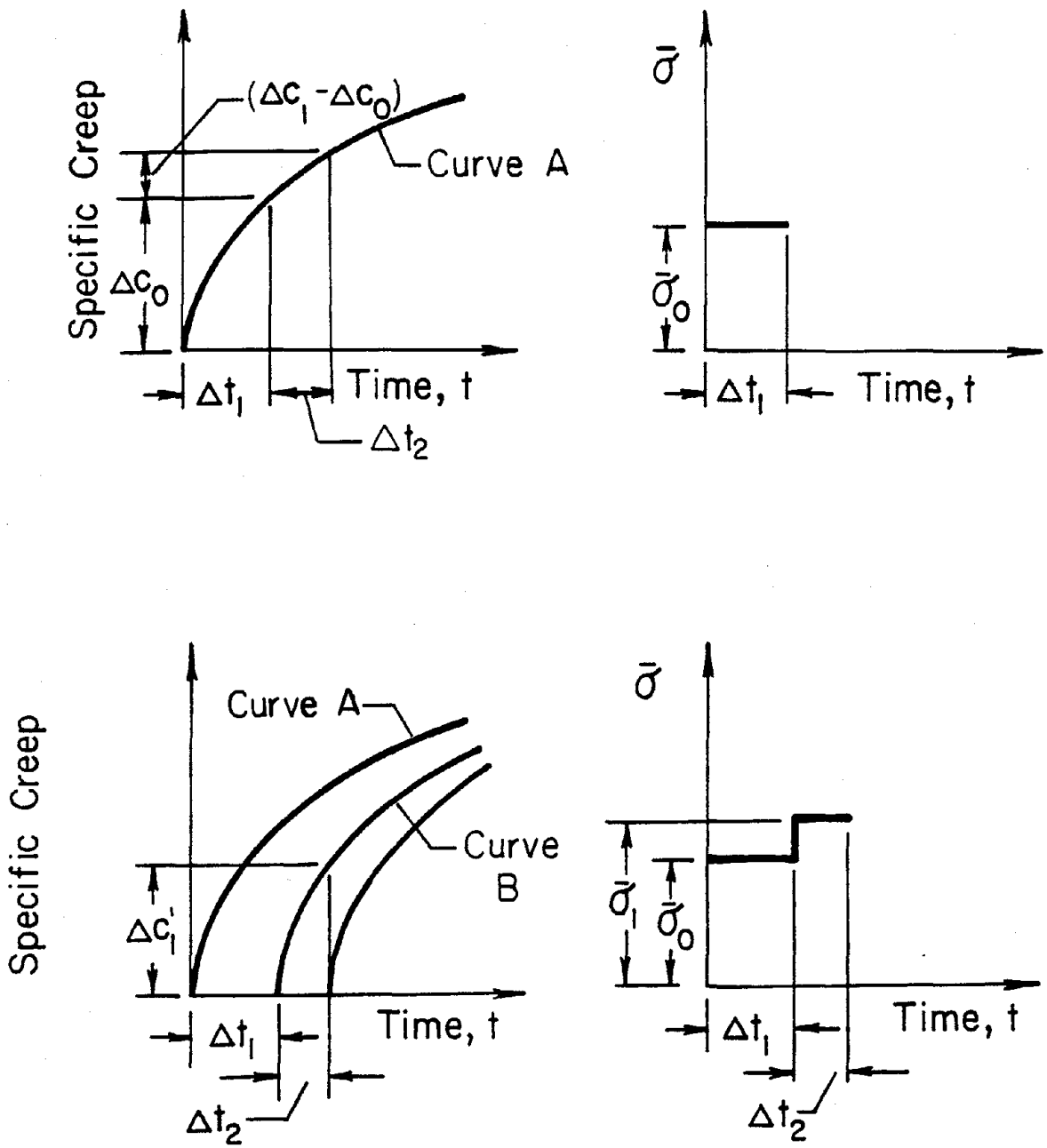
Figure 3.3 Specific Creep Curves at Various Times

Step 3. Incremental strains are calculated using the incremental displacements found in step 2, from which the corresponding initial creep strains are subtracted to yield the stress causing strains which are utilized to calculate the incremental stresses in different directions. These incremental stresses are added to the stresses due to loads to yield new stresses at the end of the time interval Δt_1. These total stresses are used in Equation 3.8 to calcualte a new equivalent stress, $\bar{\sigma}_1$.

Step 4. It is assumed that the incremental stresses calculated in step 3 begin to act in the system at the end of the first time interval Δt_1 and remain acting for an indefinite period of time, thus contributing to creep in the structure. The specific creep curve which predicts creep due to these stress increments starts at time Δt_1 and is shown as curve B in Figure 3.3. Since no mathematical interpretation can be given to an expression for the incremental equivalent stress, in contrast to that for the total equivalent stress given by Equation 3.8, a different approach must be used in the calculation of creep contribution from these incremental stresses.

To compute the initial strains for the second time interval, Δt_2, it is necessary to consider (1) the instantaneous elastic stresses and (2) the incremental stresses from the time interval Δt_1. The incremental equivalent creep strain for the time interval Δt_2 due to the elastic stresses is given by

$$\Delta \bar{\varepsilon}_0{}^{cr} = \bar{\sigma}_0 \ (\Delta C_1 - \Delta C_0), \tag{3.15}$$

in which ΔC_1 is the specific creep strain in Curve A at the end of time $(\Delta t_1 + \Delta t_2)$ as shown in Figure 3.3. The contribution from the incremental stresses, on the other hand, is given by

$$\Delta \bar{\varepsilon}_1{}^{cr} = (\bar{\sigma}_1 - \bar{\sigma}_0) \ (\Delta C_1{}'), \tag{3.16}$$

where $\Delta C_1{}'$ is the specific creep increment for the time interval Δt_2 on Curve B.

Thus, by the principle of superposition, the total incremental equivalent creep strain in the time interval Δt_2 is given by

$$\Delta \bar{\varepsilon}^{cr} = \Delta \bar{\varepsilon}_0{}^{cr} + \Delta \bar{\varepsilon}_1{}^{cr}, \tag{3.17}$$

or

$$\Delta \bar{\varepsilon}^{cr} = \bar{\sigma}_0(\Delta C_1 - \Delta C_0) + (\bar{\sigma}_1 - \bar{\sigma}_0)(\Delta C_1{}'). \tag{3.18}$$

Equations 3.13 are used once again to calculate individual components of the incremental initial strains for the time interval Δt_2 in which stress levels at the end of the first time interval Δt_1 are utilized. Steps 2 and 3 are then repeated to yield the incremental as well as total values of displacements, strains and stresses. It should be noted, however, that the incremental values are algebraically added to those existing at the end of the previous time interval.

Step 5. The procedure described in step 4 for calculation of the equivalent creep strain can be generalized as follows: For the nth time interval, there are (n-1) stress increments that contribute to the total incremental equivalent creep strain. Hence, Equation 3.17 generalizes to

$$\Delta \bar{\varepsilon}^{cr} = \Delta \bar{\varepsilon}_0{}^{cr} + \sum_{i=1}^{n-1} \Delta \bar{\varepsilon}_i{}^{cr} \tag{3.19}$$

or

$$\Delta \bar{\varepsilon}^{cr} = \bar{\sigma}_0[\Delta C_n - \Delta C_{(n-1)}]$$
$$+ \sum_{i=1}^{n-1} [\bar{\sigma}_i + \bar{\sigma}_{(i-1)}][\Delta C'_{(n-i+1)} - \Delta C'_{(n-i)}] \tag{3.20}$$

The steps described above to compute creep strain increments, and the corresponding changes in stresses due to sustained loads, are carried out as long as the incremental creep strains during a time interval are significant. It should be emphasized that this procedure does not take into

account any unloading due to the external loads. A computer program is developed to incorporate the above described methodology and is utilized to compute creep strains in composite masonry walls; some results of these analyses are given in the following section.

Example Problems

Creep Analysis of a Single Wythe Wall

In order to verify the validity of the proposed creep model and the correctness of the computer coding of the solution procedure, a single wythe brick wall is analyzed. This is a long wall and its height is 8 ft. The cross section of the wall is analyzed considering it to be under the condition of plane strain. Vertical rollers are provided at the two sides of the cross section as shown in Figure 3.4. The vertical rollers inhibit the strain in the horizontal direction and thus make the elasticity and creep equations simple to work out by hand calculations. The material properties of brick masonry are calculated on the basis of their strengths measured in the laboratory and formulas given in Reference (108). The elastic modulus and Poisson's ratio of brick masonry are computed as 2000 ksi and 0.25, respectively.

The wall is subjected to a uniformly distributed vertical load of 0.03125 k/in over its entire width. It is shown by Anand and Yalamanchili (17) that the failure in composite masonry initiates at the above mentioned magnitude of the load intensity. As the dimensions of the wall and the intensity of load are known, the elastic stress as well as the incremental stresses due to creep in the wall can be calculated from basic principles. These calculations are presented in Appendix A. A comparison of the analytical results with those obtained by the computer program are also given. For the computer solution, the problem is modelled by linear
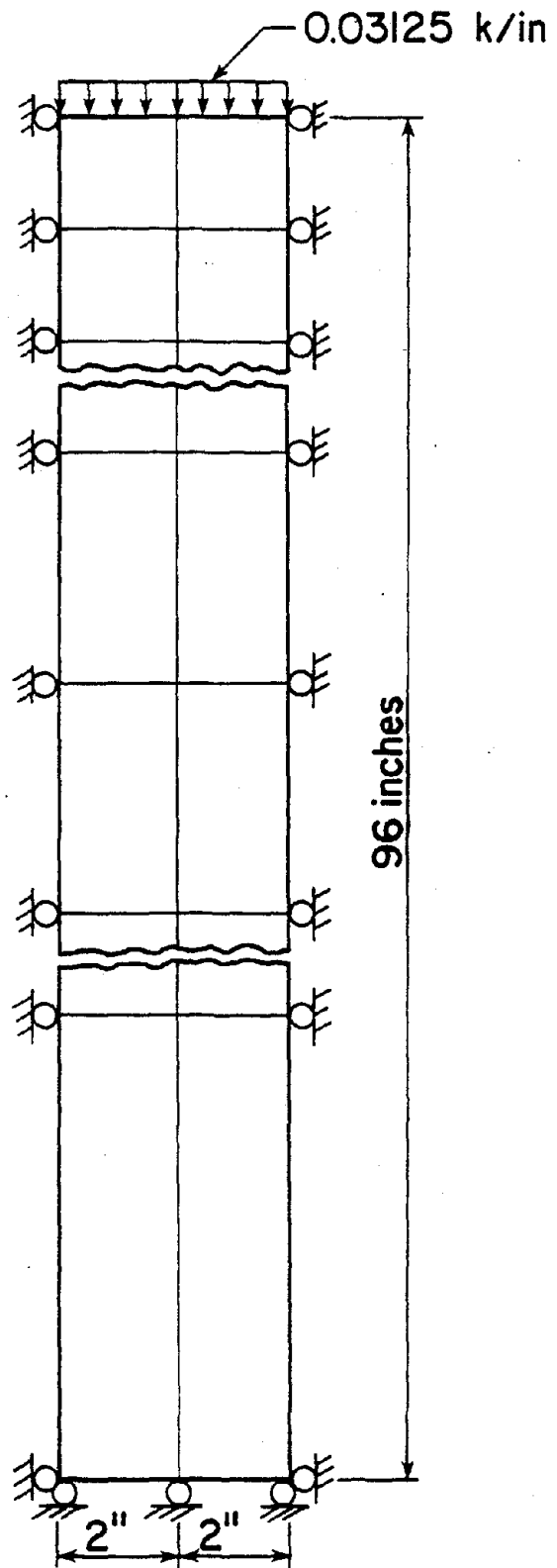
Figure 3.4   Single Wythe Brick Wall

quadrilateral elements. It is shown that the results obtained by using the computer program are in good agreement with those obtained from the analytical solution.

Creep Analysis of a Composite Wall

A composite wall shown in Figure 3.5 is analyzed. The wall is 10 ft. high and its cross section consists of an 8 in. concrete block wythe connected to a 4 in brick wythe through a 2 in. thick grouted collar joint. It is assumed that the external loads due to dead weight of the slab and the live loads act only on the concrete block wythe at the top of the wall. It is further assumed that the diaphragm action of the floor slab provides a lateral support at the top of the wall.

The creep behavior of the individual wythes has been taken from the available literature and is shown in Figure 3.2. In addition, the creep behavior of the grouted collar joint is assumed to follow that of the concrete block wythe. Numerical values corresponding to creep curves in Figure 3.2 are provided as data at every 10 day interval in the computer program. As the wall is very long, it is in a state of plane strain and thus only a unit length of the cross section need be analyzed.

It is known from working with the previous models (6-8) that most of the load transfer from the loaded wythe to the unloaded wythe occurs near the top of the wall. Consequently, a relatively fine finite element mesh is provided near the top of the wall as shown in Figure 3.5. The total number of quadrilateral elements and nodal points used in the analysis are 350 and 390, respectively. The block wythe is subjected to a load of 20 kips per foot. That leads to a uniform pressure of 0.21 ksi which is 20% of the concrete block wythe strength measured in the laboratory. The material properties for various constituents of the composite

p = 0.21 ksi

120"

Number of Elements = 350

Number of Nodes = 390

Band Width = 34
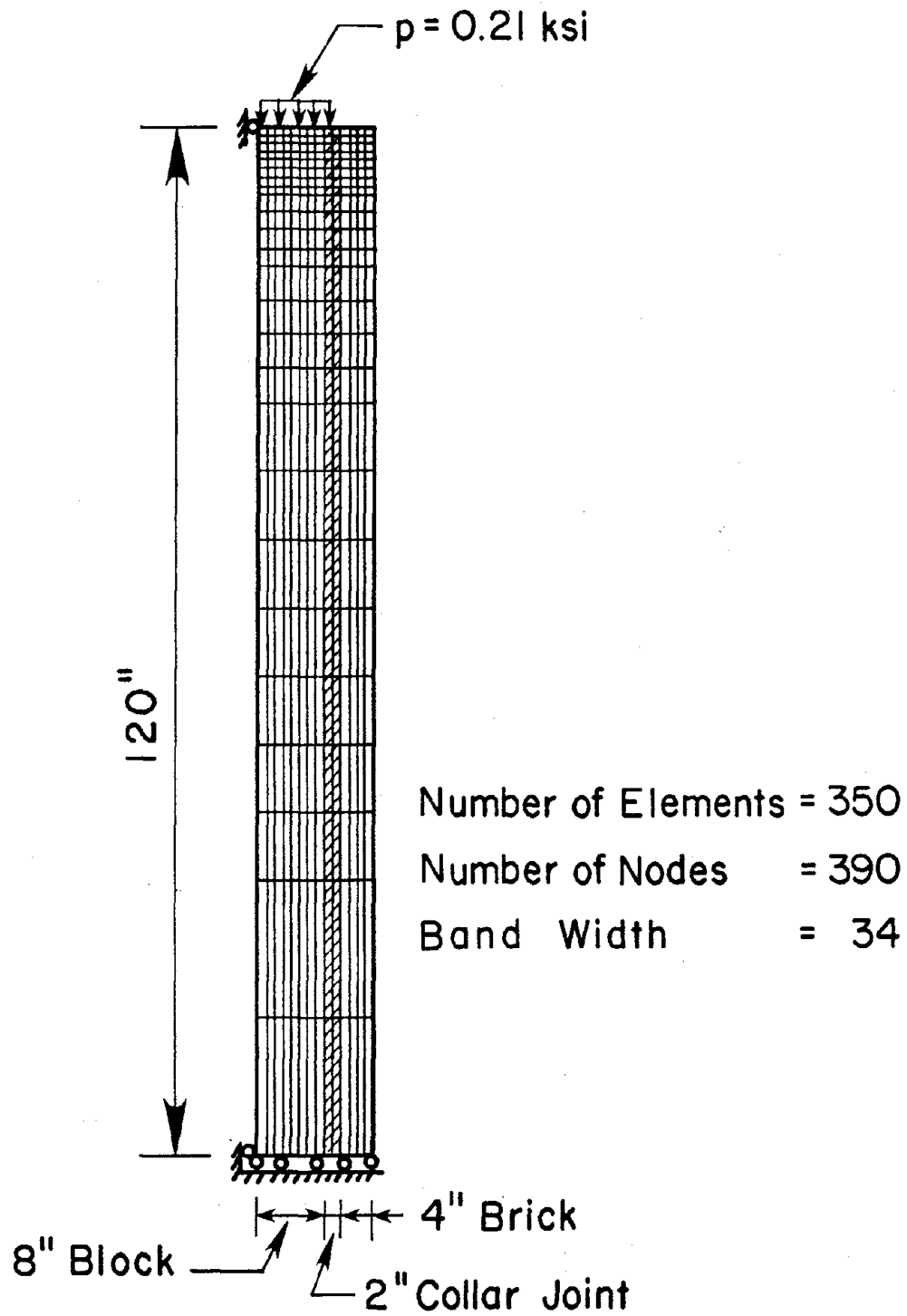
8" Block

2" Collar Joint

4" Brick

Figure 3.5   Finite Element Mesh of Composite Masonry Wall

wall are computed based on their laboratory compressive strengths as prescribed in References (105, 108) and given in Table 3.1.

Table 3.1. Material Properties

Material	Elastic Modulus, E (ksi)	Poisson's Ratio
Concrete Block	1,040	0.25
Brick	2,000	0.25
Grout	1,600	0.20

Before the creep analysis is carried out, it is desirable to check whether the conditions for which the principle of superposition is applicable are satisfied (24): (1) As required, both the brick and the block masonry are assumed to be linearly viscoelastic within the range of the applied loads (8); (2) The maximum load permitted by the Brick Institute of America on a brick wall is equal to 20% of the brick masonry strength (108) which is within the 40% strength limit necessary for application of the principle of superposition and (3) As no unloading is considered, strains always increase with the time as required. As all three of these conditions are satisfied in this example, the applicability of the previously outlined superposition procedure is valid.

Results and Discussion

The wall is initially analyzed for the instantaneously applied loads, after which the effect of creep in the wall due to sustained loads is examined for up to 300 days at which time most of the creep should have

occured, as is obvious from Figure 3.2. Starting from zero days, this total time is discretized into 10 intervals of five days each, seven intervals of 10 days each, and nine interval of 20 days each to yield a total of 26 time steps to obtain the complete solution. Some typical results for various regions of the composite wall are plotted in Figures 3.6 through 3.11, in which the results for an elastic analysis are labeled as zero days, whereas those for the creep analysis are indicated by the respective number of days after the load application.

Figure 3.6 shows the shear strain in the collar joint at various times. It is evident that due to the load transfer from the loaded block wythe to the unloaded brick wythe near the very top of the wall, the maximum shear strain occurs in the top 6 inches of the wall. The magnitude of this maximum shear strain is approximately five times greater than the average shear strain in the collar joint. As the materials creep with time, the shear strain in the collar joint also increases, and its magnitude at 300 days is approximately twice as much as at the time of load application. The rate of strain increase is large in the beginning and slows down appreciably with time. However, the shape of the shear strain diagram remains essentially the same. As far as the shear stress variations are concerned, Figure 3.7 shows no substantial changes due to creep. The slight increase in stress during the early period of creep and eventual decrease during the later time period is due to different creep behavior of the concrete block and brick wythes, as shown in Figure 3.2.

Normal vertical strains in the collar joint at various heights are shown in Figure 3.8. As the load from the loaded block wythe transfers to the unloaded brick wythe in the top six inches of the collar joint,
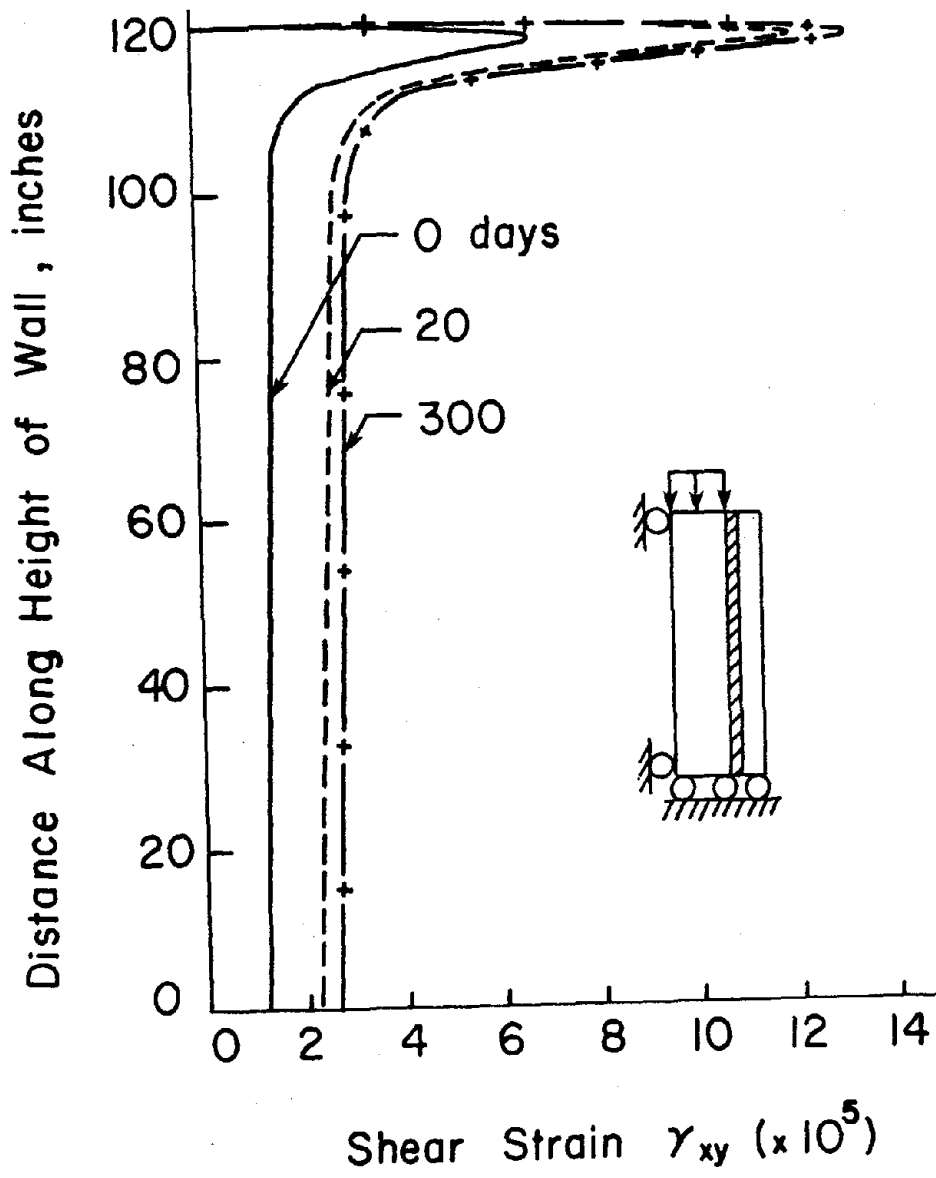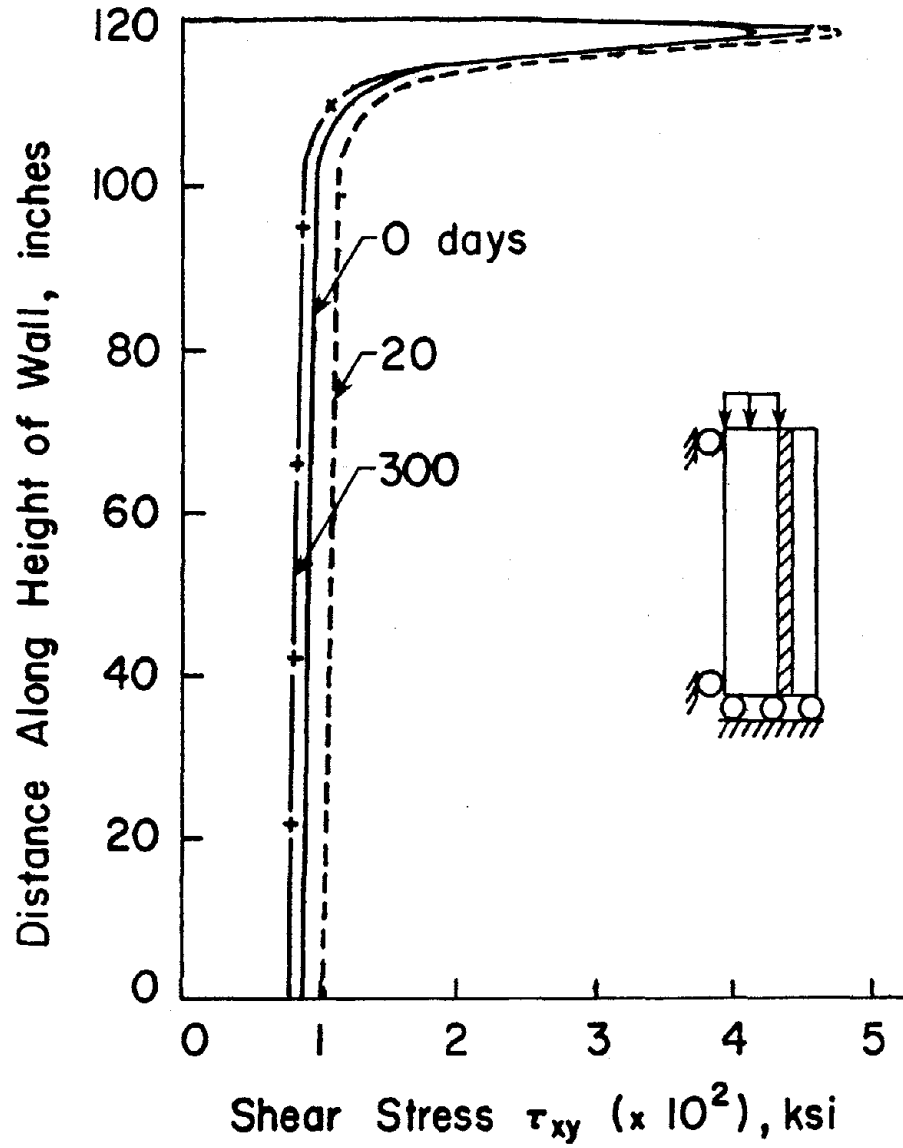
Figure 3.6   Shear Strains in the Collar Joint

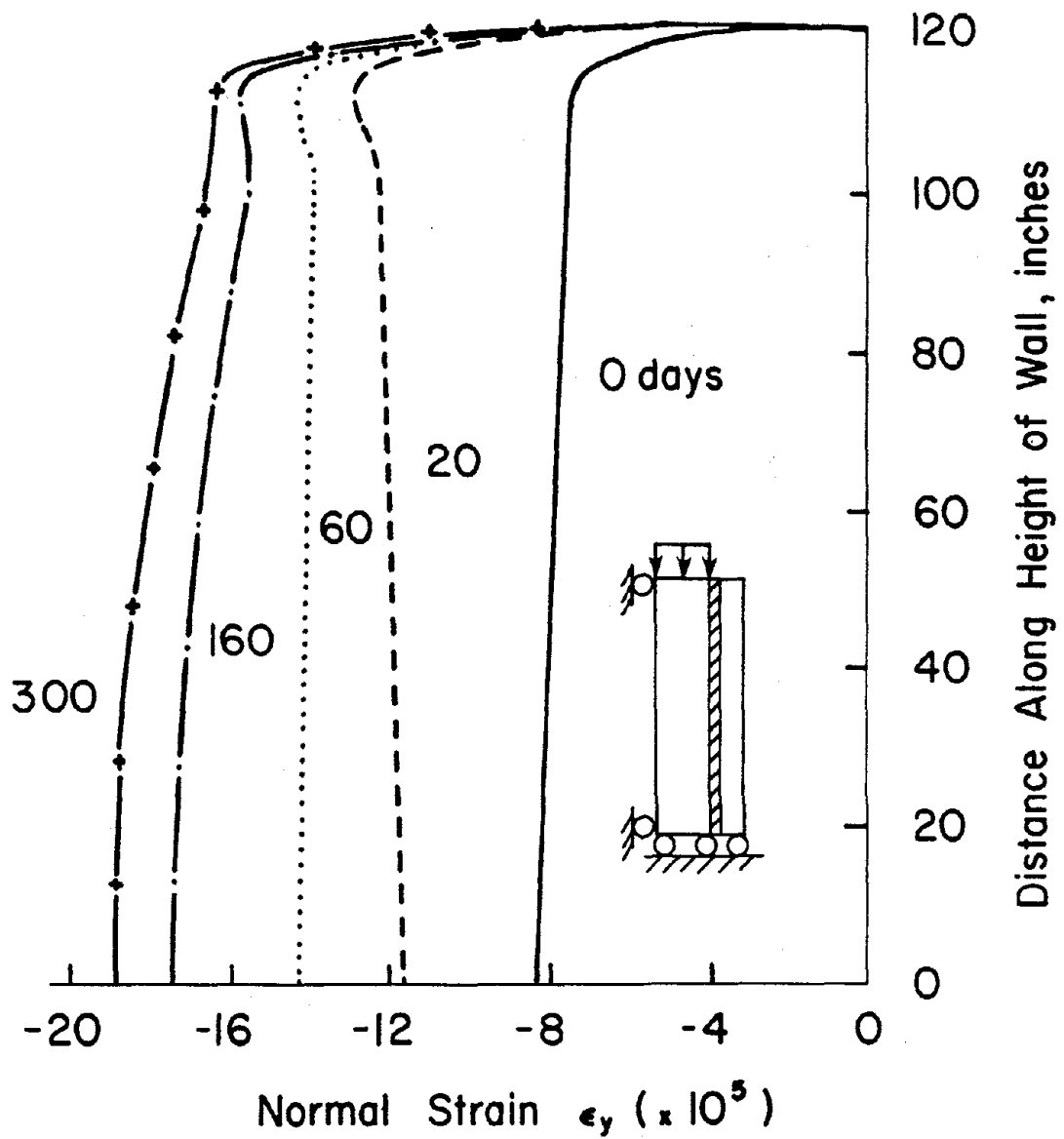Figure 3.7   Shear Stresses in the Collar Joint

Figure 3.8   Normal Vertical Strains in the Collar Joint

the normal strains in the collar joint remain essentially constant below six inches from top of the wall. With time, these normal strains increase due to creep and become approximately twice their elastic values. The normal stresses in the collar joint, as shown in Figure 3.9, on the other hand, are similar to the normal strains only at the time of instanteneous load application. Due to different creep displacements at different times in the wythes at various heights, the normal stresses in the collar joint decrease by approximately 30% during the first 20 days; however, most of this stress decrease is regained during the next 280 days. The final normal stresses are slightly smaller than those at time t = 0, indicating that there is stress relief in the collar joint due to creep. This is also substantiated in Figure 3.7 where shear stress in the collar joint at 300 days is smaller than that at zero days.

Another phenomenon of interest to investigate is the out-of-plane bending deflections of the wall due to eccentrically applied slab loads on the block wythe and their influence on the vertical normal strains at different heights of the wall. The wall is assumed to be laterally supported at the top and bottom. The horizontal out-of-plane defections of the collar joint are shown in Figure 3.10. The maximum value of this deflection at zero days, which occurs at approximately 2/3rd the height from the bottom of the wall, is less than 1/100th of an inch. The deflection increases with time due to creep and value nearly doubles after 300 days. It is evident from this figure that most of the creep deflections occur during the first 20 days.

The vertical normal strains across the width of the wall at various heights are shown in Figure 3.11. Obviously, the normal strains directly below the load are larger than those below the unloaded portion near the
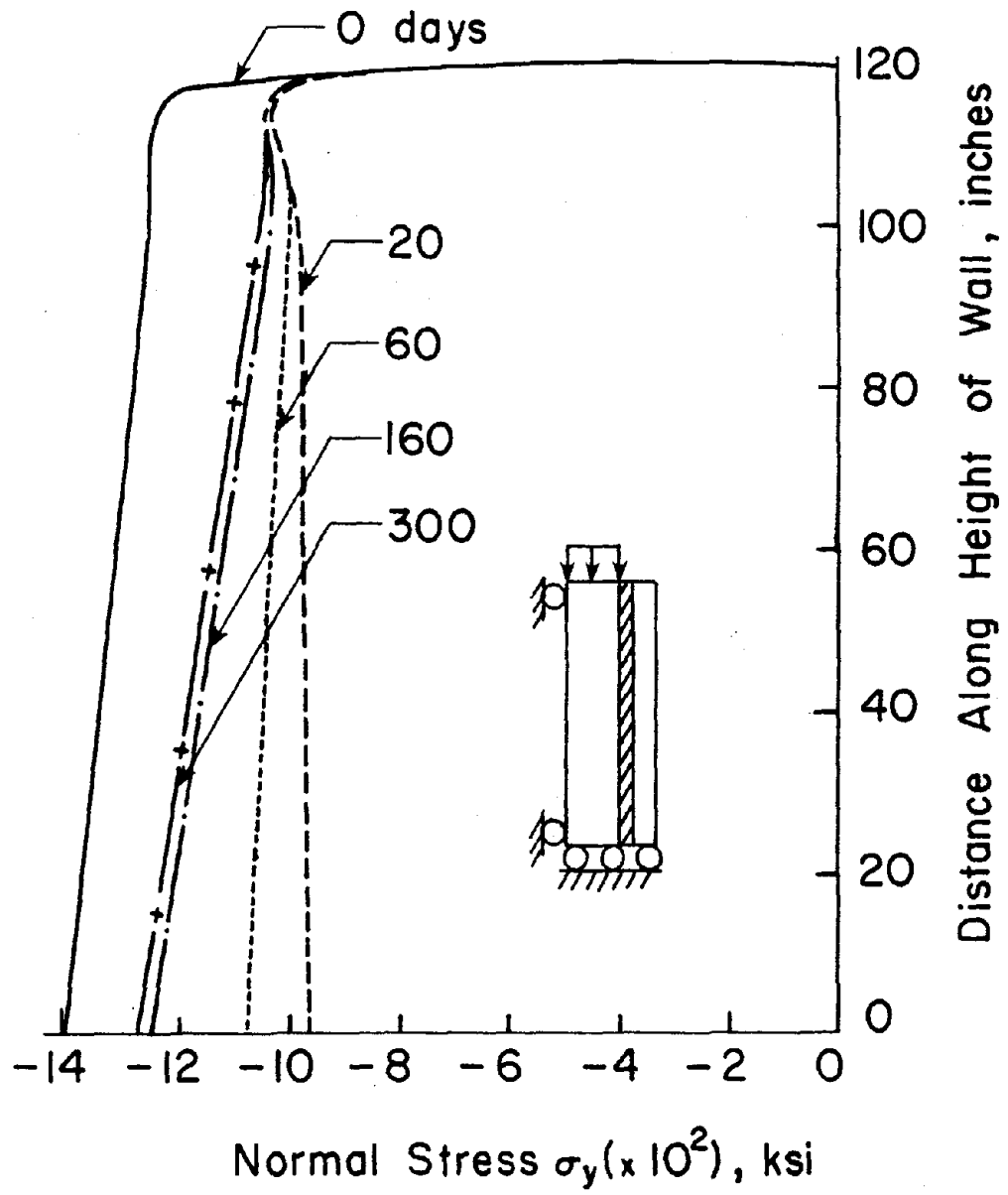
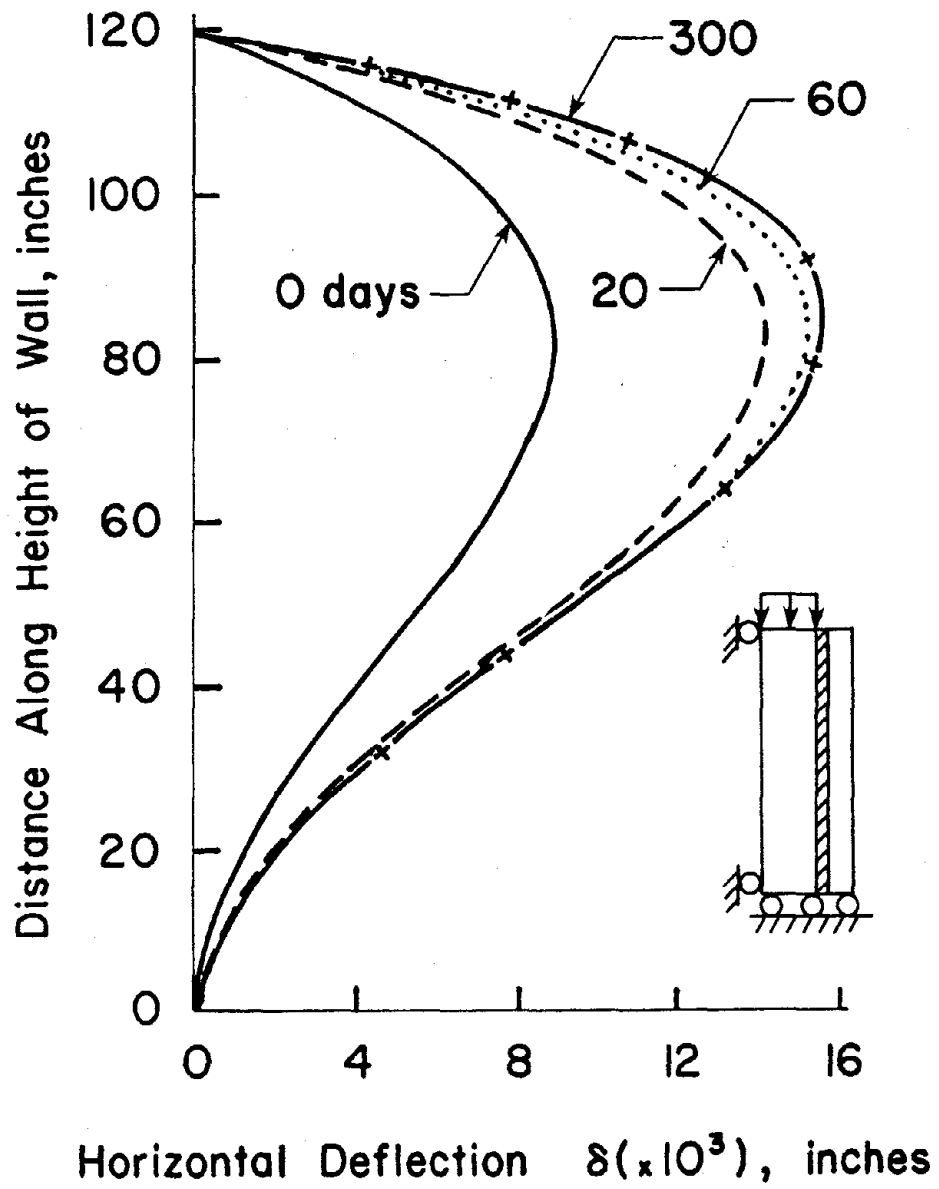Figure 3.9 Normal Vertical Stresses in the Collar Joint

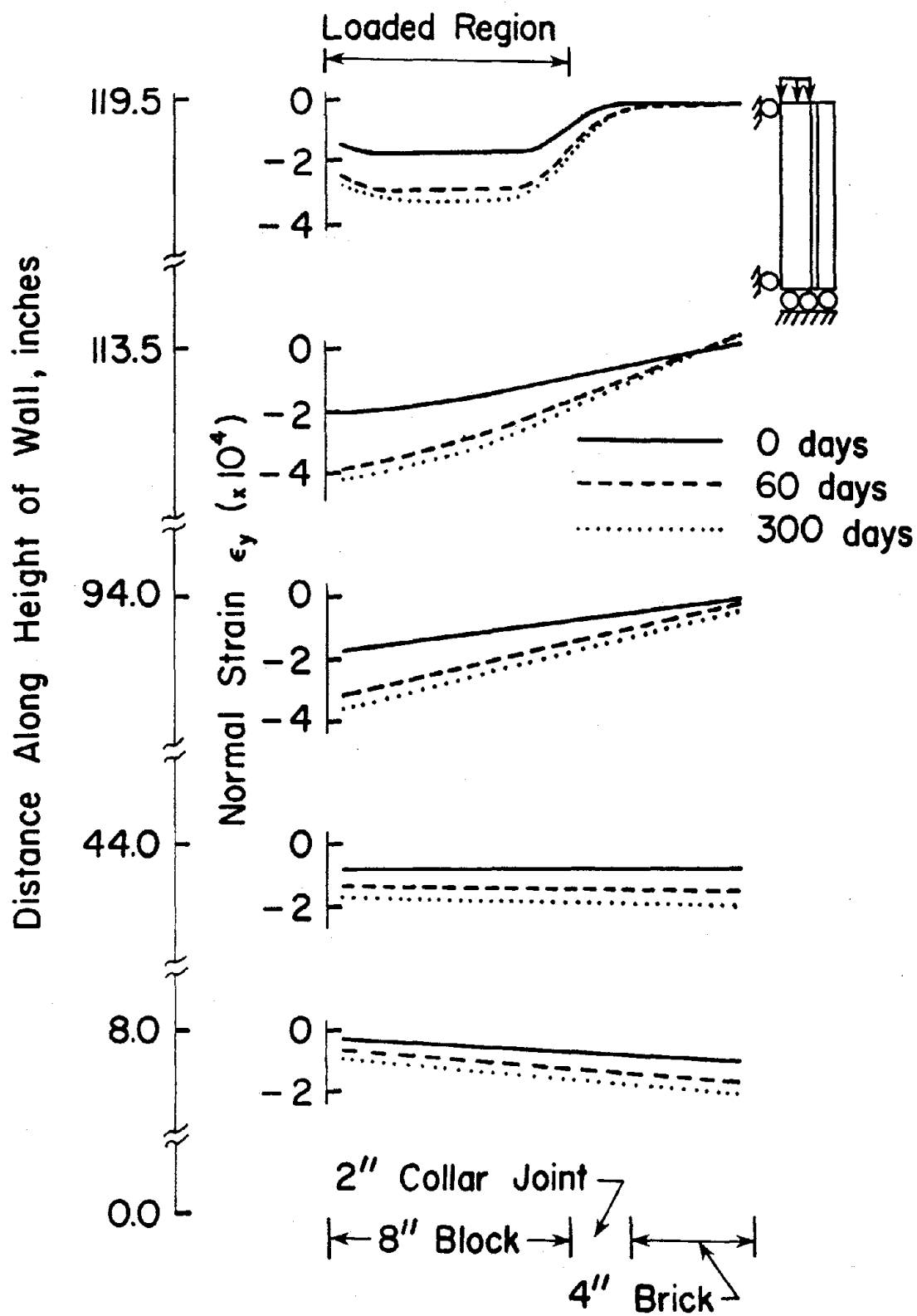Figure 3.10 Out-of-Plane Deflection of the Wall

Figure 3.11 Normal Vertical Strains in the Width of the Wall
at Different Elevations

top of the wall. As the load gradually transfers out to the unloaded

brick wythe, the normal strains in both the wythes should become equal

leading to uniform vertical movement of the whole width of the wall with

no further load transfer through the collar joint. This phenomenon has

previously been observed in walls which have been assumed to be contin-

uously supported laterally along their whole height (7). However, due

to the out-of-plane wall deflection shown in Figure 3.10, and its asso-

ciated curvature and bending stresses, the compressive normal strains

reduce in the brick wythe for the top 1/3rd height of the wall, and they

increase near the bottom of the wall. Once again, the final strains after

300 days are approximately twice their values at the time of the load

application.

It may also be of interest for the reader to find out the amount of

computational effort that was needed to perform this creep analysis.

Computations were carried out on a VAX-11/780 and a total of 26 time steps

were needed to complete the creep analysis up to 300 days. CPU time re-

quired per time step for the above problem with 390 nodes was 57.2 sec-

onds.

Conclusions

From the example problem presented, it is clear that the proposed

technique for creep analysis can be implemented successfully to estimate

creep strains (and the corresponding stress changes) in masonry walls

using the principle of superposition. The results of the elastic and creep

analysis of a long composite wall under a condition of plane strain lead

to the following conclusions:

1. All strains do increase substantially due to creep during the
   first 300 days, most of these during the first month after the
   load application.

2. The shear stresses in the collar joint remain almost constant with the elapse of time. Normal stresses in the collar joint reduce between 10% and 30% at various times.

3. The out-of-plane deflections, though rather small, double due to creep within 300 days. These deflections tend to produce different strain distributions along the height of the wall.

4. The results presented here are based on the specific creep curves shown in Figure 3.2. Similar curves for other materials must be available if the technique presented in this chapter is to be used for walls of those materials.

CHAPTER IV

ESTIMATION OF TEMPERATURE STRESSES IN

COMPOSITE MASONRY WALLS

It is reported in the literature (46, 63, 85), that strains and stresses in masonry due to temperature variations may not be *insignificant* in magnitude compared to those due to the external loads. In composite masonry walls, in particular, the effects of temperature variations may even be more important, especially on the shearing stresses in the collar joint. It is therefore, important that the effects of temperature strains be included in the analysis and design of composite masonry walls. In this research, a two-dimensional finite element model based on a plane strain condition is utilized to study the above mentioned effects. The initial strain approach is utilized to estimate stresses in the collar joint of composite walls due to differential temperatures on the inside and outside wythe faces in a wall. Computational techniques are presented in detail to investigate the effects of temperature on composite masonry walls under a state of plane strain. The theory and development necessary to determine equivalent nodal loads for thermal strains are also given. Analyses are then carried out for typical examples to show the significance of temperature strains on the stress distribution.

Temperature Strains

Many studies have been carried out to measure the thermal expansion in brick and block masonry due to the increase in temperature. A detailed review of this literature can be found in Reference (45).

The thermal strains in this study have been considered as time independent, thus yielding their maximum value based upon the assumed temperature variations in the wall. As the strains due to temperature are independent of the stresses caused by the externally applied loads, these could be considered as initial strains in the time independent stress analysis (104). For example, initial strains $\{\varepsilon_i\}$ in an isotropic material with a coefficient of thermal expansion α, due to an increase in temperature Δt may be defined as

$$\{\varepsilon_i\} = \lfloor\varepsilon_{xi}, \ \varepsilon_{yi}, \ \varepsilon_{zi}, \ \gamma_{xyi}, \ \gamma_{yzi}, \ \gamma_{zxi}\rfloor^T \tag{4.1}$$

and given by

$$\{\varepsilon_i\} = \lfloor\alpha\Delta t, \ \alpha\Delta t, \ \alpha\Delta t, \ 0, \ 0, \ 0\rfloor^T. \tag{4.2}$$

Elastic Analysis due to External Loads

In a composite masonry wall, the external loads are transmitted from a floor directly to the inner concrete block wythe. Part of these loads get transferred to the outer brick wythe through the collar joint, thus, causing shearing stresses in it.

Determination of stresses and displacements in a composite masonry wall under the plane strain condition due to in-plane loads can be easily accomplished by using the cross sectional model of the wall together with a standard plane strain finite element analysis. A detailed development of the in-plane stiffness matrix and a step by step procedure to obtain the displacements, strains and stresses may be found in standard finite element texts (101).

Analysis for Thermal Strains

Initial strains in a given structural system generally cause additional deformations and stress redistribution. In a finite element

analysis, their effect can be incorporated (1) by determining the additional equivalent loads that must be applied to the structural system and (2) by computing the additional stresses in the system from the stress producing strains (which are the strains due to the equivalent loads minus the initial strains). These additional stresses and strains are added to those due to the external loads to yield the corresponding total values due to the external loads and thermal strains. Before describing the finite element analysis procedure for temperature in detail it is desirable to present a method for computing the joint loads in an element due to initial strains.

Joint Loads in an Element due to Thermal Strains

Total strains $\{\varepsilon\}$ in a structure are equal to the sum of the strains due to the external loads and initial strains and are given as

$$\{\varepsilon\} = [C]\{\sigma\} + \{\varepsilon_i\} \qquad (4.3)$$

in which

$$\{\varepsilon\} = [\varepsilon_x, \ \varepsilon_y, \ \varepsilon_z, \ \gamma_{xy}, \ \gamma_{yz}, \ \gamma_{zx}]^T \text{ and} \qquad (4.4)$$

$$\{\sigma\} = [\sigma_x, \ \sigma_y, \ \sigma_z, \ \tau_{xy}, \ \tau_{yz}, \ \tau_{zx}]^T. \qquad (4.5)$$

$\{\varepsilon_i\}$ is defined in Equation 4.1 and $[C]$ is a matrix of elastic coefficient. Equation 4.3 can be inverted to get an expression for the stresses $\{\sigma\}$ as

$$\{\sigma\} = [D](\{\varepsilon\} - \{\varepsilon_i\}). \qquad (4.6)$$

As prescribed in the previous section, the cross-section of the wall is assumed to be in a state of plane strain, for which $\tau_{xz} = \tau_{yz} = 0$ and $\varepsilon_3 = \varepsilon_z = 0$. Thus, the stresses may again be given by Equation 4.6 in which the individual matrices can be defined as

$$\{\sigma\} = [\sigma_x, \ \sigma_y, \ \tau_{xy}]^T, \qquad (4.7)$$

$$\{\varepsilon\} = [\varepsilon_x, \ \varepsilon_y, \ \gamma_{xy}]^T, \qquad (4.8)$$

$$\{\varepsilon_i\} = [\varepsilon_{xi}, \ \varepsilon_{yi}, \ \gamma_{xyi}]^T \qquad (4.9)$$

and

$$[D] = \frac{E}{(1+v)(1-2v)} \begin{bmatrix} (1-v) & v & 0 \\ v & (1-v) & 0 \\ 0 & 0 & \dfrac{1-2v}{2} \end{bmatrix} . \qquad (4.10)$$

To compute equivalent joint loads for the initial strains, let $\{p\}$ be an 8x1 load vector which defines forces at the nodes of a linear quadrilateral element in equilibrium, that produces stresses $\{\sigma\}$ in the element. If the element is subjected to a set of virtual nodal displacements $\{u^*\}$ that produce virtual element strains $\{\varepsilon^*\}$, the principle of virtual work, then yields

$$\{u^*\}^T\{p\} = \int\{\varepsilon^*\}^T\{\sigma\} \ dV. \qquad (4.11)$$

The virtual strains may be expresses in terms of the virtual nodal displacements by

$$\{\varepsilon^*\} = [B] \ \{u^*\} \qquad (4.12)$$

where $[B]$ is the strain-displacement transformation matrix. Substituting Equation 4.12 into Equation 4.11, eliminating $\{u^*\}^T$ and utilizing Equation 4.6 yields

$$\{p\} = \int[B]^T([D]\{\varepsilon\}-[D]\{\varepsilon_i\}) \ dV \qquad (4.13)$$

or

$$\{p\} + \int[B]^T[D]\{\varepsilon_i\} \ dV = \int[B]^T[D]\{\varepsilon\} \ dV. \qquad (4.14)$$

The second term on the left hand side of Equation 4.14 yields the equivalent joint load vector $\{p_i\}$ for the initial strains and may be defined as

$$\{p_i\} = \int[B]^T[D]\{\varepsilon_i\} \ dV. \qquad (4.15)$$

As the wall is assumed to be in a state of plane strain, $\{\varepsilon_i\}$ in Equation 4.15 for the thermal strains can be expressed as

$$\{\varepsilon_i\} = (1 + \nu)[\alpha\Delta t, \ \alpha\Delta t, \ 0]^T. \qquad (4.16)$$

Thermal Analysis

As mentioned in an earlier section, thermal strains are considered time independent in this study. Their influence on displacements, strains, and stresses is easily obtained by considering these strains as initial strains, for which an elastic analysis for the equivalent joint loads due to thermal strains is performed. It should again be noted that the additional stresses due to these strains are calculated by using Equation 4.6.

To obtain the initial strains in an element, the temperature at the centroid of the element must be known. The temperatures at the inner face of the block wythe and the outer face of the brick wythe of a wall may be taken as the room temperature and atmospheric temperature, respectively. To find the temperature at any point within the wall, one needs a temperature profile across the cross section through the three different materials, namely, concrete block, grout and clay brick. The literature gives very little information about the above mentioned temperature profile. It has been reported by Glanville and Kobak (39), however, that the temperature profile from the exterior to the interior of a wall can be assumed to be a step function. A heat transfer analysis and subsequent structural analysis indicates that this assumption does not introduce serious error (39). On the basis of heat flow analysis under steady state conditions for intersecting walls, Rahman and Suter (77) used a parabolic temperature profile across the masonry wall intersection. Based upon the above mentioned information, a parabolic temperature profile, as shown

in Figure 4.1 has been assumed across the thickness of the wall in this study. This temperature profile may be expressed as

$$T(x) = (x/w-1)^2(T_1-T_2) + T_2 \qquad (4.17)$$

where $|T_1| > |T_2|$, w is the wall thickness and x is the distance from the wall interior where temperature = T_1. Similarly, if $|T_2| > |T_1|$, the parabolic temperature profile may be given by

$$T(x) = (x/w)^2(T_2-T_1) + T_1. \qquad (4.18)$$

Using the above temperature profiles, the temperatures at the centroids of various elements across the wall thickness can be obtained for different combinations of interior and exterior temperatures. The temperature changes, which are responsible for causing initial strains in the elements, are calculated by subtracting ambient, stress free temperatures at the centroids. These temperature changes are multiplied by the coefficient of thermal expansion to yield the initial strains in each element from which equivalent joint loads can be calculated using Equation 4.15. The thermal strain analysis can be carried out using these joint loads as described in Chapter III for the creep strains.

Example Problems

Analysis of a Single Element Problem

A 2 in x 2 in continuum is modelled by one linear quadrilateral element. This single element problem is analyzed for thermal gradient to verify the validity of the proposed model and the correctness of the computer coding. A plane strain condition is assumed in this analysis. Applied boundary conditions do not allow the specimen to deform in the horizontal direction. This is shown in Figure 4.2. The applied boundary conditions make the problem simple and the solution can also be obtained by hand calculations. The elastic modulus and the Poison's ratio of the

$$T(x) = \left(\frac{x}{W} - 1\right)^2 \Delta T + T2$$

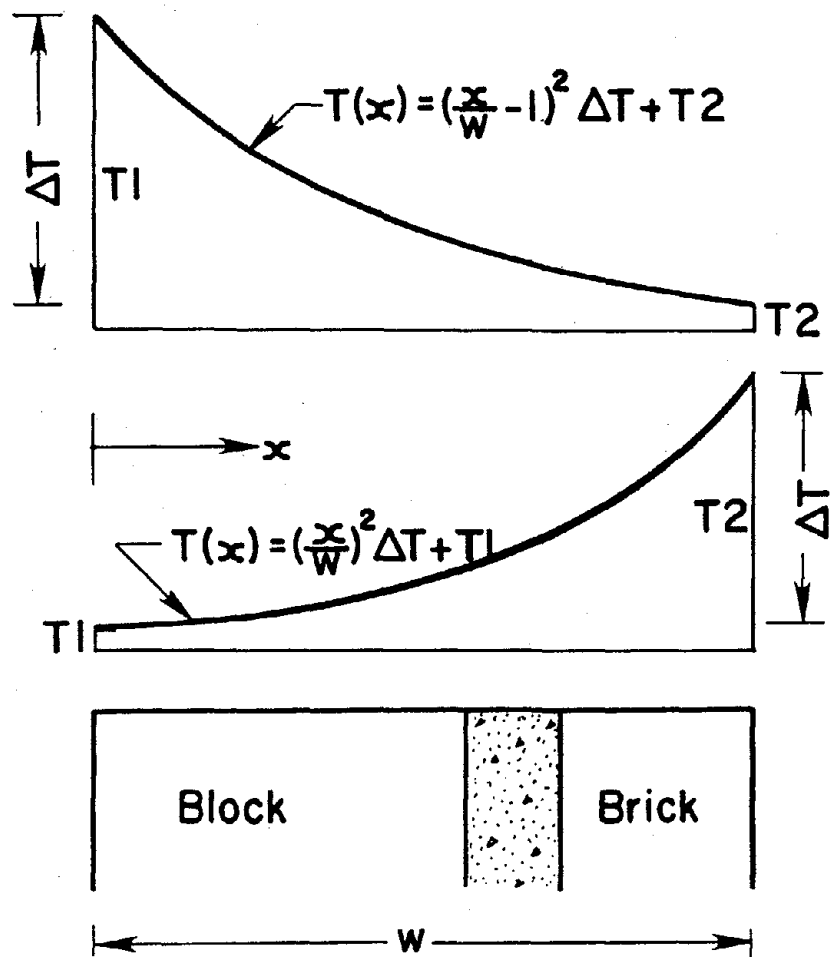$$T(x) = \left(\frac{x}{W}\right)^2 \Delta T + T1$$

Figure 4.1 Temperature Profile across the Wall Thickness
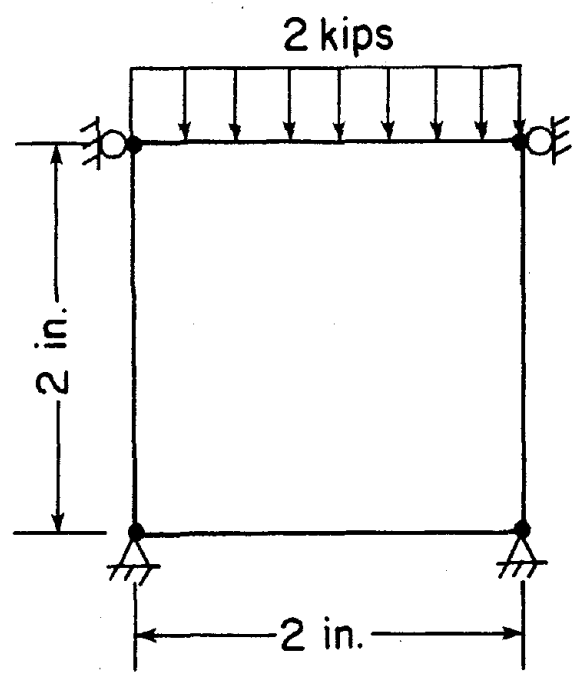
Figure 4.2 Brick Masonry Specimen Modelled by Single Element

material for this problem are assumed to be 2000 ksi and 0.25 respectively. The coefficient of thermal expansion is considered to be 4.0×10^{-5} in/in-deg.F. The specimen is subjected to a uniformly distributed load of 1.0 kip/in. The elastic stresses as well as the total strains and stresses due to different temperatures on the two sides of the specimen can be calculated from the basic principles using hand calculations. These calculations are presented in Appendix B. A comparison of analytical results with those obtained by the computer program shows that they are in good agreement with each other.

Analysis of a Composite Wall

In order to estimate the effect of thermal strains on stresses and strains in the collar joint of a composite wall, the cross-section of a long composite wall similar to that analyzed for creep strains in Chapter III is analyzed. The material properties, boundary conditions, geometry, externally applied loads and the finite element mesh of the composite wall for this analysis are the same as those for the wall analyzed in Chapter III. Linear quadrilateral elements are used to model the wall under plane strain condition. The finite element mesh is shown in Figure 3.5. The effect of a slab has been ignored in the modelling because it can be shown that the slab resistance to vertical displacement is relatively small and can be neglected.

A wide range of values for the coefficient of thermal expansion of block, grout and brick is quoted in the literature. This is possible because there is no standard for measuring the coefficient of thermal expansion for masonry materials or masonry (59). The values for the coefficient of thermal expansion that are available in the literature are shown in Table 4.1. Based upon the information summarized in this table,

the coefficients of thermal expansion for the block and brick masonry, and grout have been chosen as 5.0×10^{-6} in/in-deg.F, 3.2×10^{-6} in/in-deg.F, and 6.0×10^{-6} in/in-deg.F, respectively, in this study.

Table 4.1. Values of Coefficient of Thermal Expansion ($\alpha \times 10^6$ in/in-deg.F) for Brick, Block and Mortar as Available in the Literature.

Reference	Brick	Block	Mortar
Grimm and Fowler (46)	3.4[*]	4.3[*]	--
Jessop (59)	2.78-3.89	3.33-7.22	7.22
Rahman and Suter (77)	--	5.5[*]	--
Grimm (45)	2.2 (clay) 3.3(surface clay)	--	4.94
Spalding (86)	--	5.5	--
Lanczner (61)	3.11[*]	--	--
Plummer (73)	2.2(fire clay) 3.3(surface clay)	--	--

[*] Masonry

It is assumed that the stress-free temperature at the time of construction of the composite wall is 60°F. In order to estimate additional stresses and strains that are caused in the collar joint of the composite wall under investigation, three different sets of inside-outside temperatures are considered. These are 80°, 80°F for a uniform temperature increase of both wythes, 80°, 110°F for a 30 degree higher temperature on the outside than the inside, and 70°, -10°F representing a heated inside environment on a cold winter day. The temperatures at the centroids of various elements across the width of the wall are obtained by using one

of the appropriate Equations 4.17 or 4.18. Subtraction of the stress-free
temperature of 60°F from the element temperatures yields the temperature
changes which are utilized to compute equivalent nodal loads in the
thermal analysis described earlier.

The resulting shear strains and shear stresses in the collar joint
due to the three temperature combinations are shown in Figures 4.3 through
4.6 in which the corresponding values are also plotted for the external
loads. Note that the stresses have been taken from collar joint elements
adjacent to the brick wythe as these gave larger values than those near
the block wythe. It is evident from Figure 4.3 that the shear strain
distribution due to the external loads is different from that due to the
temperature changes. This is quite obvious as the external loads are
applied only on the block whythe whereas the temperature changes lead to
equivalent loads that are applied on both wythes in the horizontal and
vertical directions. It can also be noted that the shear strains in the
collar joint due to the temperature changes can be positive or negative
depending upon the temperature increase or decrease in the two wythes.

As the temperature change produces only normal initial strains (and
no initial shear strains), the stress causing shear strains are the same
as the final strains in the thermal analysis. This leads to shear
stresses in the collar joint due to the thermal loads which are propor-
tional to the final shear strains. Thus, the shapes of the shear strain
distribution shown in Figures 4.3 and 4.4 is similar to that of the shear
stress distributions shown in Figures 4.5 and 4.6.

It can be seen in Figure 4.5 that the largest value of the shear
stress due to the temperature change alone is equal to -20 psi which oc-
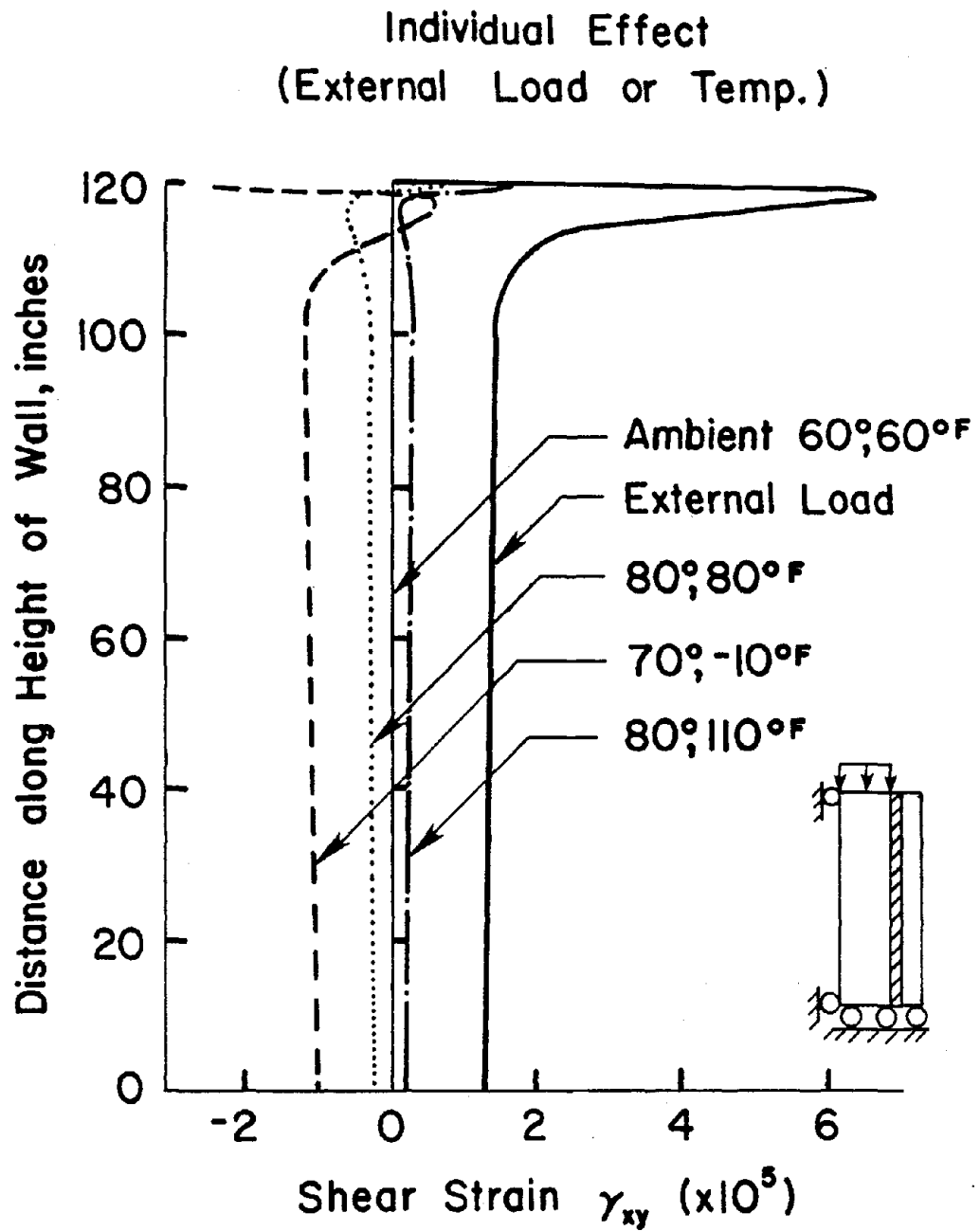curs at the top of the wall for a temperature combination of 70°, -10°F.
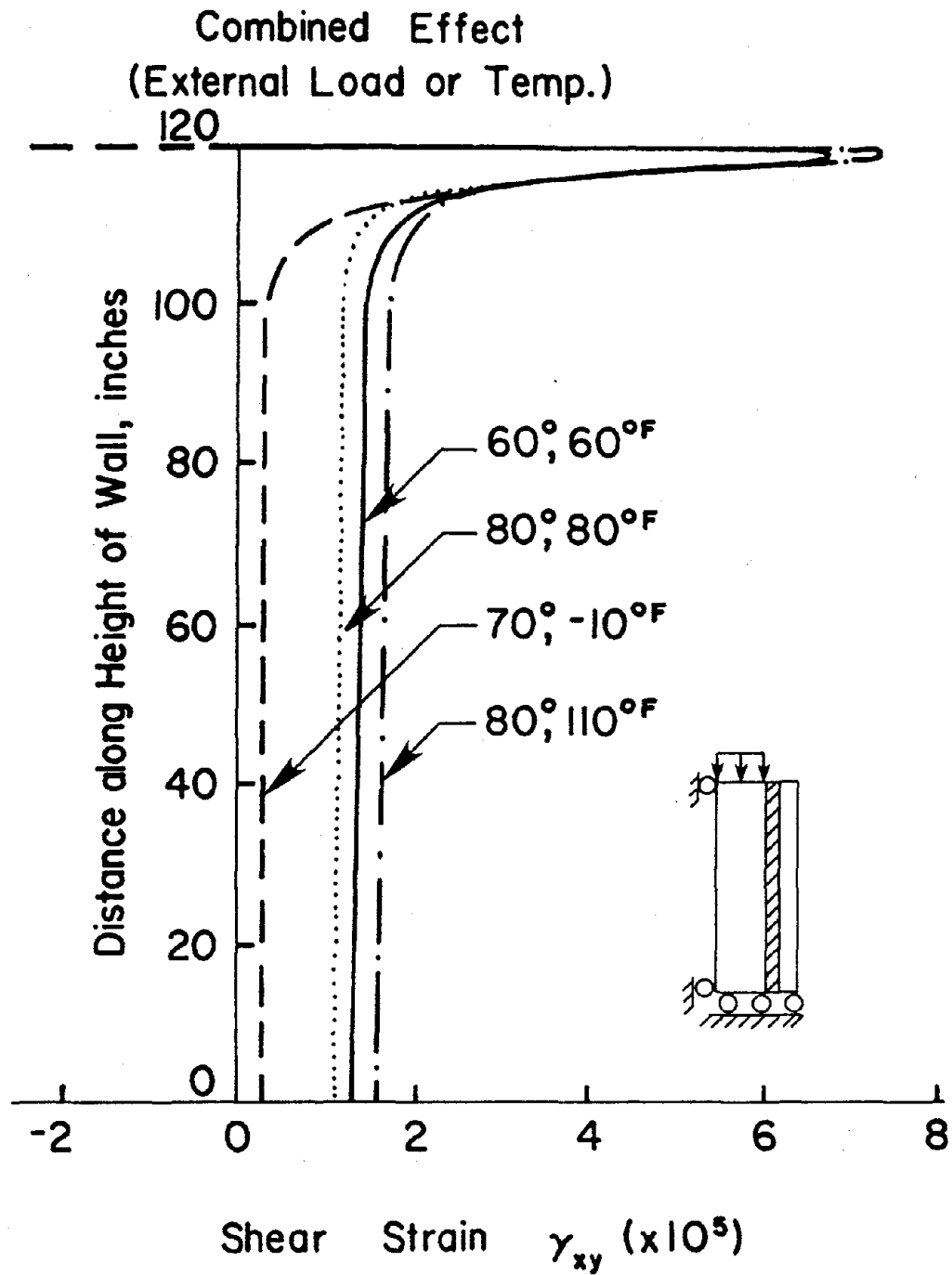
Individual Effect
(External Load or Temp.)

Figure 4.3 Collar Joint Shear Strains due to
Loads or Temperature

Figure 4.4 Collar Joint Shear Strains due to
Loads or Temperature

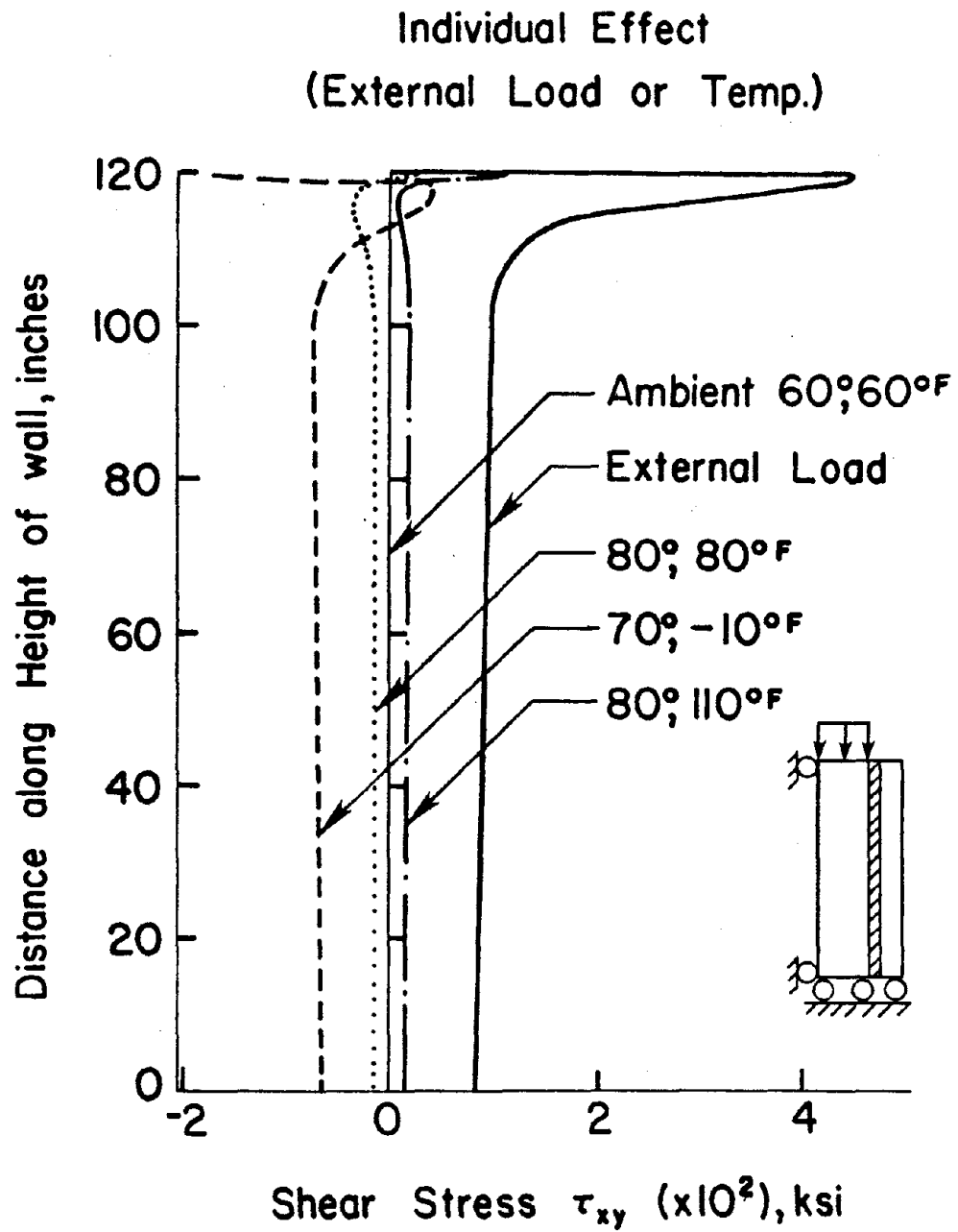## Individual Effect
(External Load or Temp.)

Figure 4.5 Collar Joint Shear Stresses due to
Loads or Temperature

Combined Effect
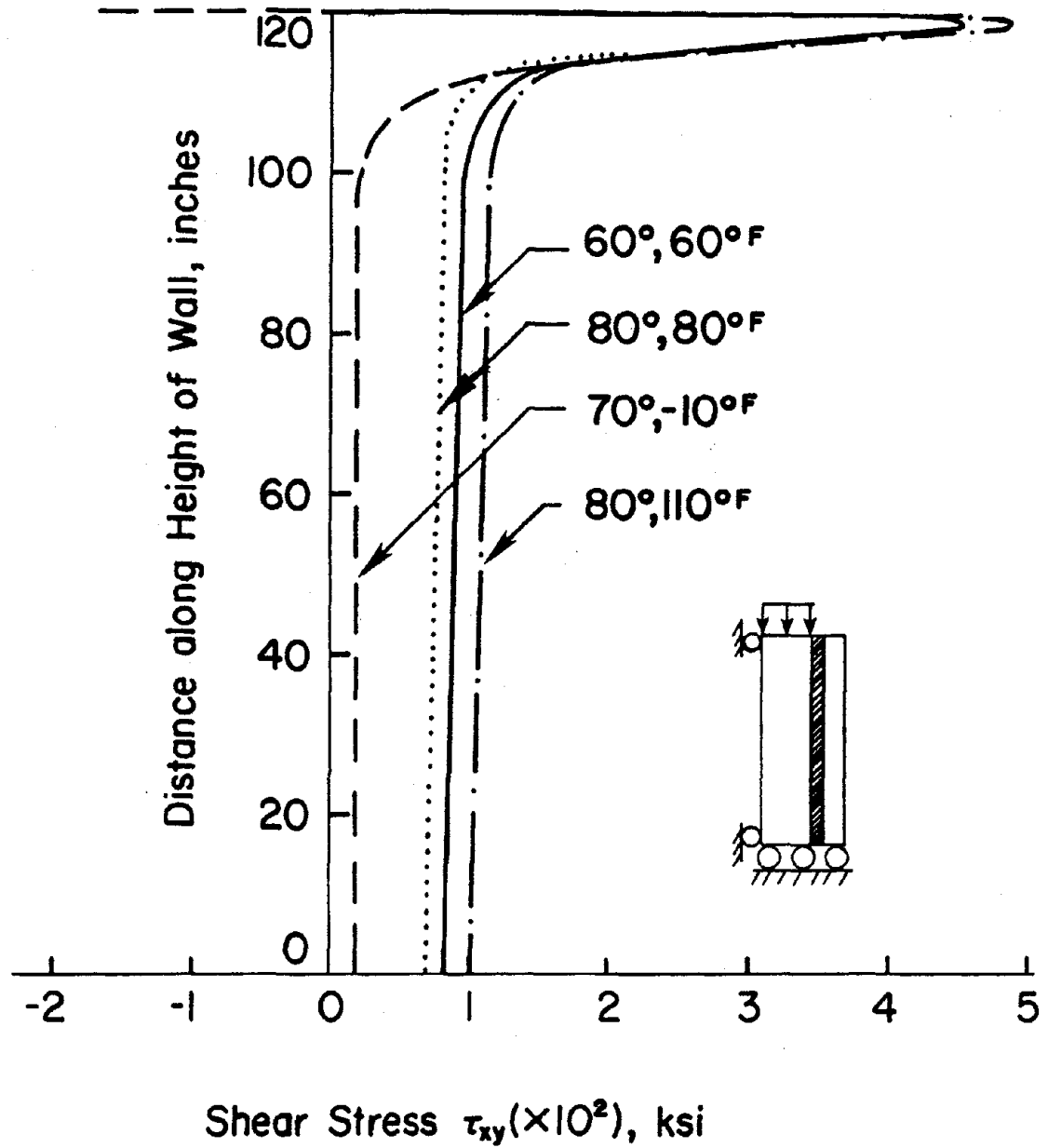## (External Load and Temp.)

Figure 4.6   Collar Joint Shear Stresses due to Loads and
             Temperature

The maximum shear stress in the collar joint due to the external loads alone, on the other hand, is equal to 46 psi and it occurs at approximately 2 in. from the top of the wall. The maximum shear stress due to the combined effect of the external loads and temperature changes occurs for a temperature combination of 80°, 110°F at about 2 in. from the top and has a value of 50 psi. This indicates that the increase in shear stresses in the collar joint due to the specified temperature changes is only 4 psi which is approximately 8% of the stress due to external loads.

The normal vertical strains in the collar joint due to the external loads and temperature changes are shown in Figures 4.7 and 4.8. It is seen that the vertical strains are compressive due to the external loads as well as due to 70°, -10°F temperature combination whereas they are tensile due to increases in temperatures to 80°, 80°F or 80°, 110°F. The temperature strains are of the order of one to two times larger than those due to the external loads. These strains are mostly uniform in the whole height of the wall except at the top where the strains due to the external loads are zero and, due to the temperature changes, are approximately 20 to 50% larger than their average values.

The normal stresses in the collar joint due to the external loads and temperature changes are plotted in Figures 4.9 and 4.10. The normal stress is zero at the top of the wall both due to the external loads and thermal strains. As the load transfers from the loaded wythe to the unloaded wythe in the top 5 to 6 in. length of the wall, the normal stress in the collar joint becomes uniform from this height downwards. The maximum normal stress due to the external loads is equal to 150 psi compressive. Due to an increase in the temperature combination to 80°, 110°F, the total compressive stress in the collar joint increases to 270
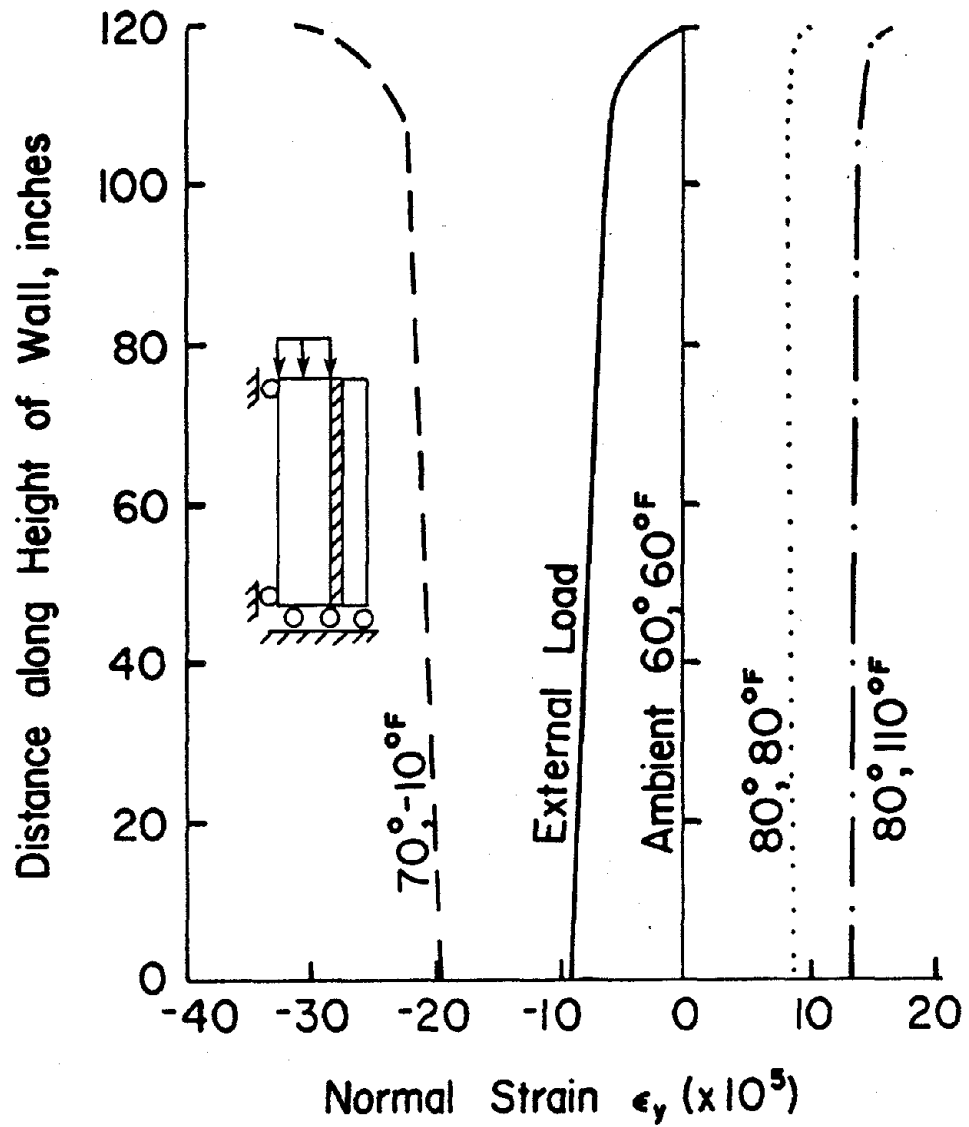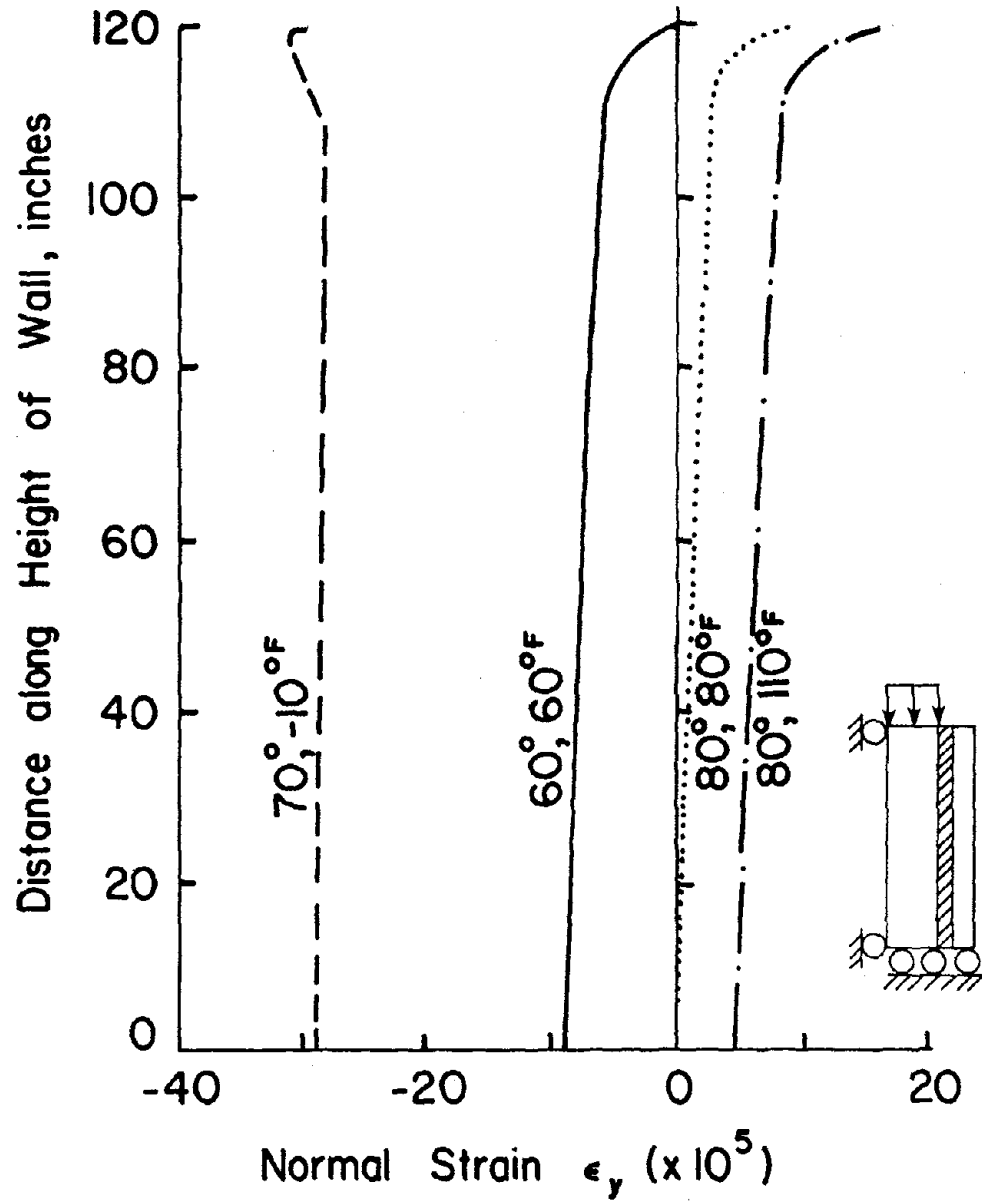
Figure 4.7   Collar Joint Normal Strains due to
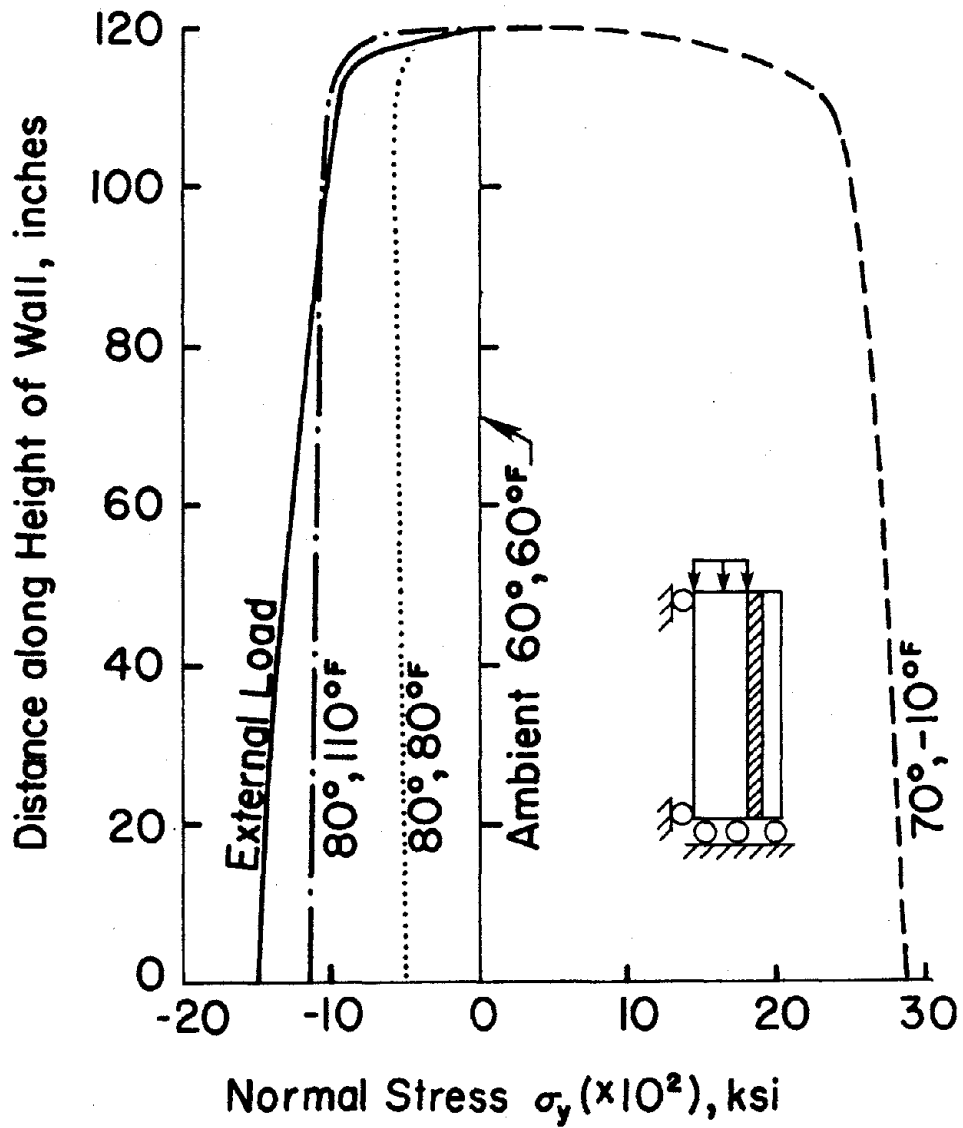Loads or Temperature

Combined Effect
(External Load and Temp.)

Figure 4.8   Collar Joint Normal Strains due to Loads and
Temperature

Figure 4.9 Collar Joint Normal Stresses due to Loads or Temperature
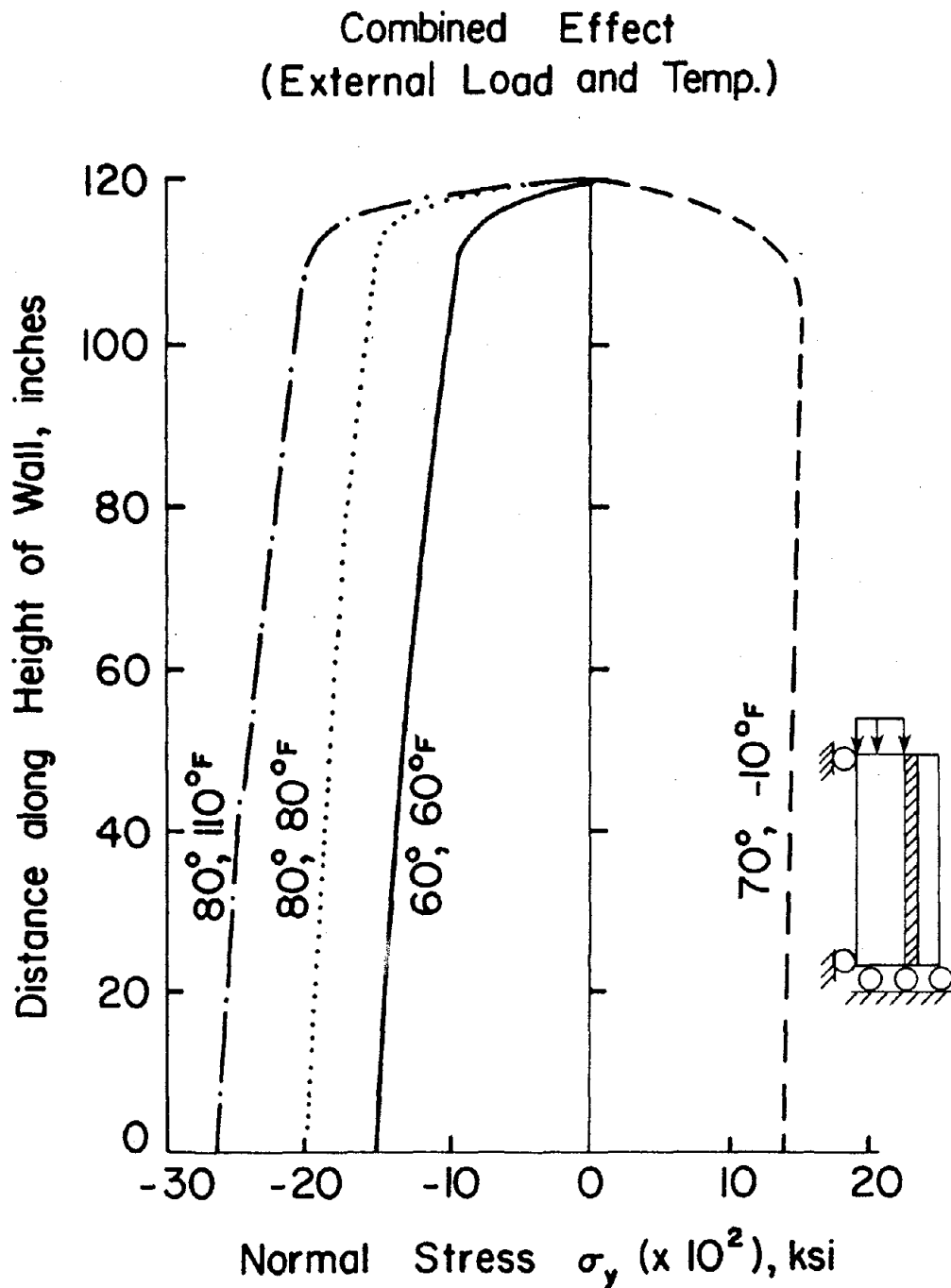
Combined Effect
(External Load and Temp.)

Figure 4.10   Collar Joint Normal Stresses due to Loads and
Temperature

psi whereas a temperature combination of 70°, -10°F together with the external loads produces a tensile stress in the collar joint of approximately 135 psi.

As the grout in the collar joint is a tension-weak material, it should be of interest to compute the largest amount of tension in the collar joint by considering the action of only the dead loads and temperature changes. It is estimated that half of the external loads are always present as dead loads, which yield a compressive stress in the collar joint of 75 psi. Combining this with a temperature combination of 70°, -10°F, which produces a tensile stress of 285 psi due to the temperature change alone, leads to a maximum tensile stress in the collar joint of 210 psi due to the combined effects of the dead loads and temperature changes. This computed tensile stress is not the interface tensile stress, rather this stress exist in the grout of the collar joint away from the interface. The average laboratory compressive strength of the grout used in the test specimens was 2,625 psi. Considering the tensile strength to be 10% of the compressive strength, the maximum tensile stress of grout at failure can be assumed as 260 psi, which is larger than the maximum value of tensile stress in the collar joint computed above.

Conclusions

The results of the elastic and thermal analysis of a long composite wall under condition of plane strain lead to the following conclusions:

1. The shear stresses and strains in the collar joint do not undergo any substantial changes due to the realistic temperature variations assumed in the analysis. Particularly, the maximum value of the collar joint shear stress only changes from 46 to 50 psi, which is well within the failure range.

2. The normal stresses in the collar joint can change from a compressive value of 150 psi for the external loads alone to a tensile value of 210 psi for the dead loads and assumed

temperature changes. Although these stresses are smaller than the tensile failure limit stress of the grouted collar joint, the value is quite large to give the desirable factor of safety against a tensile failure. Accordingly, vertical tension steel must be provided in the collar joint to inhibit tensile failure.

3. It can be seen in Figure 4.6 that the maximum value of the shear stress, which occurs near the very top, is equal to 50 psi whereas the average value in the major portion of the wall is only 12 psi. The average failure shear stress in the collar joint obtained experimentally, on the other hand, is approximately 60 psi; however, its distribution is unknown. It is impossible, therefore, at this point to predict a factor of safety against shear failure unless detailed shear stress distributions within the collar joint can be estimated from measured strains.

CHAPTER V

DEVELOPMENT OF VARIABLE-NODE-NUMBER

ISOPARAMETRIC ELEMENTS

In the previous two chapters, the cross-sections of composite masonry walls have been analyzed using linear rectangular plane strain finite elements. The horizontal displacement plots in Figure 3.10 indicate that the displacement field in the wall caused by vertical loads only on the block wythe contains general functions of order not less than three. Hence, elements with displacement functions of order three or higher along the vertical direction are required to model the cross section of a composite wall accurately. Elements with second order displacement function may yield correct results if the finite element mesh is very fine along the vertical direction.

In composite masonry walls, when only the block wythe is loaded, load transfer from the block wythe to the brick wythe occurs through the shearing stresses in the collar joint. Hence, the shear stresses at the block wythe-collar joint interface are the most critical stresses in a composite wall. Since, one of the main objectives in this research is to estimate the interface stresses accurately, very fine meshes are provided along the horizontal direction in the vicinity of the interface. Hence, it is expected that the elements with quadratic displacement functions along the horizontal direction would to be able to correctly model the displacement field of the wall.

The plots of collar joint shear stresses given in Chapter III and Chapter IV show that the shear stress variation is not uniform. The

maximum value of the shear stress occurs within the top 2 to 3 inches of the wall. Hence, to obtain the correct magnitude of the shearing stresses and the exact locations of their occurence, one must provide a very fine mesh along the vertical direction at the top few inches of the wall if lower order (second order) elements are used. On the other hand, a relatively coarse mesh may be used if higher order elements are chosen for modelling the wall. The analysis of the cross section of a wall modelled by either lower order elements in a very fine mesh or regular higher order elements in a relatively coarse mesh becomes expensive. Hence, an alternative way to model the composite walls more economically has been suggested in this study.

It can be stated from the above discussion that the composite masonry walls can be modelled efficiently if one employs elements that have higher order displacement function along the vertical direction and lower order displacement function along the horizontal direction to discretize the cross section of the wall. These types of elements with different displacement functions in two different directions are called variable-node-number elements. In this study, attention has been focussed towards developing variable-node-number elements that can be used to obtain correct stresses in the collar joint through efficient modelling of the composite walls. For the most economical analysis, the higher order variable-node-number elements may be used to model the collar joint at the block-collar joint and brick-collar joint interfaces and quadratic elements may be used to model the block and brick wythes. The transition from the higher order elements in the collar joint to the quadratic elements in the block and brick wythes can also be achieved by using variable-node-number elements. A finite element mesh for the top portion

of a composite masonry wall shown in Figure 5.1 demonstrates the use of variable-node-number elements as interface and transition elements.

Variable-Node-Number Isoparametric Elements

The concept of variable-node-number isoparametric elements was first introduced by Zienkiewicz (101) in 1970. During the last few years, different types of variable-node-number elements have been developed by researchers (29,30,89,95) to model their specific problems. It has been shown by the above researchers that the stresses and strains can be significantly improved and the cost of analysis can be decreased considerably by using variable-node-number elements. For maximum accuracy, Bathe (23) suggested that the elements should be as nearly rectangular as possible and the noncorner nodes should in general be located at their natural coordinate positions. The use of variable-node-number elements is most effective for two-dimensional problems. In three-dimensional analysis, the use of incompatible modes can in some cases decrease the analysis cost considerably.

Three types of variable-node-number isoparametric serendipity elements are developed in this study. The elements with local coordinate system and node numbering are shown in Figure 5.2. Element VISO10 has cubic displacement functions along both the vertical directions and quadratic displacement functions along the horizontal directions. It is a ten noded element. Element VISR9 has cubic displacement function along the right vertical side and element VISL9 has cubic displacement function along the left vertical side. Both VISR9 and VISL9 elements have quadratic displacement functions along the other three sides. They are nine noded elements.
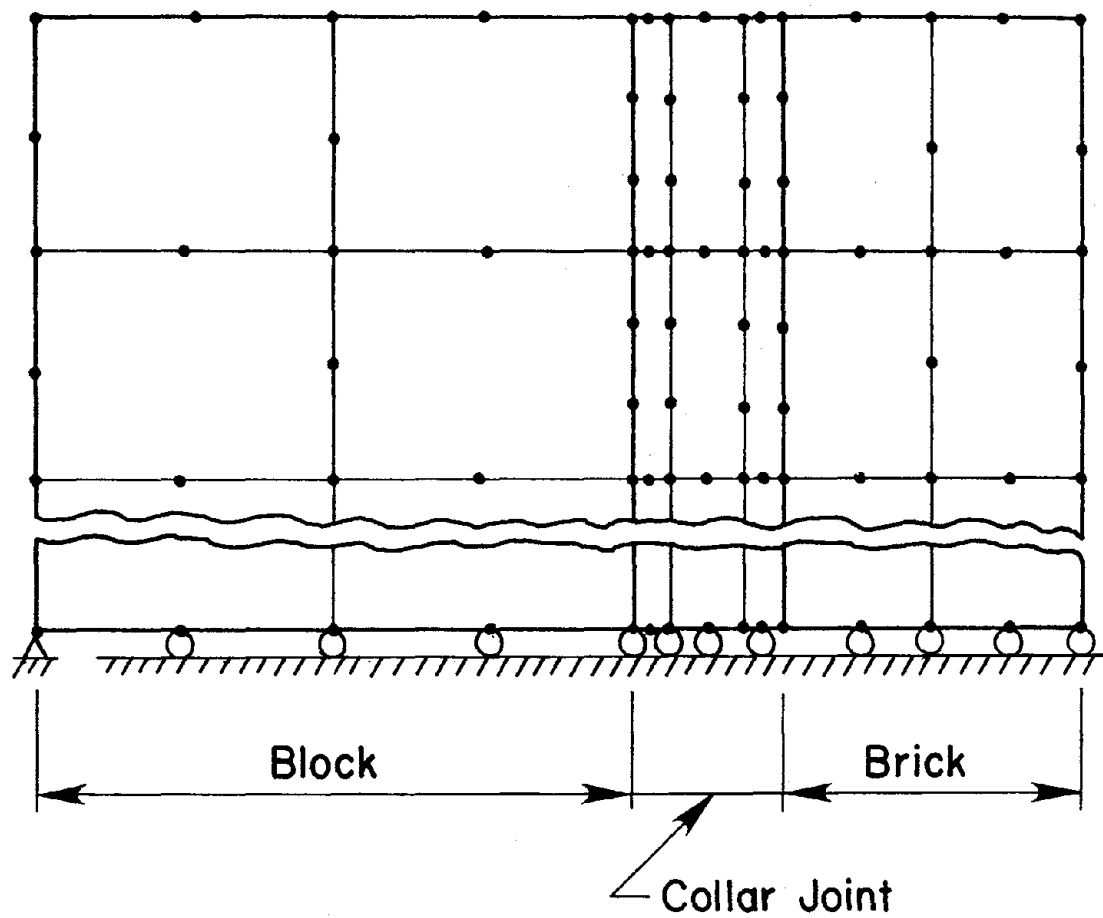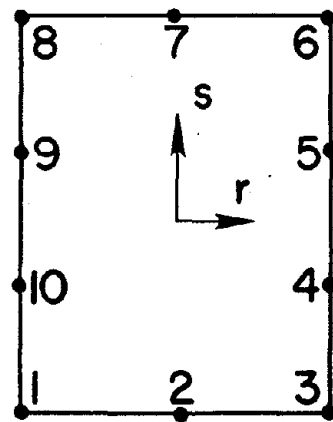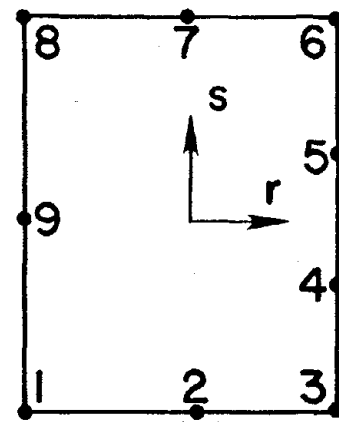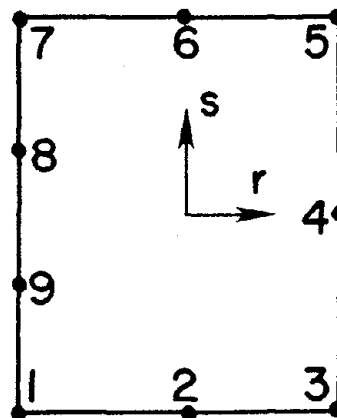
Figure 5.1   Variable-Node-Number Elements Used as Interface and
Transition Elements

Figure 5.2 Variable-Node-Number Elements

Derivation of the Shape Functions (N)

The shape functions for the elements VISO10, VISR9 and VISL9 have been derived using the technique suggested by Taylor (88). In this procedure, for m-th order serendipity elements the side shape function N_{ij} are constructed as products of m-th order Lagrange interpolation functions along the nodal edge together with first-order functions in all other directions. The corner shape functions are then constructed by subtracting appropriate proportions of the edge shape functions from the basic first-order Lagrange product interpolation for the corner node to produce zeroes at the nodes of all edges joining the corners.

Element VISO10

This element is a ten noded variable-node-number isoparametric serendipity element. The side shape functions (N_2, N_4, N_5, N_7, N_9, and N_{10}) of this type of element are available in the literature (23). They are listed below:

$$N_2 = 1/2(1-r^2)(1-s),$$

$$N_4 = \{(1-s^2)+1/16(27s^3+7s^2-27s-7)\}\{1/2(1+r)\},$$

$$N_5 = \{1/16(-27s^3-9s^2+27s+9)\}\{1/2(1+r)\},$$

$$N_7 = 1/2(1-r^2)(1+s),$$

$$N_9 = \{1/16(-27s^3-9s^2+27s+9)\}\{1/2(1-r)\} \text{ and}$$

$$N_{10} = \{(1-s^2)+1/16(27s^3+7s^2-27s-7)\}\{1/2(1-r)\}.$$

(5.1)

The corner shape functions are constructed and the steps are shown in Figures 5.3 through 5.6. N_A, N_B, N_C, and N_D shown in figures are the basic first-order Lagrange product interpolations. The shape function for the corner node 1 is obtained by subtracting half of the shape function of node 2, one third of the shape function of node 9 and two third of the shape function of node 10 from the basic first-order Lagrange
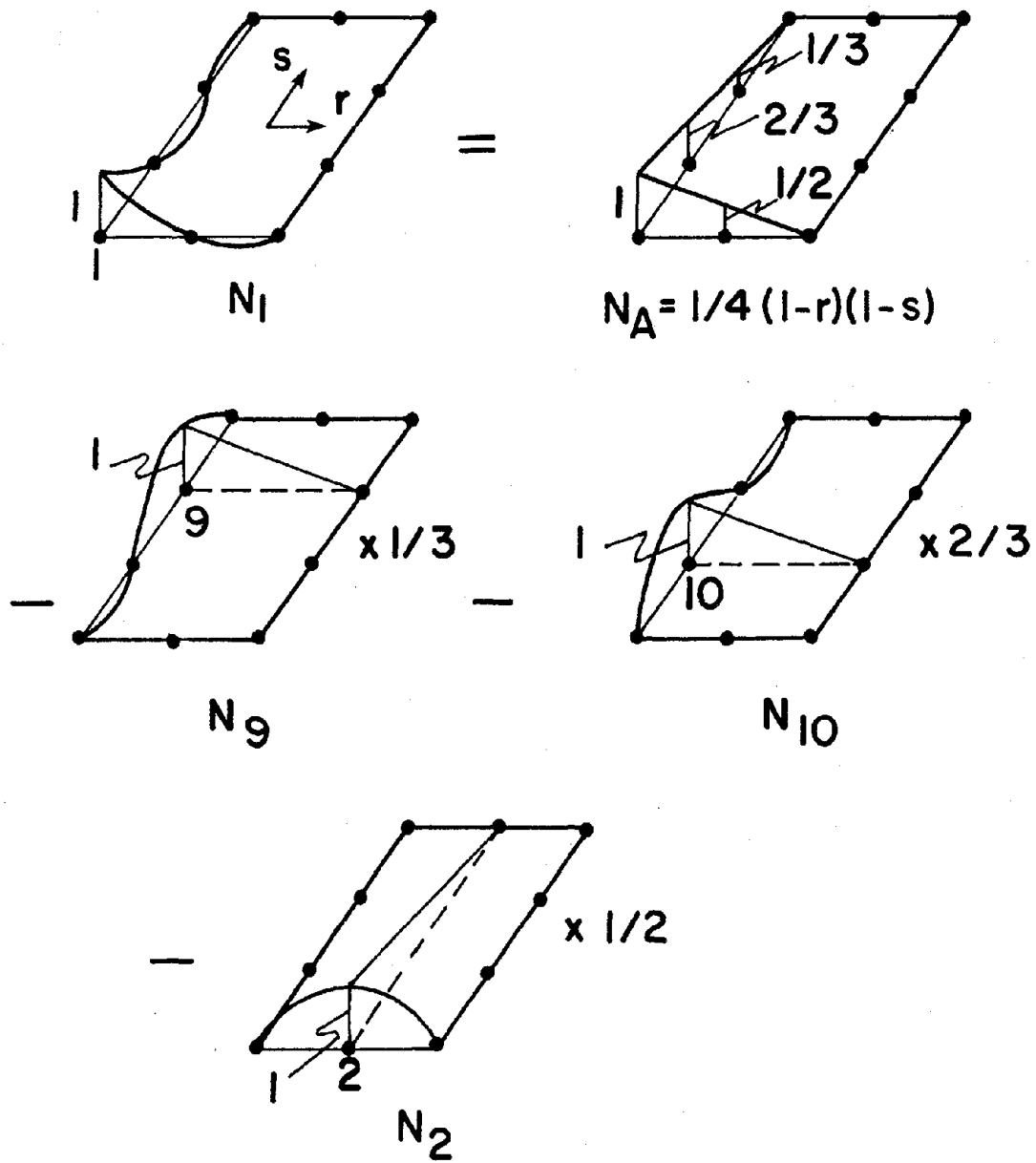
$$N_A = 1/4\,(1-r)(1-s)$$

$$N_1 = 1/4(1-r)(1-s) - 1/2\,N_2 - 1/3\,N_9 - 2/3\,N_{10}$$

Figure 5.3   Shape Function N_1 of VISO10 Element

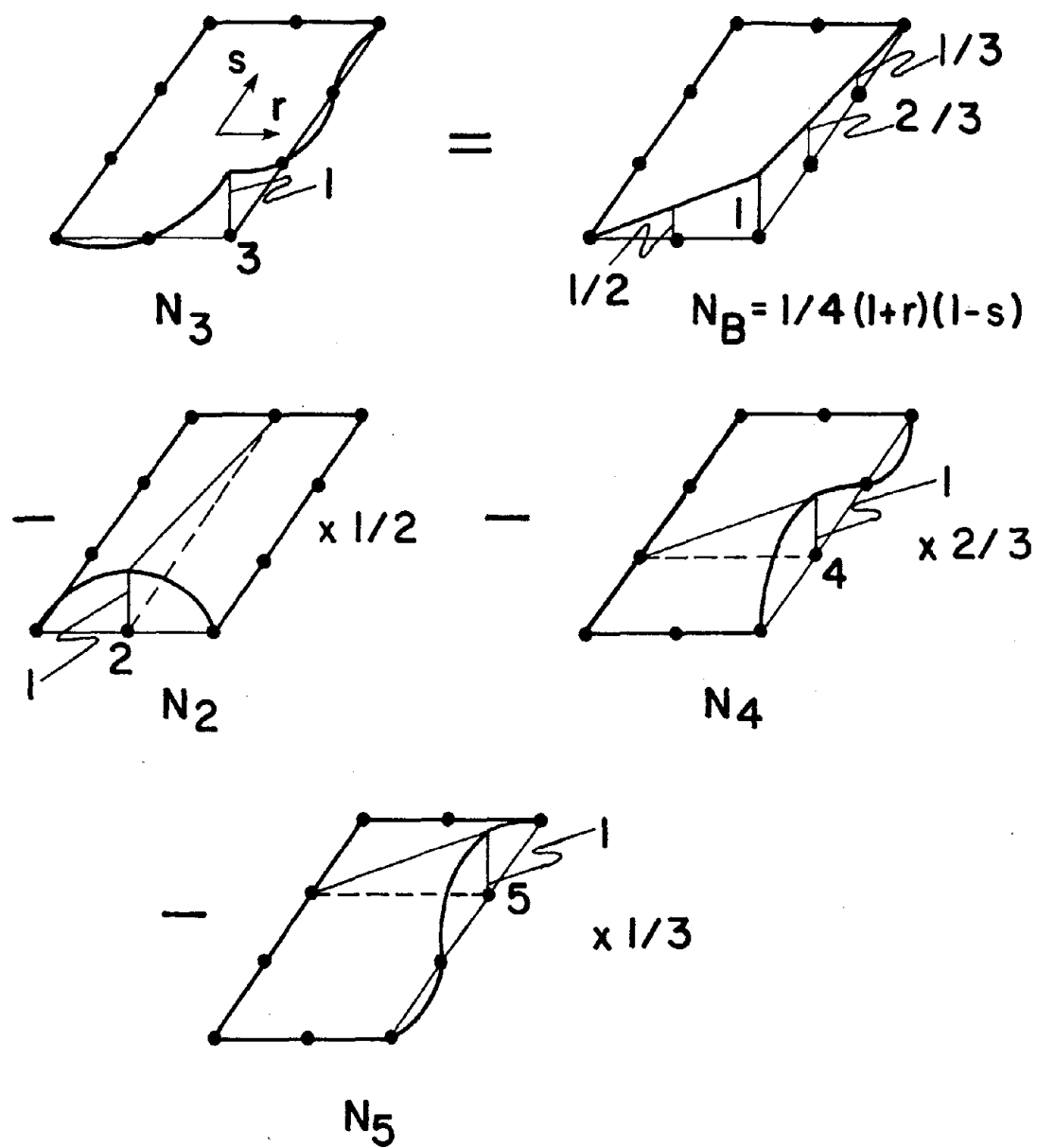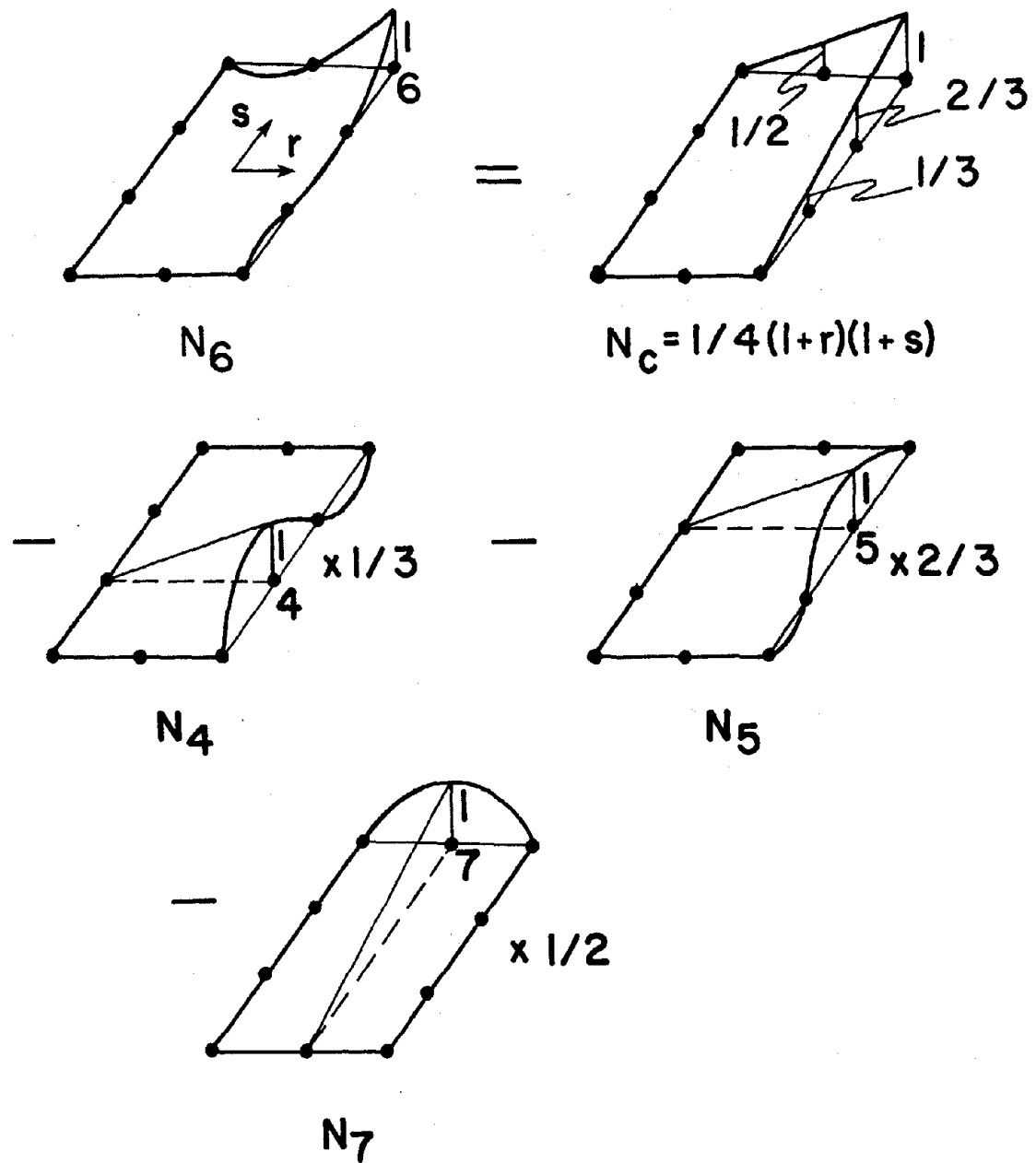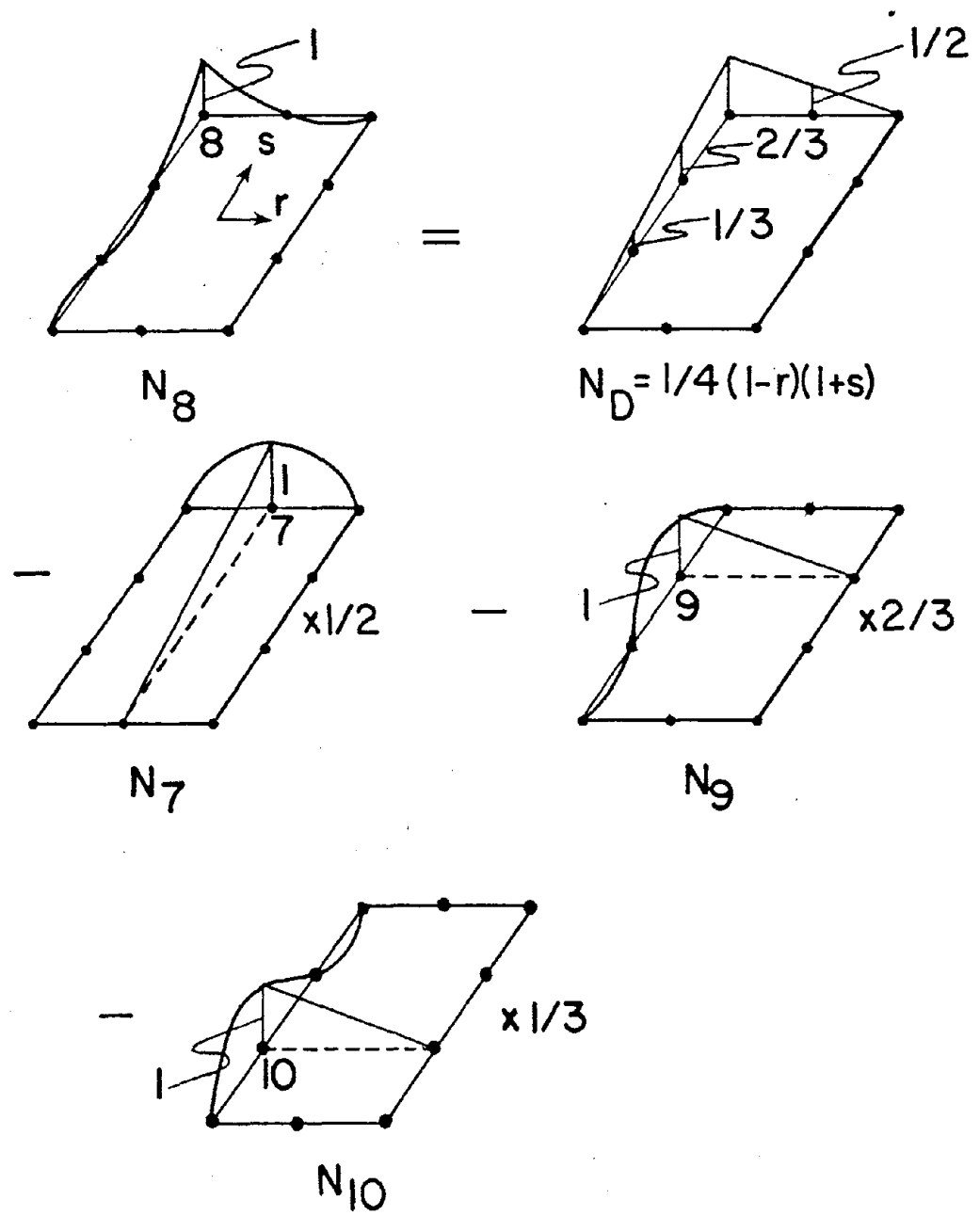$$N_3 = 1/4\,(1+r)(1-s) - 1/2\,N_2 - 2/3\,N_4 - 1/3\,N_5$$

Figure 5.4   Shape Function N₃ of VISO10 Element

$$N_6 = 1/4\,(1+r)(1+s) - 1/3\,N_4 - 2/3\,N_5 - 1/2\,N_7$$

Figure 5.5   Shape Function N_6 of VISO10 Element

$$N_8 = 1/4(1-r)(1+s) - 1/2\,N_7 - 2/3\,N_9 - 1/3\,N_{10}$$

Figure 5.6   Shape Function N_8 of VISO10 Element

product interpolation of node number 1. The shape functions for the other corner nodes are obtained following similar procedures. The derived corner shape functions are

$$N_1 = 1/4(1-r)(1-s)-1/4(1-r^2)(1-s)-1/96(-27s^3-9s^2+27s+9)$$
$$(1-r)-2/3\{(1-s^2)+1/16(27s^3+7s^2-27s-7)\}\{1/2(1-r)\},$$

$$N_3 = 1/4(1+r)(1-s)-1/4(1-r^2)(1-s)-1/96(-27s^3-9s^2+27s+9)$$
$$(1+r)-2/3\{(1-s^2)+1/16(27s^3+7s^2-27s-7)\}\{1/2(1+r)\},$$

$$N_6 = 1/4(1+r)(1+s)-1/4(1-r^2)(1+s)-1/48(-27s^3-9s^2+27s+9)$$
$$(1+r)-1/3\{(1-s^2)+1/16(27s^3+7s^2-27s-7)\}\{1/2(1+r)\} \text{ and}$$

$$N_8 = 1/4(1-r)(1+s)-1/4(1-r^2)(1+s)-1/48(-27s^3-9s^2+27s+9)$$
$$(1-r)-1/3\{(1-s^2)+1/16(27s^3+7s^2-27s-7)\}\{1/2(1-r)\}.$$

(5.2)

Element VISL9

This element is a nine noded variable-node-number isoparametric serendipity element. The displacement function along the vertical direction of the left side of the element is cubic. For the remaining three sides, the displacement functions are quadratic. The shape functions for the nodes (N_2, N_4, N_6, N_8 and N_9) which are located between the corner nodes are available in the literature (23). These shape functions are

$$N_2 = 1/2(1-r^2)(1-s),$$
$$N_4 = 1/2(1-s^2)(1+r),$$
$$N_6 = 1/2(1-r^2)(1+s),$$
$$N_8 = 1/32(-27s^3-9s^2+27s+9)(1-r) \text{ and}$$
$$N_9 = \{(1-s^2)+1/16(27s^3+7s^2-27s-7)\}\{1/2(1-r)\}.$$

(5.3)

The shape functions for the nodes at the corners of the element are developed and the steps are shown in Figures 5.7 through 5.10. In these figures N_A, N_B, N_C and N_D represent the basic first-order Lagrange product interpolations. The shape function for the corner node 1 is obtained by
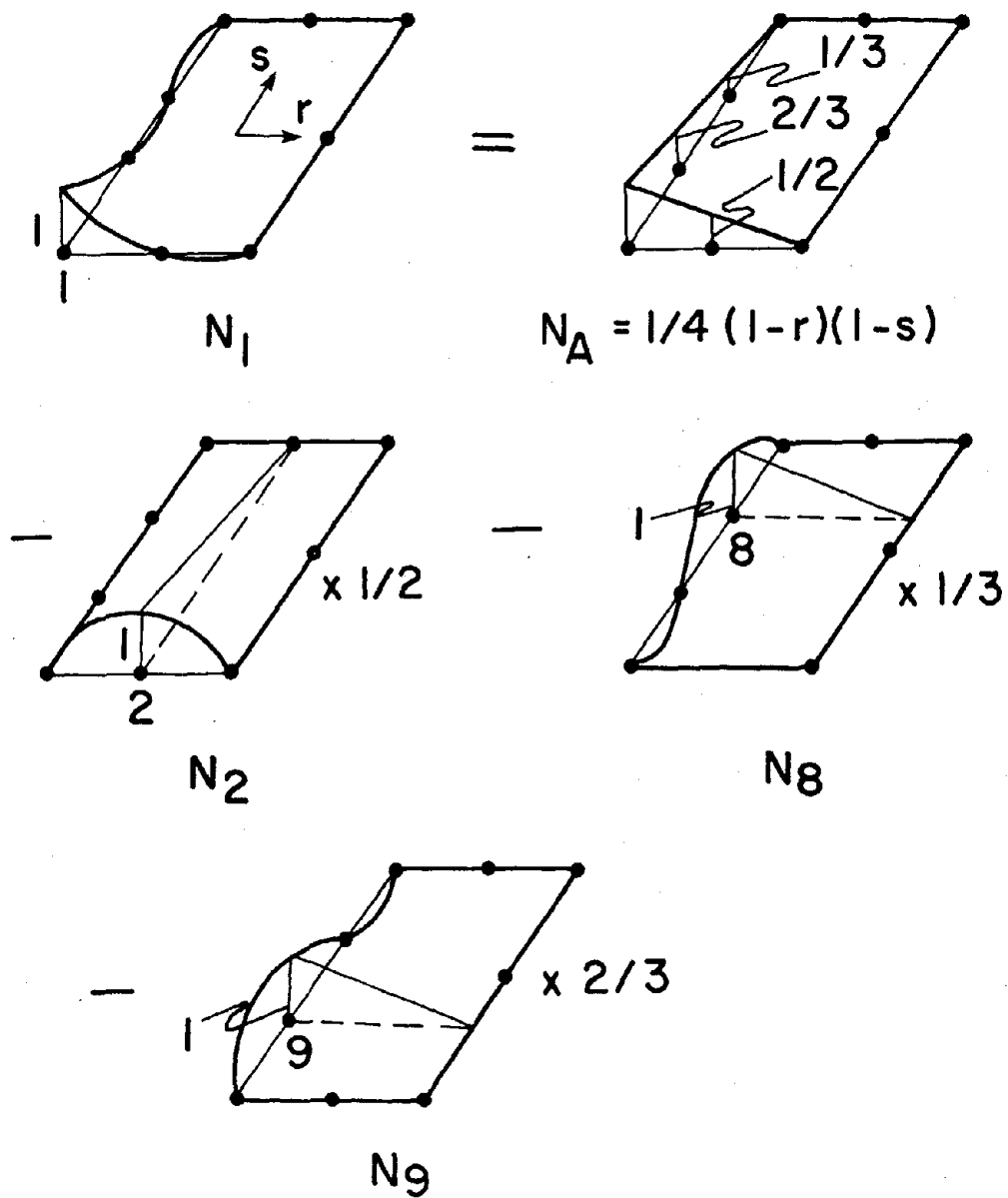
$$N_1 = 1/4\,(1-r)(1-s) - 1/2\,N_2 - 1/3\,N_8 - 2/3\,N_9$$

Figure 5.7 Shape Function N_1 of VISL9 Element
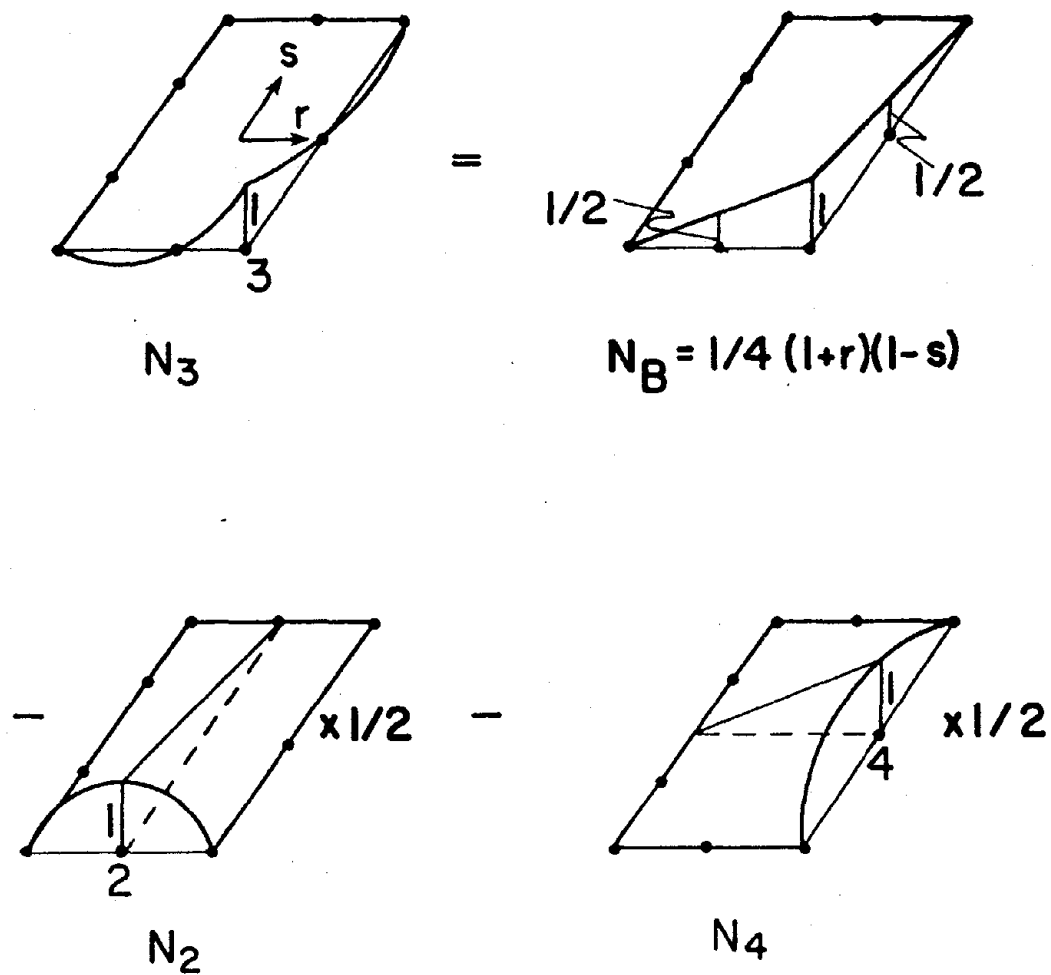
$$N_3 = 1/4\,(1+r)(1-s) - 1/2\,N_2 - 1/2\,N_4$$

Figure 5.8 Shape Function N_3 of VISL9 Element

$$N_5 = 1/4(1+r)(1+s) - 1/4 N_4 - 1/2 N_6$$

Figure 5.9   Shape Function N_5 of VISL9 Element
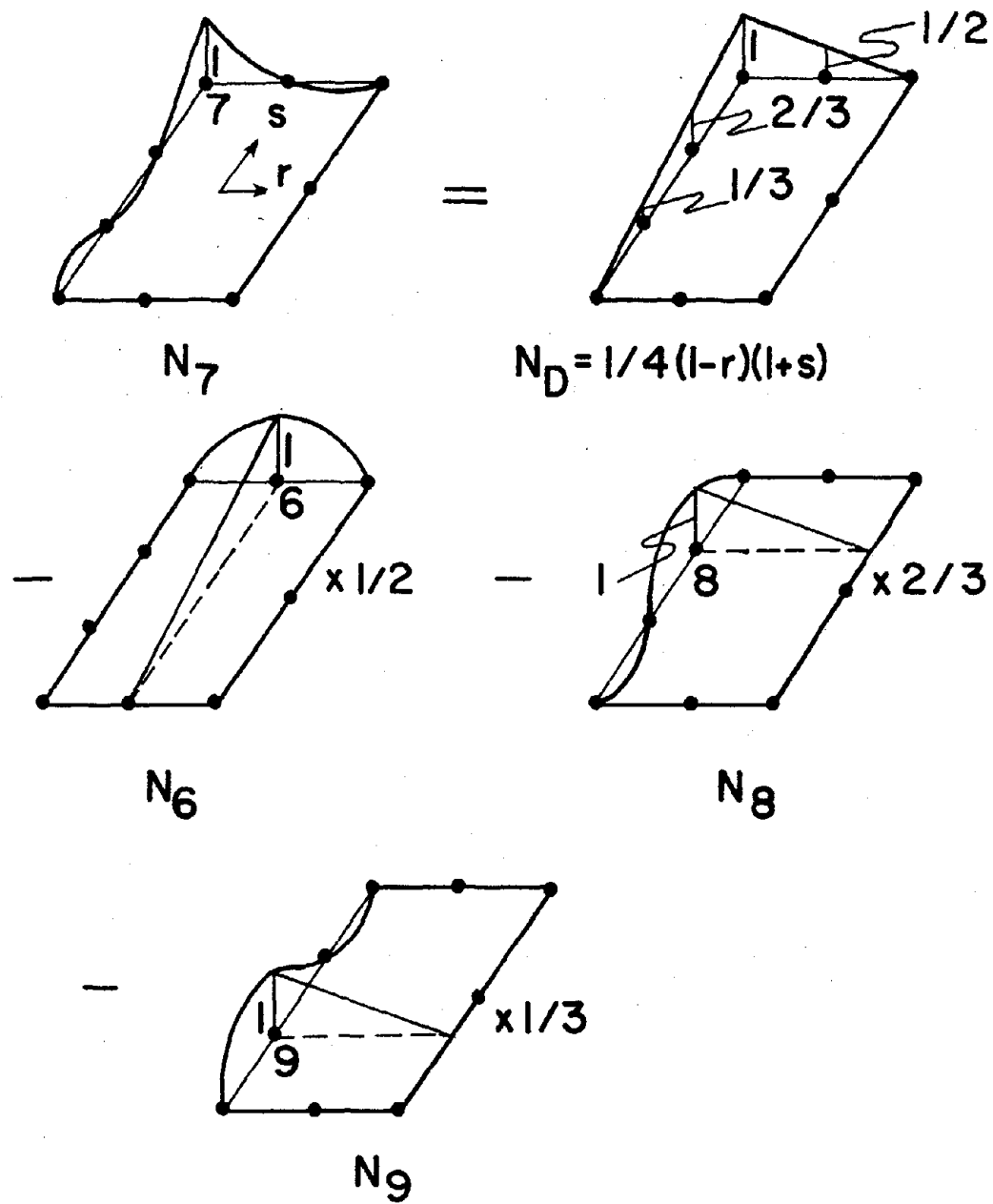
$$N_D = 1/4\,(1-r)(1+s)$$

$$N_7 = 1/4\,(1-r)(1+s) - 1/2\,N_6 - 2/3\,N_8 - 1/3\,N_9$$

Figure 5.10   Shape Function N_7 of VISL9 Element

subtracting half of the shape function of node 2, one-third of the shape function of node 8 and two-third of the shape function of node 9 from the basic first-order Lagrange product interpolation of node 1. Other corner node shape functions are obtained by following procedures similar to this. The derived shape functions are given below.

$$N_1 = 1/4(1-r)(1-s)-1/4(1-r^2)(1-s)-1/96(-27s^3-9s^2+27s+9)$$
$$(1-r)-2/3\{(1-s^2)+1/16(27s^3+7s^2-27s-7)\}\{1/2(1-r)\},$$

$$N_3 = 1/4(1+r)(1-s)-1/4(1-r^2)(1-s)-1/4(1-s^2)(1+r),$$

$$N_5 = 1/4(1+r)(1+s)-1/4(1-s^2)(1+r)-1/4(1-r^2)(1+s) \text{ and}$$

$$N_7 = 1/4(1-r)(1+s)-1/4(1-r^2)(1+s)-1/48(-27s^3-9s^2+27s+9)$$
$$(1-r)-1/3\{(1-s^2)+1/16(27s^3+7s^2-27s-7)\}\{1/2(1-r)\}.$$

$$(5.4)$$

Element VISR9

This is a nine noded variable-node-number isoparametric serendipity element with cubic displacement function in the vertical direction of the right side of the element. For the other three sides of the element, the displacement functions are quadratic. The shape functions for the nodes (N_2, N_4, N_5, N_7, and N_9) which are located between the corner nodes are given in the literature (23). These shape functions are listed below.

$$N_2 = 1/2(1-r^2)(1-s),$$

$$N_4 = \{(1-s^2)+1/16(27s^3+7s^2-27s-7)\}\{1/2(1+r)\},$$

$$N_5 = 1/32(-27s^3-9s^2-27s+9)(1+r),$$

$$N_7 = 1/2(1-r^2)(1+s) \text{ and}$$

$$N_9 = 1/2(1-s^2)(1-r).$$

$$(5.5)$$

The shape functions for the corner nodes are developed employing the aboved mentioned shape functions for the interior nodes. In Figures 5.11 through 5.14 the steps for deriving the shape functions for the corner nodes are given in detail. N_A, N_B, N_C and N_D in these figures are the basic
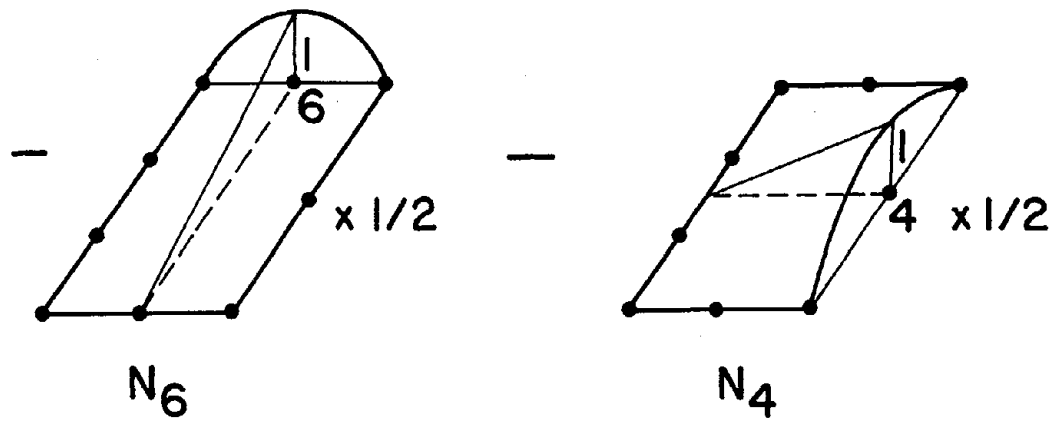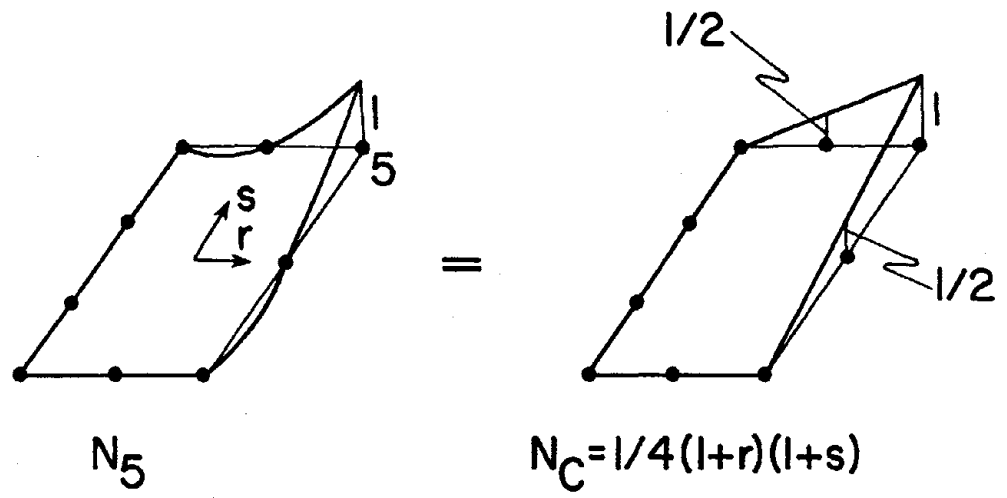
$$N_A = 1/4(1-r)(1-s)$$
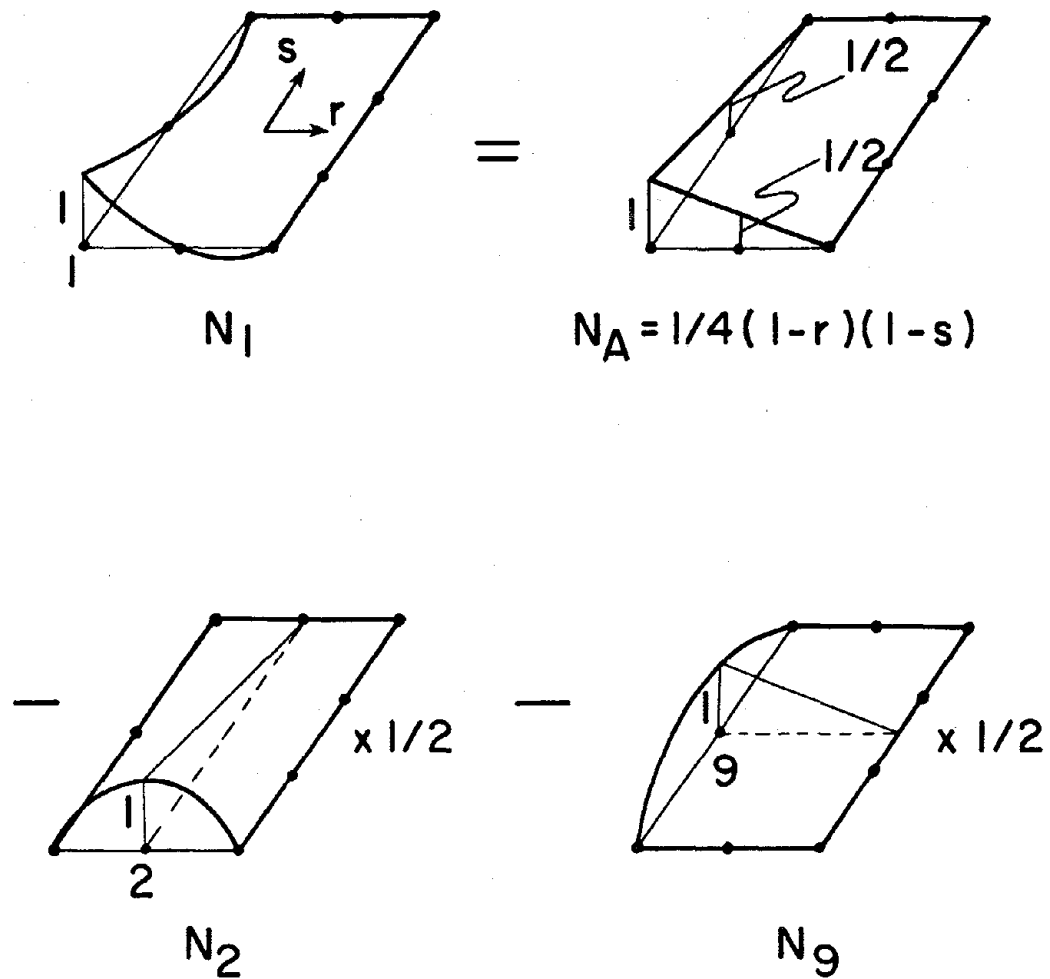
$$N_1 = 1/4(1-r)(1-s) - 1/2 N_2 - 1/2 N_9$$

Figure 5.11   Shape Function N_1 of VISR9 Element
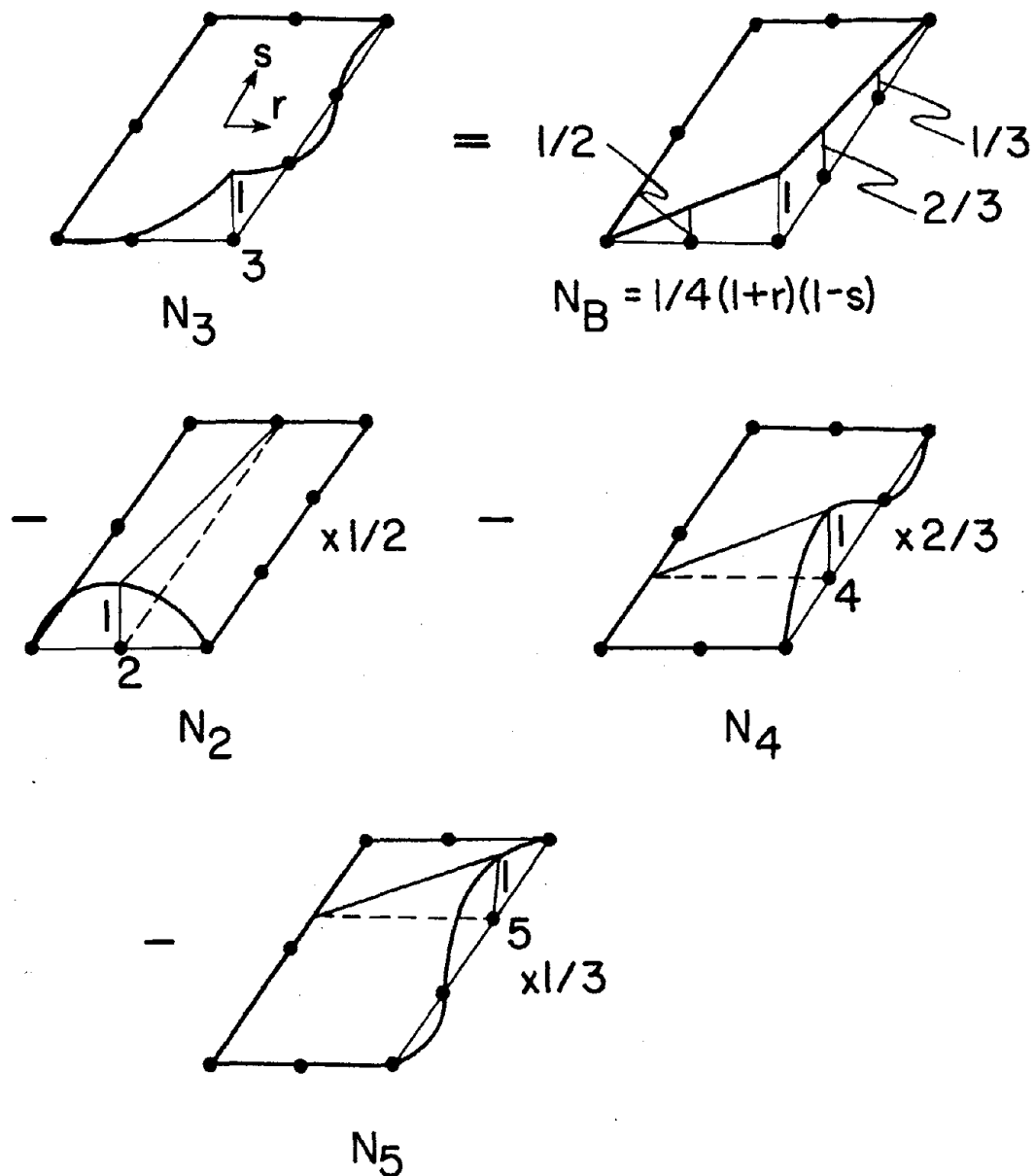
$$N_3 = 1/4 (1+r)(1-s) - 1/2 N_2 - 2/3 N_4 - 1/3 N_5$$

Figure 5.12   Shape Function N_3 of VISR9 Element
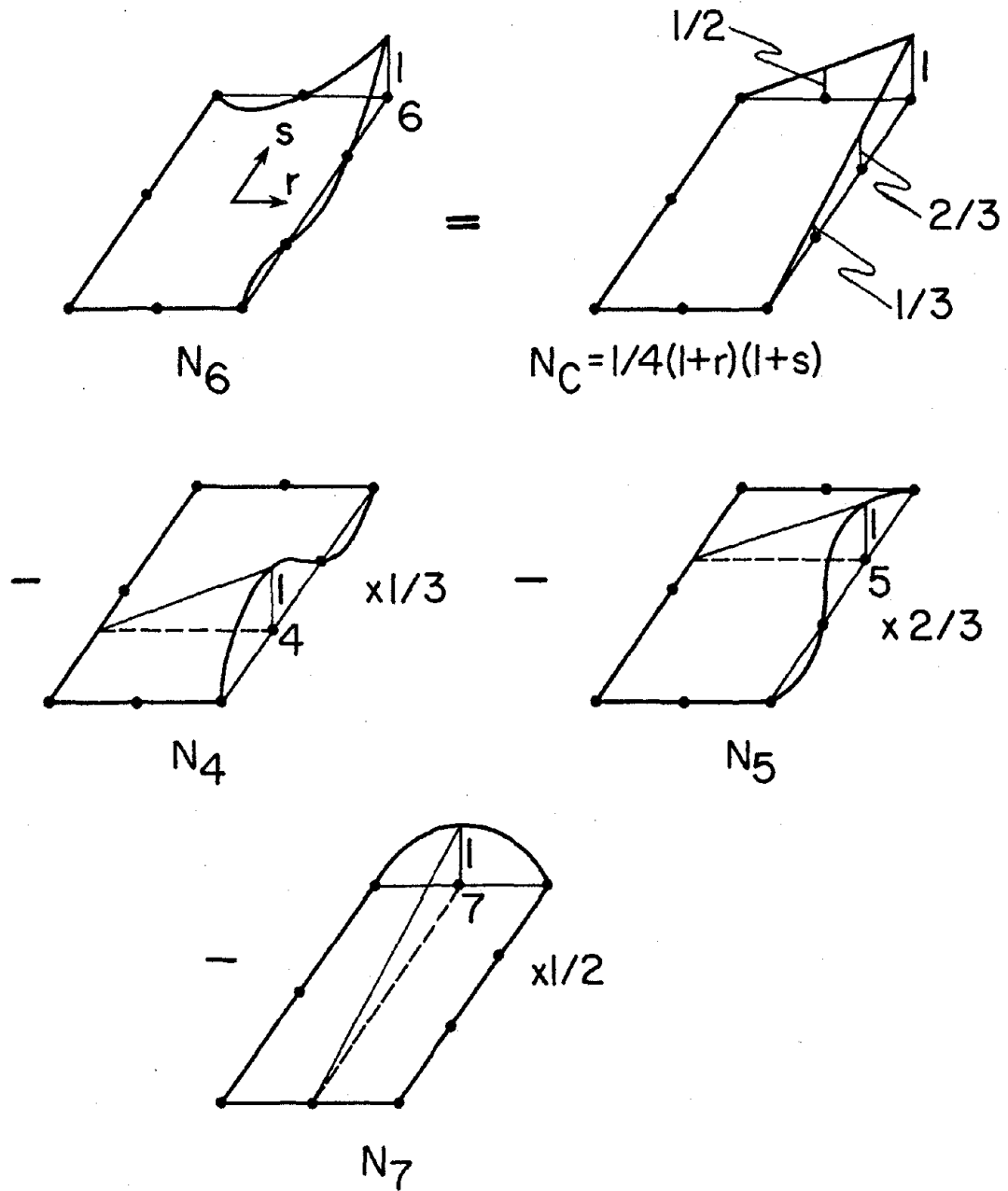
$$N_6 = 1/4(1+r)(1+s) - 1/3N_4 - 2/3N_5 - 1/2N_7$$

Figure 5.13   Shape Function N_6 of VISR9 Element
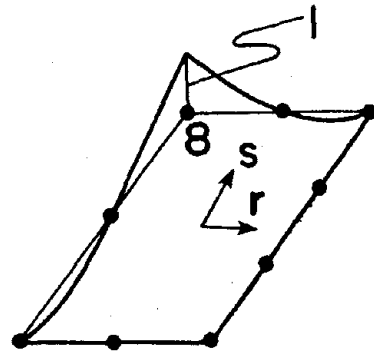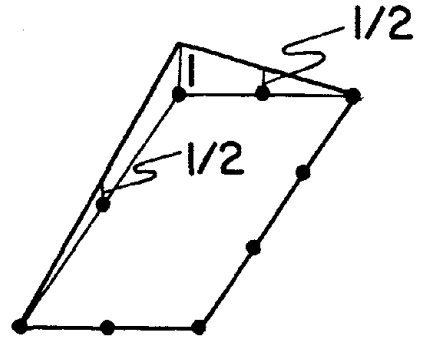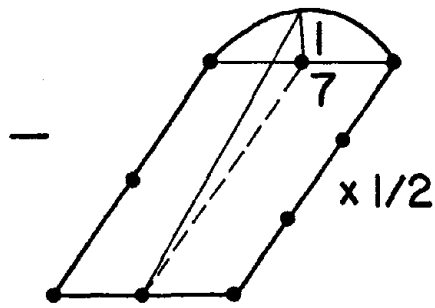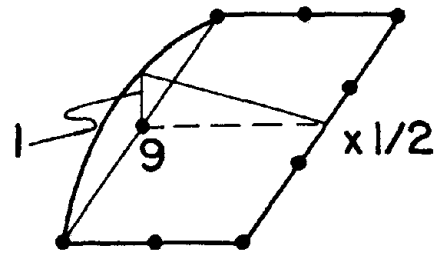
$$N_8 = 1/4(1-r)(1+s) - 1/2N_7 - 1/2N_9$$

Figure 5.14 Shape Function N_8 of VISR9 Element

first-order Lagrange product interpolations. The shape function for node 1 is obtained by subtracting half of the shape function of node 2 and half of the shape function of node 9 from the basic first-order Lagrange product interpolation of node 1. The shape functions of other corner nodes are obtained by following similar procedures. The derived shape functions for the corner nodes are

$$N_1 = 1/4(1-r)(1-s)-1/4(1-r^2)(1-s)-1/4(1-s^2)(1-r),$$

$$N_3 = 1/4(1+r)(1-s)-1/4(1-r^2)(1-s)-1/3\{(1-s^2)+1/16(27s^3$$

$$+7s^2-27s-7)\}(1+r)-1/96(-27s^3-9s^2+27s+9)(1+r),$$

$$N_6 = 1/4(1+r)(1+s)-1/4(1-r^2)(1+s)-1/6\{(1-s^2)+1/16(27s^3$$

$$+7s^2-27s-7)\}(1+r)-1/48(-27s^3-9s^2+27s+9)(1+r) \text{ and}$$

$$N_8 = 1/4(1-r)(1+s)-1/4(1-r^2)(1+s)-1/4(1-s^2)(1-r).$$

(5.6)

Derivation of the Strain-Displacement Matrices (B)

The strain-displacement matrices for the elements VISO10, VISR9 and VISL9 have been derived following the standard procedure given in the text (101). From the chain-rule

$$
\begin{Bmatrix} \dfrac{\partial}{\partial r} \\ \dfrac{\partial}{\partial s} \end{Bmatrix}
=
\begin{bmatrix} \dfrac{\partial x}{\partial r} & \dfrac{\partial y}{\partial r} \\ \dfrac{\partial x}{\partial s} & \dfrac{\partial y}{\partial s} \end{bmatrix}
\begin{Bmatrix} \dfrac{\partial}{\partial x} \\ \dfrac{\partial}{\partial y} \end{Bmatrix}
= [J]
\begin{Bmatrix} \dfrac{\partial}{\partial x} \\ \dfrac{\partial}{\partial y} \end{Bmatrix}
$$

(5.7)

in which $[J]$ is the Jacobian matrix. Pre-multiplying both sides by the inverse of the Jacobian matrix, $[J]^{-1}$, Equation 5.7 becomes

$$
\begin{Bmatrix} \dfrac{\partial}{\partial x} \\ \dfrac{\partial}{\partial y} \end{Bmatrix}
= [J]^{-1}
\begin{Bmatrix} \dfrac{\partial}{\partial r} \\ \dfrac{\partial}{\partial s} \end{Bmatrix}.
$$

(5.8)

From the definition of a shape function, the coordinate transformation can be expressed as

$x = \Sigma N_i x_i$ and

$y = \Sigma N_i y_i$, $i = 1, 2, 3, \ldots\ldots$total number of nodes,   (5.9)

where x_i, y_i are the global x and y coordinates of the nodal points. The displacement within an element can be expressed as

$u = \Sigma N_i u_i$

$v = \Sigma N_i v_i$, $i = 1, 2, 3, \ldots\ldots$total number of nodes,   (5.10)

where u_i, v_i are the nodal displacements.

Therefore, from Equation 5.7 and Equation 5.9, the Jacobian matrix is given as

$$[J] = \begin{bmatrix} \dfrac{\partial x}{\partial r} & \dfrac{\partial y}{\partial r} \\[2ex] \dfrac{\partial x}{\partial s} & \dfrac{\partial y}{\partial s} \end{bmatrix} = \begin{bmatrix} J_{11} & J_{12} \\[2ex] J_{21} & J_{22} \end{bmatrix} \qquad (5.11)$$

where

$J_{11} = \Sigma (\partial N_i/\partial r) x_i$,

$J_{12} = \Sigma (\partial N_i/\partial r) y_i$,

$J_{21} = \Sigma (\partial N_i/\partial s) x_i$ and

$J_{22} = \Sigma (\partial N_i/\partial s) y_i$, $i = 1, 2, 3, \ldots$total number of nodes.

From Equation 5.10, the strain-displacement relations can be given as

$\varepsilon_x = \partial u/\partial x = \Sigma (\partial N_i/\partial x) u_i$

$\varepsilon_y = \partial v/\partial y = \Sigma (\partial N_i/\partial y) v_i$

and

$\gamma_{xy} = \partial u/\partial y + \partial v/\partial x = \Sigma\{(\partial N_i/\partial y) u_i + (\partial N_i/\partial x) v_i\}$ (5.12)

where

$$\partial N_i/\partial x = [1 \ 0] \ [J]^{-1} \begin{Bmatrix} \partial N_i/\partial r \\ \partial N_i/\partial s \end{Bmatrix}$$

$$\partial N_i/\partial y = [0 \ 1] \ [J]^{-1} \begin{Bmatrix} \partial N_i/\partial r \\ \partial N_i/\partial s \end{Bmatrix} \ , \ i = 1, \ 2, \ 3, \ \ldots \text{total number of nodes.}$$

Therefore, the strain-displacement matrix, B, for an element can be obtained from Equation 5.12. The elements of the strain-displacement matrices (B) for VISO10, VISL9 and VISR9 elements are given below.

Element VISO10

The strain-displacement matrix, B (3 x 20) for the VISO10 element obtained by Equation 5.12 can be explicitly expressed as

$$B_{1,1} = [1 \ 0] \ [J]^{-1} \begin{Bmatrix} 1/32 \ (9s^3-9s^2-s+1)+1/2(1-s)r \\ 1/32(1-r)(-27s^2+18s+1)+1/4(1-r^2) \end{Bmatrix}$$

$$B_{1,3} = [1 \ 0] \ [J]^{-1} \begin{Bmatrix} -r(1-s) \\ -1/2(1-r^2) \end{Bmatrix}$$

$$B_{1,5} = [1 \ 0] \ [J]^{-1} \begin{Bmatrix} 1/32(-9s^3+9s^2+s-1)+1/2(1-s)r \\ 1/32(1+r)(-27s^2+18s+1)+1/4(1-r^2) \end{Bmatrix}$$

$$B_{1,7} = [1 \ 0] \ [J]^{-1} \begin{Bmatrix} 1/2(1-s^2)+1/32(27s^3+7s^2-27s-7) \\ 1/32(81s^2+14s-27)(1+r)-s(1+r) \end{Bmatrix}$$

$$B_{1,9} = [1 \ 0] \ [J]^{-1} \begin{Bmatrix} 1/32(-27s^3-9s^2+27s+9) \\ 1/32(-81s^2-18s+27)(1+r) \end{Bmatrix}$$

$$B_{1,11} = [1 \ 0] \ [J]^{-1} \begin{Bmatrix} 1/32(9s^3+9s^2-s-1)+1/2(1+s) \\ 1/32(1+r)(27s^2+18s-1)-1/4(1-r^2) \end{Bmatrix}$$

$$B_{1,13} = [1 \ 0] \ [J]^{-1} \begin{Bmatrix} -r(1+s) \\ 1/2(1-r^2) \end{Bmatrix}$$

$$B_{1,15} = [1 \ 0] \ [J]^{-1} \begin{Bmatrix} 1/32(-9s^3-9s^2+s+1)+1/2(1+s)r \\ 1/32(1-r)(27s^2+18s-1)-1/4(1-r^2) \end{Bmatrix}$$

$$B_{1,17} = [1 \quad 0] \; [J]^{-1} \begin{Bmatrix} 1/32(27s^3+9s^2-27s-9) \\ 1/32(-81s^2-18s+27)(1-r) \end{Bmatrix}$$

$$B_{1,19} = [1 \quad 0] \; [J]^{-1} \begin{Bmatrix} 1/32(-27s^3+9s^2+27s-9) \\ 1/32(1-r)(81s^2-18s-27) \end{Bmatrix}$$

$$B_{2,2} = [0 \quad 1] \; [J]^{-1} \begin{Bmatrix} 1/32(9s^3-9s^2-s+1)+1/2(1-s)r \\ 1/32(1-r)(-27s^2+18s+1)+1/4(1-r^2) \end{Bmatrix}$$

$$B_{2,4} = [0 \quad 1] \; [J]^{-1} \begin{Bmatrix} -r(1-s) \\ -1/2(1-r^2) \end{Bmatrix}$$

$$B_{2,6} = [0 \quad 1] \; [J]^{-1} \begin{Bmatrix} 1/32(-9s^3+9s^2+s-1)+1/2(1-s)r \\ 1/32(1+r)(-27s^2+18s+1)+1/4(1-r^2) \end{Bmatrix}$$

$$B_{2,8} = [0 \quad 1] \; [J]^{-1} \begin{Bmatrix} 1/2(27s^3-9s^2-27s+9) \\ 1/32(81s^2+14s-27)(1+r)-s(1+r) \end{Bmatrix}$$

$$B_{2,10} = [0 \quad 1] \; [J]^{-1} \begin{Bmatrix} 1/32(-27s^3-9s^2+27s+9) \\ 1/32(-81s^2-18s+27)(1+r) \end{Bmatrix}$$

$$B_{2,12} = [0 \quad 1] \; [J]^{-1} \begin{Bmatrix} 1/32(9s^3+9s^2-s-1)+1/2(1+s) \\ 1/32(1+r)(27s^2+18s-1)-1/4(1-r^2) \end{Bmatrix}$$

$$B_{2,14} = [0 \quad 1] \; [J]^{-1} \begin{Bmatrix} -r(1+s) \\ 1/2(1-r^2) \end{Bmatrix}$$

$$B_{2,16} = [0 \quad 1] \; [J]^{-1} \begin{Bmatrix} 1/32(-9s^3-9s^2+s+1)+1/2(1+s)r \\ 1/32(1-r)(27s^2+18s-1)-1/4(1-r^2) \end{Bmatrix}$$

$$B_{2,18} = [0 \quad 1] \; [J]^{-1} \begin{Bmatrix} 1/32(27s^3+9s^2-27s-9) \\ 1/32(-81s^2-18s+27)(1-r) \end{Bmatrix}$$

$$B_{2,20} = [0 \quad 1] \; [J]^{-1} \begin{Bmatrix} 1/32(-27s^3+9s^2+27s-9) \\ 1/32(1-r)(81s^2-18s-27) \end{Bmatrix} .$$

$B_{3,1} = B_{2,2}, \quad B_{3,5} = B_{2,6}, \quad B_{3,9} = B_{2,10}, \quad B_{3,13} = B_{2,14}, \quad B_{3,17} = B_{2,18},$

$B_{3,2} = B_{1,1}, \quad B_{3,6} = B_{1,5}, \quad B_{3,10} = B_{1,9}, \quad B_{3,14} = B_{1,13}, \quad B_{3,18} = B_{1,17},$

$B_{3,3} = B_{2,4}, \quad B_{3,7} = B_{2,8}, \quad B_{3,11} = B_{2,12}, \quad B_{3,15} = B_{2,16}, \quad B_{3,19} =$

$B_{2,20}$, $B_{3,4} = B_{1,3}$, $B_{3,8} = B_{1,7}$, $B_{3,12} = B_{1,11}$, $B_{3,16} = B_{1,15}$, $B_{3,20}$

$= B_{1,19}$,

and

$B_{1,2} = B_{1,4} = B_{1,6} = B_{1,8} = B_{1,10} = B_{1,12} = B_{1,14} = B_{1,16} = B_{1,18} = B_{1,20}$

$= B_{2,1} = B_{2,3} = B_{2,5} = B_{2,7} = B_{2,9} = B_{2,11} = B_{2,13} = B_{2,15} = B_{2,17} =$

$B_{2,19} = 0$.

Element VISL9

The strain-displacement matrix, B (3 x 18) for the VISL9 element obtained by Equation 5.12 can be explicitly expressed as

$$B_{1,1} = [1 \ 0] \ [J]^{-1} \begin{Bmatrix} 1/32(9s^3-9s^2-s+1)+1/2(1-s)r \\ 1/32(1-r)(-27s^2+18s+1)-1/4(1-r^2) \end{Bmatrix}$$

$$B_{1,3} = [1 \ 0] \ [J]^{-1} \begin{Bmatrix} -r(1-s) \\ -1/2(1-r^2) \end{Bmatrix}$$

$$B_{1,5} = [1 \ 0] \ [J]^{-1} \begin{Bmatrix} 1/4(s^2-s+2r-2rs) \\ 1/4(1+r)(r+2s) \end{Bmatrix}$$

$$B_{1,7} = [1 \ 0] \ [J]^{-1} \begin{Bmatrix} 1/2(1-s^2) \\ -s(1+r) \end{Bmatrix}$$

$$B_{1,9} = [1 \ 0] \ [J]^{-1} \begin{Bmatrix} 1/4(s^2+s+2r+2rs) \\ 1/4(1+r)(r+2s) \end{Bmatrix}$$

$$B_{1,11} = [1 \ 0] \ [J]^{-1} \begin{Bmatrix} -r(1+s) \\ 1/2(1-r^2) \end{Bmatrix}$$

$$B_{1,13} = [1 \ 0] \ [J]^{-1} \begin{Bmatrix} 1/32(-9s^3-9s^2+s+1)+1/2(1+s)r \\ 1/32(1-r)(27s^2+18s-1)-1/4(1-r^2) \end{Bmatrix}$$

$$B_{1,15} = [1 \ 0] \ [J]^{-1} \begin{Bmatrix} 1/32(27s^3+9s^2-27s-9) \\ 1/32(-81s^2-18s+27)(1-r) \end{Bmatrix}$$

$$B_{1,17} = [1 \ 0] \ [J]^{-1} \begin{Bmatrix} 1/32(-27s^3+9s^2+27s-9) \\ 1/32(81s^2-18s-27)(1-r) \end{Bmatrix}$$

$$B_{2,2} = [0 \ 1] \ [J]^{-1} \begin{Bmatrix} 1/32(9s^3-9s^2-s+1)+1/2(1-s)r \\ 1/32(1-r)(-27s^2+18s+1)-1/4(1-r^2) \end{Bmatrix}$$

$$B_{2,4} = [0 \ 1] \ [J]^{-1} \begin{Bmatrix} -r(1-s) \\ -1/2(1-r^2) \end{Bmatrix}$$

$$B_{2,6} = [0 \ 1] \ [J]^{-1} \begin{Bmatrix} 1/4(s^2-s+2r-2rs) \\ 1/4(1+r)(r+2s) \end{Bmatrix}$$

$$B_{2,8} = [0 \ 1] \ [J]^{-1} \begin{Bmatrix} 1/2(1-s^2) \\ -s(1+r) \end{Bmatrix}$$

$$B_{2,10} = [0 \ 1] \ [J]^{-1} \begin{Bmatrix} 1/4(s^2+s+2r+2rs) \\ 1/4(1+r)(r+2s) \end{Bmatrix}$$

$$B_{2,12} = [0 \ 1] \ [J]^{-1} \begin{Bmatrix} -r(1+s) \\ 1/2(1-r^2) \end{Bmatrix}$$

$$B_{2,14} = [0 \ 1] \ [J]^{-1} \begin{Bmatrix} 1/32(-9s^3-9s^2+s+1)+1/2(1+s)r \\ 1/32(1-r)(27s^2+18s-1)-1/4(1-r^2) \end{Bmatrix}$$

$$B_{2,16} = [0 \ 1] \ [J]^{-1} \begin{Bmatrix} 1/32(27s^3+9s^2-27s-9) \\ 1/32(-81s^2-18s+27)(1-r) \end{Bmatrix}$$

$$B_{2,18} = [0 \ 1] \ [J]^{-1} \begin{Bmatrix} 1/32(-27s^3+9s^2+27s-9) \\ 1/32(81s^2-18s-27)(1-r) \end{Bmatrix} .$$

$B_{3,1} = B_{2,2}, \quad B_{3,5} = B_{2,6}, \quad B_{3,9} = B_{2,10}, \quad B_{3,13} = B_{2,14}, \quad B_{3,17} = B_{2,18},$

$B_{3,2} = B_{1,1}, \quad B_{3,6} = B_{1,5}, \quad B_{3,10} = B_{1,9}, \quad B_{3,14} = B_{1,13}, \quad B_{3,18} = B_{1,17},$

$B_{3,3} = B_{2,4}, \quad B_{3,7} = B_{2,8}, \quad B_{3,11} = B_{2,12}, \quad B_{3,15} = B_{2,16}, \quad B_{3,4} = B_{1,3},$

$B_{3,8} = B_{1,7}, \quad B_{3,12} = B_{1,11}, \quad B_{3,16} = B_{1,15},$

and

$B_{1,2} = B_{1,4} = B_{1,6} = B_{1,8} = B_{1,10} = B_{1,12} = B_{1,14} = B_{1,16} = B_{1,18} = B_{2,1}$

$= B_{2,3} = B_{2,5} = B_{2,7} = B_{2,9} = B_{2,11} = B_{2,13} = B_{2,15} = B_{2,17} = 0.$

Element VISR9

The strain-displacement matrix, B (3 x 18) for the VISR9 element obtained by Equation 5.12 can be explicitly expressed as

$$B_{1,1} = [1 \ 0] \ [J]^{-1} \begin{Bmatrix} 1/4(1-s)(2r+s) \\ 1/4(1-r)(r+2s) \end{Bmatrix}$$

$$B_{1,3} = [1 \ 0] \ [J]^{-1} \begin{Bmatrix} -r(1-s) \\ -1/2(1-r^2) \end{Bmatrix}$$

$$B_{1,5} = [1 \ 0] \ [J]^{-1} \begin{Bmatrix} 1/32(-9s^3+9s^2+s-1)+1/2(1-s)r \\ 1/32(1+r)(-27s^2+18s+1)+1/4(1-r^2) \end{Bmatrix}$$

$$B_{1,7} = [1 \ 0] \ [J]^{-1} \begin{Bmatrix} 1/32(27s^3-9s^2-27s+9) \\ 1/32(81s^2-18s-27)(1+r) \end{Bmatrix}$$

$$B_{1,9} = [1 \ 0] \ [J]^{-1} \begin{Bmatrix} 1/32(-27s^3-9s^2+27s+9) \\ 1/32(-81s^2-18s+27)(1+r) \end{Bmatrix}$$

$$B_{1,11} = [1 \ 0] \ [J]^{-1} \begin{Bmatrix} 1/32(9s^3+9s^2-s-1)+1/2(1+s)r \\ 1/32(1+r)(27s^2+18s-1)-1/4(1-r^2) \end{Bmatrix}$$

$$B_{1,13} = [1 \ 0] \ [J]^{-1} \begin{Bmatrix} -r(1+s) \\ 1/2(1-r^2) \end{Bmatrix}$$

$$B_{1,15} = [1 \ 0] \ [J]^{-1} \begin{Bmatrix} 1/4(1+s)(2r-s) \\ 1/4(1-r)(2s-r) \end{Bmatrix}$$

$$B_{1,17} = [1 \ 0] \ [J]^{-1} \begin{Bmatrix} -1/2(1-s^2) \\ -s(1-r) \end{Bmatrix}$$

$$B_{2,2} = [0 \ 1] \ [J]^{-1} \begin{Bmatrix} 1/4(1-s)(2r+s) \\ 1/4(1-r)(r+2s) \end{Bmatrix}$$

$$B_{2,4} = [0 \ 1] \ [J]^{-1} \begin{Bmatrix} -r(1-s) \\ -1/2(1-r^2) \end{Bmatrix}$$

$$B_{2,6} = [0 \ 1] \ [J]^{-1} \begin{Bmatrix} 1/32(-9s^3+9s^2+s-1)+1/2(1-s)r \\ 1/32(1+r)(-27s^2+18s+1)+1/4(1-r^2) \end{Bmatrix}$$

$$B_{2,8} = [0 \ 1] \ [J]^{-1} \begin{Bmatrix} 1/32(27s^3 - 9s^2 - 27s + 9) \\ 1/32(81s^2 - 18s - 27)(1+r) \end{Bmatrix}$$

$$B_{2,10} = [0 \ 1] \ [J]^{-1} \begin{Bmatrix} 1/32(-27s^3 - 9s^2 + 27s + 9) \\ 1/32(-81s^2 - 18s + 27)(1+r) \end{Bmatrix}$$

$$B_{2,12} = [0 \ 1] \ [J]^{-1} \begin{Bmatrix} 1/32(9s^3 + 9s^2 - s - 1) + 1/2(1+s)r \\ 1/32(1+r)(27s^2 + 18s - 1) - 1/4(1-r^2) \end{Bmatrix}$$

$$B_{2,14} = [0 \ 1] \ [J]^{-1} \begin{Bmatrix} -r(1+s) \\ 1/2(1-r^2) \end{Bmatrix}$$

$$B_{2,16} = [0 \ 1] \ [J]^{-1} \begin{Bmatrix} 1/4(1+s)(2r-s) \\ 1/4(1-r)(2s-r) \end{Bmatrix}$$

$$B_{2,18} = [0 \ 1] \ [J]^{-1} \begin{Bmatrix} -1/2(1-s^2) \\ -s(1-r) \end{Bmatrix} .$$

$B_{3,1} = B_{2,2}, \quad B_{3,5} = B_{2,6}, \quad B_{3,9} = B_{2,10}, \quad B_{3,13} = B_{2,14}, \quad B_{3,17} = B_{2,18},$

$B_{3,2} = B_{1,1}, \quad B_{3,6} = B_{1,5}, \quad B_{3,10} = B_{1,9}, \quad B_{3,14} = B_{1,13}, \quad B_{3,18} = B_{1,17},$

$B_{3,3} = B_{2,4}, \quad B_{3,7} = B_{2,8}, \quad B_{3,11} = B_{2,12}, \quad B_{3,15} = B_{2,16}, \quad B_{3,4} = B_{1,3},$

$B_{3,8} = B_{1,7}, \quad B_{3,12} = B_{1,11}, \quad B_{3,16} = B_{1,15},$

and

$B_{1,2} = B_{1,4} = B_{1,6} = B_{1,8} = B_{1,10} = B_{1,12} = B_{1,14} = B_{1,16} = B_{1,18} = B_{2,1}$

$= B_{2,3} = B_{2,5} = B_{2,7} = B_{2,9} = B_{2,11} = B_{2,13} = B_{2,15} = B_{2,17} = 0.$

Formulation of the Stiffness Matrices (k)

The stiffness matrices for the elements VISO10, VISL9 and VISR9 can be formulated as (101)

$$[k] = \int [B]^T [D] [B] \ dV \tag{5.13}$$

where $[k]$ = element stiffness matrix, $[B]$ = strain-displacement matrix and $[D]$ = stress-strain relationship matrix. For a constant thickness, t of the element

$$[k] = t \int [B]^T [D][B] \ dA \tag{5.14}$$

or

$$[k] = t \iint [B]^T [D][B] \ dxdy. \tag{5.15}$$

The above expression can be expressed in terms of the local (r, s) co-ordinate system as

$$[k] = t \iint [B]^T [D][B] det[J] \ drds. \tag{5.16}$$

The above equation can be integrated by Gaussian numerical integration formulae to obtain the stiffness matrix.

Performance of the Elements
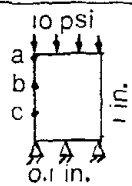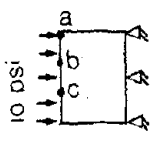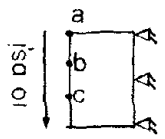
Two example problems have been considered to evaluate the performance of the variable-node-number elements. At this point, the ability of these elements to predict the correct displacements is examined. The accuracy of the elements in predicting correct stresses is tested after the optimal stress points are determined. This is discussed in the next section.

Example 1

A single ten noded variable-node-number element VISO10 is tested for vertical, horizontal and shear loads. The vertical and horizontal dimensions of the element are 1 inch and 0.1 inch, respectively. The modulus of elasticity and Poisson's ratio of the material are assumed to be 1000 psi and 0.30, respectively. Displacements at three different locations for each of the three loading conditions are computed. A two-dimensional 12 noded regular cubic element having the same dimensions and the same material properties as the variable-node-number element is ana-lyzed for the three loading conditions. The magnitude of the loads ap-plied on the cubic element is same as the magnitude of the loads applied on the variable-node-number element. The displacements in the

variable-node-number element are compared with the corresponding dis-
placements in the regular cubic element. The results of the comparative
study is given in Table 5.1. The comparative study shows that the dis-
placements obtained by variable-node-number elements are in good agree-
ment with that obtained by regular cubic elements. This agreement between
the displacements indicates that the variable-node-number elements are
capable of predicting displacements accurately.

Table 5.1. Comparison of Displacements Obtained From General
Cubic Element and Ten Noded Variable-Node-Number
Element (VISO10)

Loading	Points	Horizontal Displ.(in)		Vertical Displ.(in)	
		10 Noded	12 Noded	10 Noded	12 Noded
	a	-0.230×10^{-2}	-0.230×10^{-2}	-0.898×10^{-1}	-0.898×10^{-1}
	b	-0.186×10^{-2}	-0.187×10^{-2}	-0.595×10^{-1}	-0.595×10^{-1}
	c	-0.220×10^{-2}	-0.220×10^{-2}	-0.287×10^{-1}	-0.287×10^{-1}
	a	0.851×10^{-3}	0.851×10^{-3}	0.554×10^{-3}	0.554×10^{-3}
	b	0.743×10^{-3}	0.743×10^{-3}	-0.123×10^{-4}	-0.124×10^{-4}
	c	0.743×10^{-3}	0.743×10^{-3}	0.123×10^{-4}	0.124×10^{-4}
	a	-0.751×10^{-3}	-0.751×10^{-3}	-0.291×10^{-2}	-0.291×10^{-2}
	b	0.119×10^{-3}	0.119×10^{-3}	-0.260×10^{-2}	-0.260×10^{-2}
	b	-0.119×10^{-3}	-0.119×10^{-3}	-0.260×10^{-2}	-0.260×10^{-2}

Example 2

In this example, the combined behavior of the three types of the
variable-node-number elements (VISO10, VISL9, VISR9) is studied. A
continuum is modelled by the above mentioned elements. The geometry of
the mesh and the loading conditions are shown in Figure 5.15. The modulus
of elasticity and Poisson's ratio of the material are assumed to be 2000
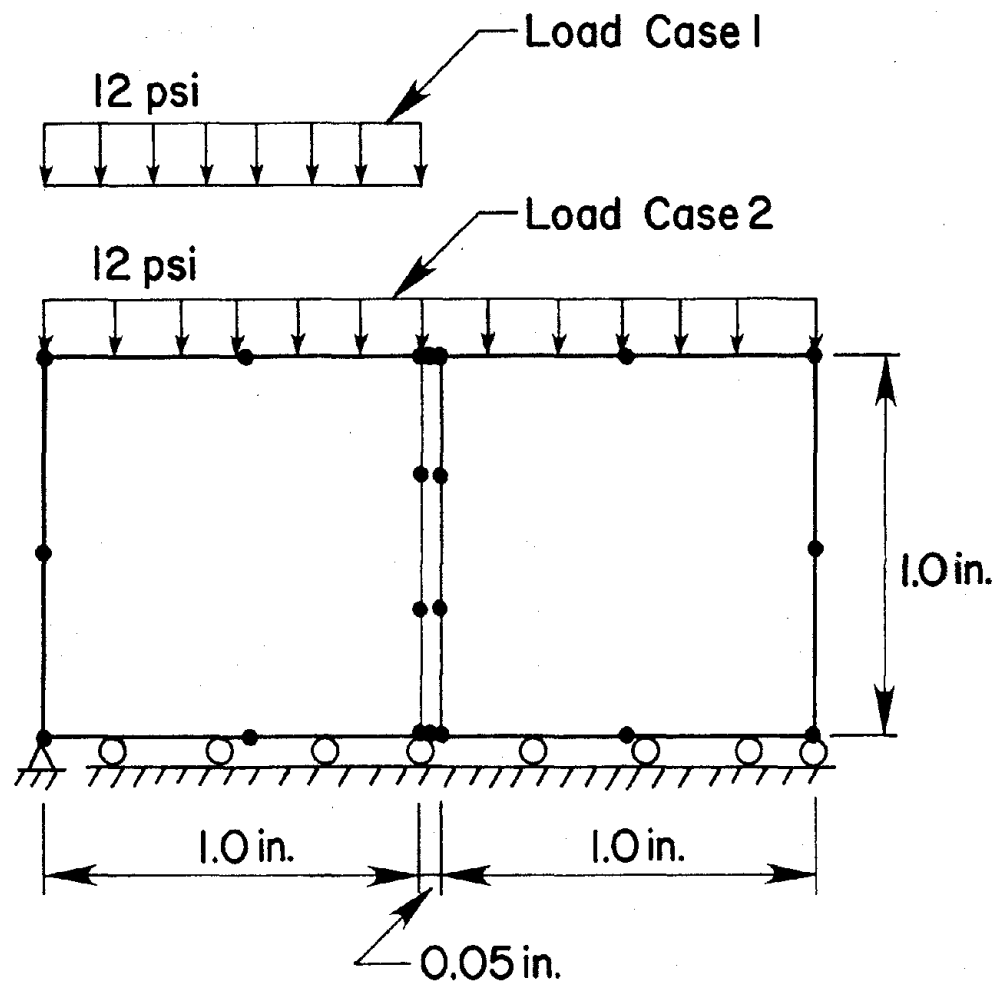
Figure 5.15 Finite Element Mesh of Three Different Types of
Variable-Node-Number Elements

psi and 0.25 respectively. The same continuum is also modelled by regular quadratic elements. The vertical displacements at the top along the horizontal direction are plotted for both the loading cases and are shown in Figure 5.16. The results obtained by variable-node-number elements completely coincide with the results obtained by quadratic elements. This shows that the newly developed elements are capable of predicting the displacements accurately.

Optimal Stress Points

In finite elements, there exist unique points at which the stresses have higher accuracy than at any other points. These points are called optimal stress points. The stresses at these points have the same degree of accuracy as the nodal displacements. The reasons for the presence of optimal stress points and a procedure to determine the locations of such points for general isoparametric elements are discussed by Barlow (22). It has been shown in this research that Barlow's procedure to locate the optimal stress points can be used for variable-node-number elements also.

In this study, the main objective behind developing the ten noded variable-node-number element (VISO10) was to use it for modelling the collar joint at the interfaces of composite masonry walls. On the other hand, the nine noded variable-node-number elements are essentially developed to serve as transition elements in the finite element mesh. For this reason, optimal stress points have been determined only for the ten noded (VISO10) element. The procedure and associated calculations for determining the optimal stress points for VISO10 element are given below.
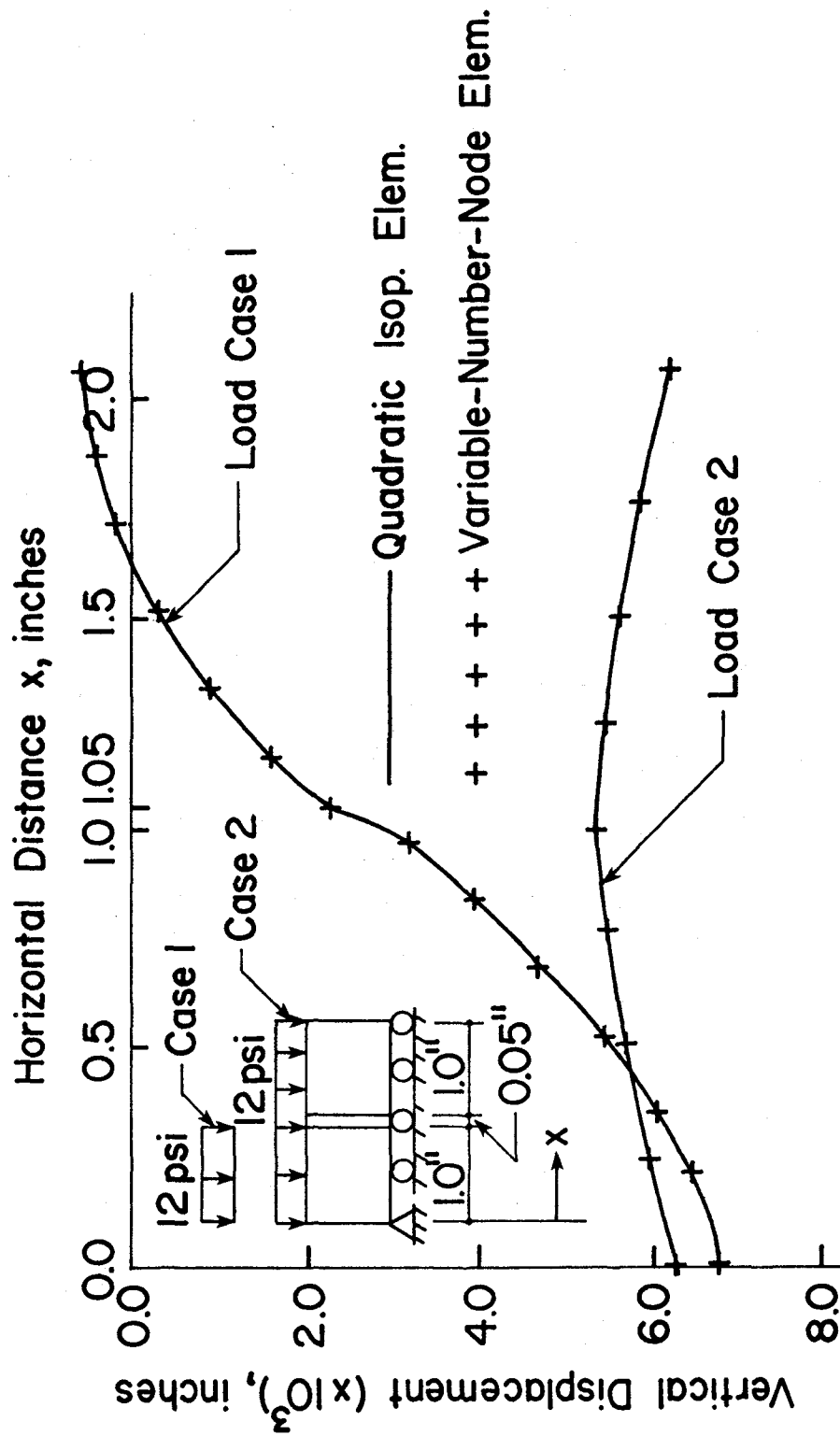
Figure 5.16 Vertical Displacements at the Top along the
Horizontal Direction

VISO10 Element

The displacement function, ϕ_a for this element contains polynomial terms up to a complete quadratic with three additional cubic and one additional fourth order terms and thus

$$\phi_a = \alpha_1 + \alpha_2 r + \alpha_3 s + \alpha_4 r^2 + \alpha_5 rs + \alpha_6 s^2 + \alpha_7 r^2 s + \alpha_8 rs^2 + \alpha_9 s^3 + \alpha_{10} rs^3 \qquad (5.17)$$

where α's are the coefficients and r, s are the non-dimensional coordinates measured from the center. The suffix a is used to denote the displacement field which can be exactly represented, in all respects, by the function. The above displacement function can be written in the form

$$[u_a, v_a] = [1, r, s, r^2, rs, s^2, r^2 s, rs^2, s^3, rs^3] \, [\alpha_u, \alpha_v] \qquad (5.18)$$

It has been stated in Chapter III that the displacement field of composite masonry walls supported at the bottom and horizontally restrained at the top is cubic. Since, VISO10 elements will be used to discretize the composite masonry walls, these elements will model a cubic displacement field of the form

$$[u_b, v_b] = [1, r, s, r^2, rs, s^2, r^3, r^2 s, rs^2, s^3] \, [\beta_u, \beta_v] \qquad (5.19)$$

where β's are the coefficients and suffix b is used to denote the displacement field which is required to be represented.

The nodal displacements $[u_a, v_a]$ in the element field may be derived in terms of α's, by inserting the relevant nodal co-ordinates in Equation 5.18. This can be written in the form

$$[u_a, v_a] = [A] \, [\alpha_u, \alpha_v] \qquad (5.20)$$

where

$$[A] = \begin{bmatrix} 1 & -1 & -1 & 1 & 1 & 1 & -1 & -1 & -1 & 1 \\ 1 & 0 & -1 & 0 & 0 & 1 & 0 & 0 & -1 & 0 \\ 1 & 1 & -1 & 1 & -1 & 1 & -1 & 1 & -1 & -1 \\ 1 & 1 & -1/3 & 1 & -1/3 & 1/9 & -1/3 & 1/9 & -1/27 & -1/27 \\ 1 & 1 & 1/3 & 1 & 1/3 & 1/9 & 1/3 & 1/9 & 1/27 & 1/27 \\ 1 & 1 & 1 & 1 & 1 & 1 & 1 & 1 & 1 & 1 \\ 1 & 0 & 1 & 0 & 0 & 1 & 0 & 0 & 1 & 0 \\ 1 & -1 & 1 & 1 & -1 & 1 & 1 & -1 & 1 & -1 \\ 1 & -1 & 1/3 & 1 & -1/3 & 1/9 & 1/3 & -1/9 & 1/27 & -1/27 \\ 1 & -1 & -1/3 & 1 & 1/3 & 1/9 & -1/3 & -1/9 & -1/27 & 1/27 \end{bmatrix} . \qquad (5.21)$$

Similarly in the required field from Equation 5.19

$$[u_b, v_b] = [B] \, [\beta_u, \beta_v] \qquad (5.22)$$

where

$$[B] = \begin{bmatrix} 1 & -1 & -1 & 1 & 1 & 1 & -1 & -1 & -1 & -1 \\ 1 & 0 & -1 & 0 & 0 & 1 & 0 & 0 & 0 & -1 \\ 1 & 1 & -1 & 1 & -1 & 1 & 1 & -1 & 1 & -1 \\ 1 & 1 & -1/3 & 1 & -1/3 & 1/9 & 1 & -1/3 & 1/9 & -1/27 \\ 1 & 1 & 1/3 & 1 & 1/3 & 1/9 & 1 & 1/3 & 1/9 & 1/27 \\ 1 & 1 & 1 & 1 & 1 & 1 & 1 & 1 & 1 & 1 \\ 1 & 0 & 1 & 0 & 0 & 1 & 0 & 0 & 0 & 1 \\ 1 & -1 & 1 & 1 & -1 & 1 & -1 & 1 & -1 & 1 \\ 1 & -1 & 1/3 & 1 & -1/3 & 1/9 & -1 & 1/3 & -1/9 & 1/27 \\ 1 & -1 & -1/3 & 1 & 1/3 & 1/9 & -1 & -1/3 & -1/9 & -1/27 \end{bmatrix} . \qquad (5.23)$$

If the element is capable of representing the nodal displacements in the field to a good degree of accuracy then the values of the two nodal displacements in Equations 5.20 and 5.22 may be approximately equated

$$[A] \, [\alpha_u, \alpha_v] = [B] \, [\beta_u, \beta_v] \qquad (5.24)$$

which gives

$$[\alpha_u, \alpha_v] = [A]^{-1}[B] \, [\beta_u, \beta_v] \qquad (5.25)$$

where

$$[A]^{-1}[B] = \begin{bmatrix} 1 & 0 & 0 & 0 & 0 & 0 & 0 & 0 & 0 & 0 \\ 0 & 1 & 0 & 0 & 0 & 0 & 1 & 0 & 0 & 0 \\ 0 & 0 & 1 & 0 & 0 & 0 & 0 & 0 & 0 & 0 \\ 0 & 0 & 0 & 1 & 0 & 0 & 0 & 0 & 0 & 0 \\ 0 & 0 & 0 & 0 & 1 & 0 & 0 & 0 & 0 & 0 \\ 0 & 0 & 0 & 0 & 0 & 1 & 0 & 0 & 0 & 0 \\ 0 & 0 & 0 & 0 & 0 & 0 & 0 & 1 & 0 & 0 \\ 0 & 0 & 0 & 0 & 0 & 0 & 0 & 0 & 1 & 0 \\ 0 & 0 & 0 & 0 & 0 & 0 & 0 & 0 & 0 & 1 \\ 0 & 0 & 0 & 0 & 0 & 0 & 0 & 0 & 0 & 0 \end{bmatrix} . \qquad (5.26)$$

The derivatives of the displacements, required in the calculation of the strains, are

$$\begin{bmatrix} \dfrac{\partial u}{\partial x} & \dfrac{\partial v}{\partial x} \\[2mm] \dfrac{\partial u}{\partial y} & \dfrac{\partial v}{\partial y} \end{bmatrix} = \begin{bmatrix} \dfrac{\partial r}{\partial x} & \dfrac{\partial s}{\partial x} \\[2mm] \dfrac{\partial r}{\partial y} & \dfrac{\partial s}{\partial y} \end{bmatrix} \begin{bmatrix} \dfrac{\partial u}{\partial r} & \dfrac{\partial v}{\partial r} \\[2mm] \dfrac{\partial u}{\partial s} & \dfrac{\partial v}{\partial s} \end{bmatrix} \qquad (5.27)$$

where

$$[u, v] = [u_a, v_a] \text{ or } [u_b, v_b].$$

The Jacobian of r and s with respect to x and y is independent of the strain field and is function of element geometry only. The strains, and hence the stresses, in the two fields are equal when the derivatives of the displacements, with respect to the non-dimensional coordinates are equal. The derivatives of the displacements are

$$\begin{bmatrix} \dfrac{\partial u_a}{\partial r} & \dfrac{\partial v_a}{\partial r} \\[2mm] \dfrac{\partial u_a}{\partial s} & \dfrac{\partial v_a}{\partial s} \end{bmatrix} = \begin{bmatrix} 0 & 1 & 0 & 2r & s & 0 & 2rs & s^2 & 0 & s^3 \\ 0 & 0 & 1 & 0 & r & 2s & r^2 & 2rs & 3s^2 & 3rs^2 \end{bmatrix} \begin{Bmatrix} \alpha_u \\ \alpha_v \end{Bmatrix} \qquad (5.28)$$

and

$$\begin{bmatrix} \dfrac{\partial u_b}{\partial r} & \dfrac{\partial v_b}{\partial r} \\[2mm] \dfrac{\partial u_b}{\partial s} & \dfrac{\partial v_b}{\partial s} \end{bmatrix} = \begin{bmatrix} 0 & 1 & 0 & 2r & s & 0 & 3r^2 & 2rs & s^2 & 0 \\ 0 & 0 & 1 & 0 & r & 2s & 0 & r^2 & 2rs & 3s^2 \end{bmatrix} \begin{Bmatrix} \beta_u \\ \beta_v \end{Bmatrix}. \qquad (5.29)$$

Equating Equations 5.28 and 5.29 and substituting for $[\alpha_u, \alpha_v]$ from Equation 5.25 yields

$$\begin{bmatrix} 0 & 1 & 0 & 2r & s & 0 & 1 & 2rs & s^2 & 0 \\ 0 & 0 & 1 & 0 & r & 2s & 0 & r^2 & 2rs & 3s^2 \end{bmatrix} \begin{Bmatrix} \beta_u \\ \beta_v \end{Bmatrix} =$$
$$\begin{bmatrix} 0 & 1 & 0 & 2r & s & 0 & 3r^2 & 2rs & s^2 & 0 \\ 0 & 0 & 1 & 0 & r & 2s & 0 & r^2 & 2rs & 3s^2 \end{bmatrix} \begin{Bmatrix} \beta_u \\ \beta_v \end{Bmatrix}. \qquad (5.30)$$

The above equation is satisfied for all values of β's, only when

$$r = \pm 1/\sqrt{3}. \qquad (5.31)$$

Hence, if the element is used to represent a general cubic displacement field, the stresses at any point along the two lines within the element drawn at $r = \pm 1/\sqrt{3}$ will have the same degree of accuracy as the nodal displacements. It should be noted that the displacement function of the element in the vertical direction is cubic and hence the optimal stress locations are independent of s when the element is used to represent a cubic displacement field.

Examples

Several examples are now presented which demonstrate the importance and use of optimal stress locations. In these examples, cantilever beams

are modelled by quadratic and cubic-quadratic (VISO10) elements. The beams are subjected to axial loads, tranverse loads at the free ends, uniformly distributed vertical loads and moments at the free ends.

In the first example, it is shown that the stresses anywhere within the element is correct when the order of the displacement function of the element is more than or equal to the order of the displacement field of the problem. The rest of the examples show that the stresses are correct only at the optimal stress locations when the order of the displacement function of the element is less than the order of the displacement field of the problem. Other than the first example problem which is modelled by quadratic elements, all the other example problems are modelled by ten noded variable-node-number element (VISO10).

Example 1

A cantilever beam, 10 inches long and 2 inches deep is analyzed using a mesh of 5 quadratic isoparametric plane stress elements as shown in Figure 5.17. The beam is subjected to an end moment and an axial load separately. For both the loading cases, stresses are calculated at 30 different locations within each element. The locations of these points in the local coordinates (r,s) are r = -0.77459, -0.57735, 0.0, 0.57735, 0.77459 and s = 0.0, 0.2, 0.4, 0.57735, 0.77459, 0.9.

The normal and shearing stresses within each element at all the 30 locations are compared with the corresponding stresses based upon single beam theory. The stresses for both the load cases obtained by finite element analysis are in excellent agreement with those obtained by beam theory. A cantilever beam subjected to pure bending and axial loads produces quadratic and linear displacement fields repectively. The quadratic element which is used to model the beam has terms of a complete
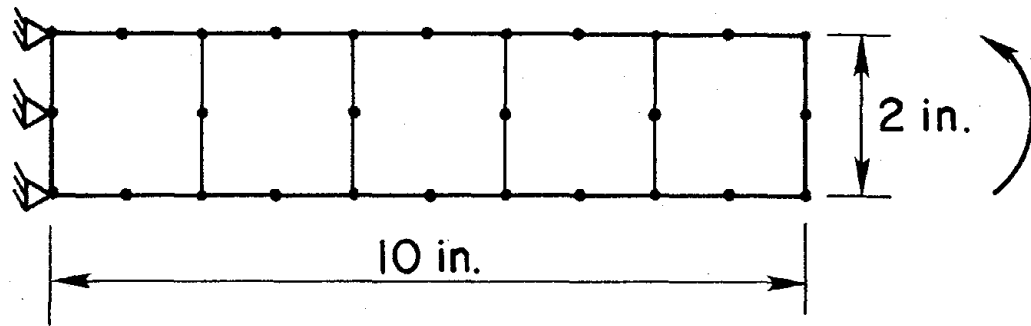
(a)
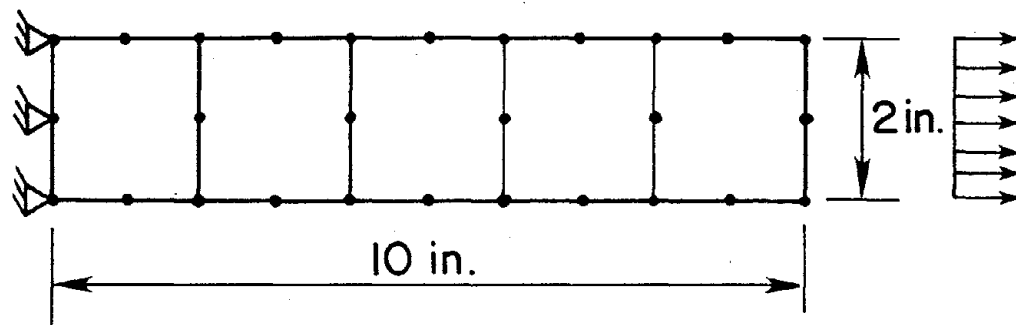
(b)

Figure 5.17   Finite Element Mesh of the Cantilever Beam

quadratic polynomial in its displacement function. Therefore, the representation of the beam by quadratic elements is exact in all its attributes and hence, in this situation optimal stress locations are not necessary to find the correct stresses, rather the stresses are correct everywhere within the element.

Example 2

Shearing stresses in a cantilever beam subjected to a concentrated load at its free end are computed using a mesh of 8 rectangular 10 noded variable-node-number elements (VISO10). Stresses are calculated at many arbitrary points within each element. In Figures 5.18 and 5.19, the shear stress variation along the horizontal axis at s = 0.77459 and 0.9 are plotted, respectively. These stresses are wildly oscillatory and hence it is important to know the optimal stress locations for such elements to predict the acceptable stresses.

The shearing stress distributions along the horizontal axis of the beam at s = 0.77459 and 0.9 are computed from beam theory and are plotted on the shearing stress distribution curves at s = 0.77459 and 0.9 obtained from finite element analysis. The theoretical curves intersect with the finite element curves at two points in each element. At a distance sufficiently away from the support, these intersection points within each element are at $r = \pm 1/\sqrt{3}$ (location of optimal stress points determined earlier). This shows that the stresses obtained by a mesh of VISO10 elements at $r = \pm 1/\sqrt{3}$ for any value of s are same as those given by beam theory at those locations. The cantilever beam subjected to a concentrated load at the free end has cubic displacement fields in both the horizontal and vertical directions. VISO10 elements have a cubic displacement function along the vertical direction and a quadratic
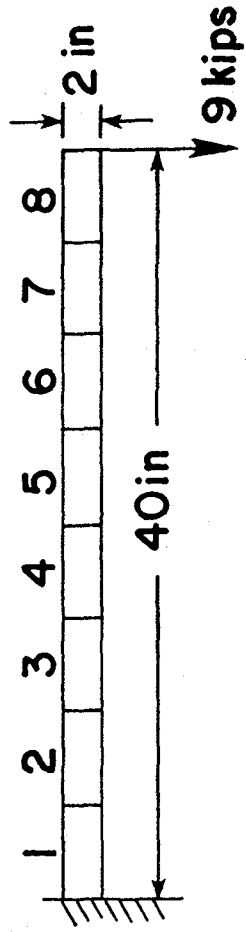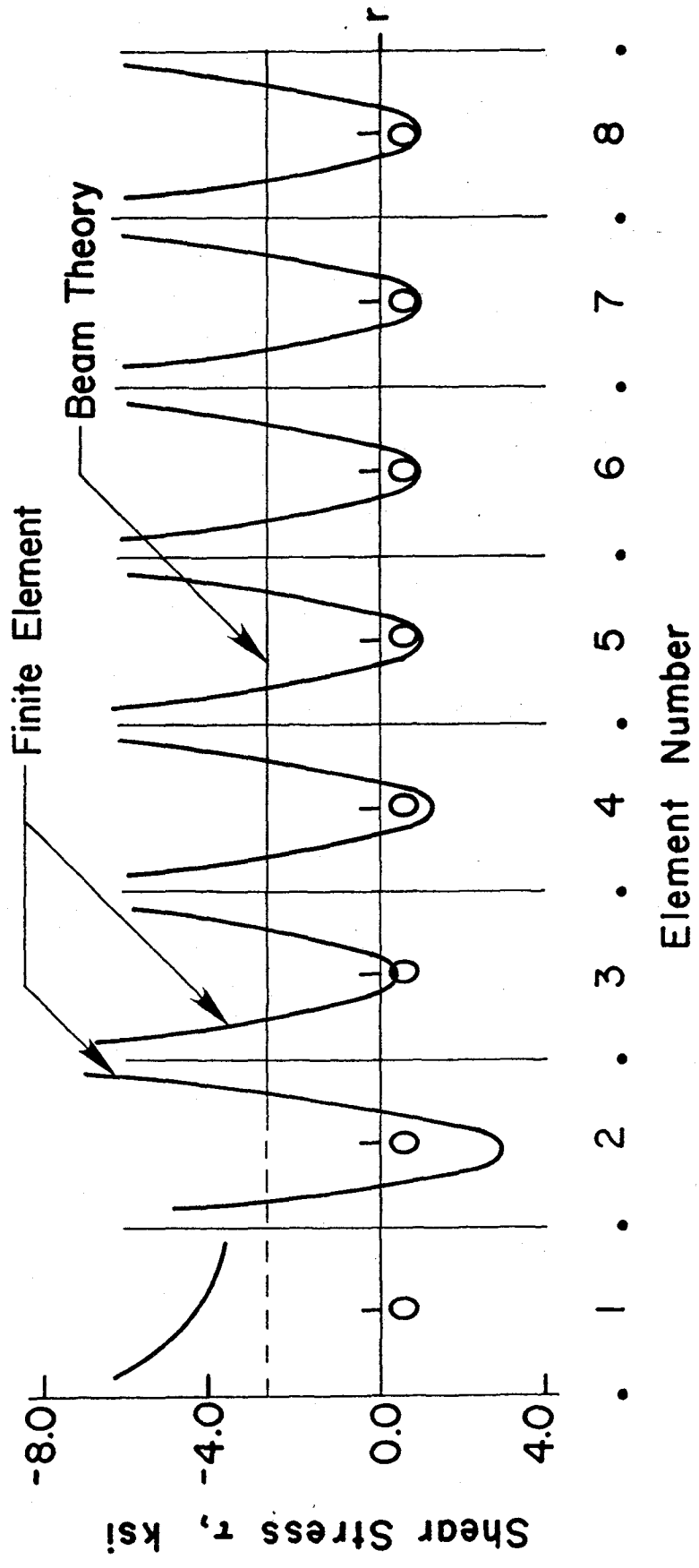
Figure 5.18 Variation of Shear Stress τ along s = 0.77459 for
a Cantilever Beam Subjected to a Concentrated Load
at the Free End
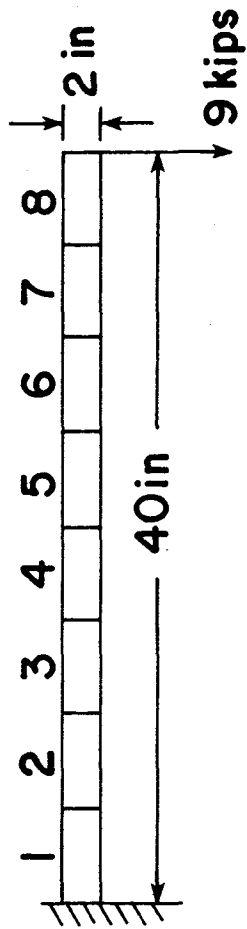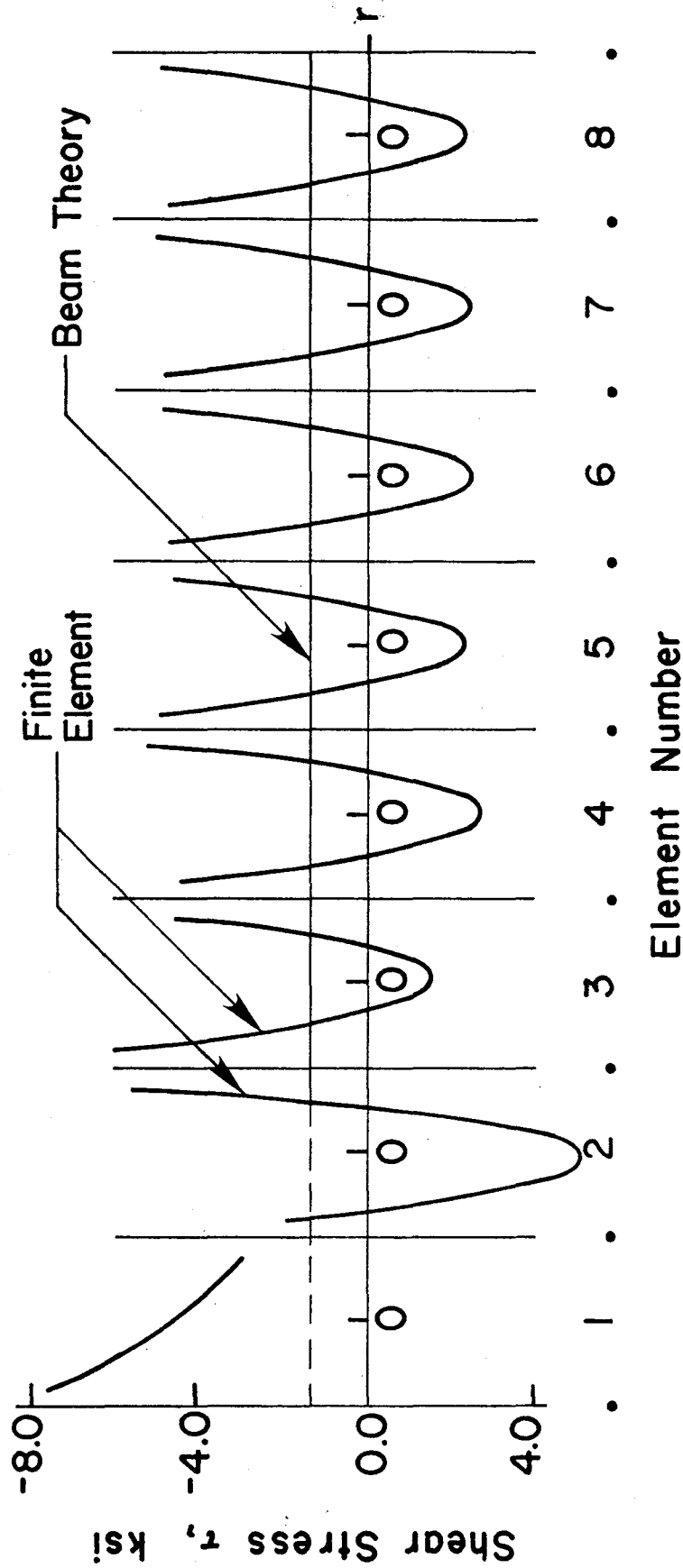
Figure 5.19 Variation of Shear Stress τ along s = 0.9 for a
Cantilever Beam Subjected to a Concentrated
Load at the Free End

displacement function along the horizontal direction. Therefore, VISO10 elements can represent the displacement field in the vertical direction exactly and hence optimal stress locations are independent of s. On the other hand, the order of the displacement field in the horizontal direction is more than the order of the displacement polynomial of the element. Therefore, the optimal stress locations are dependent upon r and it is necessary to know the locations of optimal stress points for accurate prediction of stresses.

Example 3

A cantilever beam in this example is modelled by 8 rectangular 10 noded variable-node-number isoparametric elements as shown in example 2. The beam in this case is subjected to uniformly distributed loads over its entire length. Shear stress distributions along the horizontal axis at s = 0.0 and 0.77459 are obtained by beam theory and finite element analysis and are plotted. These are shown in Figures 5.20 and 5.21. The shear stresses are extremely oscillatory; however, acceptable values of stresses exist at the optimal stress locations.

It is now known that the optimal stress locations for VISO10 elements are at $r = \pm 1/\sqrt{3}$ and independent of s. Figures 5.20 and 5.21 show that at a distance sufficiently away from the support, the computed shear stresses (finite element solution) are indistinguishable from the theoretical stresses (beam theory solution) at the optimal stress locations.

Efficiency of VISO10 Element in Modelling Composite Masonry Walls

The performance of 10 noded variable-node-number elements (VISO10) when used to model composite masonry walls is studied. In this study, composite walls with 2 inch collar joints are modelled and only the
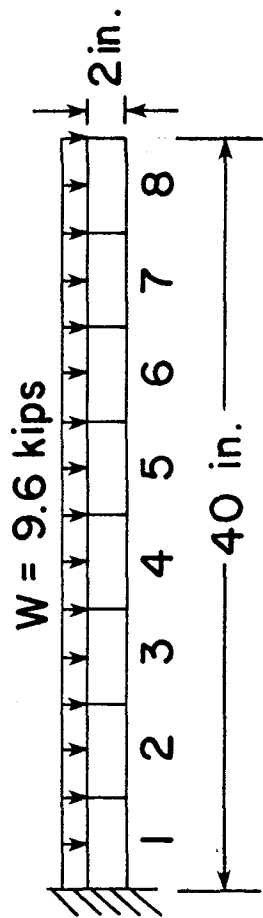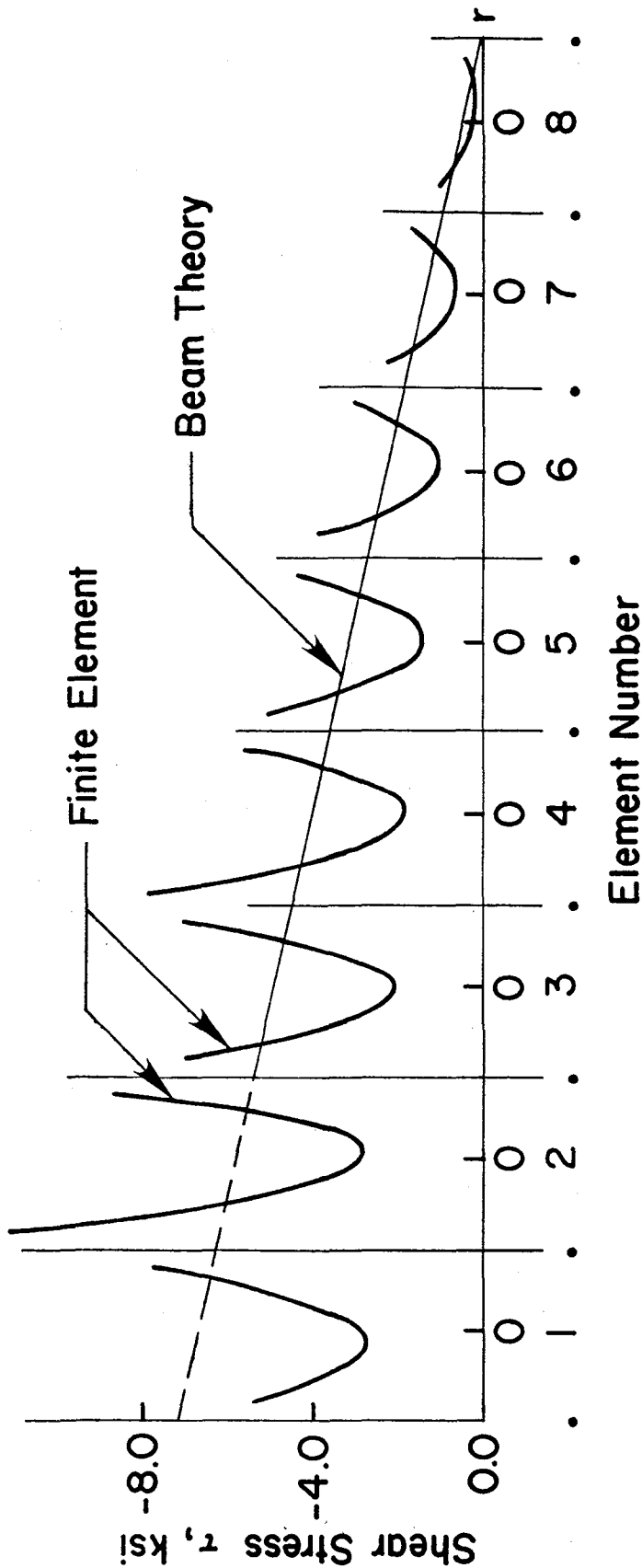
Figure 5.20   Variation of Shear Stress τ along s = 0.0 for a
Cantilever Beam Subjected to a Uniformly
Distributed Load
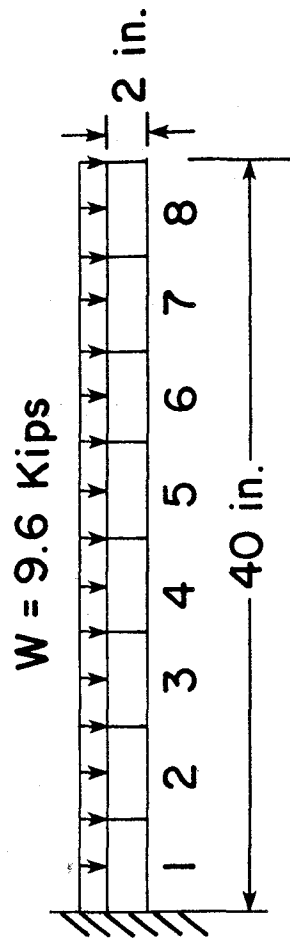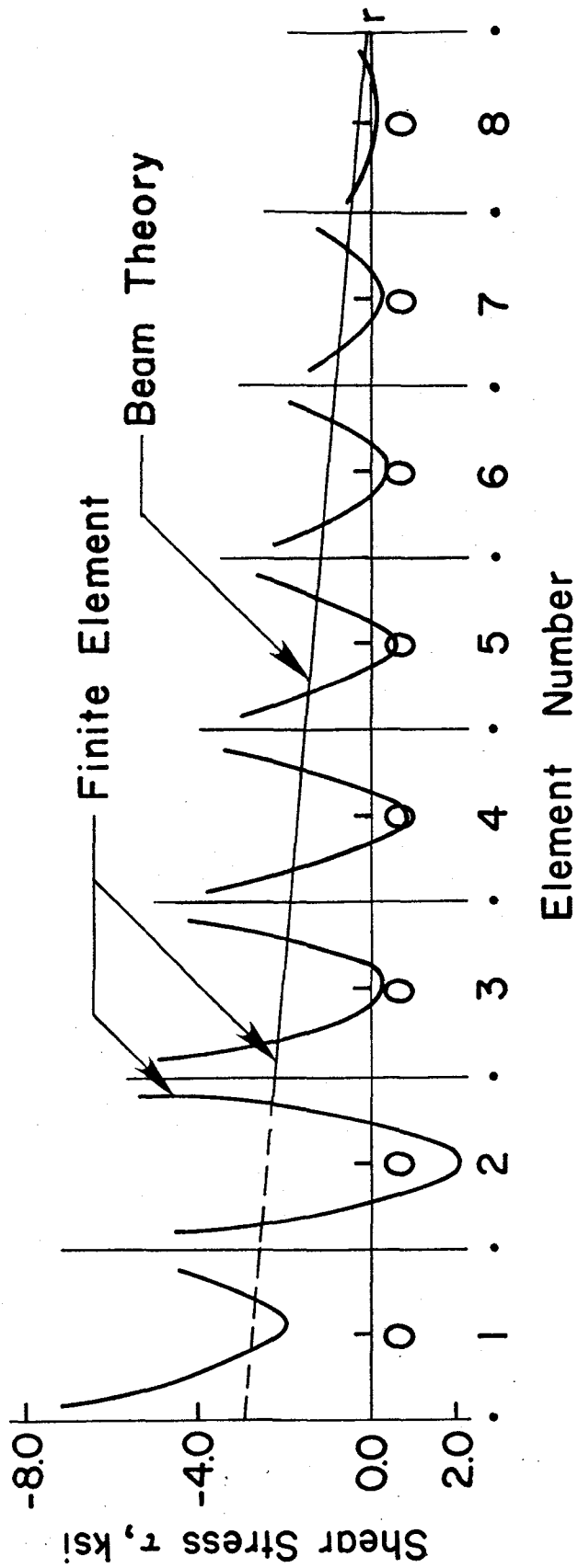
Figure 5.21   Variation of Shear Stress τ along s = 0.77459 for a
Cantilever Beam Subjected to a Uniformly
Distributed Load

shearing stresses in the collar joints are considered to evaluate the performance of the elements. The results obtained using a mesh of VISO10 elements are compared with that obtained using a mesh of linear elements. The objective here is to see how efficiently a coarse mesh of VISO10 elements can reproduce the results obtained by a very fine mesh of linear elements. The effect of mesh refinement on the collar joint shear stresses is also studied. Lastly, the effectiveness of VISO10 element in providing the vertical flexibility in the loaded block wythe is examined.

A composite masonry wall modelled by linear elements is shown in Figure 5.22. In this model, a very fine mesh at the top of the wall along the vertical direction and a relatively coarse mesh in the horizontal direction are provided. This mesh is defined as Mesh 1. Other finite element meshes, Mesh 2, Mesh 3, Mesh 4 and Mesh 5 of VISO10 elements are shown in Figures 5.23 through 5.26. In Mesh 6 two-dimensional cubic elements are used to model the block wythe while the rest of the wall is modelled by VISO10 elements. The geometry of this mesh is same as that of Mesh 5.

The shearing stresses in the collar joint obtained from various meshes are plotted and are shown in Figures 5.27, 5.29, 5.30. Figure 5.27 shows the plots of shearing stresses in the collar joint obtained using Mesh 1 and Mesh 2. The stress distribution within the top few inches of the wall obtained by Mesh 2 is in good agreement with that obtained by Mesh 1. This is mainly because, in the top 4 inches of the wall, both the meshes provide the same number of degrees of freedom in both horizontal and vertical directions. The two distributions of shearing stresses are different at a distance of six inches from the top of the

0.1753 k/in^2

4
|
4
6

20

20

Mesh 1

All Linear Elements
No. of Elements = 168
No. of Nodes = 198

20

20

25
inches

Block
Wythe

Brick Wythe

Collar Joint
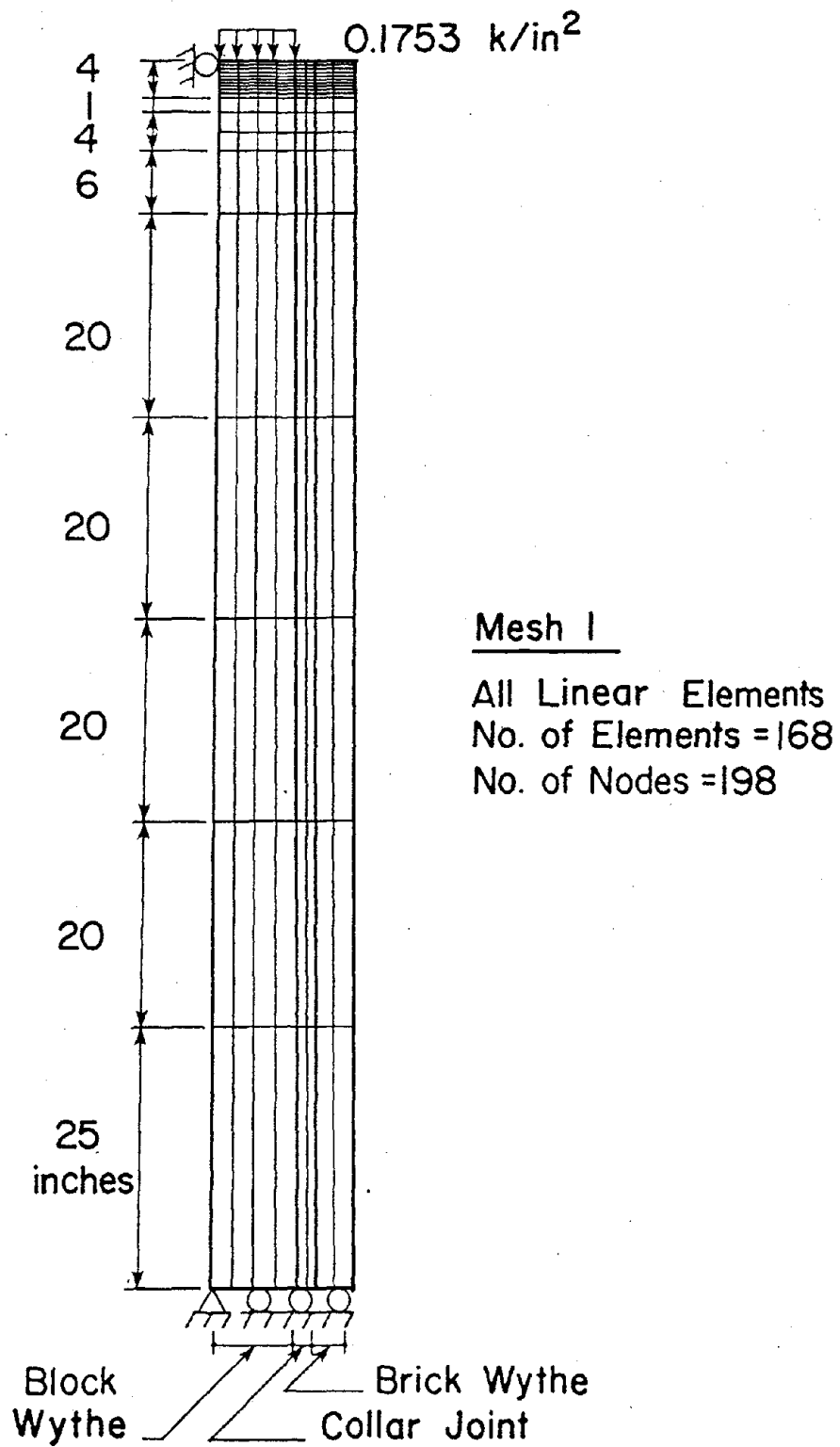
Figure 5.22 Mesh 1, A Finite Element Mesh of Linear Quadrilateral
Elements

0.1753 k/in^2

4

6

48

Mesh 2

All VISO 10 Elements
No. of Elements = 28
No. of Nodes = 142

62
inches

Block
Wythe

Brick Wythe

Collar Joint
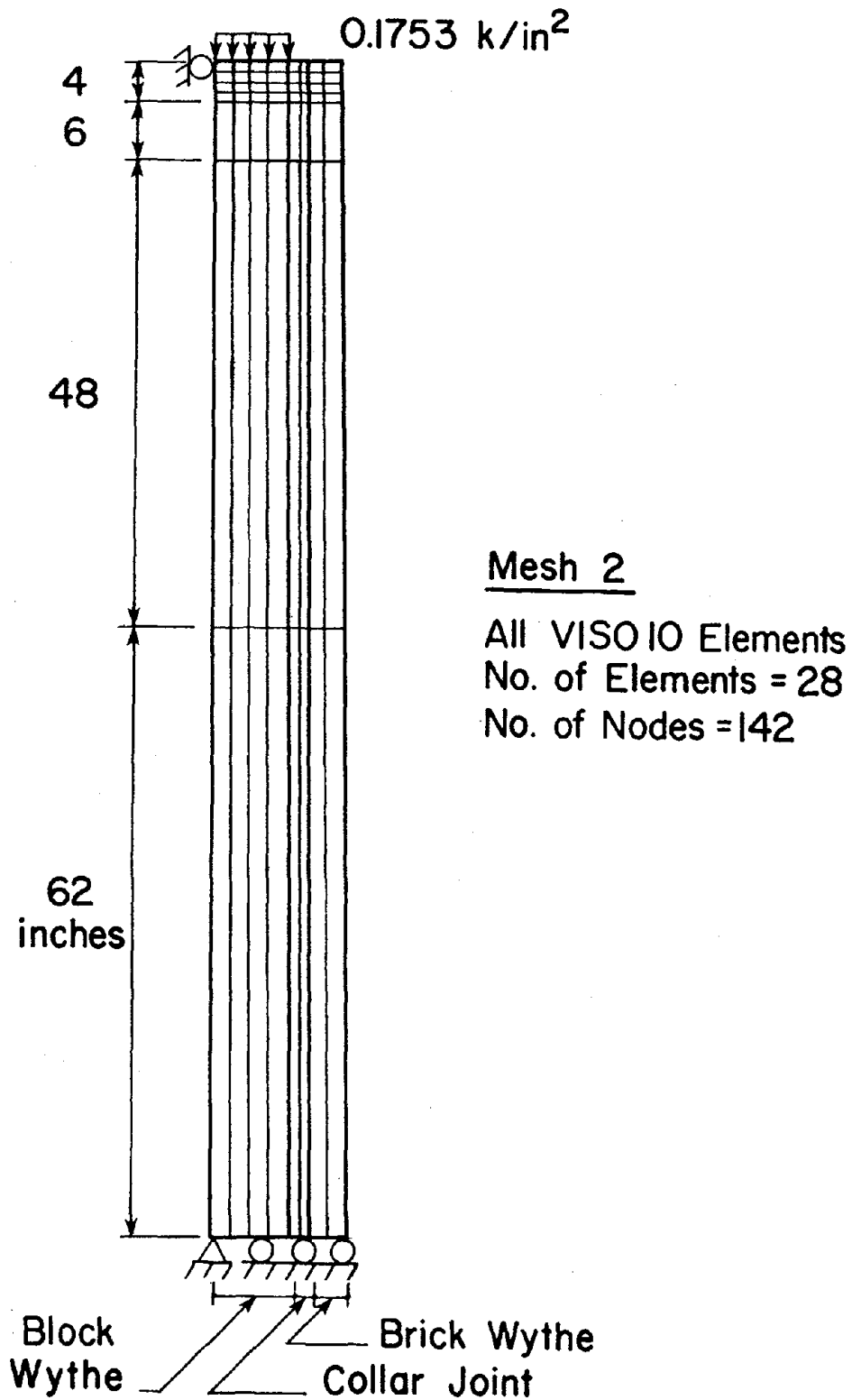
Figure 5.23   Mesh 2, A Finite Element Mesh of VISO10 Elements
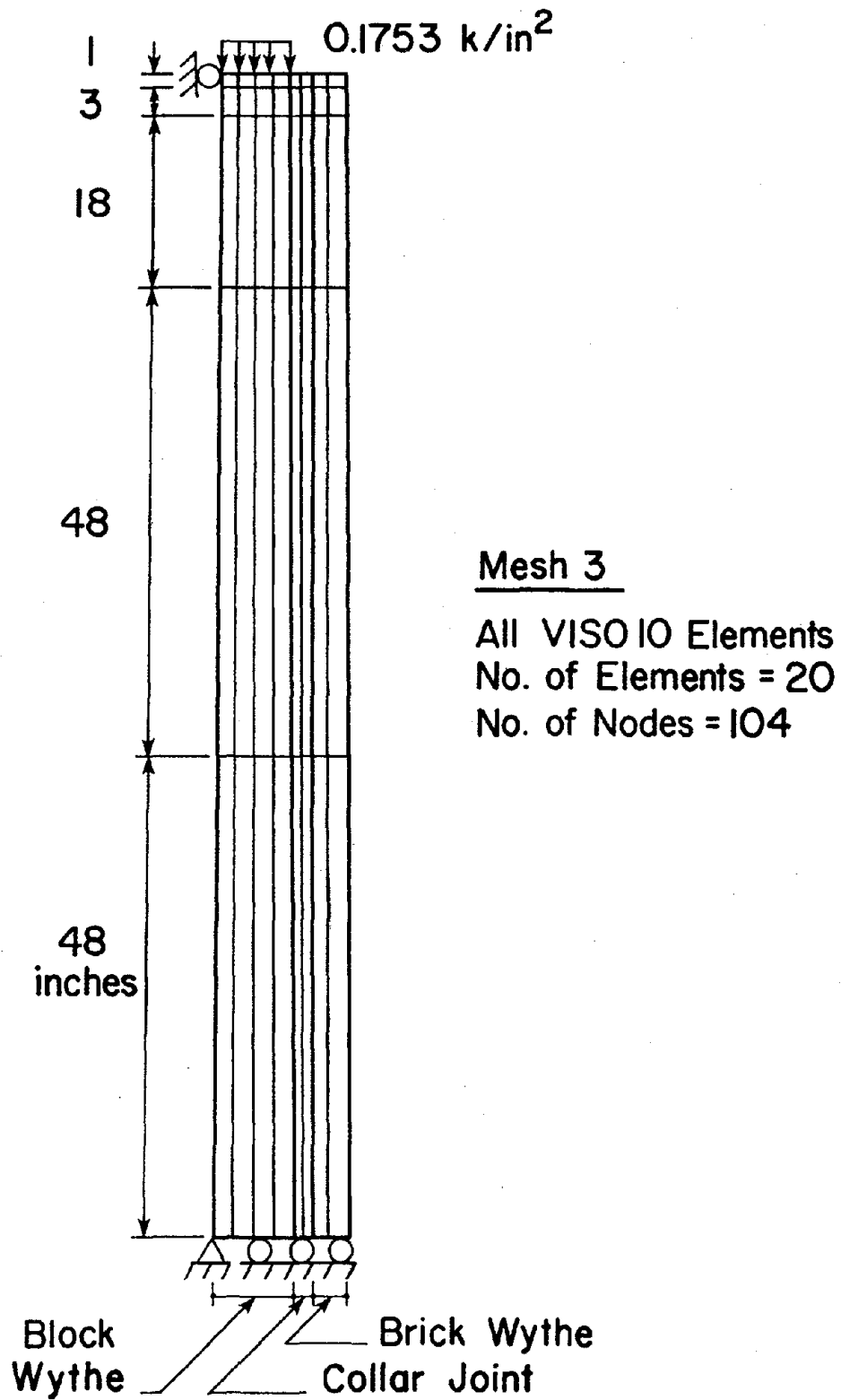
Figure 5.24 Mesh 3, A Finite Element Mesh of VISO10 Elements
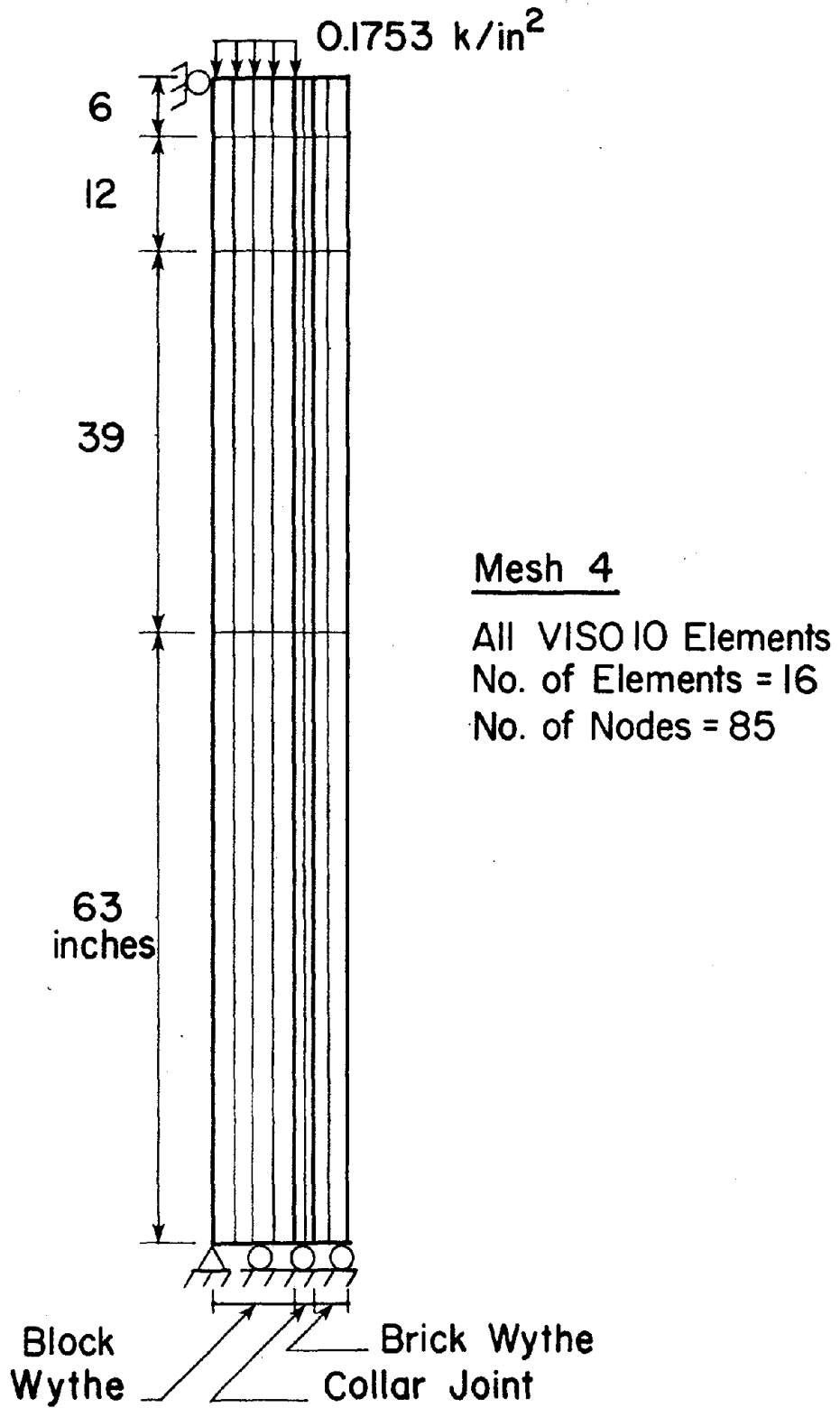
Figure 5.25   Mesh 4, A Finite Element Mesh of VISO10 Elements
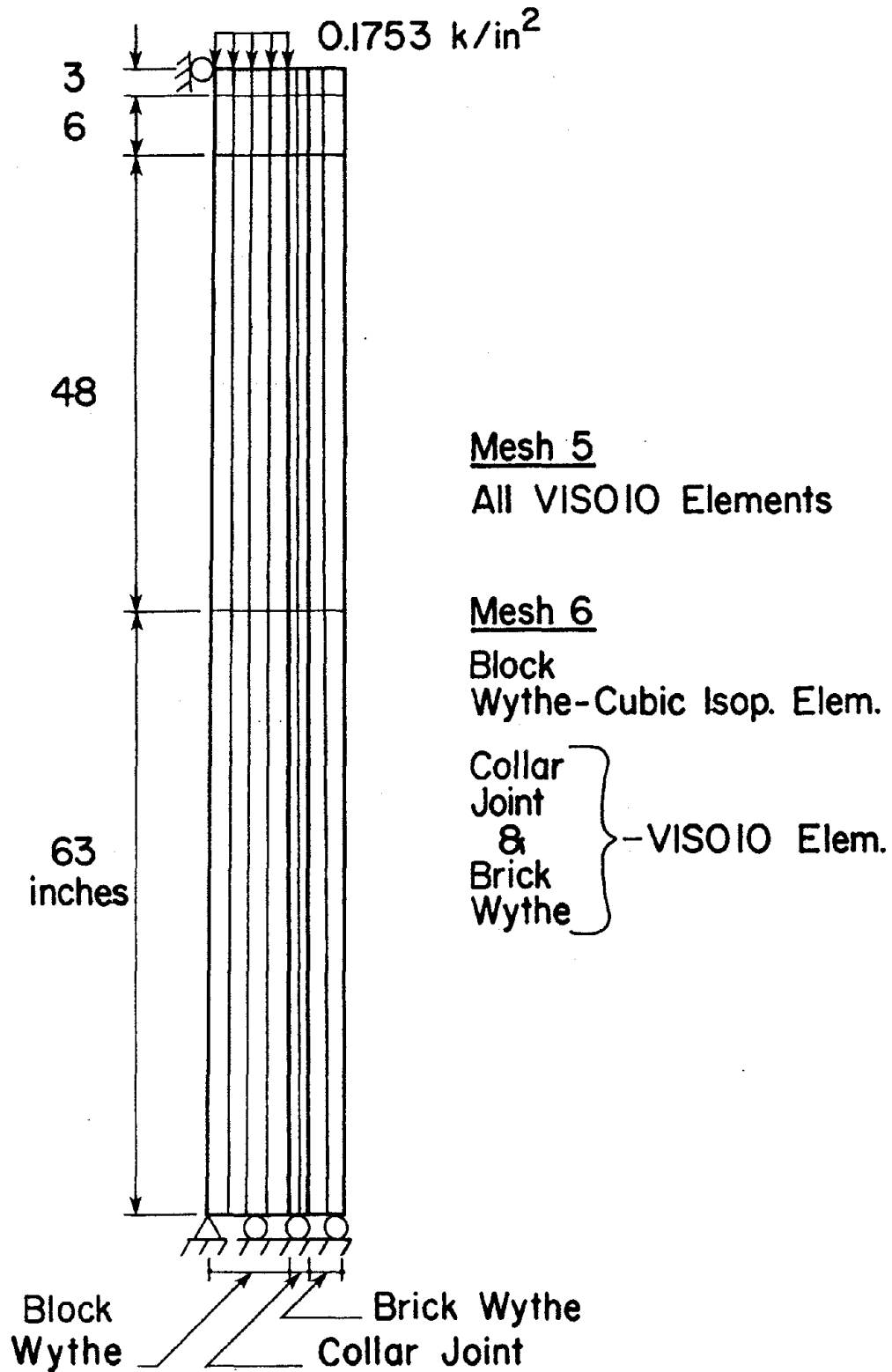
Figure 5.26   Mesh 5, A Finite Element Mesh of VISO10 Elements and
Mesh 6, A Finite Element Mesh of Cubic Quadrilateral
and VISO10 Elements
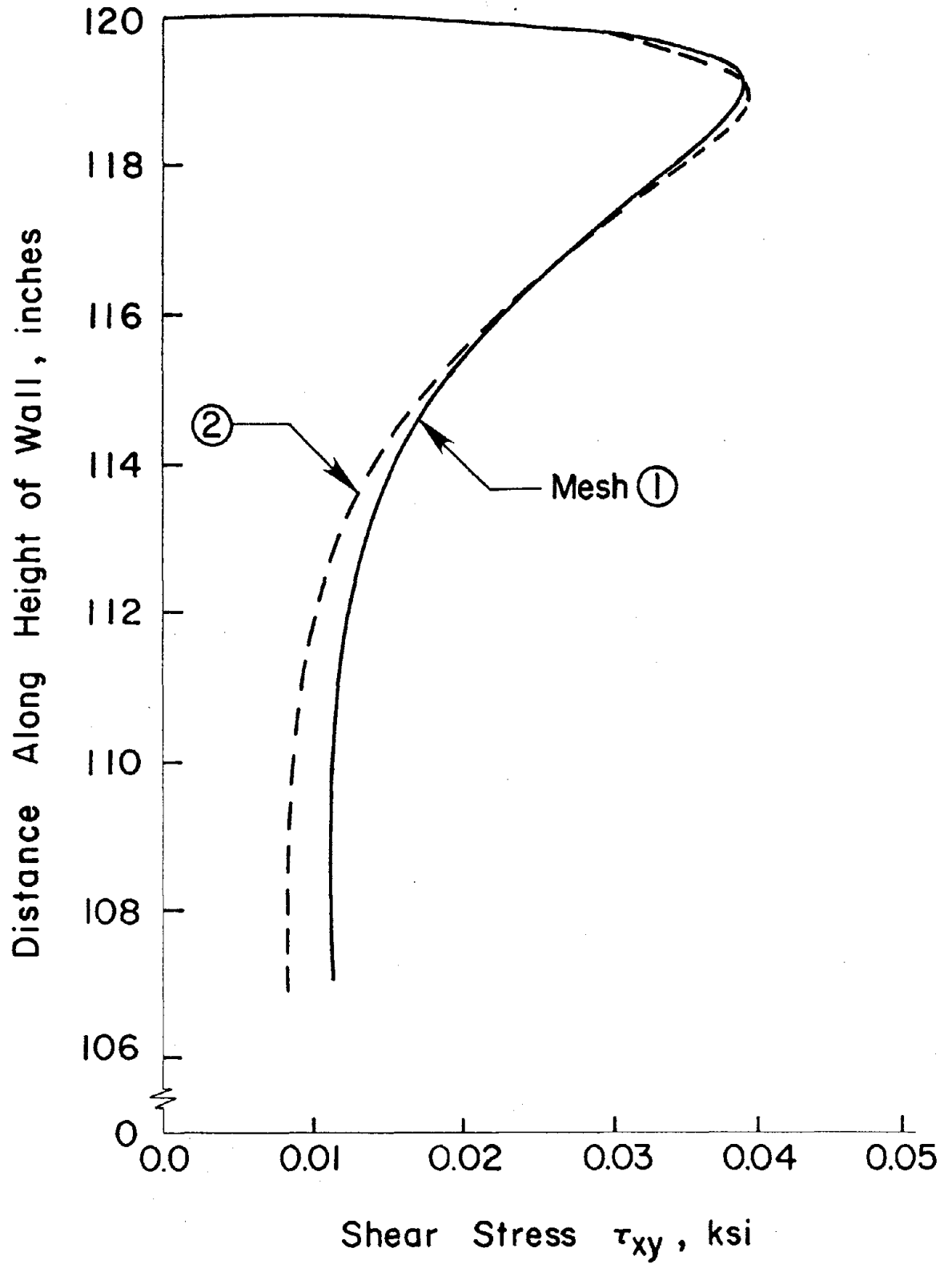
Figure 5.27   Shear Stresses in the Collar Joint Obtained by
Mesh 1 and Mesh 2
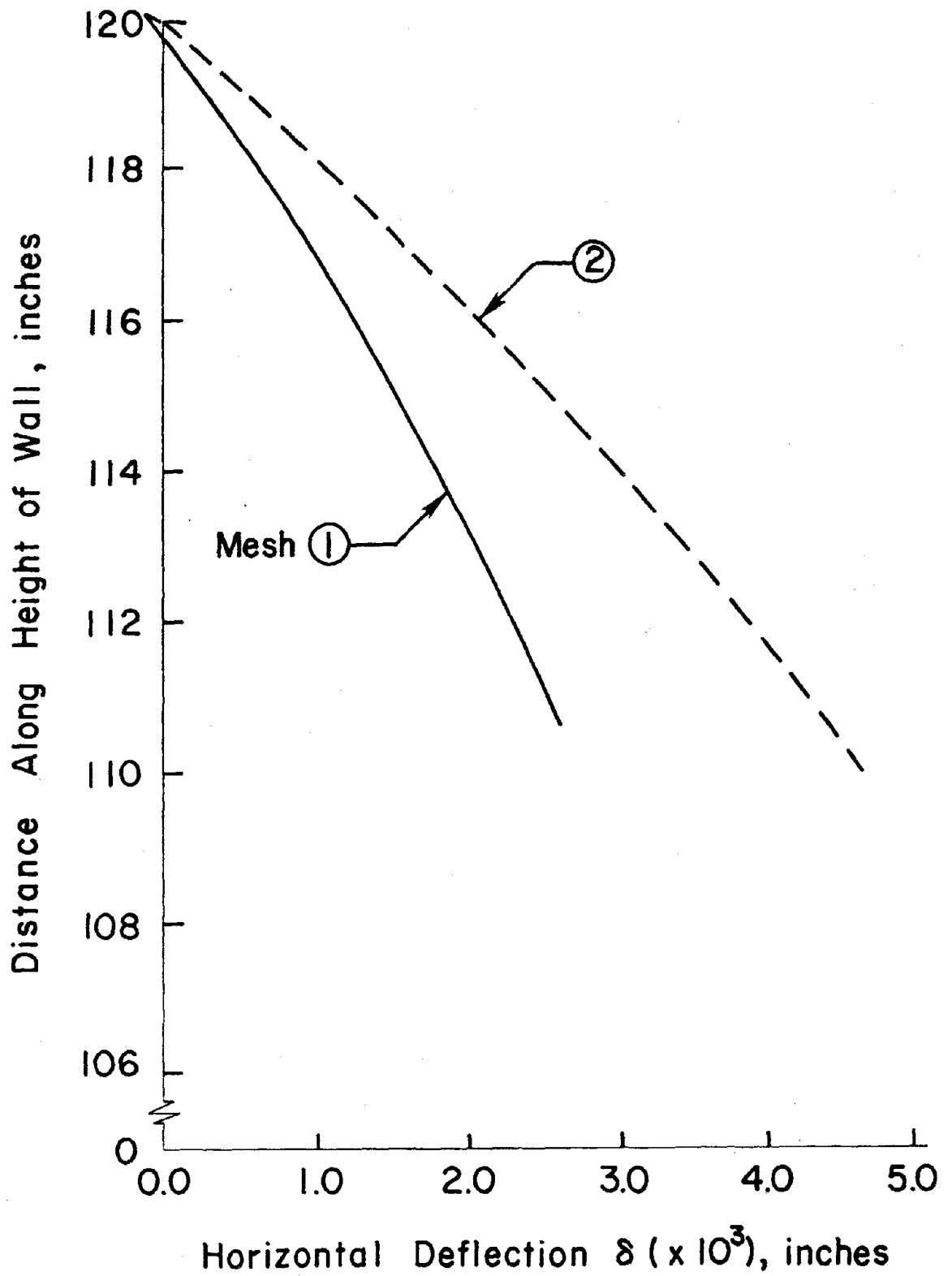
Figure 5.28 Out-of-Plane Deflection of the Wall Obtained by
Mesh 1 and Mesh 2
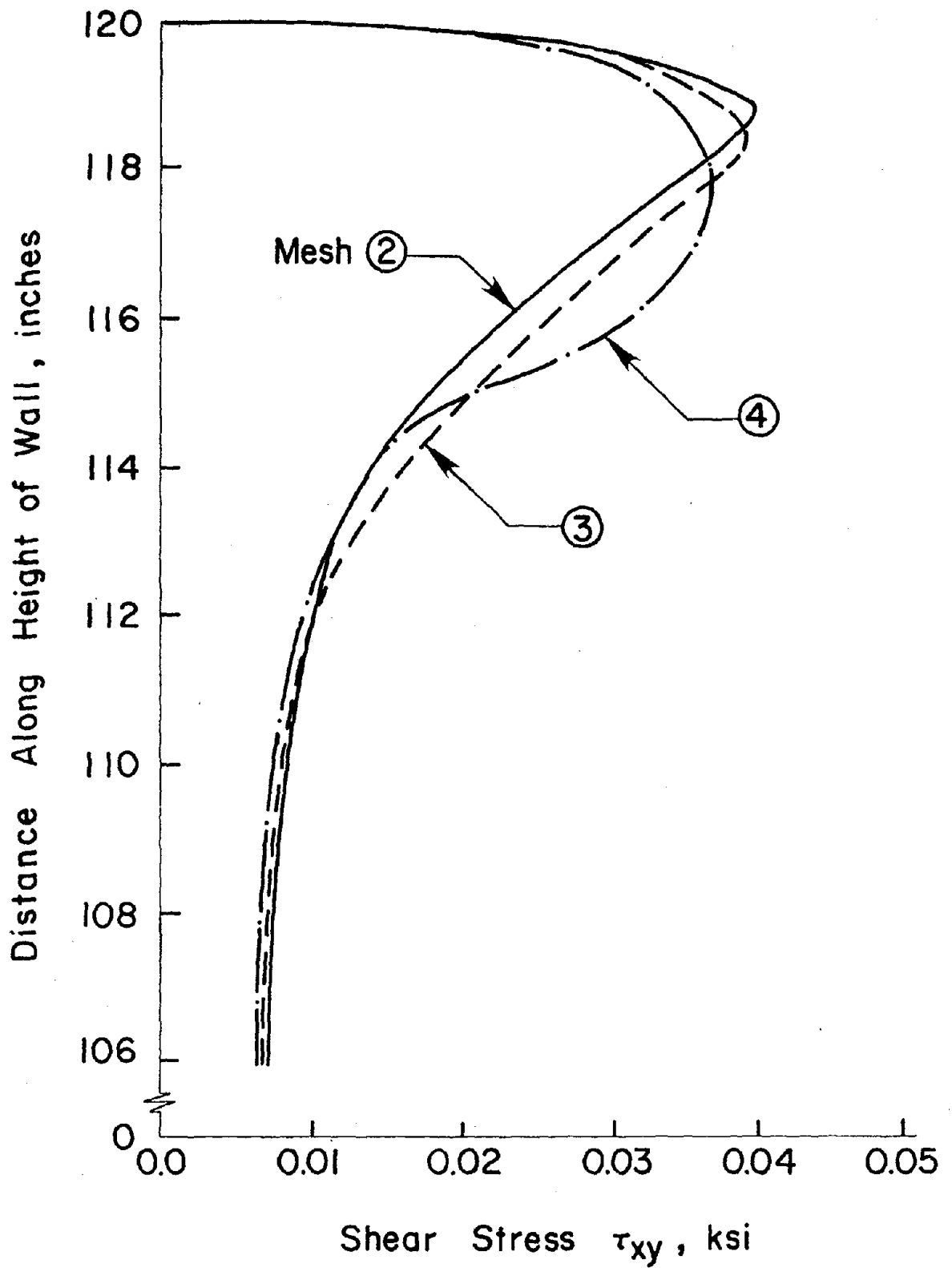
Figure 5.29   Shear Stresses in the Collar Joint Obtained by Mesh 2, Mesh 3 and Mesh 4
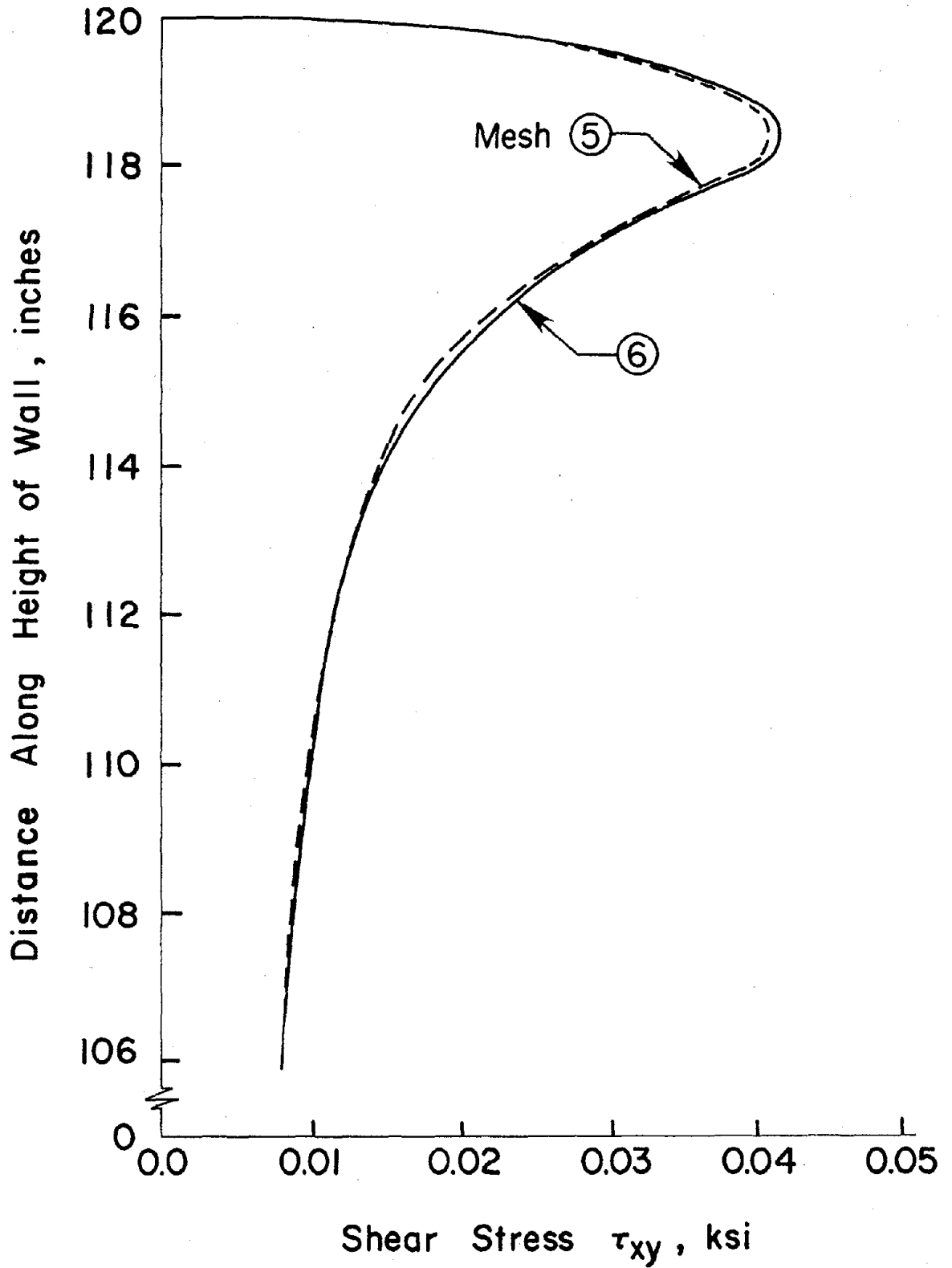
Figure 5.30   Shear Stresses in the Collar Joint Obtained by Mesh 5 and Mesh 6

wall. The mesh of linear elements predicts higher shear stresses than that predicted by the mesh of VISO10 elements. The shear stress is a function of both the horizontal and the vertical deflections. In the collar joint, the horizontal deflections cause negative shear stresses which are subtracted from the positive shear stresses caused by the vertical deformations to get the final shear stresses. The horizontal displacements within the top few inches of the wall obtained by using Mesh 1 and Mesh 2 are shown in Figure 5.28. Mesh 1 predicts less horizontal displacements than that predicted by Mesh 2. The linear elements of Mesh 1 cannot exactly represent the cubic displacement field of the wall and consequently, they predicts less negative shear stress than those predicted by Mesh 2 of elements having displacement functions of 3rd order. At a distance of 6 inches from the top of the wall, the load intensity on the entire width of the wall becomes almost uniform. Hence, the vertical displacements obtained by using Mesh 1 are almost same as the vertical displacements obtained by using Mesh 2. This results in equal positive shear stresses in both the cases. The negative shear stresses in Mesh 1 being less than that in Mesh 2 cause larger total shearing stresses in Mesh 1. However, the difference in shearing stresses between these two cases is not significantly different.

In Figure 5.29, shearing stresses in the collar joint obtained using Mesh 2, Mesh 3 and Mesh 4 are plotted. All these meshes consist of 10 noded variable-node-number elements. Among these three meshes, Mesh 2 is the finest and Mesh 4 is the coarsest. The plots show that for a coarser mesh, the magnitude of the peak shearing stress decreases and its location moves downwards, away from the top of the wall. The plots in Figure 5.29 show that Mesh 2 predicts the highest magnitude of peak stress

and Mesh 4 predicts the lowest magnitude of peak stress. The shear stress distribution obtained by Mesh 3 is very close to that obtained by Mesh 2. This indicates that a very coarse mesh of VISO10 elements can be used to model the composite masonry walls without any loss of accuracy in stresses.

The effectiveness of VISO10 elements in modelling the block wythes in composite masonry walls is studied comparing the shearing stresses in the collar joint obtained from Mesh 5 of VISO10 elements with that obtained from Mesh 6 in which the block wythe is modelled with cubic elements. The Mesh 5 and Mesh 6 are same in fineness; the only difference is in the type of elements used in two cases. The shearing stresses in the collar joint are shown in Figure 5.30. The shearing stresses obtained by Mesh 5 are in good agreement with those obtained by Mesh 6. This shows that the displacement field produced in the block wythe by the vertical loads can be modelled correctly by VISO10 elements.

CHAPTER VI

INTERFACE BEHAVIOR IN COMPOSITE WALLS

In general, the interface of two dissimilar materials is weak in shear. Hence, there may exist planes of weakness in the composite masonry walls at the block wythe-collar joint and brick wythe-collar joint interfaces. The behavior of interfaces in composite masonry may be assumed to be similar to the behavior of the joints in rocks. For numerical modelling of jointed rocks, a special joint/interface element was first developed by Goodman et al. (42). Page (71) used Goodman's joint element to model the mortar joints in single wythe brick masonry. The concept of "interface element" may be used in composite masonry walls for modelling the interfaces. Before arriving at a decision about the type of interface element to be used for modelling the interfaces in composite masonry walls, it is important to understand clearly the behavior of the interfaces and to review the characteristics of the existing joint elements.

Dilatancy

Dilatancy means volumetric change accompanying deformation. The term dilation is used to mean thickening of a joint undergoing shear deformation at constant normal stress. Dilatancy should not be confused with lateral strain caused by the Poisson's effect. Poisson's ratio is an elastic property that relates normal strains in one direction to normal strains in another. Dilatancy, on the other hand, relates normal strains to shearing strains. Typically, joints (specially natural rock joints) have some roughness. Their shear strength is due to overriding and fracturing through the asperities. Overriding creats a dilation. It is

the characteristic of rough joints in shear. Dilatancy properties of discontinuities are governed by the roughness of the adjacent surfaces. When joints are very smooth, their dilation may be insignificant. If a dilatant joint is subjected to transverse restraint during shearing, there will be an increase in the shear stiffness of the joints, and, more importantly, an increase in the normal stress on the joint. For a given point, at a given starting normal stress, the normal stress increase due to a shear displacement certainly depends on how stiff the medium adjacent to the joint is.

In composite masonry walls, the brick and block faces are smooth at the brick wythe-collar joint and block wythe-collar joint interfaces respectively. Hence, the dilation in these joints is not expected to be significant. The coarse aggregates of grout in two inch thick collar joints may cause a little dilation in the interfaces. This dilation cannot affect the shearing stiffness and the state of normal stress at the interface because both the brick and the block wythes have very little transverse stiffness and also these wythes are not horizontally retrained. For the above mentioned reasons, in the numerical modelling of the interfaces in composite masonry walls, the effects of dilatancy have been ignored.

History of Joint/Interface Elements

In the past few years, many two and three-dimensional joint/interface elements have been proposed. These elements have been developed to model the joints in rocks and the interfaces in soil-structure problems. Most joint elements are planar and are assumed to have zero thickness when deriving a stiffness matrix. The rotational stiffness and the effect of dilation have also been introduced in some joint/interface elements. The

chronology of development of the joint/interface elements, including the pertinent characteristics of each, is described in Table 6.1.

Table 6.1. Chronology of Development of Joint/Interface Elements

Date	Reference	Characteristics of Joint Element
1968	Goodman, R. E. et al. (42)	Two-dimensional linear element, no thickness.
1970	Mahtab, M.A. (64)	Three-dimensional, no thickness.
1970	Zienkiewicz, O.C. et al. (103)	Two-dimensional, isoparametric formulation, essentially like a solid element, no thickness.
1971	Heuze, F.E. et al. (54)	Two-dimensional, strain soften-ing considered, no thickness.
1971	Noorishad, J. (70)	Two-dimensional, fluid flow problems, no thickness.
1971	Heuze, F.E. and Goodman, R.E. (53)	Two-dimensional, strain soften-ing considered, dilation consi-dered, no thickness.
1972	St. John, C.M. (87)	Two and three-dimensional, no thickness.
1972	de Rouvray, A.L. and Goodman, R.E. (80)	Two-dimensional, strain soften-ing and dilation considered, no thickness and no explicit coupling between opening and reclosing tendencies.
1972	Goodman, R.E., and Dubois, J. (40)	Two-dimensional, strain soften-ing and dilation considered, no thickness, no explicit coupling between opening and reclosing tendencies, iteration by load transfer.
1973	Ghaboussi, J. et al. (38)	Two-dimensional, axi-symmetric, dilation considered, relative displacement as independent degree of freedom.

Table 6.1 (Continued)

1974	Gale, J.E. et al. (37)	Two-dimensional, fluid flow problems, no thickness.
1975	Ngo, D. (68)	Two-dimensional quadratic element, no thickness.
1975	Schafer, H. (82)	One and two-dimensional bond elements for reinforced concrete.
1976	Sharma, H.D. et al. (84)	Two-dimensional quadratic element.
1976	Hilber, H.M. and Taylor, R.L. (55)	Two-dimensional, fluid flow problems.
1976	Desai, C.S. (32)	Axisymmetric, modified form of Goodman's element (42).
1977	Goodman, R.E. and St. John, C. (41)	Two-dimensional, strain softening and dilation considered, rotational stiffness, no thickness.
1977	Wilson, E.L. (95)	Two and three-dimensional elements, relative displacements as independent degrees of freedom.
1978	Hittinger, M. and Goodman, R.E. (58)	Two-dimensional quadratic element, strain softening and dilation considered, rotational stiffness and no thickness.
1978	Herrmann, L.R. (51)	Similar to Goodman's elements, constraint condition used.
1978	Buragohain, D.N. and Shah, V.L.(27)	Curved isoparametric, relative displacements as independent degrees of freedom.
1979	Heuze, F.E. (52)	Two-dimensional, dilation considered, rotational stiffness and no thickness.
1979	Pande, G.N. and Sharma, K.G. (72)	8-noded isoparametric, relative displacement as an independent parameter.
1981	Xiurun, G. (99)	Two-dimensional, dilation considered, no thickness.

Table 6.1 (Continued)

1981	Van Dillen, D.E. and Ewing, R.D. (90)	Two and three-dimensional, dilation considered.
1981	Desai, C.S. (33)	Two and three-dimensional, with thickness, material model for dynamic case.
1983	Katona, M.G. (60)	Element derived from virtual work principle, constraint condition.
1985	Mehlorn, G. and Kauser, M. (66)	One and two-dimensional contact elements for reinforced concrete.
1985	Beer, G. (25)	Shell to shell interface element, relative displacement as independent degree of freedom.

Proposed Thin Interface Element

If the interfaces in composite masonry walls are assumed to act as planes of weakness then they can be represented by a thin layer of isoparametric continuum elements (interface elements), the shear stress-strain properties of which are typically derived from laboratory tests on the interfaces. The interface element proposed in this research is similar to that developed by Desai and co-workers (33,34). This type of interface element has also been used successfully by Haggblad and Nordgren (47) to solve nonlinear soil-structure interaction problems.

The proposed interface element is essentially a solid element of small finite thickness. This element represents a thin layer of material between the block wythe and collar joint or the brick wythe and collar joint. Figure 6.1 shows schematically the proposed thin layer interface element for simulation of the interface behavior. The proposed interface
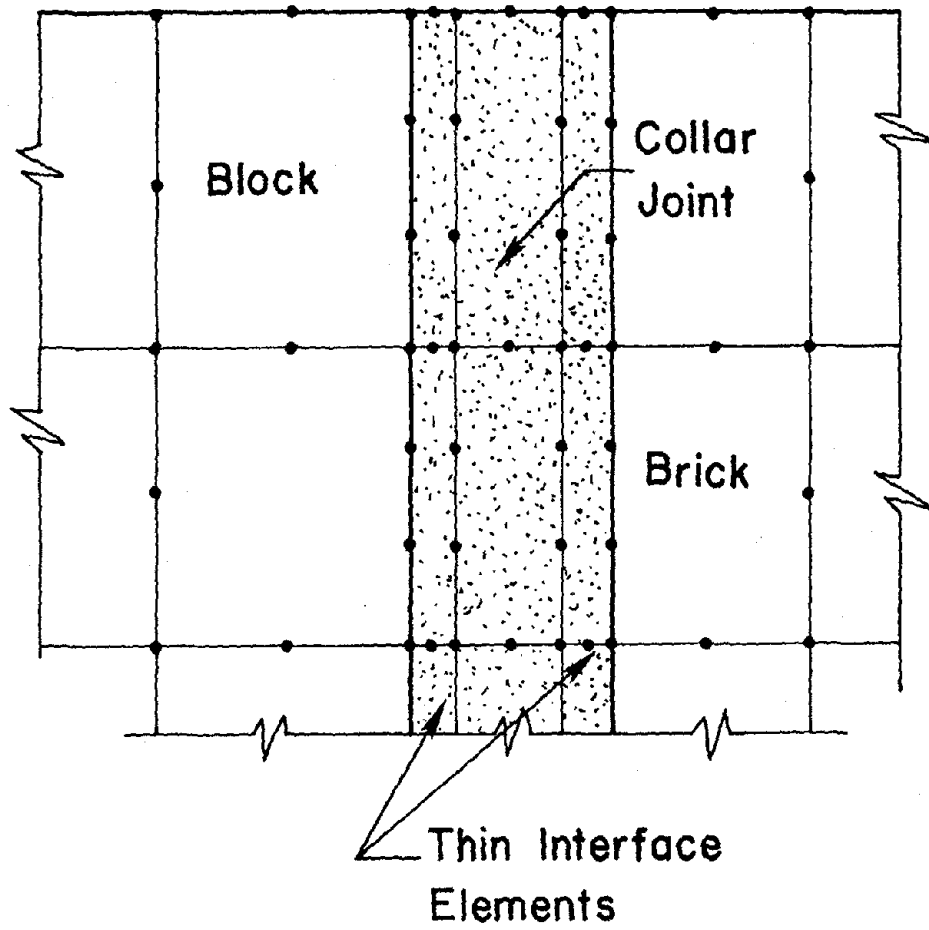
Figure 6.1 Thin Interface Element

element is like a solid 10 noded variable-node-number isoparametric (VISO10) element. The thickness of this element can be determined following the procedure suggested by Desai, et al. (34). The aspect ratio of this type of interface element is generally very high but it does not create numerical problems. It has been shown by Pande and Sharma (72) that even on small word length machines, aspect ratios of thousands apparently do not create numerical problems. They have concluded that on accurate machines, it is possible to adopt very small thickness of interfaces without numerical ill-conditioning. Regarding the mid-side nodes of the proposed interface element along the thickness direction, it is felt that although the thickness of the interface element may be very small, sharp variations in the strains of adjacent continuum elements can take place and a linear interpolation of strains is required. Hence, the mid-side nodes along the thickness direction have been retained in the proposed interface element.

Constitutive Matrix, [C]

The constitutive relations for the interface element are defined differently from the constitutive relations for any other solid element. The constitutive matrix [C] is expressed as

$$[C] = \begin{bmatrix} [C_{nn}] & [C_{ns}] \\ \\ [C_{sn}] & [C_{ss}] \end{bmatrix} \tag{6.1}$$

where $[C_{nn}]$ = normal component, $[C_{ss}]$ = shear component and $[C_{ns}]$, $[C_{sn}]$ represent coupling effects between normal and shear behavior. In the present research these effects are neglected because it is difficult to determine the coupling terms from laboratory tests. The normal behavior of the interface element is evaluated just as for the adjacent solid

elements. The shear part $[C_{ss}]$, of the interface constitutive relationship matrix can be obtained by using the results of direct shear tests for various interfaces. The procedure is outlined in detail elsewhere (34,47). For linear elastic behavior of the interface, the constitutive matrix [C] for two dimensional case can be expressed as

$$[C] = \begin{bmatrix} C_1 & C_2 & 0 \\ C_2 & C_1 & 0 \\ 0 & 0 & G \end{bmatrix} \qquad (6.2)$$

where for plane strain case

$$C_1 = E(1-v)/(1+v)(1-2v)$$

$$C_2 = Ev/(1+v)(1-2v)$$

and for plane stress case,

$$C_1 = E/(1-v^2)$$

$$C_2 = Ev/(1-v^2)$$

where

E is the elastic modulus, v is Poisson's ratio and G is the shear modulus of the interface.

Determination of the Shear Modulus, G

It is mentioned earlier that the shear component, G, of the constitutive matrix is determined from the results of direct shear tests. But, there are no appropriate and sufficient results available from the direct shear tests for the brick wythe-collar joint or block wythe-collar joint interfaces to determine the value of G. Hence, a different approach is followed for determining the value of G of the interface using the test results of Williams and Geschwindner (94). Some important features of the test procedure and the results are discussed below.

The specimens were constructed consisting of two brick wythes and one solid concrete block wythe in a symmetrical arrangement as shown in Figure 6.2. These wythes were joined together by 3/8 inch collar joint filled in with either mortar or grout. The load was applied through the centroid of the assembly and the horizontal displacements in the faces of the brick wythes and the vertical displacements of the top of the block wythe were recorded. The failure load was considered to be the load which caused the initial collar joint failure. It was reported that for S-type of mortar in the collar joint without any reinforcement, the average value of the shear bond strength of the test triplets was 54.5 psi. A plot of shear bond stress vs. vertical displacement of the top of the block was also presented. A part of this plot for the specimen having Type S mortar as the collar joint material is reproduced in Figure 6.3.

In order to compute the shear modulus G, one needs a plot of shear bond stress vs. shear strain of the interface or a plot of shear stress vs. vertical displacement of the interface due to the shear load corresponding to the shear bond stress. In this research, the shear modulus G for the interface is computed from the shear stress-vertical displacement relationship. A detailed procedure for obtaining the vertical displacement of the interface (for the specimen in which Type S mortar is used as the collar joint material) from the measured vertical displacement of the top of the middle block wythe is stated below.

In the collar joint, two narrow strips are considered as the interfaces with finite thicknesses. The displacement configurations of the specimen at different levels of load transfer from the loaded block wythe to the unloaded brick wythe is shown in Figure 6.4. When the load is applied on the block wythe, the block wythe deforms vertically by an

Brick Masonry Wythe (units 4"x4"x12")

3/8" Collar Joint

Concrete Block Masonry Wythe (units 8"x8"x16")

(a) Isometric View

17-5/8"

15-5/8

3-5/8"

5-5/8

3-5/8

15-5/8"

3

(a) Side View

(b) Front View
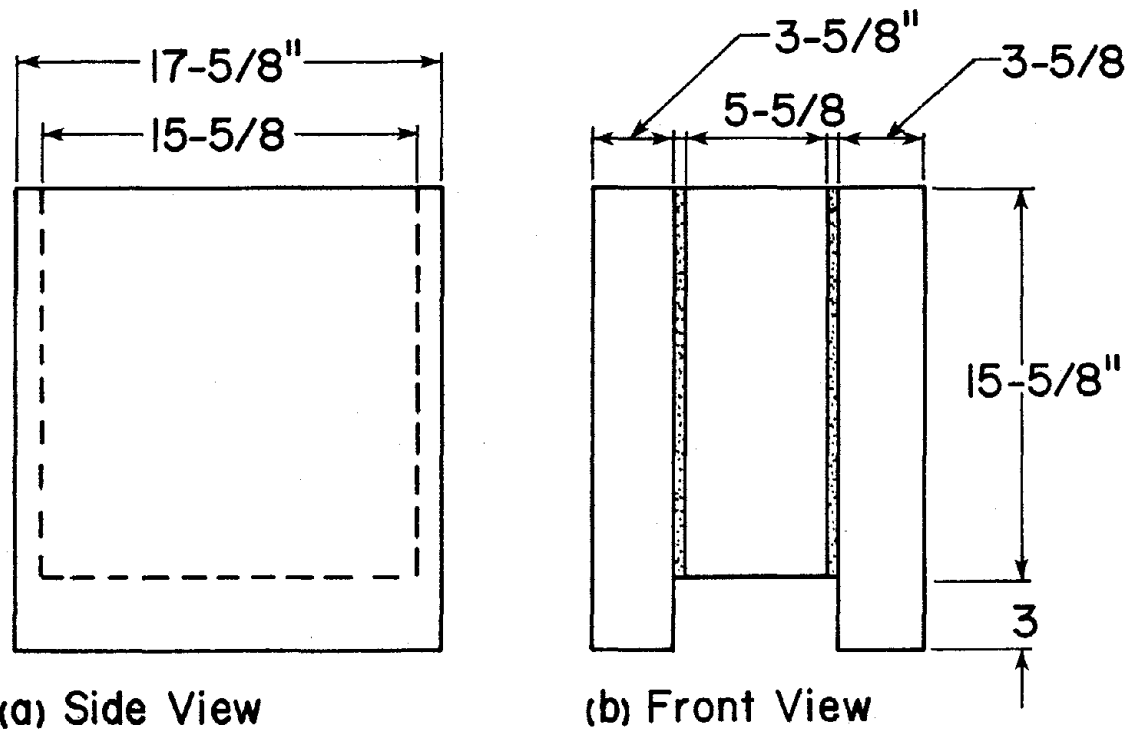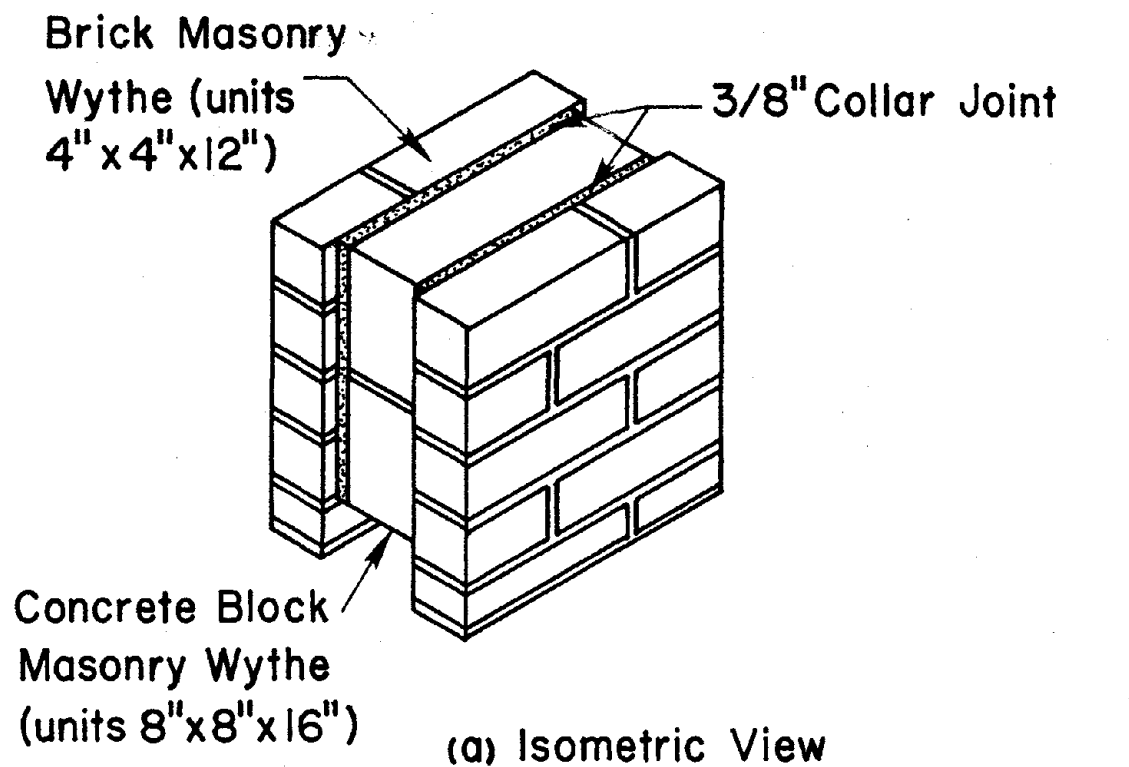
Figure 6.2 Williams and Geschwindner's (94) Specimen
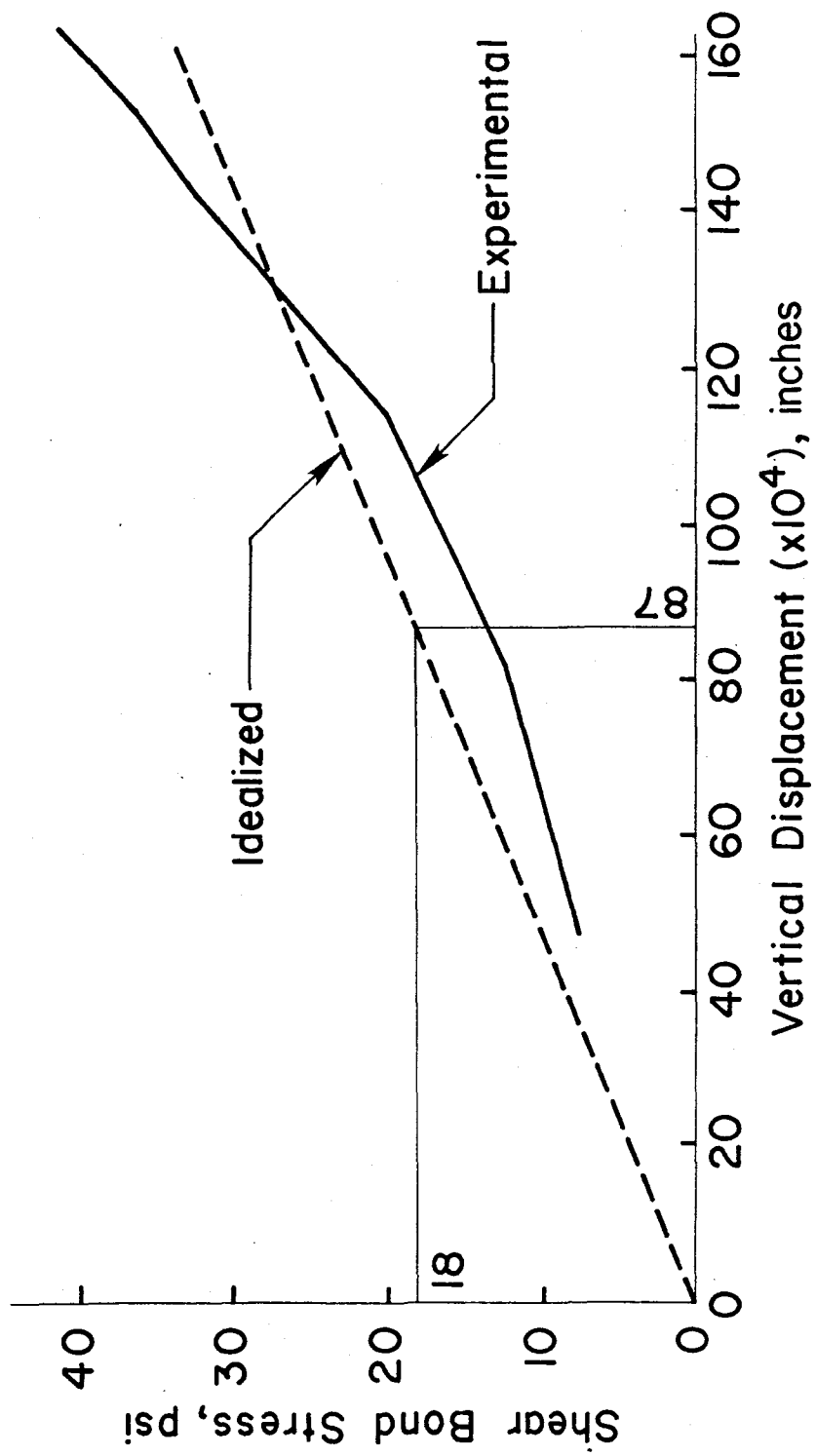
Figure 6.3   Shear Bond Stress vs. Vertical Displacement at the Top of the Block Wythe (94)
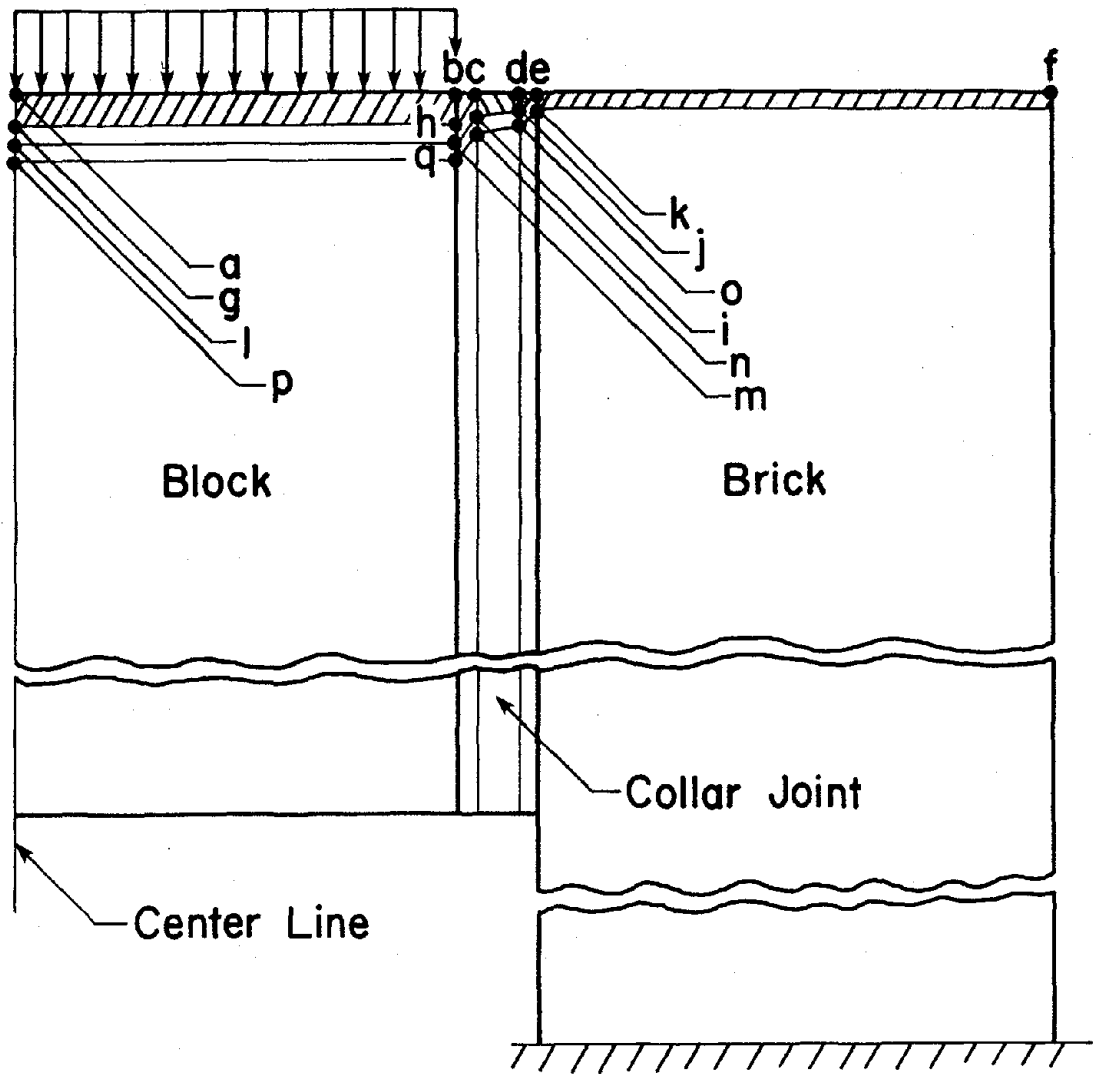
Figure 6.4   Assumed Displacement Configuration of Williams and
             Geschwindner's Specimen (94)

amount bh causing a shearing strain defined by the angle bch at the block
wythe-collar joint interface. This shearing strain depends upon the
characteristics of the interface. Due to the shearing strain in the
block-collar joint interface, the vertical load on the block wythe par-
tially transfers out to the collar joint as shear load. This shear load
causes shear deformation in the collar joint and vertical deformation dj
in the brick wythe-collar joint interface. The shear deformation in the
collar joint and the vertical deformation dj yields total deformation ci
on the block side of the collar joint. Because of the joint deformation
in the brick-collar joint interface, the shear load is transfered from
the collar joint to the brick wythe. The shear load is assumed to act
uniformly over the entire height of the brick wythe which is supported
at the bottom. This shear load causes vertical displacement ek in the
brick wythe. It is obvious from the boundary conditions of the specimen
that the total deformation ci in the collar joint and ek in the brick
cause the block wythe to deform vertically by the same amount. Hence,
the total vertical displacement at the top of the block wythe is ap, which
is the sum of the two interface displacements; the collar joint shear
deformation and the brick deformation. Thus, subtracting the collar joint
shear and brick deformations from the total block deformation, one can
obtain the total interface deformation. If the load-deformation behavior
for both the interfaces is assumed to be the same, then the total inter-
face deformation may be divided by two to get the deformation of one
interface. The shear strain at the interface can be obtained by dividing
the interface deformation by the assumed thickness of the interface.

Following the above procedure, the shear modulus of the joints cor-
responding to different assumed interface thicknesses are computed. Only

S-type mortar as the collar joint material is considered and the nonlinear shear stress-vertical displacement curve is approximated as linear. It is shown that the joint deformation of the composite triplet specimen does not depend upon the thickness of the interface.

The solid load-bearing concrete blocks of Williams and Geshwindner's specimen (94) are constructed of normal weight concrete and its elastic modulus and Poisson's ratio are assumed to be 1600 ksi and 0.25, respectively. The compressive strength of brick is 20,800 psi and that of mortar is 1420 psi. The modulus of elasticity of brick and mortar are computed based on their compressive strengths following the procedure prescribed in References (108,81) and the values are found to be 2000 ksi and 1420 ksi respectively. The Poisson's ratio of mortar is assumed as 0.2.

For computing the shear modulus of the interface, four arbitrary joint thicknesses and an arbitrary average shear stress level of 18 psi are considered. Calculations for estimating the magnitude of the shear modulus of the interface are given below.

(1) Vertical deformation of the brick wythe, Δ_{Br} (assuming uniform shear distribution along the height of brick wythe):

$$\Delta_{Br} = WL/2AE + WL'/AE \tag{6.3}$$

where

> W = total shear force acting on brick wythe
>   = 18x15.625 lbs = 281.25 lbs.,
>
> L = length of the brick wythe on which shear force acts
>   = 15.625 in.,
>
> A = area of cross-section. For plane strain case, thickness
>   is assumed to be 1. Hence, A = 3.625 in^2,
>
> E = modulus of elasticity and
>
> L'= length of the block wythe from the bottom of the

collar joint to the top of the support
= 3 inches.

Hence, Δ_{Br} = (281.25x15.625)/(2x3.625x2000,000)
+(281.25x3)/(3.625x2000,000)
= 0.000419 inches.

(2) Shear deformation of the collar joint:

The shear modulus of the collar joint,

$$G = E/2(1+v) = 1420,000/2(1+0.2) = 591,667 \text{ psi.} \qquad (6.4)$$

The shear strain, γ can be obtained from the shear stress, τ

and the shear modulus, G as

$\gamma = \tau/G = 18/591,667 = 0.0000304$

Assume interface thickness = 0.002 inches, then

collar joint thickness = 0.375-0.002-0.002 = 0.371 inches.

Hence, the shear deformation, d_1 can be obtained as

$d_1 = \gamma$ x 0.371 = 0.0000112 inch.

Assume interface thickness = 0.06 inches.

Collar joint thickness = 0.375-0.006-0.006 = 0.255 inches.

The shear deformation, d_2 can be obtained as

$d_2 = \gamma$ x 0.255 = 0.0000077 inches.

Assume interface thickness = 0.1 inches.

Collar joint thickness = 0.375-0.1-0.1 = 0.175 inches.

The shear deformation, d_3 can be obtained as

$d_3 = \gamma$ x 0.175 = 0.00000532 inches.

Assume interface thickness = 0.1875 inches.

Collar joint thickness = 0.375-0.1875-0.1875 = 0.

The shear deformation d_4 is given by

$d_4 = \gamma$ x 0 = 0.

(3) Total deformation of the block, δ_{Total} at the top corresponding to 18

psi shear stress can be obtained from Figure 6.3 and is

δ_{Total} = 0.0087 inches.

(4) The joint deformations, δ_i assuming identical behavior of block-
wythe collar joint and brick wythe-collar joint interfaces can be
obtained for different assumed interface thicknesses from the above
information and are given as

Interface thickness = 0.0020 in., δ_1 = 0.00413 inches

            = 0.0600 in., δ_2 = 0.00413 inches

            = 0.1000 in., δ_3 = 0.00413 inches

            = 0.1875 in., δ_4 = 0.00414 inches.

The joint deformations are the same for all the four interface
thicknesses. This is due to the fact that the shear deformation in the
collar joint is very small compared to the total deformation in the block.
Although the vertical deformations for all the four thicknesses of the
interface are the same, the shearing strains will not be the same as it
is a function of the joint thickness. Thus, the shearing modulus of
elasticity will be different for interfaces with different thicknesses.
The shearing modulus of an interface of the specimen whose thickness is
assumed to be equal to half of the collar joint thickness is determined
next.

Thickness of the interface = 0.1875 inches.

Shearing strain = 0.00414/0.1875 = 0.02208.

Shearing modulus = 18/0.02208 = 815 psi.

The shearing modulus of the joint will remain constant for all stress
levels because the average shear stress vs. vertical displacement curve
of the specimen is approximated to be linear and the material is assumed
to be linear elastic.

The magnitude of the shearing modulus of elasticity of the interface of Williams and Geschwindner's test specimen appears to be very low when compared against the shear modulus of the collar joint material. The shear modulus, G_E of the collar joint material (Type S mortar) computed from the modulus of elasticity of mortar is about 726 times larger than the interface shear modulus, G_{jt}. Page (71) and Ali and Page (2) presented shear stress vs. shear strain curves for mortar joints in single wythe clay brick and solid concrete block masonry, respectively. The normal stress vs. normal strain curves were derived indirectly from prism tests and the shearing stress vs. shearing strain curves were derived from brickwork couplets with sloping bed joints by subtracting brick deformations from total deformations measured on a gage length encompassing several bricks and joints. It was observed that the varying ratio of shear to normal stress did not have any significant influence on the shear stress vs. shear strain curves for masonry. For the mortar joints in clay brick masonry the shearing modulus, G_E, is calculated from the modulus of elasticity obtained from the normal stress vs. normal strain curve given by Page (71). Also, the shearing modulus, G_{jt}, of the mortar joint is obtained from the shear stress vs. shear strain curve. It is observed that G_E is about 1.8 times larger than G_{jt}. Also, the shearing modulus, G_E of mortar in the joints of solid block masonry is derived from the normal stress-strain curves given by Ali and Page (2). The magnitude of shearing modulus, G_{jt} of mortar joint in solid block masonry computed from the shearing stress-strain curve is found to be almost same as G_E. The stress-strain curves for mortar joints presented by Page (71) and Ali and Page (2) are nonlinear and the initial linear portion of the curves are considered to find the elastic and shear modulus. Hence, the above

mentioned relationships between G_E and G_{jt} are valid only when the magnitude of stress in the mortar is very low.

The joint behavior in the above mentioned three experiments are found to be extremely different from one another. In one extreme, the joint is as strong in shear as the mortar in a continuum and in the another extreme the joint is very weak in shear. Hence, it was felt that further investigation should be conducted to arrive at a conclusion about the behavior of the interfaces in composite masonry walls. The experiments in composite masonry that has been conducted at Clemson University are considered for further investigation.

Behavior of Interfaces in Composite Masonry Walls

Composite masonry wall specimens with 3/8 inch and 2 inch collar joints were tested at Clemson University (79). These specimens were subjected to vertical loads only on the block wythe. A typical test specimen is shown in Figure 6.5. The specimen consisted of a 48 in x 48 in block wall and a 40 in x 40 in brick wall connected together by a 2 in or a 3/8 in thick collar joint. The entire top course of the block and the outside cavities of the blocks from top to bottom were grouted.

Normal strains at various locations in the middle length of the wall were measured. The locations of the strain gages are shown in Figures 6.6 and 6.7. The solution of the three-dimensional behavior of the composite masonry wall specimen is achieved by analyzing the cross section of the specimen using a two-dimensional plane strain finite element program. This is discussed in the next paragraph. The modulus of elasticity of block masonry, mortar and brick masonry are determined from the compressive strengths of masonry units and mortar following the procedure
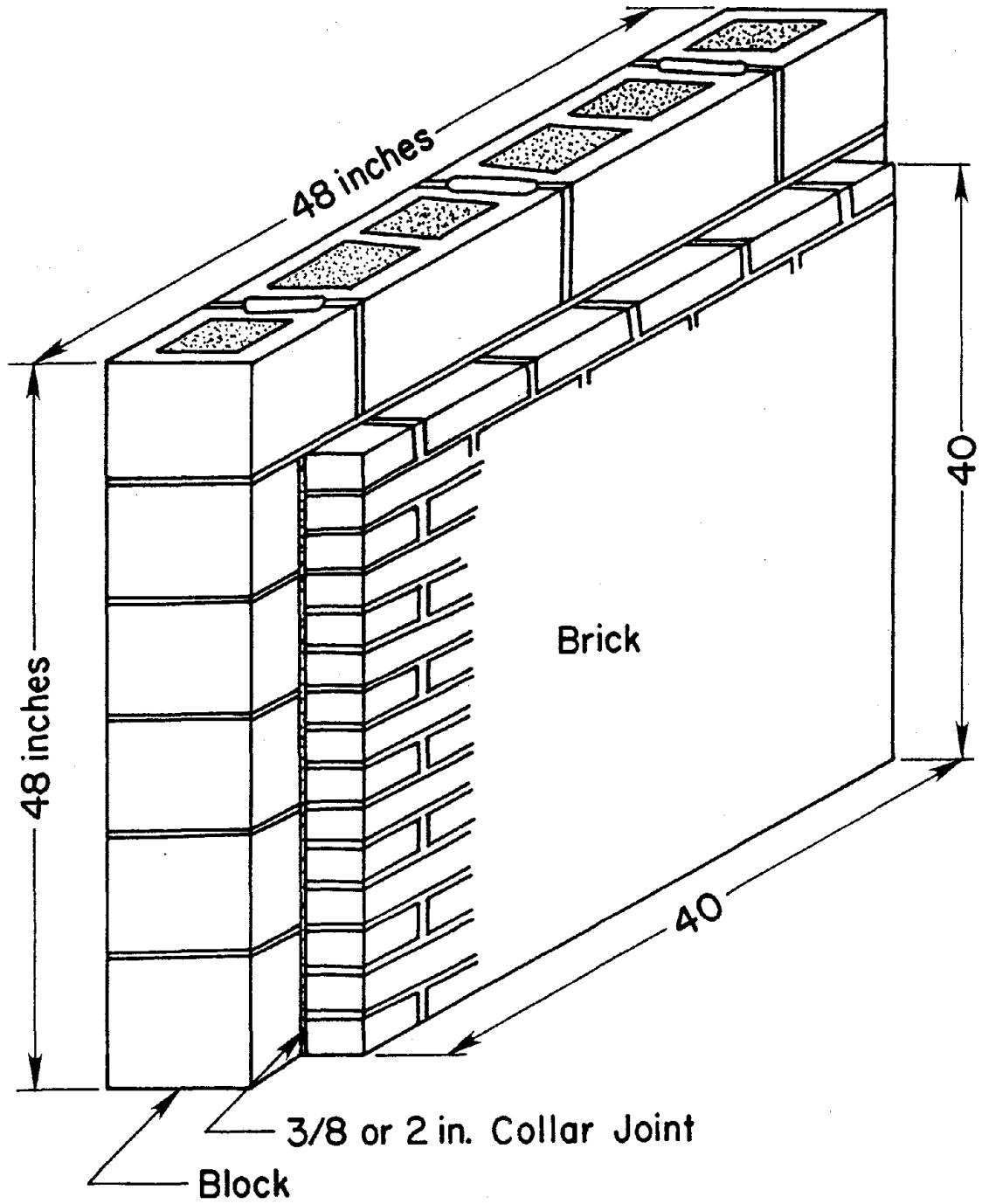
Figure 6.5   A Typical Clemson University Test Specimen
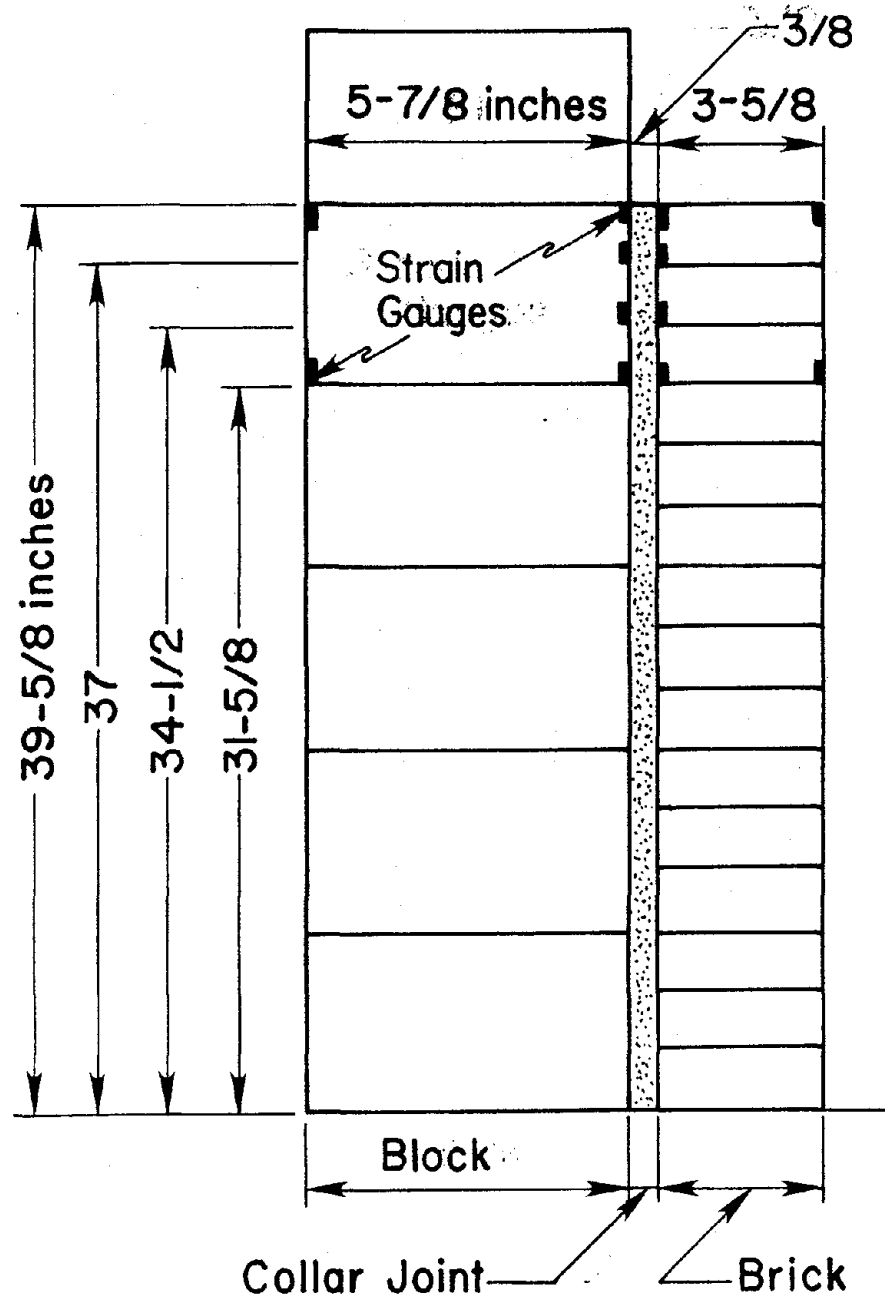
Figure 6.6 Location of Strain Gauges in the Specimen with 3/8 in
Collar Joint
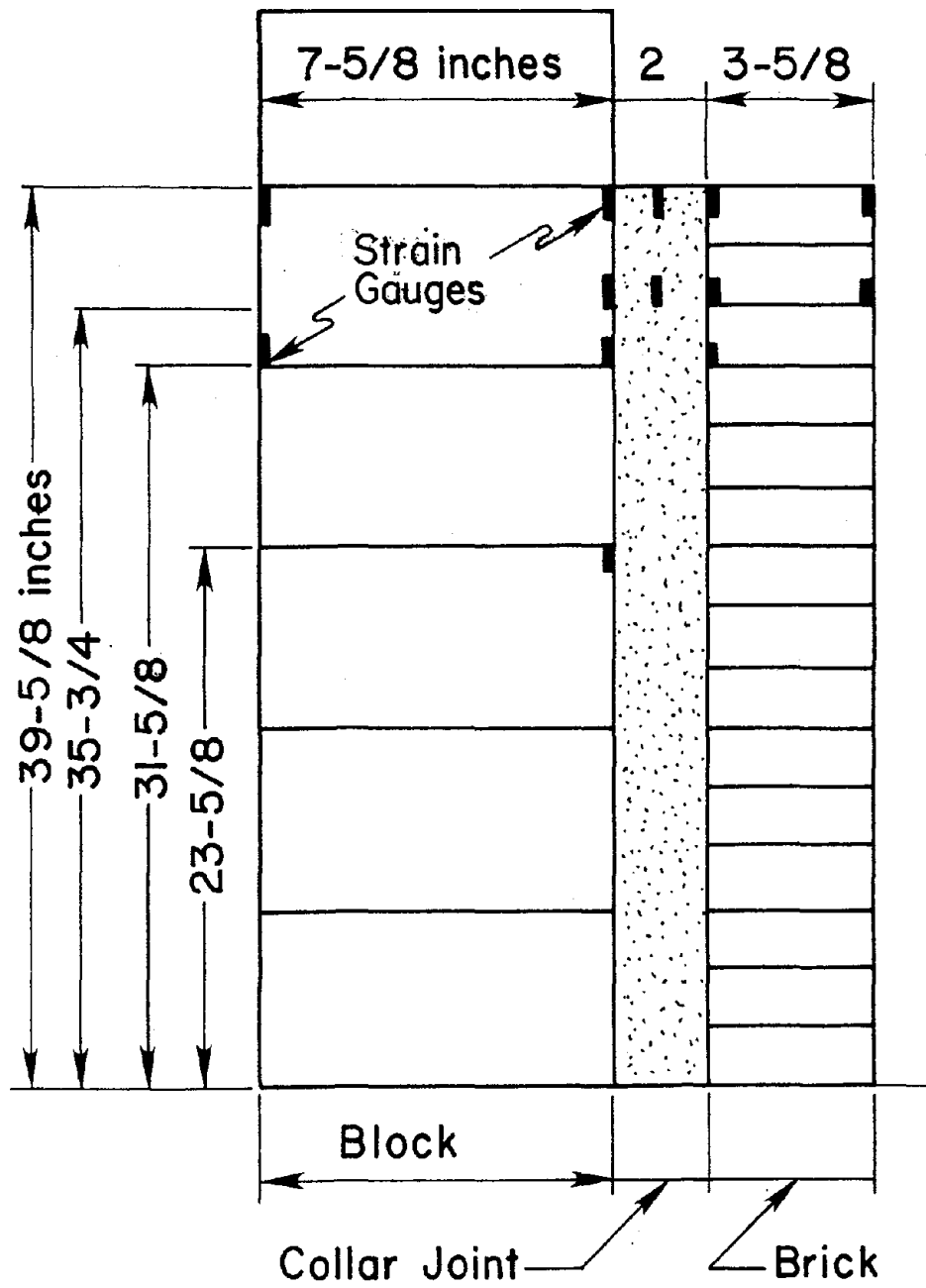
Figure 6.7 Location of Strain Gauges in the Specimen with 2 in Collar Joint

given in References (105), (81) and (108), respectively. The magnitudes of elastic modulus for block masonry, mortar and brick masonry are found to be 1075 ksi, 2480 ksi and 2950 ksi, respectively. The modulus of grouted block masonry is taken as 1600 ksi. Normal strains are computed at various locations considering (1) block wythe-collar joint and brick wythe-collar joint interfaces are very weak in shear (using interface elements assigning the shear modulus obtained from Williams and Geschwindner's test) and (2) block wythes and collar joints as well as brick wythes and collar joints are perfectly bonded together. The analytically computed normal strains are compared with experimentally measured normal strains to understand the behavior of the interface.

The strain gauges were located in the middle length of the test specimen and hence, to obtain normal strains theoretically at those locations where the strain gauges were located, the middle portion of the specimen which was ungrouted is modelled by two-dimensional plane strain finite elements. Also, in order to estimate the normal strains in the ungrouted portion of the specimen for a specific magnitude of total load on the entire length of the wall specimen, it is necessary to know the portion of the total load that acts on the ungrouted portion of the wall. During the test, a uniform vertical displacement was applied over the entire length of the specimen. As the stiffness along the length of the specimen is nonuniform, loads experienced by it at different sections along the length due to the uniform vertical displacement at the top is also expected to be nonuniform. The portion of the total load that acts on the ungrouted portion of the wall specimen is determined next.

Load Fractions for Plane Strain Models

Composite Masonry Wall Specimen
with 3/8 inch Collar Joint

The load fractions for this specimen are determined for two types

of interface behavior. For the first case, the two materials at the

interfaces are assumed to be perfectly bonded together. The grouted

portion of blocks along with bricks at one end of the wall specimen may

be considered as the sum of two simple geometric shapes as shown in Figure

6.8. In shape 1, the vertical displacement, Δ due to axial force P is

given by

$$\Delta = PL/AE \qquad (6.5)$$

where

L = length in inch,

A = cross sectional area of the block of shape 1 in square inch,

E = elastic modulus of the grouted block in psi and

P = axial force in pounds.

Sustituting the values of the parameters yields

$$\Delta = (Px48)/(7.625x4.0x1600)$$
$$= P \times 9.83 \times 10^{-4} \text{ (in)}. \qquad (6.6)$$

Shape 2 is analyzed by the finite element method as a plane strain problem

for a total axial load of 5.814 kips. The vertical displacement at the

top is found to be 0.0042 inches. The ungrouted portion of the specimen,

as shown in Figure 6.9, is also analyzed by the finite element method

considering a plane strain condition and, for a total load of 49.37 kips,

the vertical displacement is found to be 0.0053 inches.

The load that is necessary to produce a vertical displacement of

0.0053 inches in shape 2 is (5.814 x 0.0053)/0.0042 = 7.3368 kips. Also

from Equation 6.6, the load that is necessary to produce a vertical
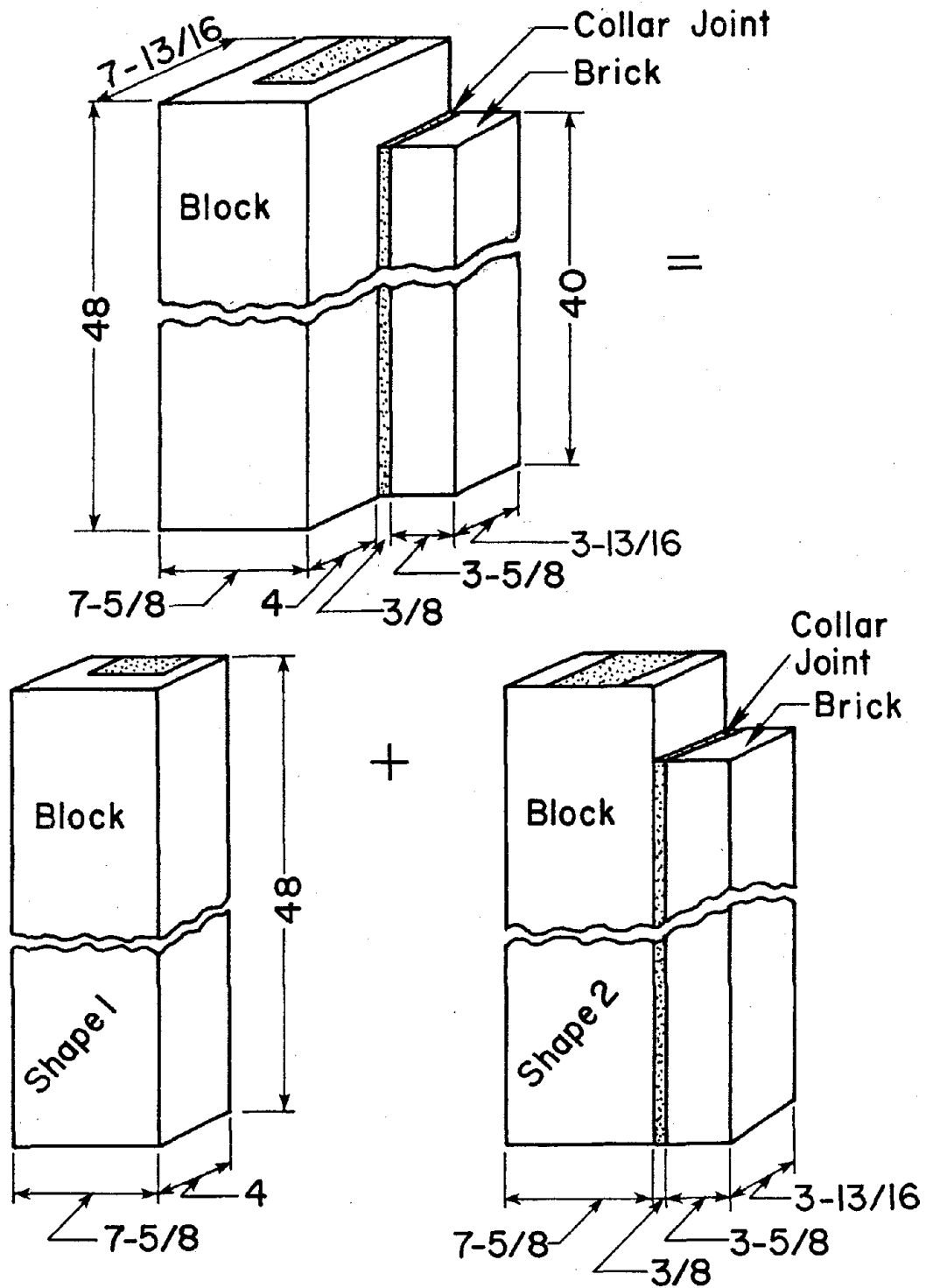
Note: All dimensions are in inches

Figure 6.8   The Grouted Block and Part of Brick Wythe at the End
of the Specimen with 3/8 in Collar Joint
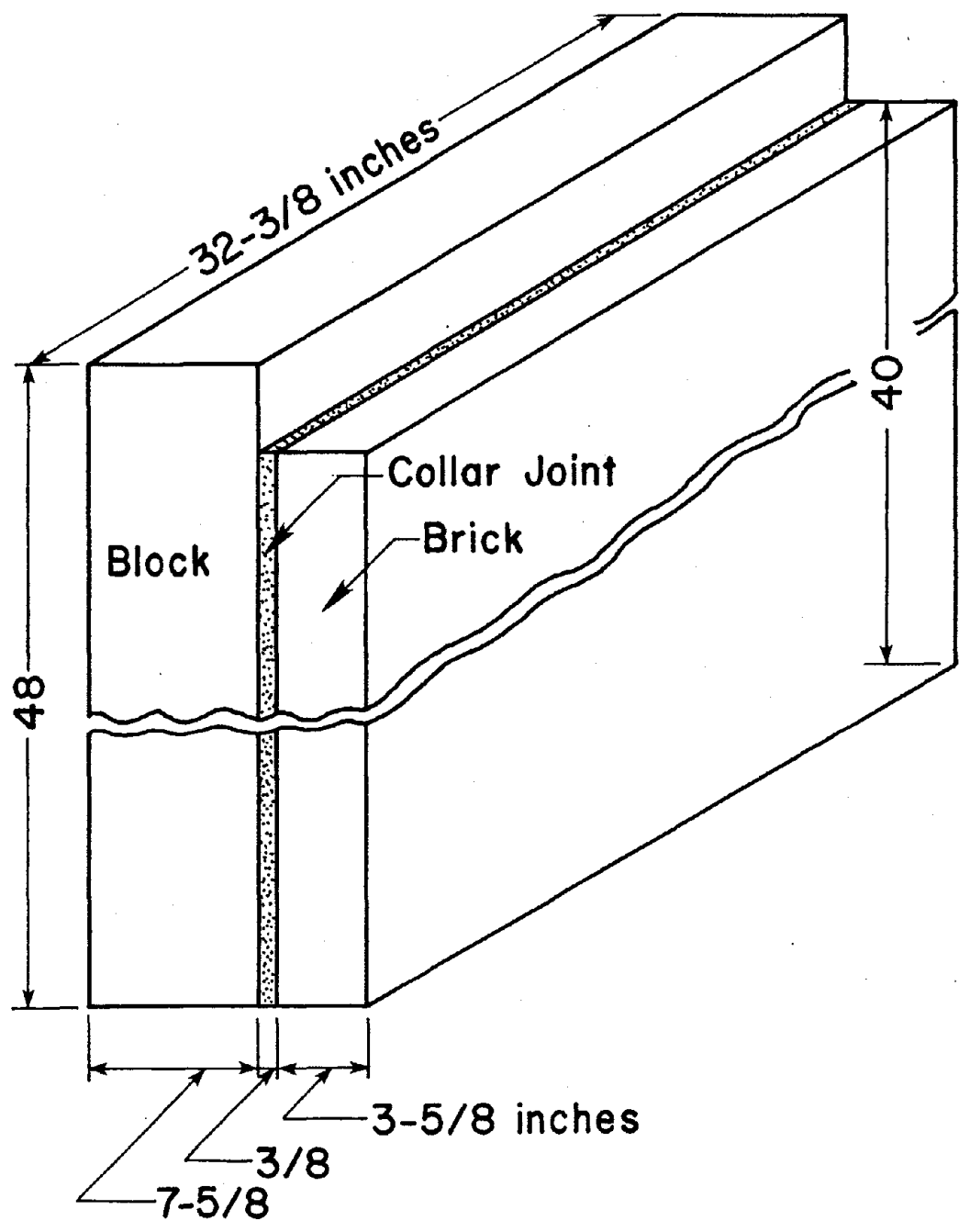
Figure 6.9 Ungrouted Portion of the Specimen with 3/8 in
Collar Joint

displacement of 0.0053 inches in shape 1 is $(0.0053 \times 10^4)/9.83 = 5.39$ kips. Therefore, the total load on the grouted portion of the blocks at the two ends of the walls is $2 \times (7.3368 + 5.39) = 25.45$ kips. Thus, the vertical load necessary to produce a uniform vertical displacement of 0.0053 inches at the top of the wall specimen over the entire length is 74.82 (=25.45 + 49.37) kips. It can be derived from the above mentioned computations that for a uniform vertical displacement, the load experienced by the ungrouted portion of the wall specimen is 0.659 (=49.37/74.82) times the total load experienced by the specimen when the interface materials are considered to be perfectly bonded together.

A second case in which the interfaces are assumed to be extremely weak in shear is considered in the estimation of load distribution between the grouted and the ungrouted portion of the composite masonry wall specimen. The block-collar joint and the brick-collar joint interfaces in shape 2 and in the ungrouted portion of the wall are modelled by interface elements. An interface thickness of 0.1875 inches and a shear modulus of 815 psi obtained from Williams and Geschwindner's test (94) are used for the interface element. Following exactly the same procedure that is adopted in the case of interfaces where the materials are assumed to be perfectly bonded together, it is obtained that for a uniform vertical displacement at the top of the wall specimen along its entire length the load experienced by the ungrouted portion of the specimen is 0.605 times the total load experienced by the entire specimen.

Composite Masonry Wall Specimen
with 2 inch Collar Joint

First, it is assumed that the two different materials at the interfaces are perfectly bonded together. Figure 6.10 shows the grouted
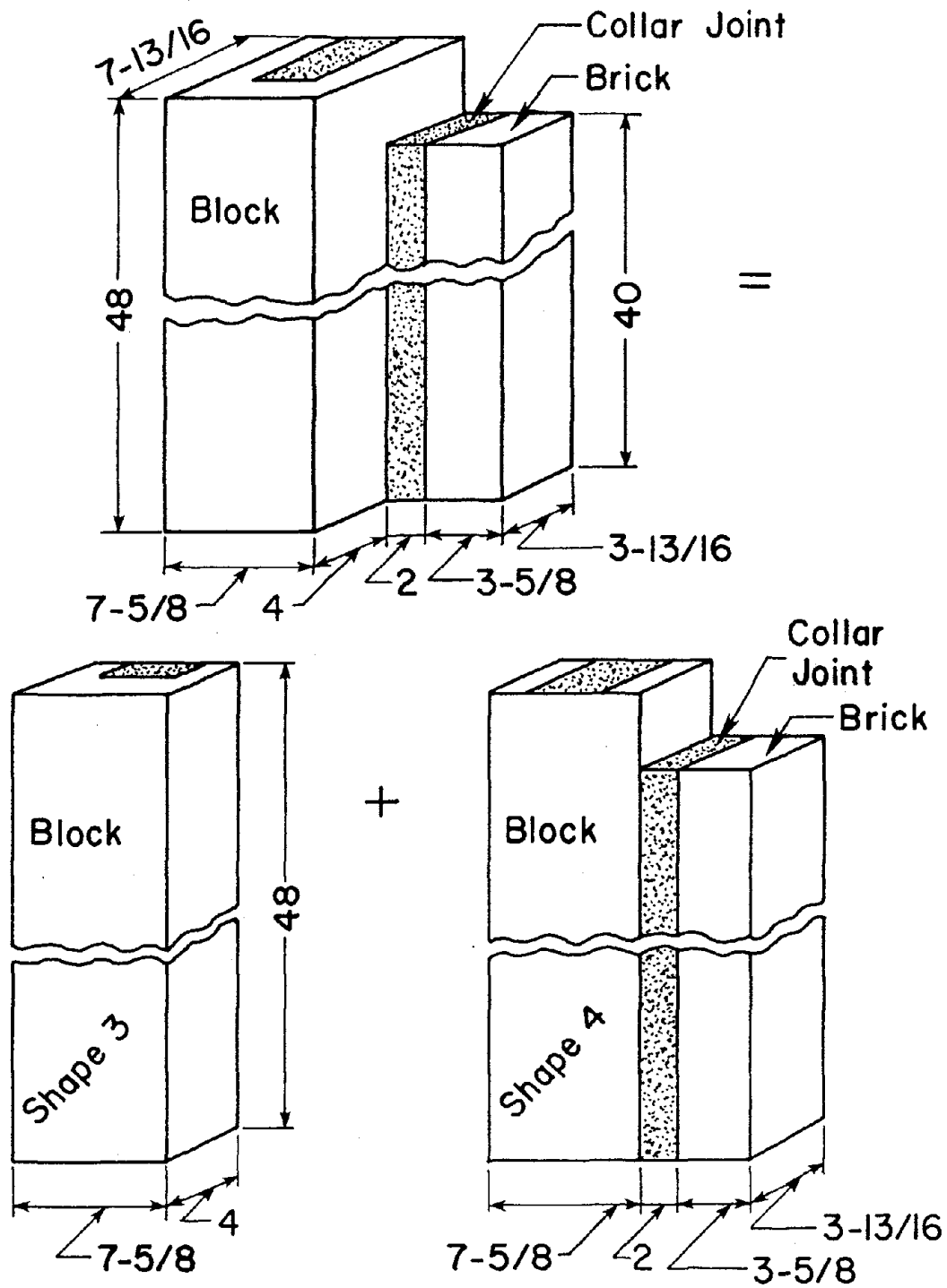
Figure 6.10   The Grouted Block and Part of Brick Wythe at the End
of the Specimen with 2 in Collar Joint

portion of blocks along with bricks at one end of the specimen which may be treated as the sum of two simple geometric shapes, shape 3 and shape 4. Using Equation 6.5, the vertical displacement Δ, in shape 3 due to axial load P can be computed as

$$\Delta = (P \times 48)/(7.625 \times 4.0 \times 1600)$$
$$= P \times 9.83 \times 10^{-4} \text{ (in)}. \tag{6.7}$$

Shape 4 and the ungrouted portion of the wall specimen as shown in Figure 6.11 are analyzed by plane strain finite elements for total vertical loads of 5.814 kips and 49.37 kips, respectively, and the corresponding vertical displacements at the top are found to be 0.0039 and 0.0050 inches.

The total load necessary to produce a vertical displacement of 0.005 inches in shape 4 is 7.4538 (=5.814 x 0.005/0.0039) kips. Also, from Equation 6.7, the total load that is necessary to produce a vertical displacement of 0.005 inches in shape 3 is 5.08 (=0.005 x 10^4/9.83) kips. Therefore, the total vertical load on the two grouted ends of the specimen is 25.06 (=(7.4538 + 5.08) x 2) kips. Thus, it is observed that for a uniform vertical displacement of 0.005 inches at the top of the specimen over its entire length, a total vertical load of 74.45 (= 49.73 + 25.06) kips is necessary. Hence, for a uniform vertical displacement, the load experience by the ungrouted portion of the specimen is 0.663 (49.37/74.45) times the total load experienced by the specimen when the two materials at the interfaces are perfectly bonded together.

Interfaces are also considered to be very weak in shear for estimating the part of total loads that acts on the ungrouted portion of the wall specimen. Shape 4 and the ungrouted portion of the specimen are analyzed using interface elements to model the interfaces. The interface thickness is assumed to be 0.1875 inches and the shear modulus is taken as that derived from Williams and Geschwindner's test. Following the
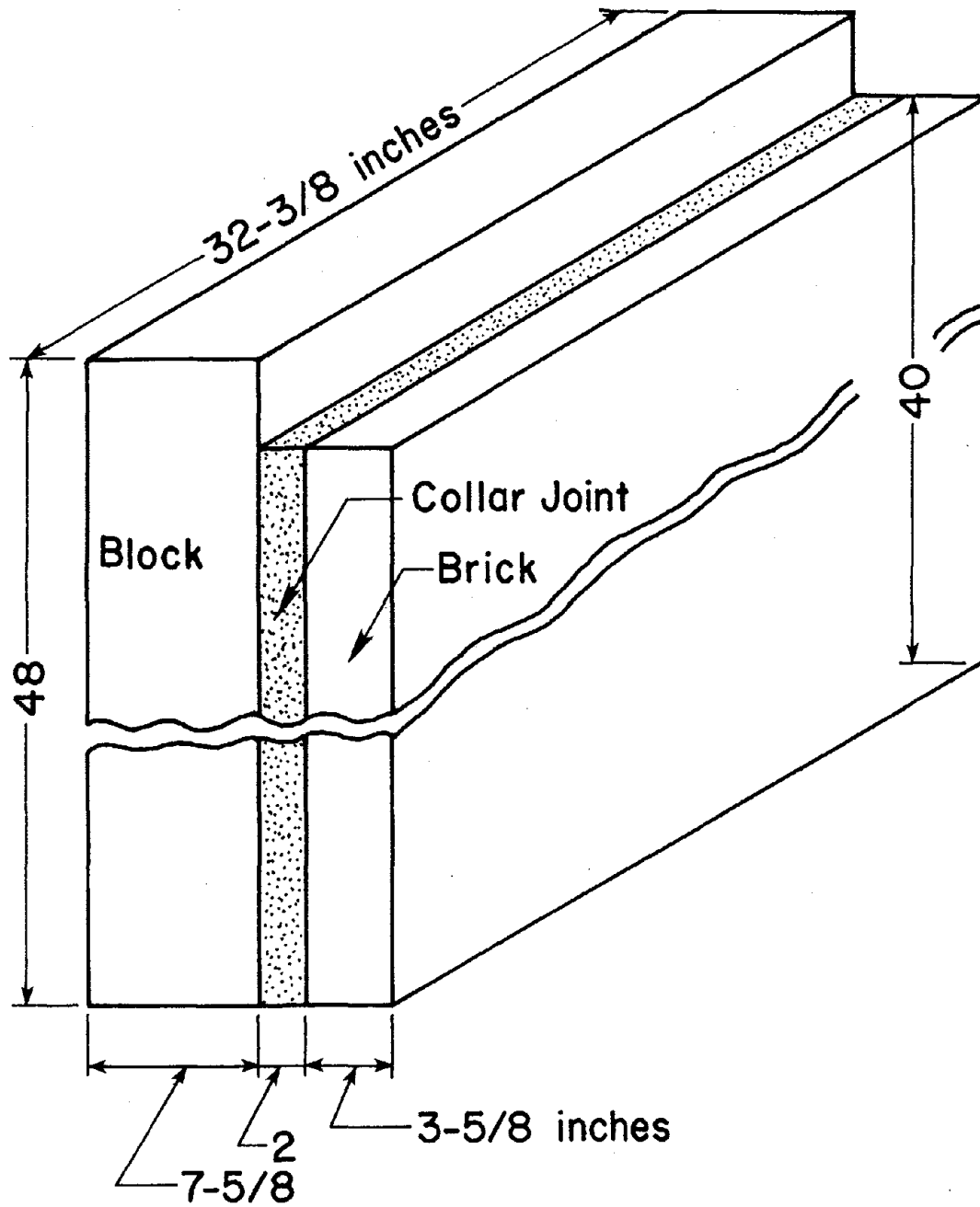
Figure 6.11   Ungrouted Portion of the Specimen with 2 in
Collar Joint

procedure as mentioned above for the case of interfaces where the materials are perfectly bonded together, it is found that for a uniform vertical displacement at the top along the length of the specimen, the load experienced by the ungrouted portion is equal to 0.606 times the total load experienced by the wall specimen.

Two-dimensional Analysis of Composite Wall Specimens

The ungrouted portions of the composite masonry wall specimens with 2 inch and 3/8 inch collar joints are analyzed by a 2-D finite element method considering plane strain condition. The experimental failure loads for a composite wall specimen with 2 inch and 3/8 inch collar joints were found to be 210 kips and 150 kips, respectively. Hence, at an arbitrary load level of 80 kips, the wall specimens are neither expected to undergo any permanent deformation nor be influenced by the nonlinearities due to cracks. At this load level, the composite masonry wall specimens are assumed to behave linearly elastically. In order to obtain strains analytically in the specimens corresponding to an 80 kips total load, a 53 (=80 x 0.663) kip load is applied on the ungrouted portion of the wall specimen with a 2 inch collar joint and a 52.7 (=80 x 0.659) kip load is applied on the ungrouted portion of the composite wall specimen with 3/8 inch collar joint when the two dissimilar materials at the interfaces in both the specimens are considered to be perfectly bonded together.

When interfaces are considered very weak in shear, 48.48 (=80 x 0.606) kip and 48.40 (=80 x 0.605) kip loads are experienced by the middle portion of the specimen with 2 inch and 3/8 inch collar joints, respectively, for a total load of 80 kips on the entire specimen. In this case, interface elements are used to model the weak interfaces. The interface

thickness is considered as 0.1875 inches for both the composite masonry wall specimens. The shear modulus of the joint elements is assigned a value of 815 psi, which is derived from Williams and Geschwindner's test (94). The normal strains obtained from these analyses are compared with the experimentally obtained normal strains.

Comparison of Analytical Results with Experimental Observations

The normal strains obtained experimentally and the normal strains computed analytically for composite wall specimens with 2 inch and 3/8 inch collar joints are plotted and shown in Figures 6.12 through 6.19. The normal strains shown in Figures 6.12 and 6.15 for composite wall specimens with 3/8 inch collar joints indicate that the magnitude of normal strains obtained experimentally agree better with the normal strains computed analytically when the interface materials are considered perfectly bonded together. Figures 6.13 and 6.14 also show the normal strains in the specimen with 3/8 inch collar joints. In Figure 6.13, the experimentally obtained normal strains are equally comparable with both the analytically computed normal strains obtained considering that the interfaces are very weak in shear and the interface materials are perfectly bonded together. It can be observed in Figure 6.14 that the experimentally observed normal strains in the blocks at the interface below the top two inches of the specimen are almost equal to the normal strains computed analytically considering that the interfaces are very weak in shear. However, within the top two inches of the specimen, the normal strains obtained analytically considering that the interfaces are very strong in shear are close to the experimental normal strains. Thus, examining the plots of the normal strains obtained analytically and
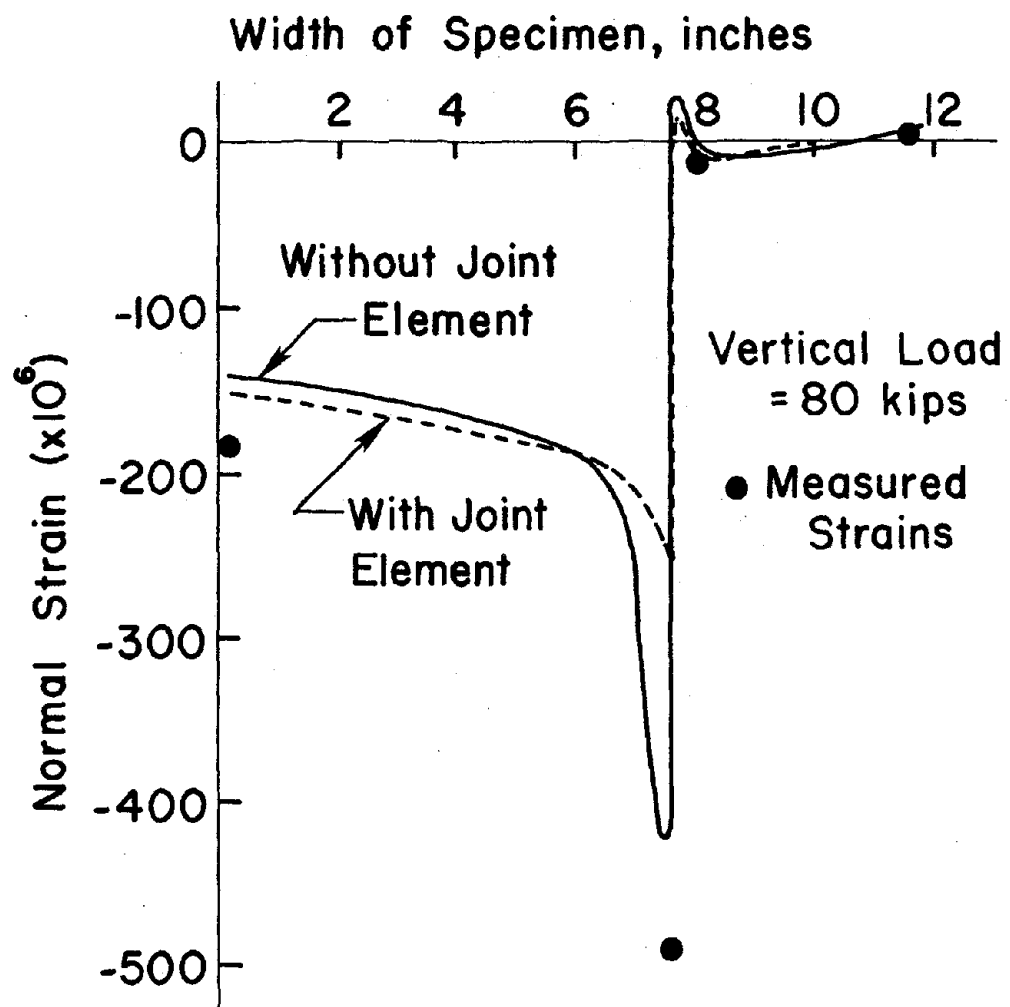
Figure 6.12 Normal Strains at a Distance of 40 in from the Bottom of the Specimen with 3/8 in Collar Joint
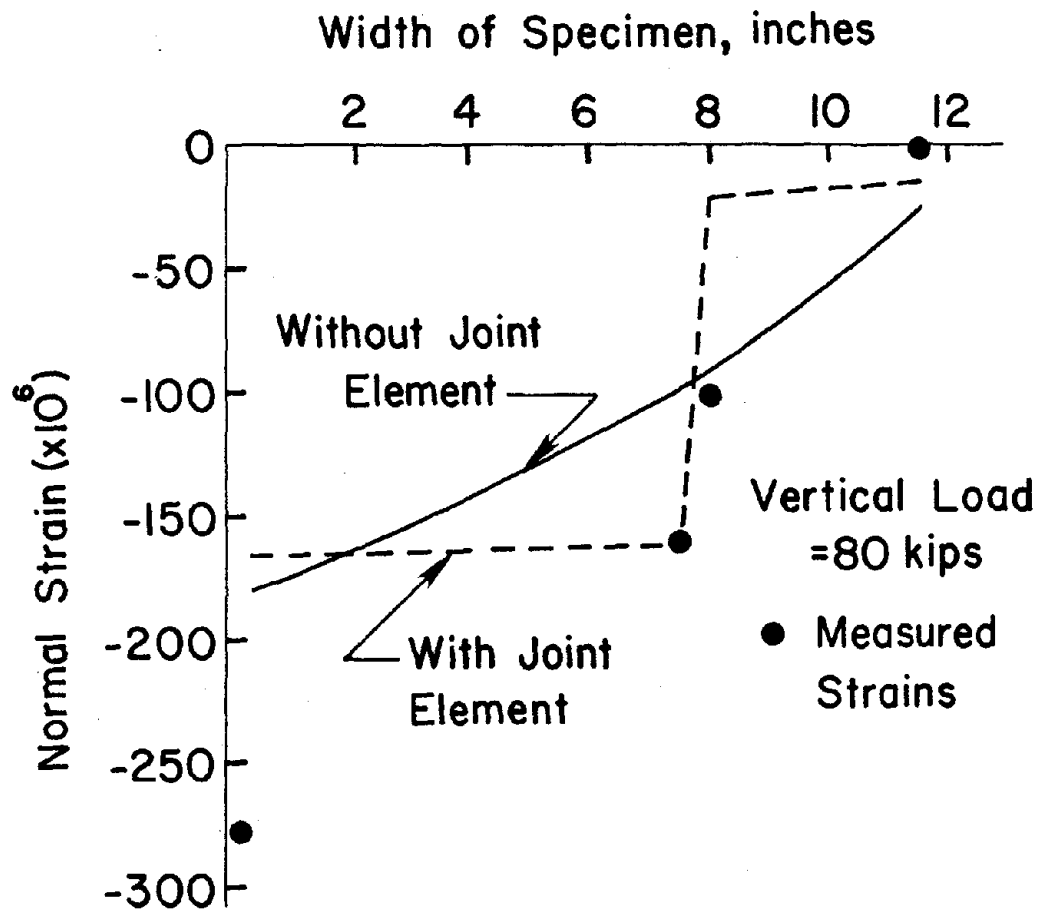
Figure 6.13   Normal Strains at a Distance of 32.37 in from the Bottom
of the Specimen with 3/8 in Collar Joint
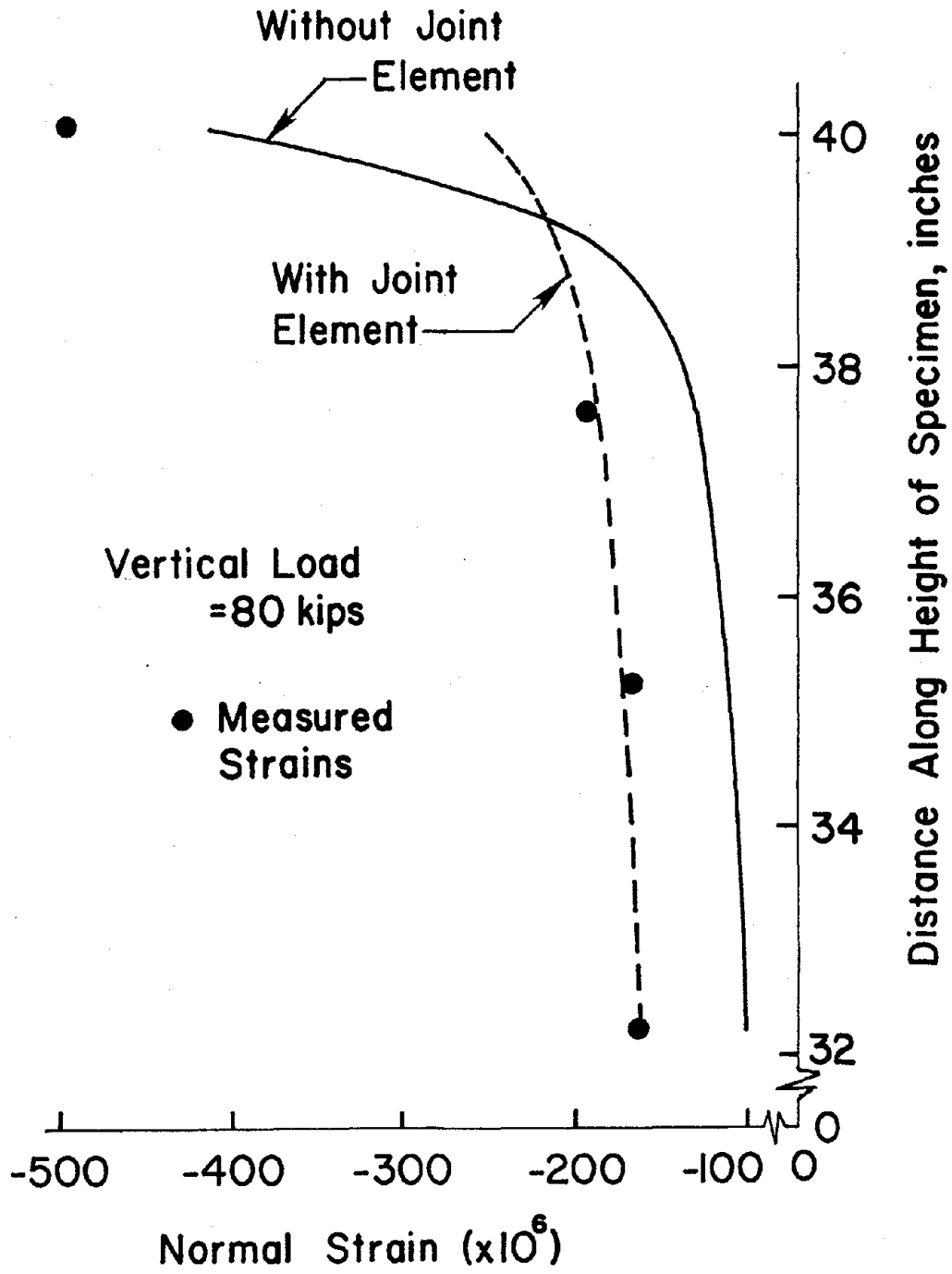
Figure 6.14   Normal Strains in the Block Wythe at Block Wythe-Collar
Joint Interface of the Specimen with 3/8 in
Collar Joint
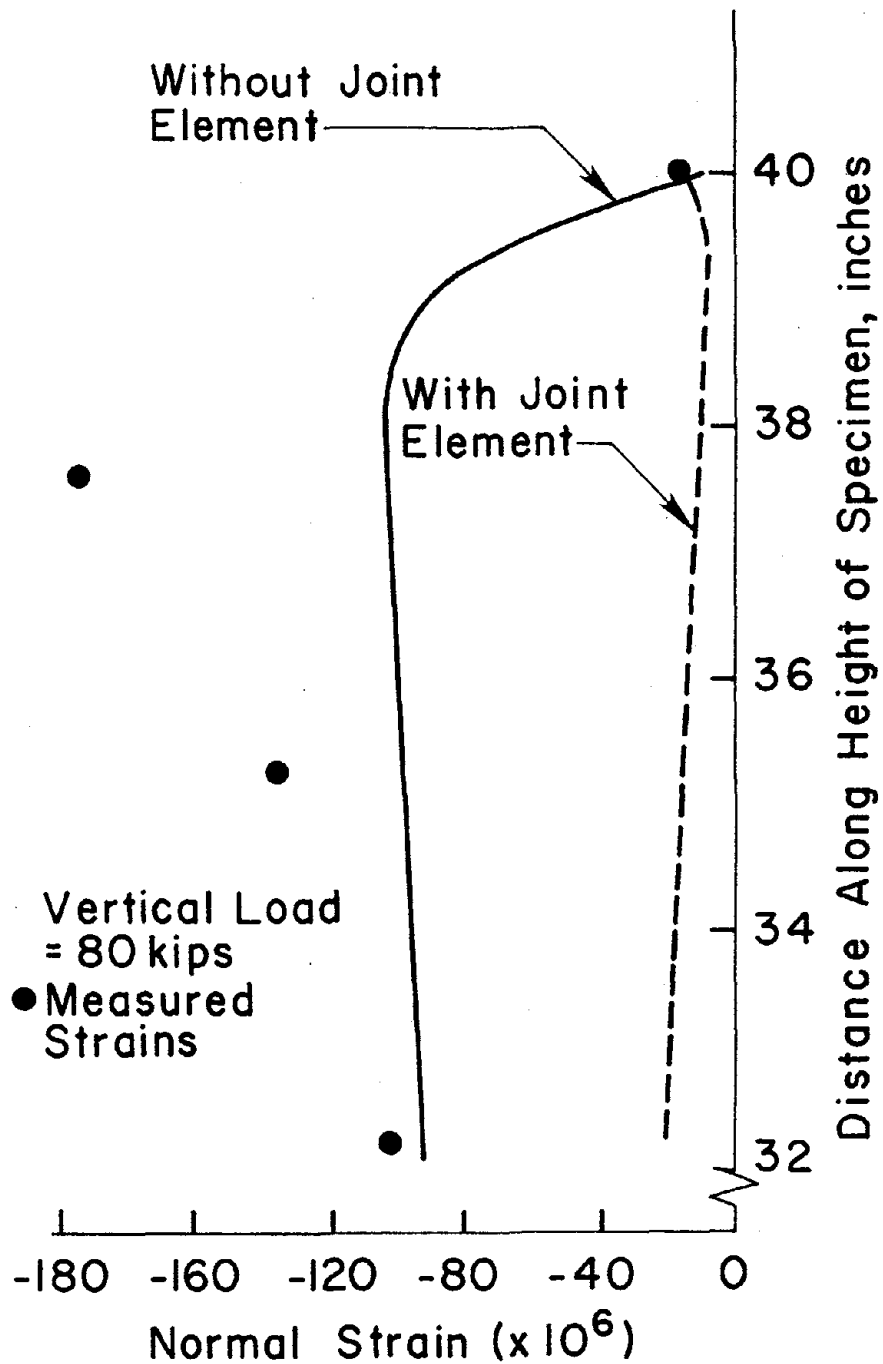
Figure 6.15   Normal Strains in the Brick Wythe at Brick Wythe-Collar
Joint Interface of the Specimen with 3/8 in
Collar Joint
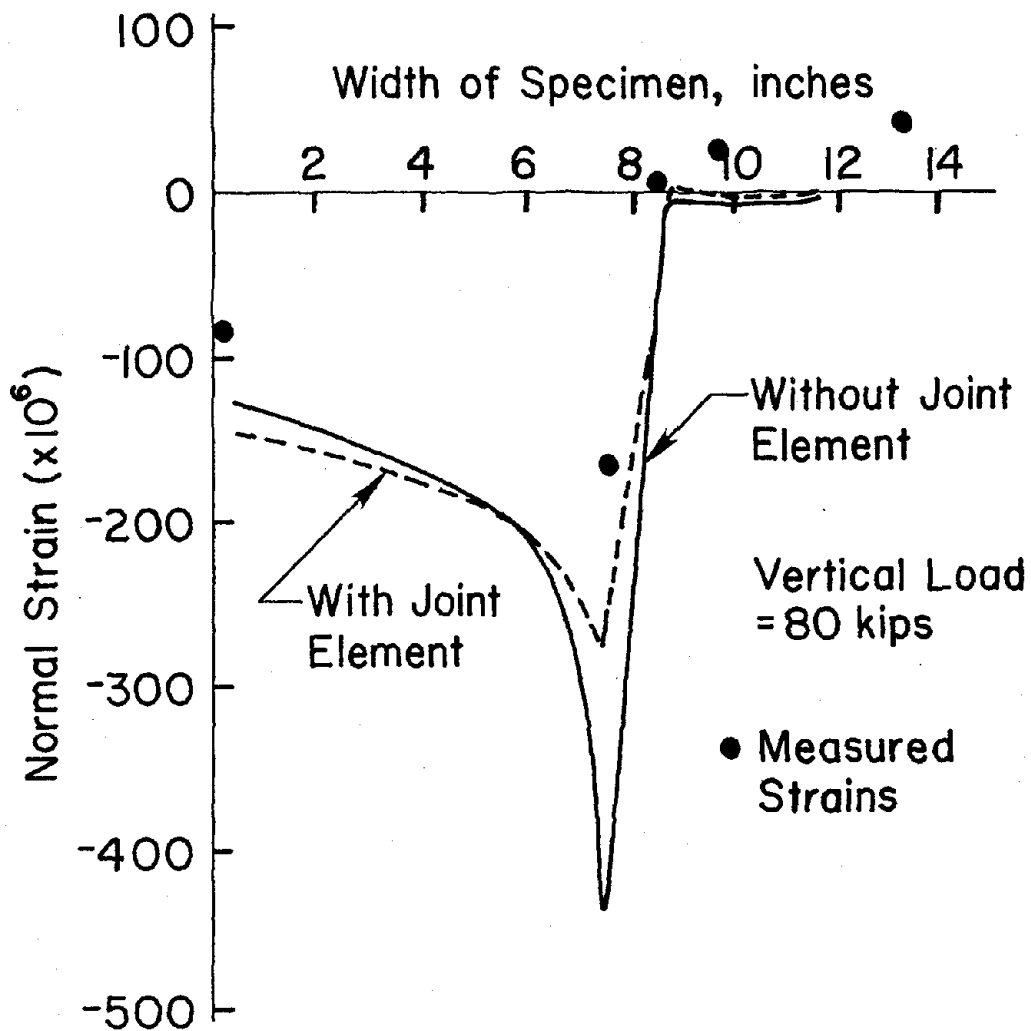
Figure 6.16 Normal strains at a Distance of 40 in from the Bottom of the Specimen with 2 in Collar Joint
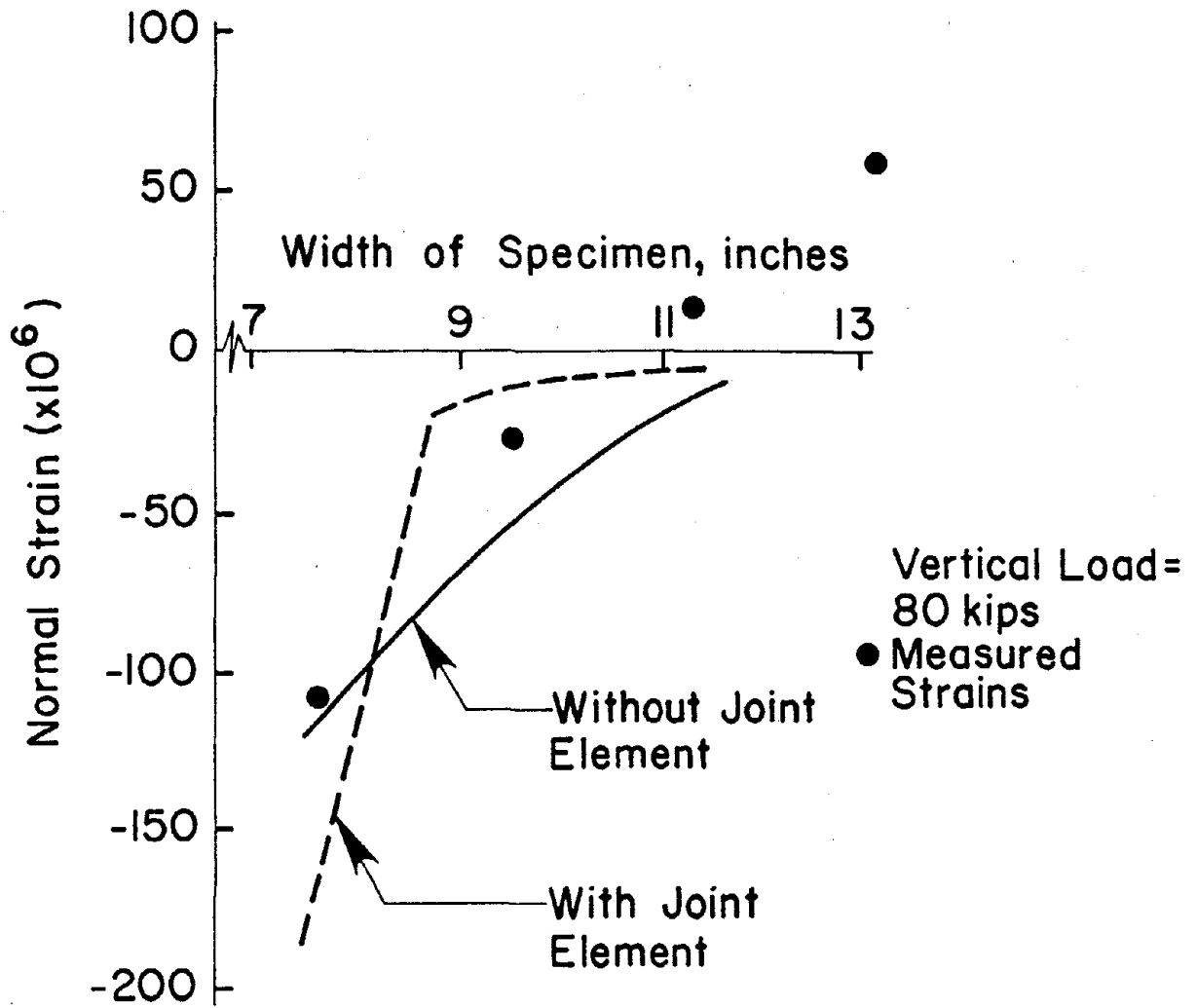
Figure 6.17 Normal Strains at a Distance of 36.25 in from the
Bottom of the Specimen with 2 in Collar Joint
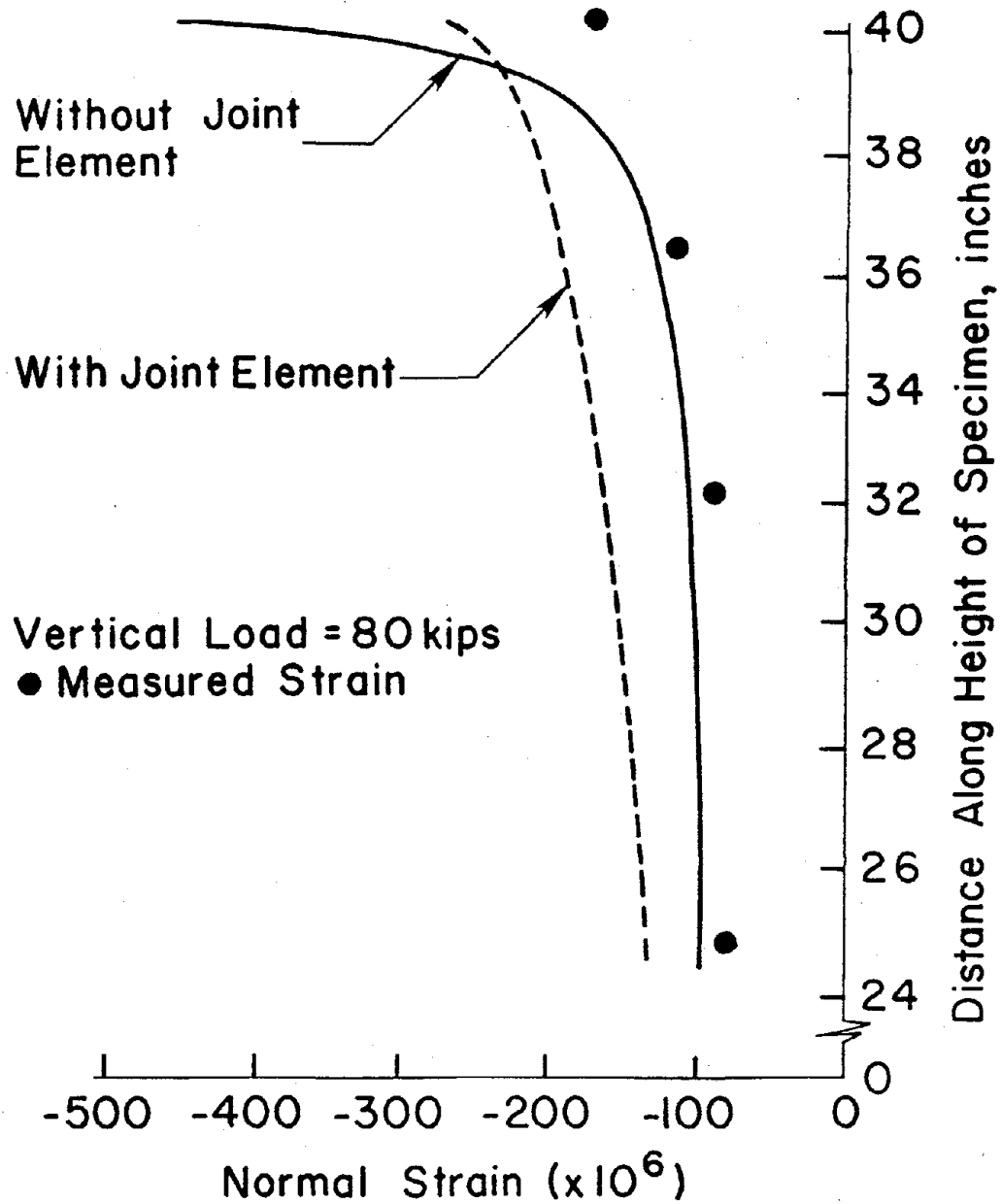
Figure 6.18 Normal strains in the Block Wythe at Block Wythe-Collar
Joint Interface of the Specimen with 2 in
Collar Joint
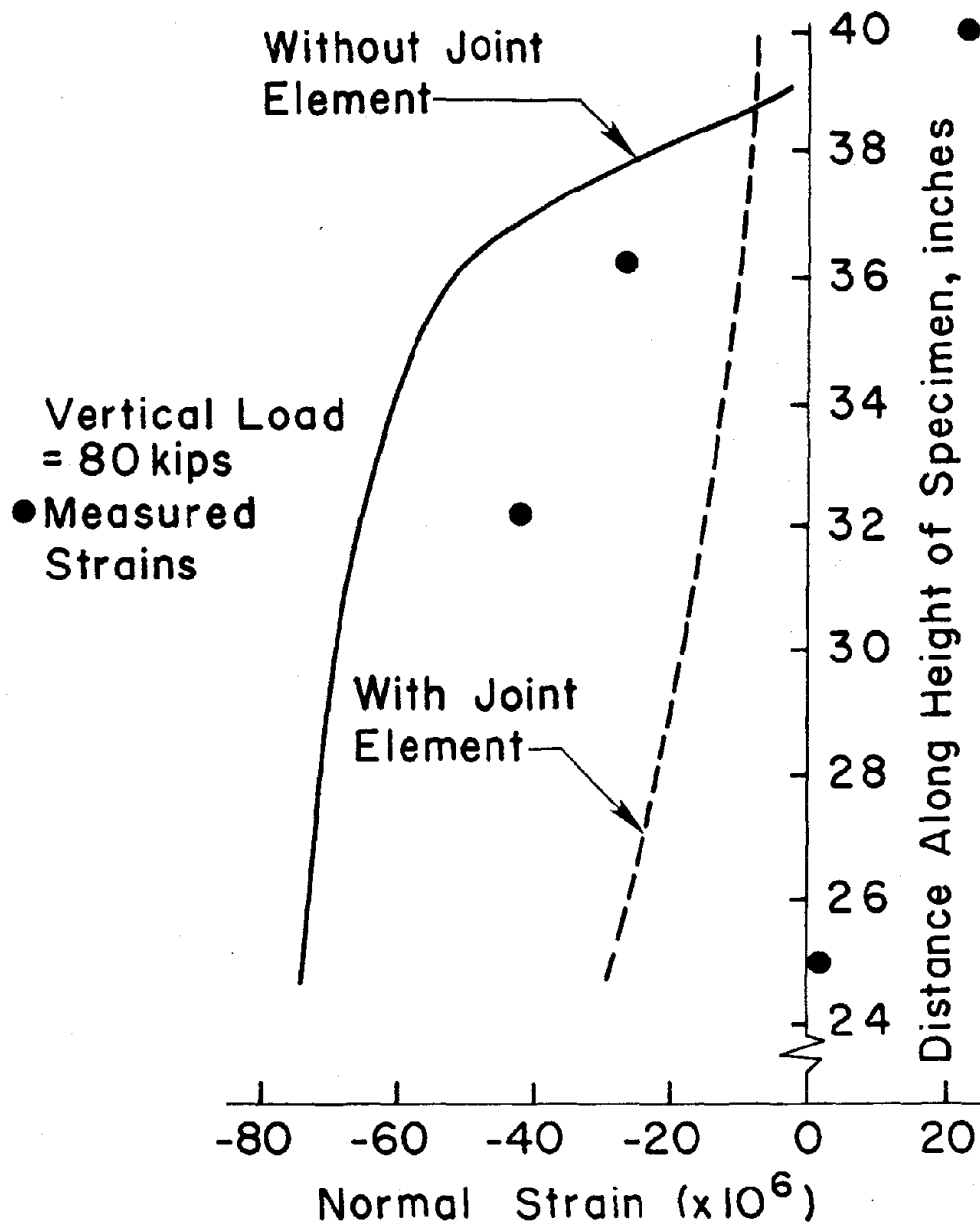
Figure 6.19   Normal Strains in the Brick Wythe at Brick Wythe-Collar
Joint Interface of the Specimen with 2 in
Collar Joint

experimentally in a composite masonry wall specimen with 3/8 inch collar joint, it can be concluded that the block-collar joint and the brick-collar joint interfaces behave more like perfectly bonded joints rather than planes of weakness.

Figures 6.16 through 6.19 show the plots of normal strains measured experimentally and theoretically in a composite wall specimen with 2 inch collar joint. In Figure 6.16, the experimentally determined normal strains are in better agreement with the theoretically computed normal strains obtained by considering that the interfaces are very weak in shear. However, it is also observed that the experimentally measured strains do not show any evidence of stress concentration (which is expected) in the block at the interface. The strain distribution, obtained analytically by considering interfaces as strong joints shows a very large strain in the block at the interface due to stress concentration. At this point, this particular normal strain differs considerably from the experimentally measured strain. In Figure 6.18, it is shown that the theoretical strains in the block at the interface that are obtained by considering the interfaces as very strong joints are almost the same as the experimentally determined strains except at one point in the block at the top of the collar joint where a stress concentration is expected. The distributions of normal strains in the specimen along the width and in the brick along the height measured experimentally are very similar to the distributions of the corresponding normal strains obtained theoretically by analyzing the composite masonry wall specimen considering the interfaces to be very strong in shear. These are shown in Figures 6.17 and 6.19, respectively. From the above mentioned plots, it is clear that the block- collar joint and the brick-collar joint interfaces behave

like strong joints in which dissimilar materials at the interface are

assumed to be perfectly bonded together.

Conclusions

1. The shearing modulus of elasticity of the interfaces of the
   composite masonry wall specimen obtained from Williams and
   Geschwindner's test (94), differ considerably from the shearing
   modulus of elasticity calculated from the shear stress
   vs. strain diagrams given by Page (71) and Ali and Page (2).
   This indicates that if one decides to model the interfaces of a
   particular wall by interface elements, it would be necessary to
   determine experimentally the values of shearing modulus of the
   interfaces for that particular wall.

2. The behavior of the interface in composite masonry walls has
   been evaluated by comparing the theoretical results with
   experimental observations. It is concluded from the comparison
   that the interface behaves like perfectly bonded joints. Hence,
   interface elements are not considered appropriate for modelling
   block wythe-collar joint interfaces, and are not used in this
   research.

CHAPTER VII

STRESSES AT THE INTERFACE OF LOADED WYTHE

AND COLLAR JOINT

In this chapter, a procedure is described to estimate correct

stresses at the block-collar joint interface when the interface in a

composite masonry wall is considered to be perfectly bonded together.

In composite walls, generally the inner block wythe is loaded and hence,

a stress discontinuity exists at the top free end in the block-collar

joint interface. It is shown here that for composite walls involving

stress discontinuities the finite element procedure can be used to obtain

reasonably correct solutions using the recommendations suggested by

Whitcomb et al. (93). It is further shown that the suggested procedure

can also be used in conjunction with the variable-number-node elements

those are developed in Chapter V to obtain correct stresses in composite

walls.

Stress Discontinuities

To illustrate the stress discontinuity at a point, consider the

problem of uniform pressure on part of a semi-infinite plane as shown in

Figure 7.1(a). The exact solution of this problem is known and is given

in Ref. (93). The boundary condition on the shearing stress is $\tau_{yx} = 0$

along $y = 0$. However, if the points $(\pm a, 0)$ are approached along $x =$

$\pm a$, then from the exact solution $\tau_{xy}(\pm a, 0) = \pm p/\pi$. Therefore, due to

stress discontinuities at the points $(\pm a, 0)$, $\tau_{xy} \neq \tau_{yx}$. The numerical

procedure is based on the assumption of a symmetric stress tensor every-

where in the continuum including the points with stress discontinuities.

(a)

(b)
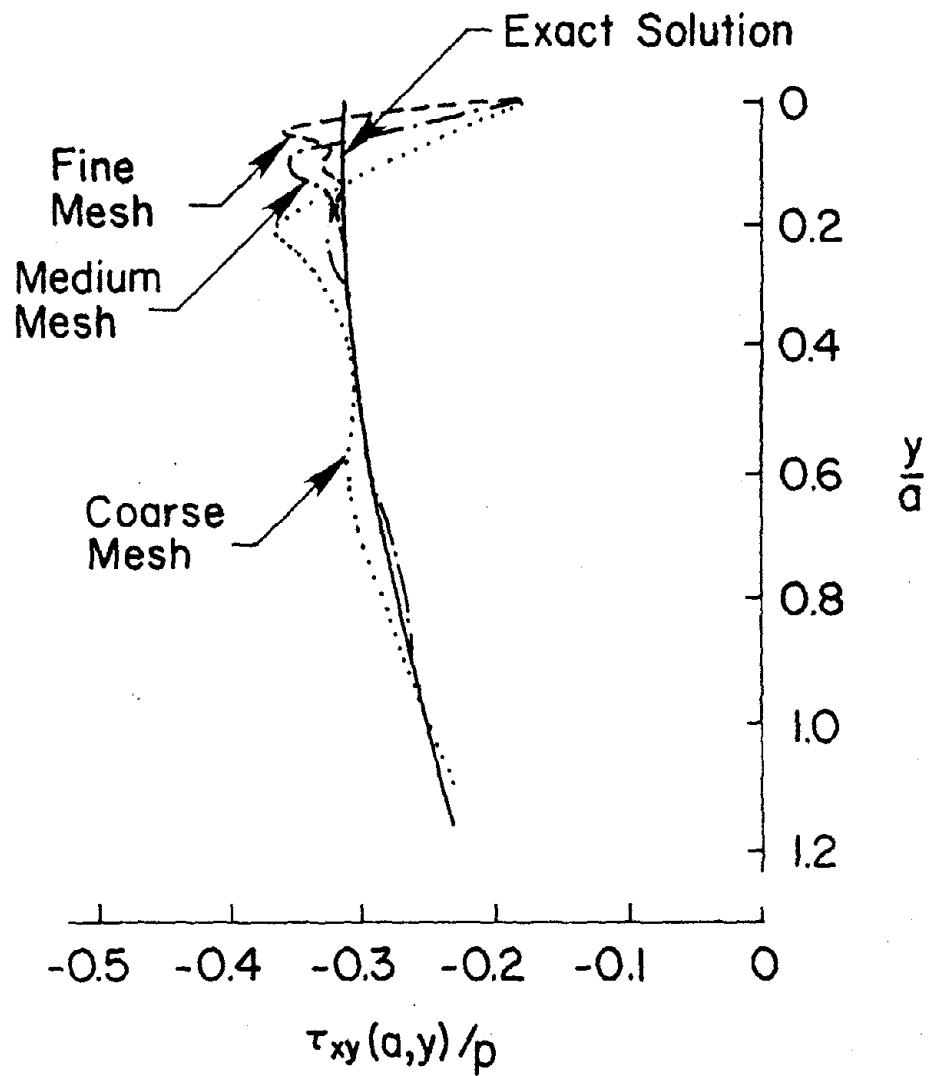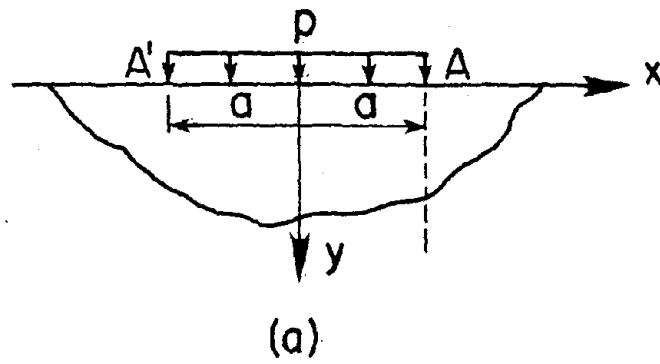
Figure 7.1 Shear Stress (τ_{xy}/p) Distribution on x = a Line

Therefore, these procedures cannot account for an unsymmetric stress tensor at these points, and this leads to difficulties. Whitcomb et al. (93) have studied how the finite element method calculates the stresses near stress discontinuities. Some important features of this study are given next.

The relevant domain of the problem shown in Figure 7.1(a) was idealized by eight noded isoparametric elements. Three meshes: coarse, medium and fine were used. The medium mesh was obtained by subdividing each element of the coarse mesh into four elements. Similarly, the fine mesh was obtained by subdividing each element of the medium mesh into four elements. Figure 7.1(b) presents the normalized shear stress distribution τ_{xy} on the line $x = a$ for $0 \leq y \leq a$. The finite element solutions with the three meshes agreed very well with the exact solution except in the immediate neiborhood of point A. It was observed that the region of disagreement was confined to the two elements nearest the discontinuity. Examining the distribution of τ_{yx} on the line $y = 0$, it was observed that region of disagreement of the finite element results with the exact results was confined to two elements on either side of point A. Based on the above observations, it was concluded that for a problem involving stress discontinuities, the finite element solutions are accurate everywhere except very near the stress discontinuities. However, the region of inaccuracy is limited to about two elements and such a region can be made very small by progressive mesh refinement.

Finite Element Solutions of Composite Masonry Walls with Stress Discontinuities

Composite masonry walls with two inch collar joints are modelled by finite elements assuming materials at the interfaces are perfectly bonded

together. Figures 7.2 and 7.3 show two finite element meshes, Mesh G and Mesh GG of composite walls, respectively, modelled by quadratic isoparametric elements. The Mesh GG in Figure 7.3 is relatively coarser than the Mesh G shown in Figure 7.2. The composite walls are also modelled by ten noded variable-number-node elements (VISO10) and the meshes are designated by G10 and GG10 and are shown in Figures 7.4 and 7.5. It is attempted to show that the very coarse mesh of VISO10 elements can also be used to predict correct stresses at the interfaces of composite masonry walls.

The normalized shear stresses in the 0.1 inch thick elements in the collar joint at the block-collar joint interface along the height of the wall with Mesh G and Mesh GG are shown in Figure 7.6. It is observed in these analyses that the shear stresses in the top two elements at the interface near the region of stress discontinuity are oscillatory. It is also noticed that the shear stress distribution predicted by Mesh G agrees well with that predicted by Mesh GG everywhere within the interface except in the top two elements. A similar situation was observed by Whitcomb et al. (93) in composite laminates subjected to stress discontinuities. Hence, the procedure suggested by Whitcomb et al.(93) to obtain accurate solutions by the finite element method for problems involving stress discontinuities can also be used for composite masonry walls. Further, since the refinement of the mesh from G to GG did not alter the predicted shear stress distribution, the Mesh G may be considered as the optimum mesh for accurate prediction of shear stresses in the collar joint at the interface. The normalized value of the maximum shear stress in the collar joint at the block wythe-collar joint interface predicted by Mesh G is 0.32.
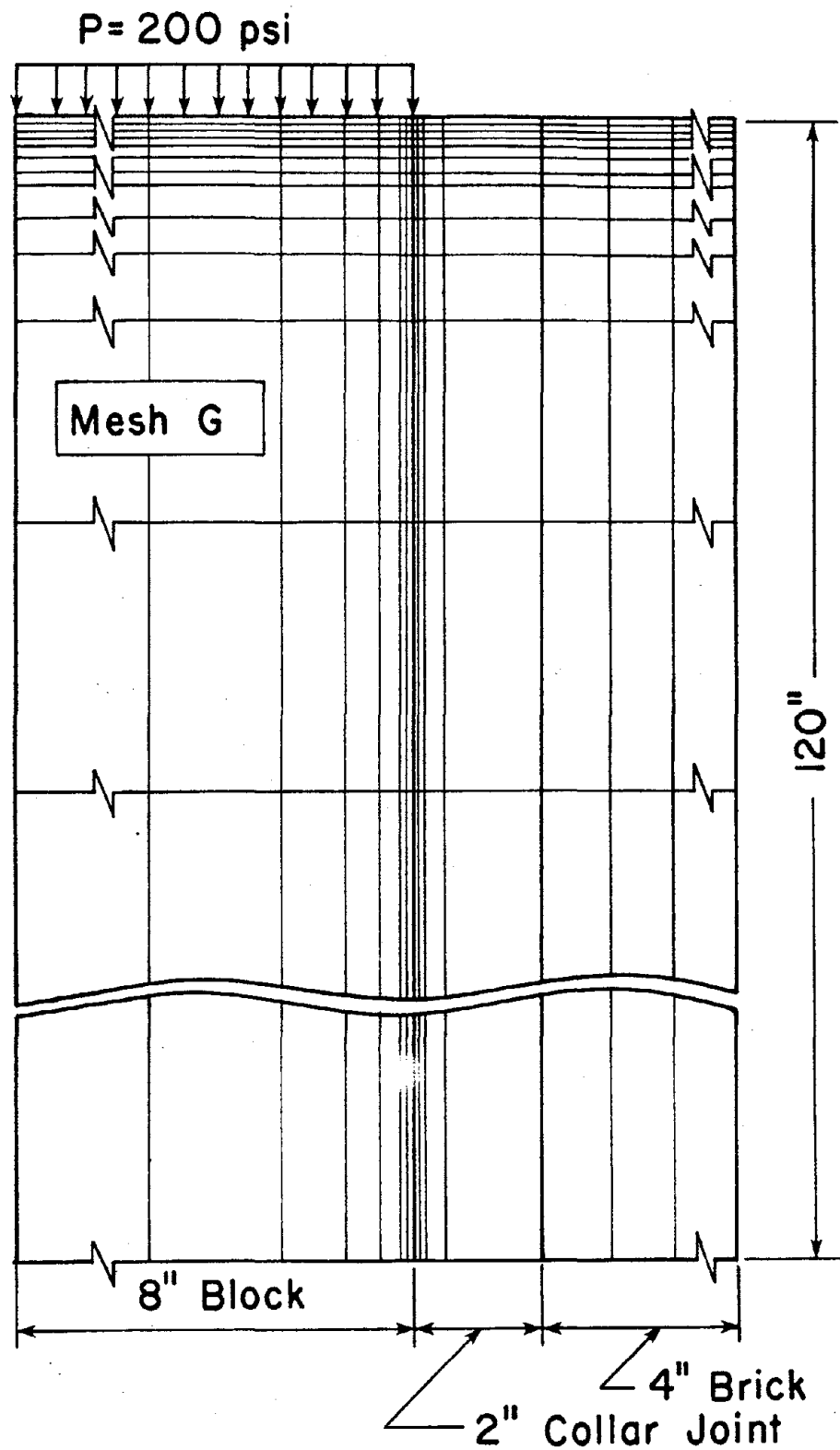
Figure 7.2 Mesh G, A Finite Element Mesh of Quadratic Isoparametric
Elements for a Composite Masonry Wall with 2 in
Collar Joint
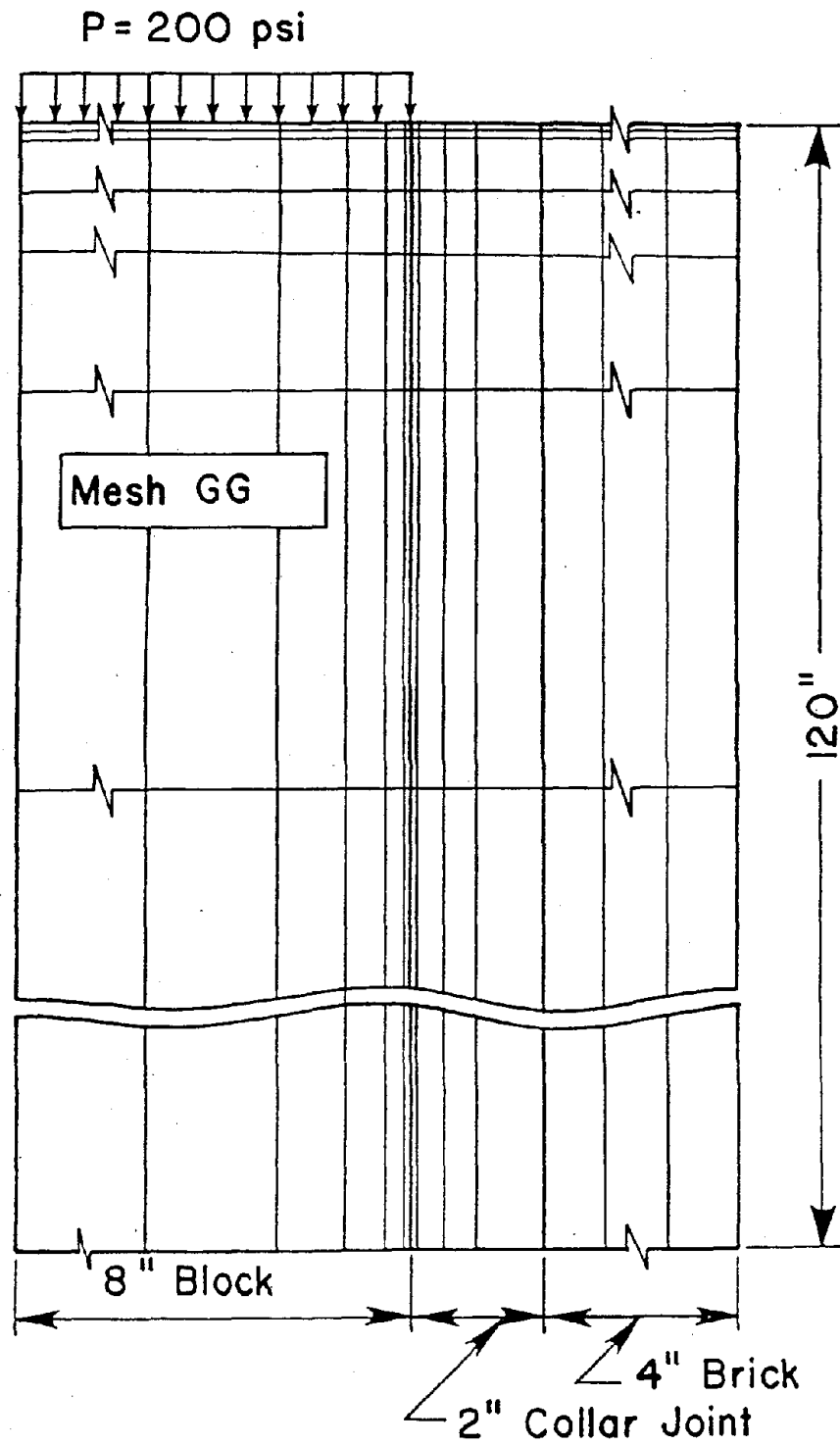
Figure 7.3 Mesh GG, A Finite Element Mesh of Quadratic Isoparametric
Elements for a Composite Masonry Wall with 2 in
Collar joint

P = 200 psi

Mesh GIO

120"

8" Block

4" Brick
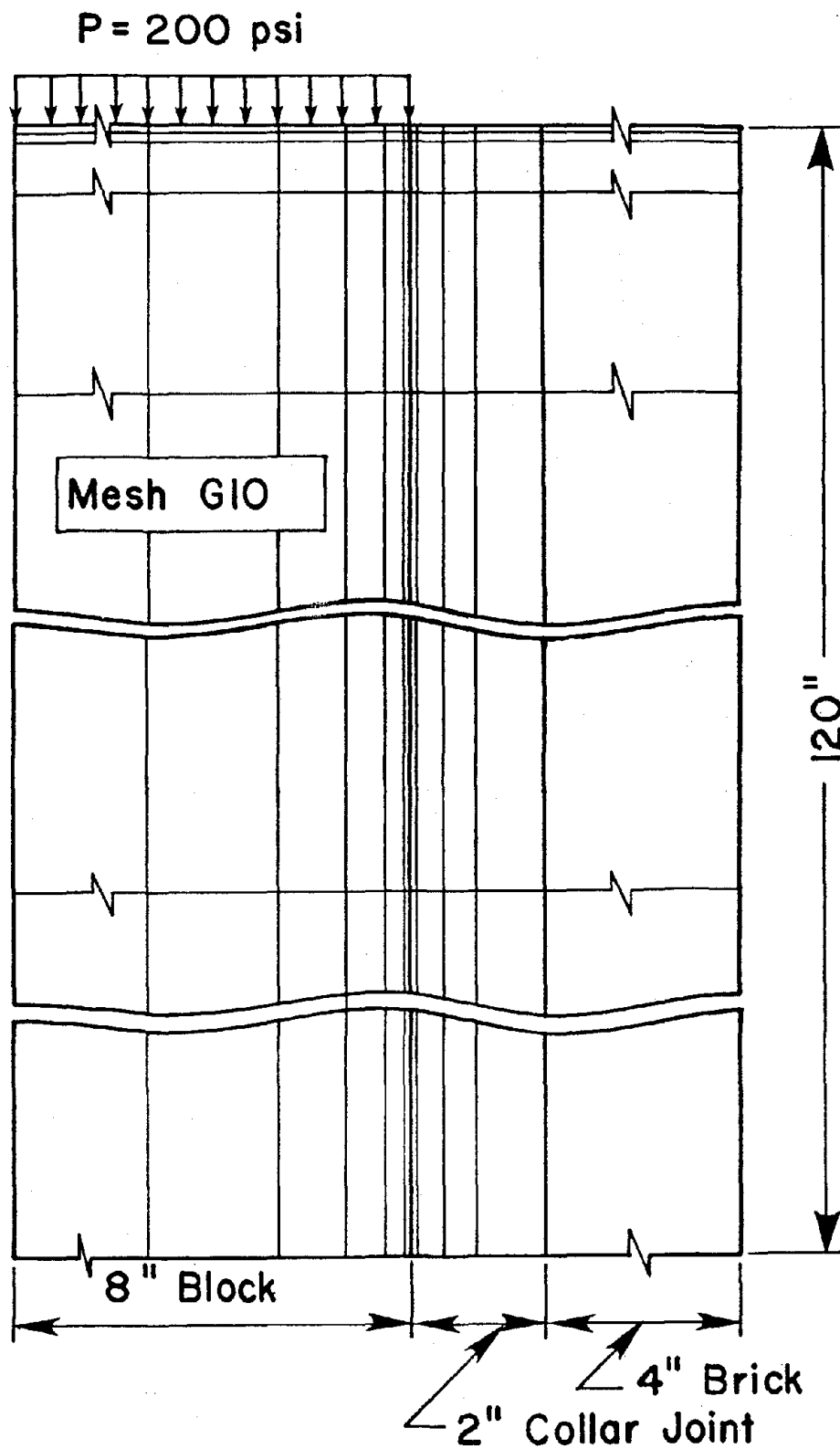
2" Collar Joint

Figure 7.4   Mesh G10, A Finite Element Mesh of VISO10 Elements
for a Composite Masonry Wall with 2 in Collar Joint
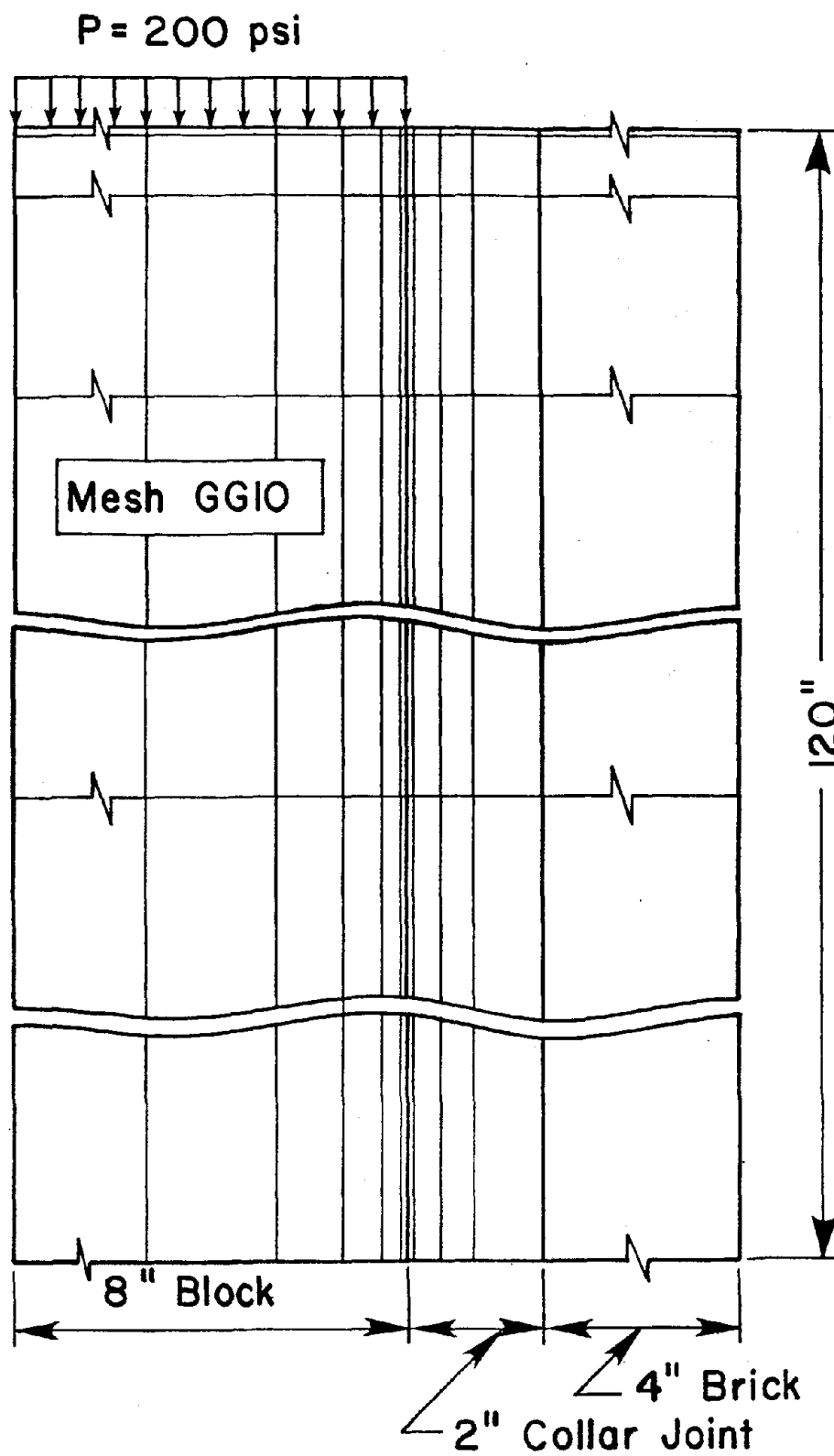
Figure 7.5   Mesh GG10, A Finite Element Mesh of VISO10 Elements
for a Composite Masonry Wall with 2 in Collar Joint

Figure 7.6 Shear Stress (τ_{xy}/p) Distribution along the
Height of the Wall with Mesh G and Mesh GG

In Figure 7.7, normalized shear stresses in the collar joint elements
of thicknesses 0.05 and 0.1 inches at the block-collar joint interface
along the height of the wall are shown. Mesh G is used in these analyses.
The shear stress distributions in two cases are absolutely indistin-
guishable everywhere in the collar joint at the interface along the height
of the wall except in the top two elements. This indicates that even for
very small widths of elements at the interface the results are disturbing
only in top two elements of the interface. Hence, by neglecting the re-
sults of the top two elements, correct shear stresses in the collar joint
at the interface could be obtained irrespective of the widths of the el-
ements used at the interface when a reasonably fine mesh is employed for
the finite element solution.

It should be noted at this point that in Figure 7.6, the maximum
predicted shear stress, neglecting the top two elements, is almost the
same as the predicted shear stress if the results of only the top most
element are neglected. On the other hand, the shear stress distributions
in Figure 7.7 indicates that when the widths of collar joint elements at
the interface are very small, the maximum shear stress neglecting the top
two elements is considerably different from the maximum shear stress when
the results of only the top most element is neglected. Moreover, in this
case where the elements at the interface are very thin, the shear stress
distribution is extremely unsmooth within the top two elements. There-
fore, in general, for a very fine mesh of quadratic isoparametric elements
used in modelling a composite wall, accurate solutions can be obtained
if the results of the top two elements are disregarded.

The shear stress distributions in the collar joint elements at the
block-collar joint interface obtained by using Mesh G10 and Mesh GG10 are

Figure 7.7 Shear Stress (τ_{xy}/p) Distribution along the Height of the Wall with Various Interface Thicknesses

shown in Figure 7.8. Ten noded variable-number-node elements (VISO10) are employed in the finite element meshes. The collar joint elements at the interfaces are 0.1 inch thick. In Mesh GG10 only one layer of very thin elements is provided at the top of the wall. The rest of the wall is modelled by a coarse mesh along the vertical direction. This is done to examine the possibility of getting accurate stresses by disregarding the results of only one element at the top of the wall in the interface when VISO10 elements are used in a very coarse mesh. The shear stress distributions obtained from Mesh G10 and Mesh GG10 agree very well with each other. In Mesh G10, when the results of the top two elements are discarded the maximum normalized shear stress is 0.323. This magnitude remains unchanged if the results of only one element at the top are disregarded. On the other hand, the maximum normalized shearing stress from mesh GG10, disregarding the results of its only layer of very thin element at the top, is 0.32. A comparison of maximum stress in Figure 7.6 with that in Figure 7.8 indicates that the maximum shear stress obtained by mesh G disregarding the results of the top two elements is same as the maximum shear stress obtained by mesh GG10 disregarding the results of only one element at the top. This is shown in Figure 7.9. The above agreement between the stresses obtained from two different meshes indicates that accurate stresses can be obtained from a mesh of VISO10 elements when the thickness of the elements in the collar joint at the interface is 0.1 inch and the results of the top most element are neglected.

The stresses in the collar joint elements having a thickness of 0.05 inch at the interface are examined to investigate further the possibility of predicting accurate stresses by disregarding the results of only one
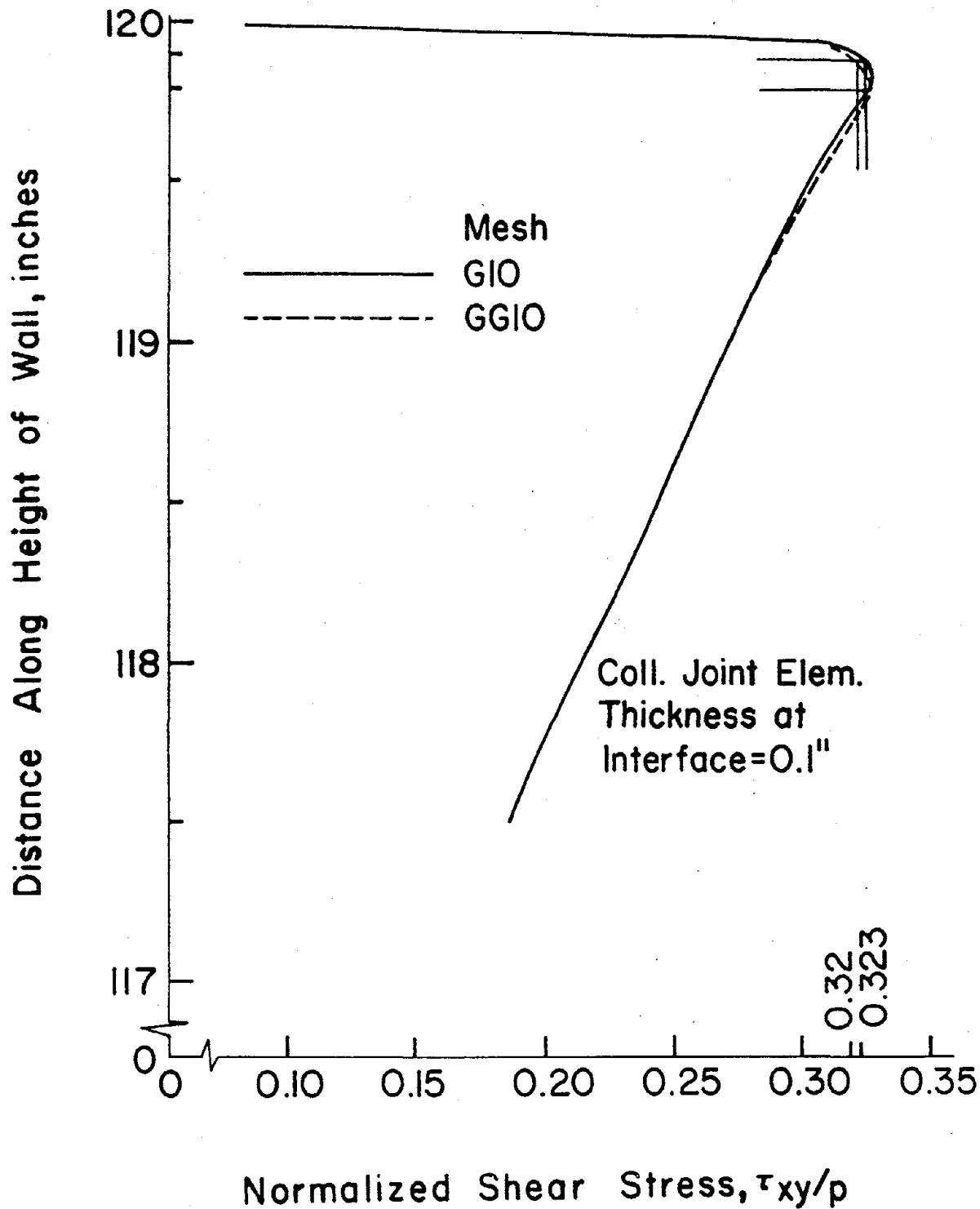
Figure 7.8 Shear Stress (τ_{xy}/p) Distribution along the Height of the Wall with Mesh G10 and Mesh GG10
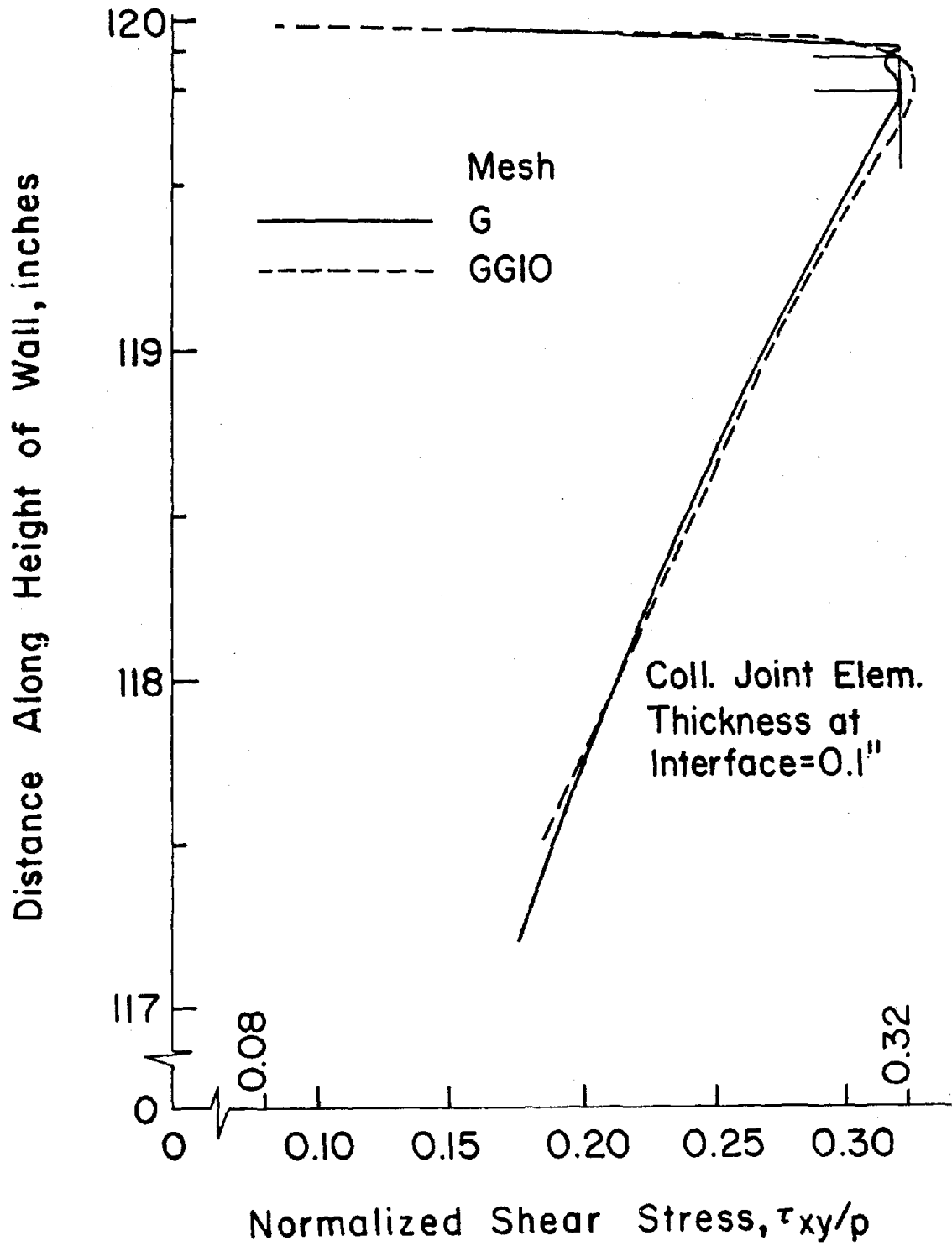
Figure 7.9   Shear Stress (τ_{xy}/p) Distribution along the
Height of the Wall with Mesh G10 and Mesh GG10

element in a mesh of VISO10 elements. In Figure 7.10, the normalized

shear stress distribution along the height of wall in the collar joint

elements at the interface having widths of 0.1 and 0.05 inch is shown.

In these analyses Mesh G10 is used. The shear stresses in the collar

joint elements with 0.1 inch thickness and the shear stresses in the

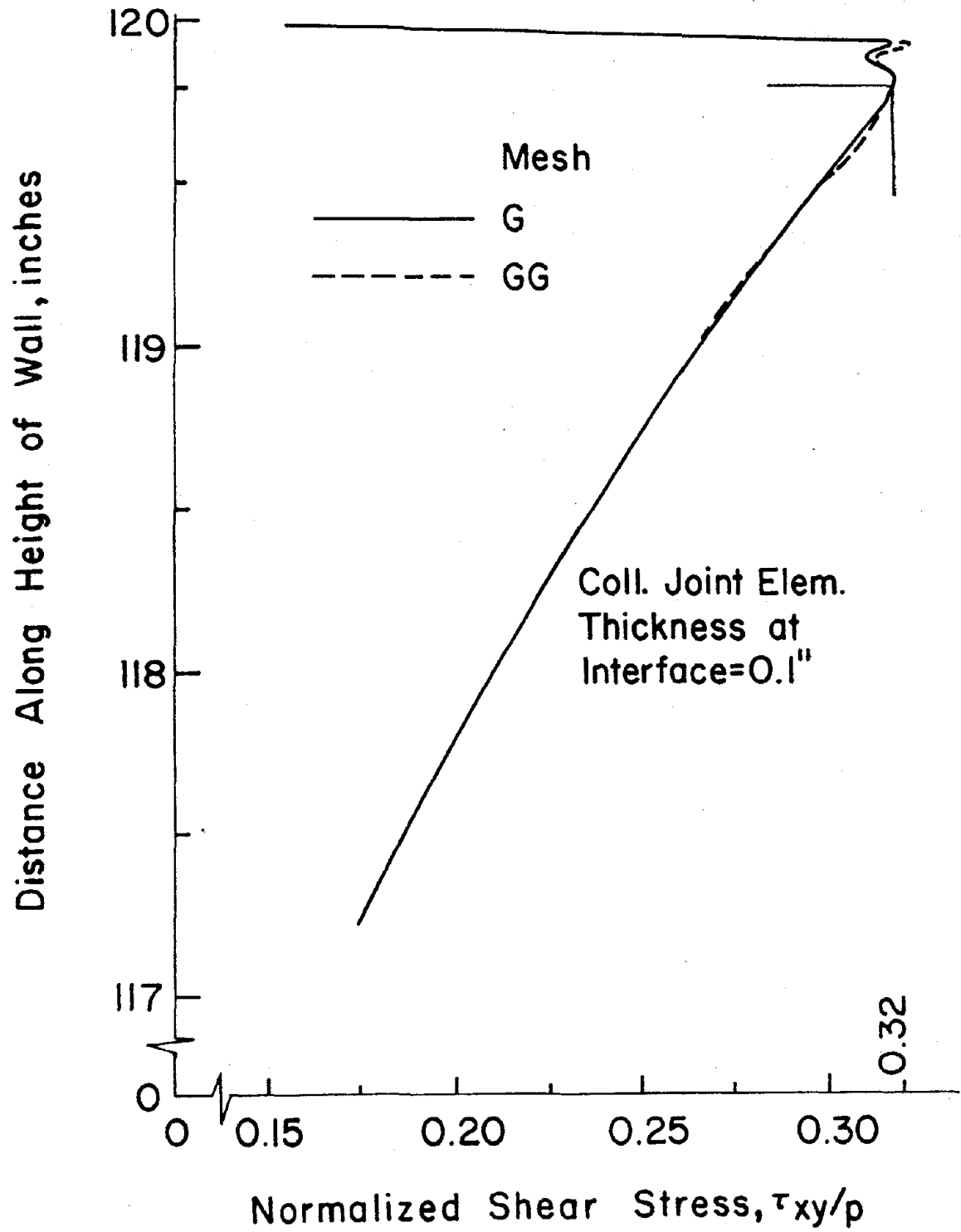collar joint elements with a thickness of 0.05 inch are in good agreement

with each other everywhere along the height of the wall except in the top

two elements. The normalized maximum shear stress, neglecting the results

of the top two elements in the 0.1 inch thick collar joint element at the

interface, is 0.323, which is comparable with the normalized maximum shear

stress of 0.335 in the 0.05 inch thick collar joint element. The pre-

dicted shear stresses in the collar joint elements of 0.05 inch thickness

are extremely oscillatory in the top two elements and the maximum stress

when the results of the top most element are disregarded differs consid-

erably from the maximum stress when the results of the top two elements

are disregarded. A reasonably accurate solution is obtained when the

results of the top two elements are disregarded. Thus, the indications

are that it may not be possible to estimate correct magnitude of stresses

by disregarding the results of only one element at the top of the inter-

face. For further investigation into this subject, normalized shear

stresses in the collar joint elements having thickness of 0.05 inch for

the Meshes G, G10, and GG10 are shown in Figure 7.11. For Mesh GG10, the

maximum value of normalized shear stress obtained by disregarding the

results of the top most element is 0.35. On the other hand, the maximum

normalized shear stresses obtained from Mesh G and Mesh G10 neglecting

the stresses in the top two elements are 0.33 and 0.335, respectively.

A comparison of maximum stress obtained from Mesh GG10 with that obtained
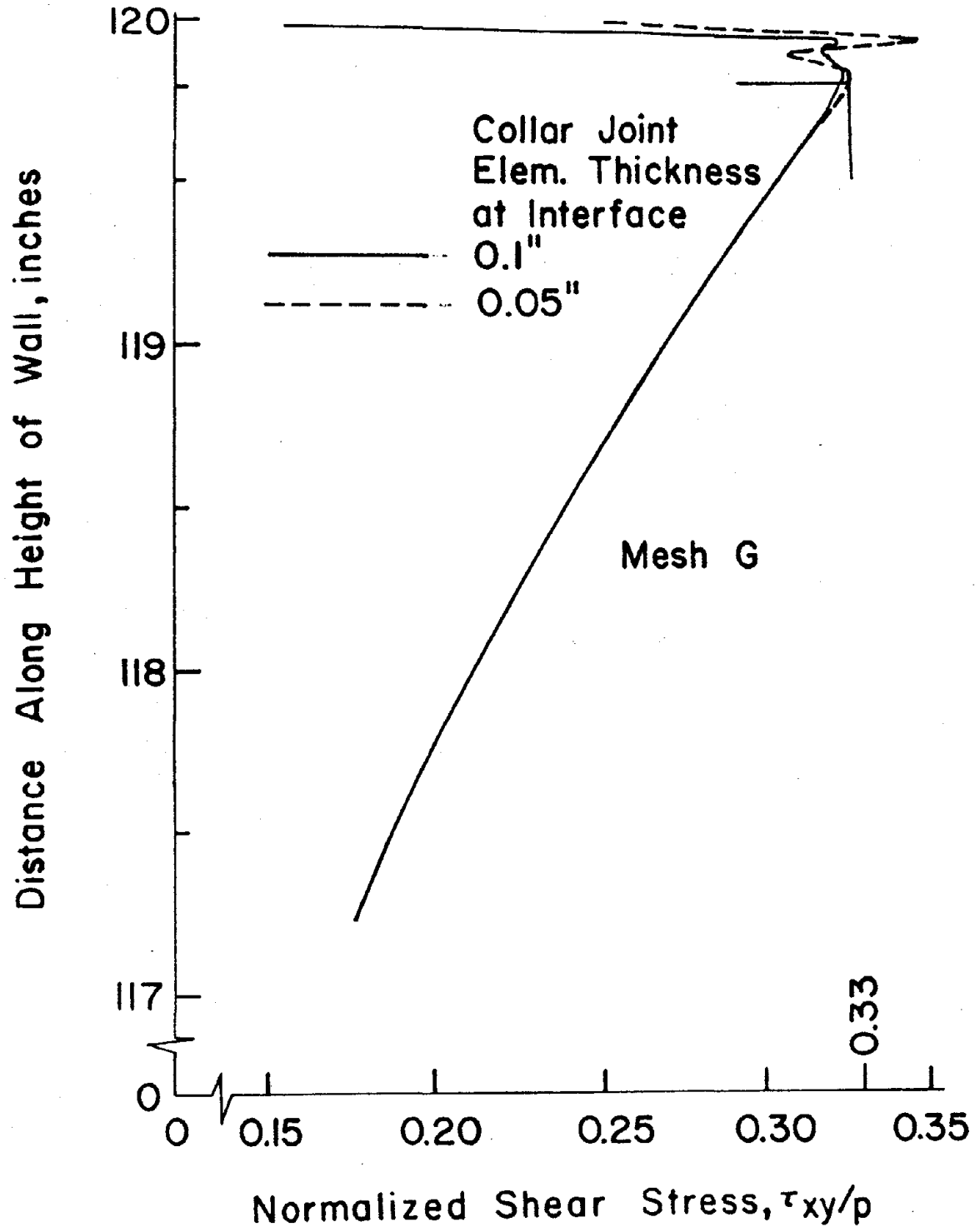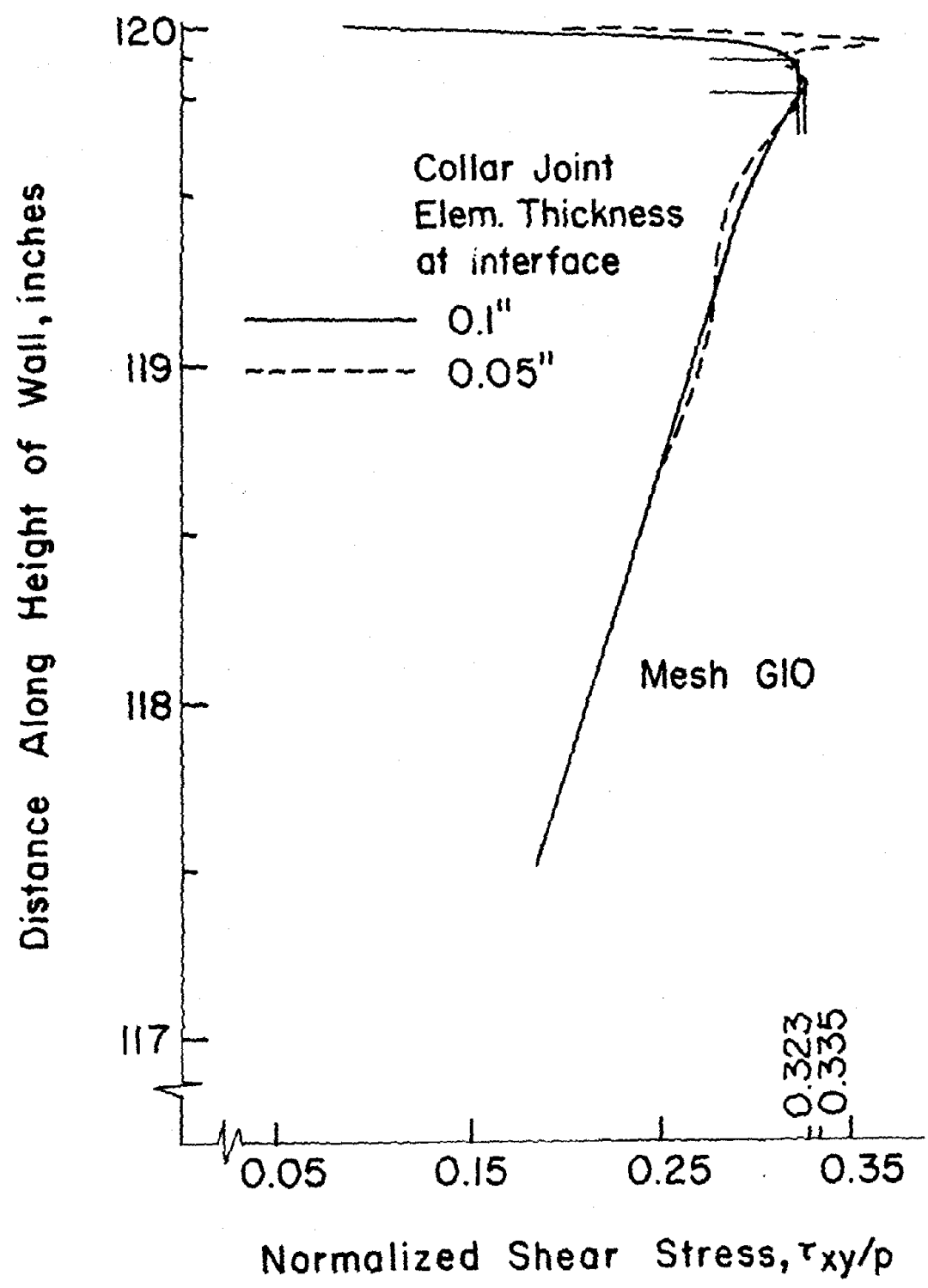
Figure 7.10   Shear Stress (τ_{xy}/p) Distribution along the Height
of the Wall with Various Interface Thicknesses
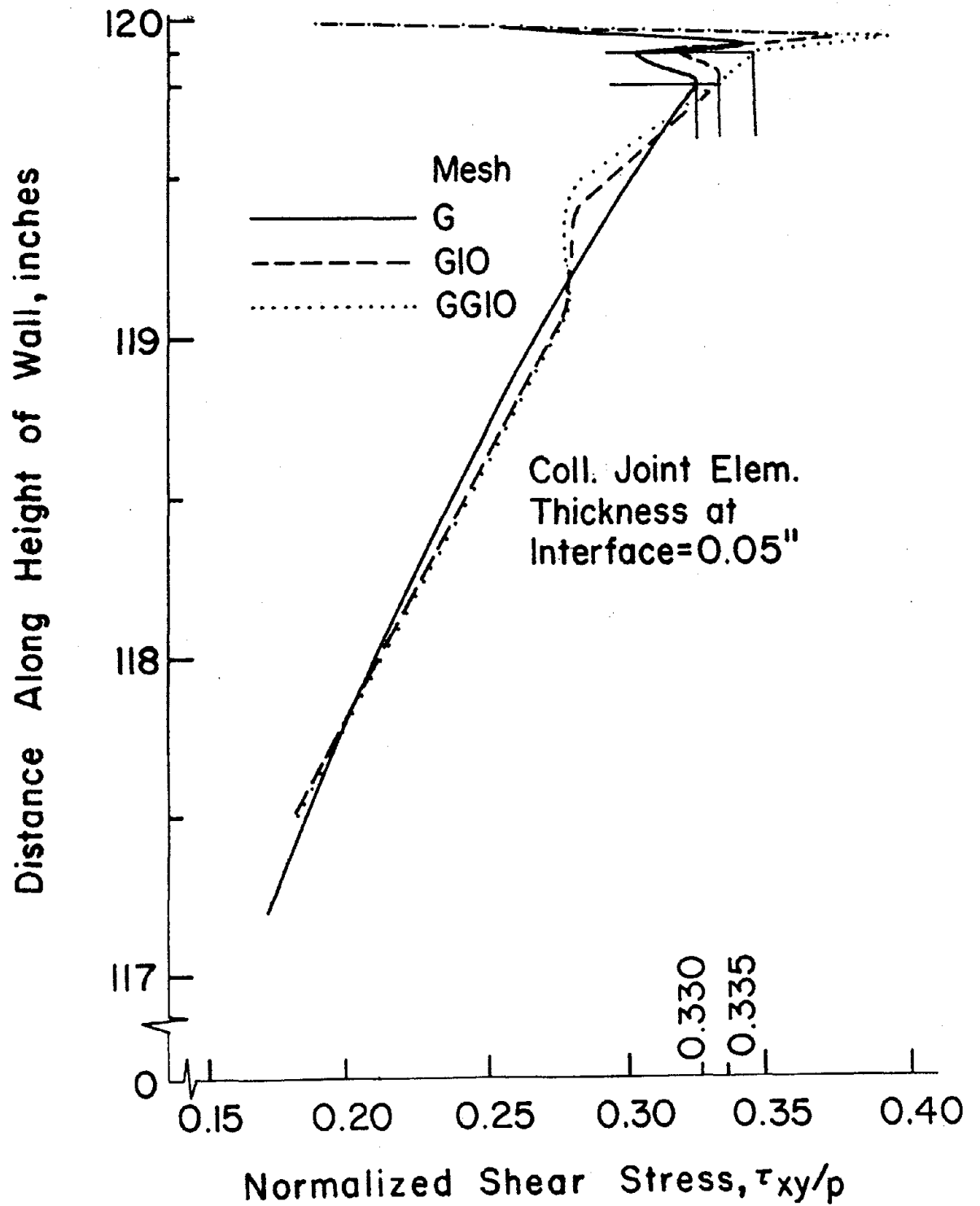
Figure 7.11 Shear Stress (τ_{xy}/p) Distribution along the Height of the Wall with Three Meshes

from Mesh G and Mesh G10 shows that a reasonably accurate solution cannot be obtained if the results of only one element at the top of the wall are disregarded.

It is also observed after a critical review of all the normalized shear stress distribution plots that in most cases the maximum shear stress obtained by disregarding the results of top two elements is about 7 to 10 per cent higher than the maximum shear stress obtained by disregarding the results of top one element. Based on this and above cited observations, it is concluded that accurate solution for composite masonry walls can be obtained by finite element analysis if the results of the top two elements at the interface are disregarded.

CHAPTER VIII

DEVELOPMENT OF FAILURE CRITERION AND

ANALYSIS OF COMPOSITE MASONRY WALLS

Current and previous studies regarding the shear stress distribution
in the collar joint of composite masonry walls indicate that when the
inner block wythe is loaded, the most critical stresses are the shear
stresses in the collar joint, particularly in the region of load appli-
cation near the top of the wall. Consequently, failure initiates in that
region and complete separation of the two wythes takes place. Recently,
the phenomenon of cracking and crack propagation in composite masonry
walls has received special attention. However, at the present there is
very little evidence that analytical models have been developed to predict
cracking in composite walls (14, 15, 17, 18).

Masonry joints have low tensile strength, high compressive strength,
and shear strength which is a function of the superimposed compression
as well as the shear bond strength between the two materials. A Coulomb
type of joint failure criterion is desirable since the failure shear
stress in this case is defined as a function of the shear bond strength,
the coefficient of friction and the associated normal stress. Several
researchers have proposed such criteria for joints based on their exper-
imental results (48, 50) which assume a uniform distribution of shear and
normal stresses within the failure planes. This is not necessarily rep-
resentative since the distribution of normal and shear stress along the
joint is not uniform. In the experimentally determined failure criteria,
the investigators ignore the effects of any localized normal stresses that

may be caused by the shearing forces acting alone on a structure in the absence of normal loads. Also, each of the proposed failure envelopes is associated with a particular type of brick, block, or mortar.

The current research is concerned with the development of an improved joint failure criterion which takes into account the variation of stresses within the joints. Only concrete block-mortar joints are being considered in this research.

The proposed improved failure criterion has been developed theoretically utilizing the experimentally determined failure envelopes. Test specimens, which were used to develop the experimental failure criteria, are analyzed by the finite element method for different combinations of the experimentally determined vertical and horizontal failure loads. It is assumed in these analyses that the crack initiation and final failure occur at the same load. Normal and shear stresses at various points along the failure plane are plotted. A failure envelope is drawn for each specimen assuming that there exists at least one point in the failure plane at which failure initiates at a specific combination of the normal and shear stresses. Thus, the actual state of stress in the failure plane is utilized in the formulation of the failure envelope. An empirical equation that describes the failure criterion is developed from these envelopes which relates the shear bond strength and coefficient of friction with the block and mortar properties.

The proposed empirical equation is utilized to analyze various specimens, for which failure loads have previously been found experimentally. It is shown that the loads for the crack initiation and failure estimated by the analysis agree well with those measured

experimentally. Details of this development are presented in the next sections.

Development of the Failure Criterion

Although various investigators have conducted experimental studies of the joint shear failure as mentioned before, only Hamid et al. (48) and Hegemier et al. (50) give details of the test procedures, material properties, and failure equations. Hence, specimens from these two references are utilized in the development of the improved joint failure criterion. It is assumed in the analyses that the interface between the block and mortar is bonded together perfectly.

Hegemier's Specimens

Test specimens used by Hegemier were triplets that consisted of three ungrouted blocks with either two bed joints or two head joints as shown in Figure 8.1 and 8.2 respectively. The component materials consisted of Grade N-1 normal weight concrete block and Type S mortar, for which the modulii of elasticity were given as 600 and 877 ksi, respectively. A value of 0.25 for the Poisson's ratio was assumed for the two materials. Based on a uniform distribution of both the normal and shear stresses on the net area of the block-mortar joints, Hegemier (50) developed the failure criteria for the bed joints and head joints, respectively, as

$$\tau = 36 - 0.89 \ \sigma \ \text{and} \tag{8.1}$$

$$\tau = 45 - 0.84 \ \sigma \tag{8.2}$$

in which τ and σ are in psi and σ is considered negative in compression.

Finite Element Analysis of Hegemier's Specimen

In order to develop a failure criterion based on the actual distribution of the normal and shear stresses in the block-mortar joints,

Hegemier's Bed Joint Specimen
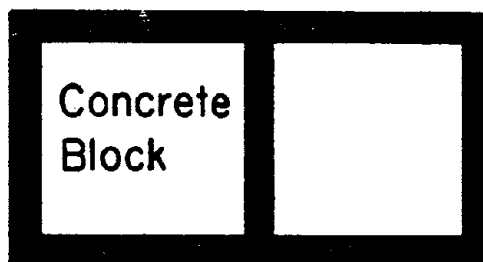
Plan
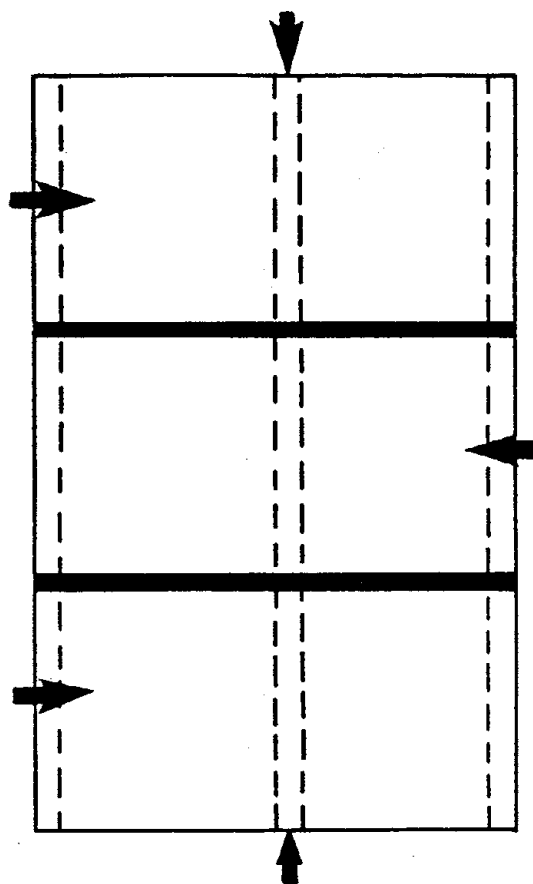
Elevation

Figure 8.1 Bed Joint Specimen Tested by Hegemier et al.

Hegemier's Head Joint Specimen
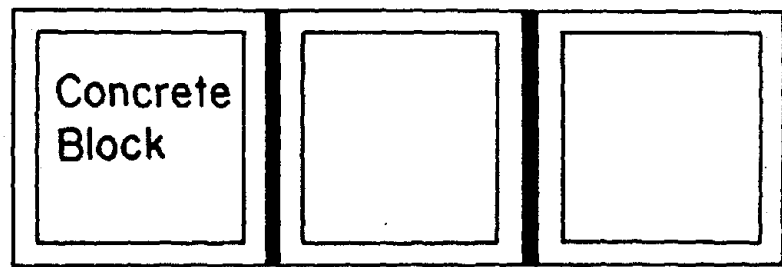
Plan
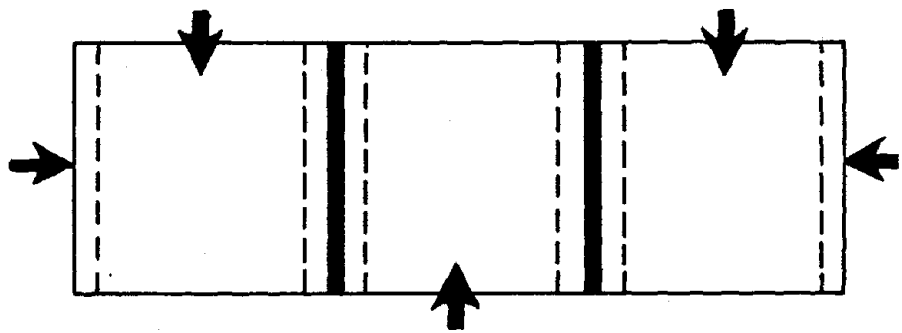
Elevation

Figure 8.2 Head Joint Specimen Tested by Hegemier et al.

the triplet is analyzed elastically using a two-dimensional plane stress

finite element program with quadratic isoparametric elements. Only one

quarter of the bed joint triplet and one half of the head joint triplet

are analyzed due to the two and one axes of symmetry in the triplets,

respectively. A sufficiently fine mesh is selected in the joint and near

the ends of the model to ensure a realistic distribution of the normal

and shear stresses in the collar joint. A typical finite element mesh

used in the analysis is shown in Figure 8.3.

Triplets with Bed Joints

This model is analyzed for three sets of arbitrarily selected failure

load combinations obtained from Equation 8.1. These load combinations,

for loads normal and parallel to the bed joint, respectively, are based

on stresses in psi of 0 and 36, 100 and 125, and 200 and 214. In order

to utilize the plane stress finite element model with uniform thickness

in the analysis of hollow block with bed joints, the elastic modulii of

the block material and mortar (given earlier as 600 ksi and 877 ksi) are

modified by the smearing technique to yield the corresponding values of

287 ksi and 420 ksi, respectively. The resulting normal and shear

stresses in the bed joint for the three load combinations are plotted by

different symbols as shown in Figure 8.4. A failure envelope is drawn

using these stress points with the assumption that for each set of the

load combinations there exist at least one point on the failure envelope

at which failure initiates. This leads to a linear expression for the

failure criterion as

$$\tau = 56-0.867 \ \sigma. \tag{8.3}$$
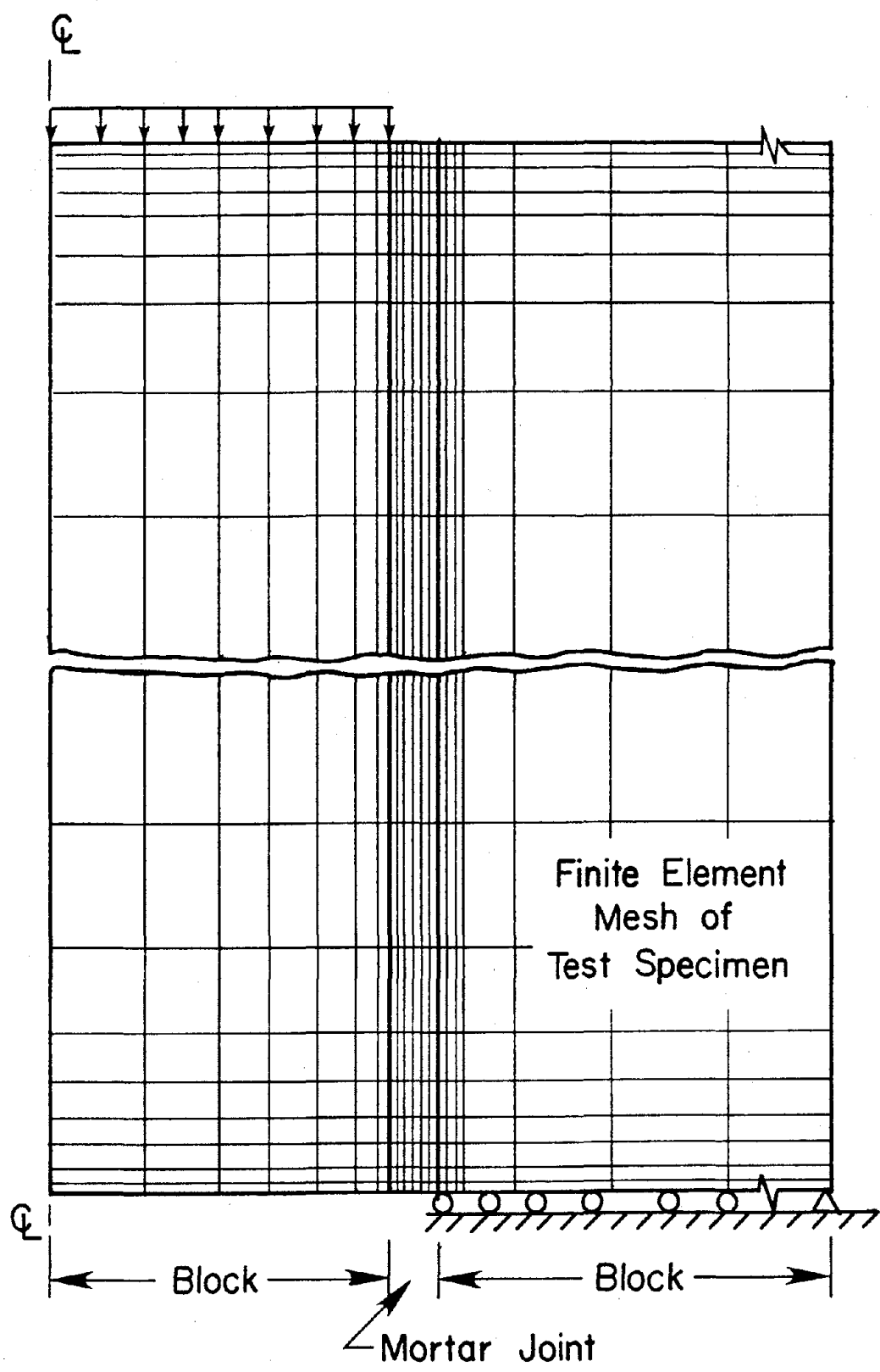
Figure 8.3 Finite Element Mesh for Hegemier's Specimen

Hegemier et al.- Bed Joint

$\tau = 56 - 0.867\,\sigma$

Shear Stress, τ (psi)

Normal Stress, σ (psi)
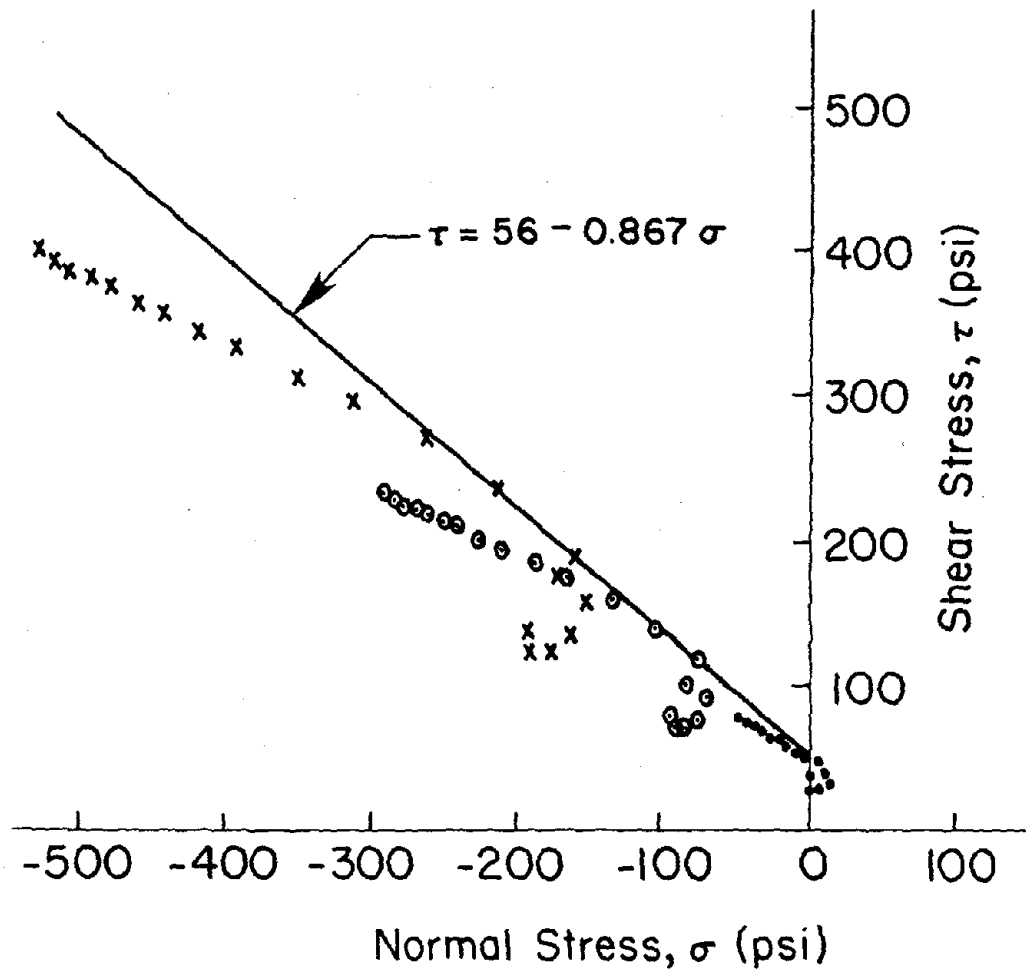
Figure 8.4 Stresses in Hegemier's Bed Joint Specimen from
Finite Element Analysis

Triplets with Head Joints

As in the case of the bed joint triplets, three sets of loads for this analysis are arbitrarily selected using Equation 8.2, which are based on the normal and shear stress combinations, respectively, in psi of 0 and 45, 100 and 129 and 200 and 213. As the mortar in the head joint is spread on the entire area, no modifications in its properties are required for the finite element analysis. On the other hand, due to the hollow nature of the concrete blocks, its elastic modulus is modified as in the case of the triplet with bed joints. The elastic modulii for the concrete blocks and mortar used in this analysis are 287 ksi and 877 ksi, respectively. The normal and shear stresses in the head joint obtained from the three loading combinations are shown with different symbols in Figure 8.5, in which a linear failure envelope based on the actual stress distribution is also drawn. The expression for the resulting failure criterion is found to be

$$\tau = 65 - 0.875 \ \sigma. \tag{8.4}$$

Hamid's Specimen

The test set-up utilized by Hamid (48) to obtain the strength of bed joints is shown in Figure 8.6. Although Hamid conducted tests with grouted and ungrouted blocks using Type N and S mortars, only his results with the ungrouted blocks and Type S mortar are used in this research. Ungrouted bed joint specimens are considered because the interfaces in these specimens can represent the behavior of block wythe-collar joint interface of composite masonry walls more closely than the interfaces of grouted bed joints. The compressive strengths of half concrete blocks tested flatwise and 2 inch mortar cubes are 2,850 psi and 3,110 psi, respectively. Assuming once again a uniform state of stress in the bed
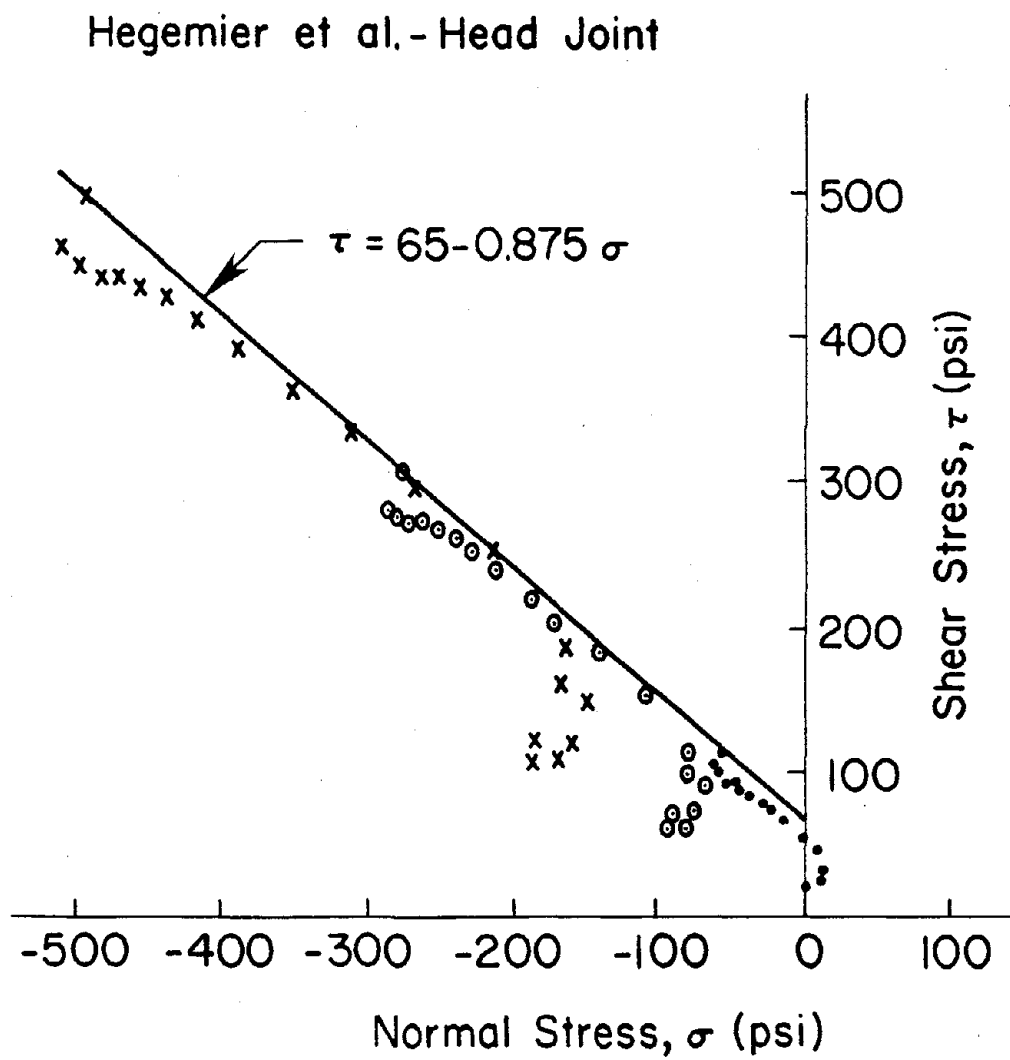
Figure 8.5 Stresses in Hegemier's Head Joint Specimen from
Finite Element Analysis

Hamid's Bed Joint Specimen
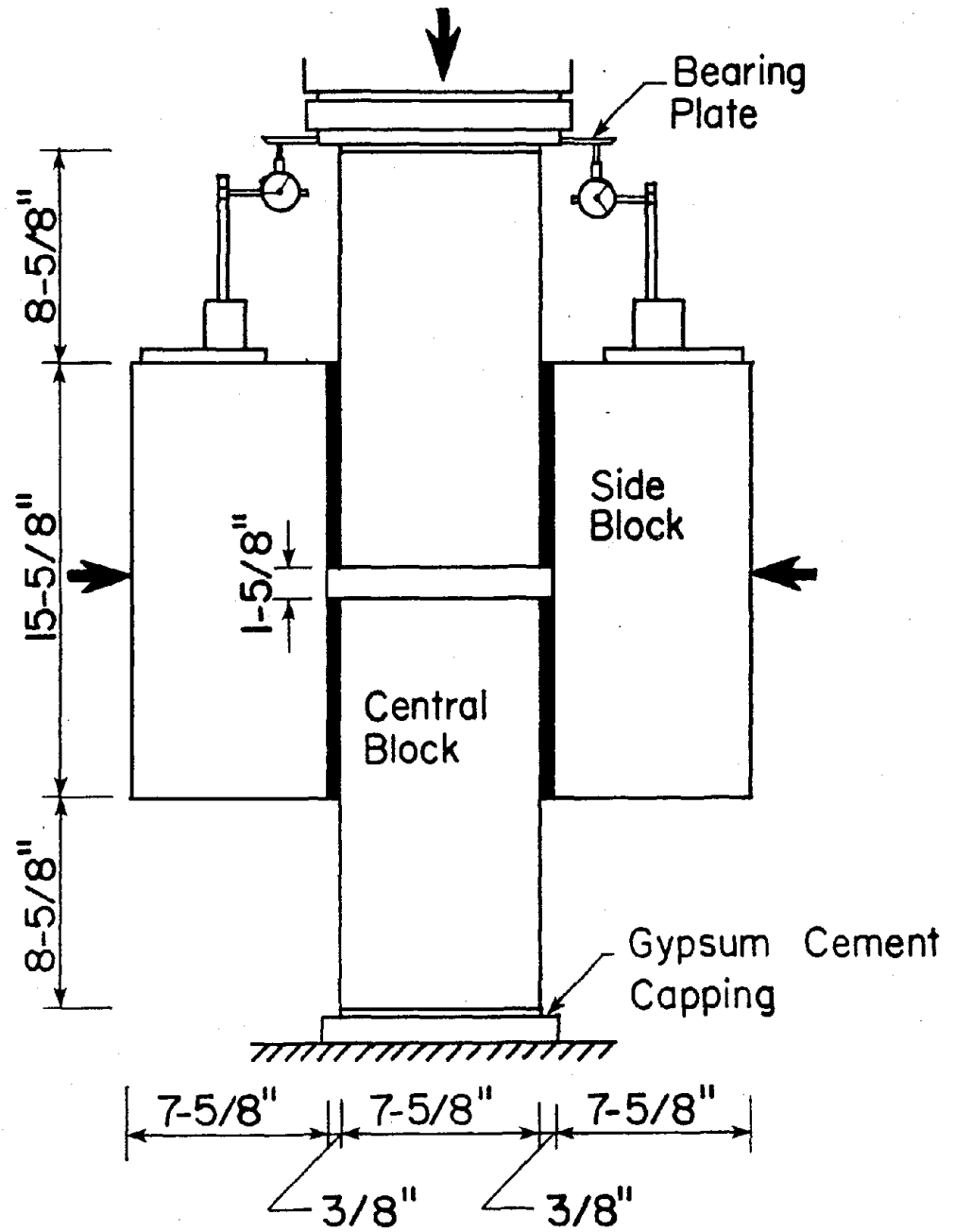
Figure 8.6 Test Arrangement Used by Hamid et al.

joints, the failure criterion determined experimentally by Hamid is given by

$$\tau = 76-1.07 \; \sigma. \tag{8.5}$$

The test procedure shown in Figure 8.6 has two axes of symmetry; thus, the finite element model of Figure 8.3 can once again be utilized. The elastic modulii to be used in the analysis are obtained from the measured compressive strengths of the concrete block and mortar. Using ACI 531-79 (104) and a compressive strength for the hollow block = 2,850 psi yields a modulus value of 1,671 ksi. The elastic modulus, E_m, in ksi, for the solid mortar material is given by (81)

$$E_m = 1,000 \; f'_m \tag{8.6}$$

in which f'_m, in psi, is the compressive strength of the mortar. Thus, E_m in this case = 3,110 ksi. However, since the mortar is placed only on the shell of the hollow concrete blocks, its modulus value to be used in the plane stress analysis must be modified to yield a value of 1,960 ksi.

As in the case of Hegemiers's model, three sets of failure loads, normal and parallel to the bed joint, are computed from Equation 8.5 for the arbitrary stress combinations, in psi, of 0 and 76, 100 and 183 and 200 and 290, repectively. The resulting normal and shear stresses in the bed joint due to these loads are plotted as before and are shown in Figure 8.7, which also shows the failure envelope based on the actual stresses. This failure criterion can be given by the expression

$$\tau = 77-1.20 \; \sigma. \tag{8.7}$$

Hamid et al. - Bed Joint

$\tau = 77 - 1.20\,\sigma$

Normal Stress, σ (psi)

Shear Stress, τ (psi)
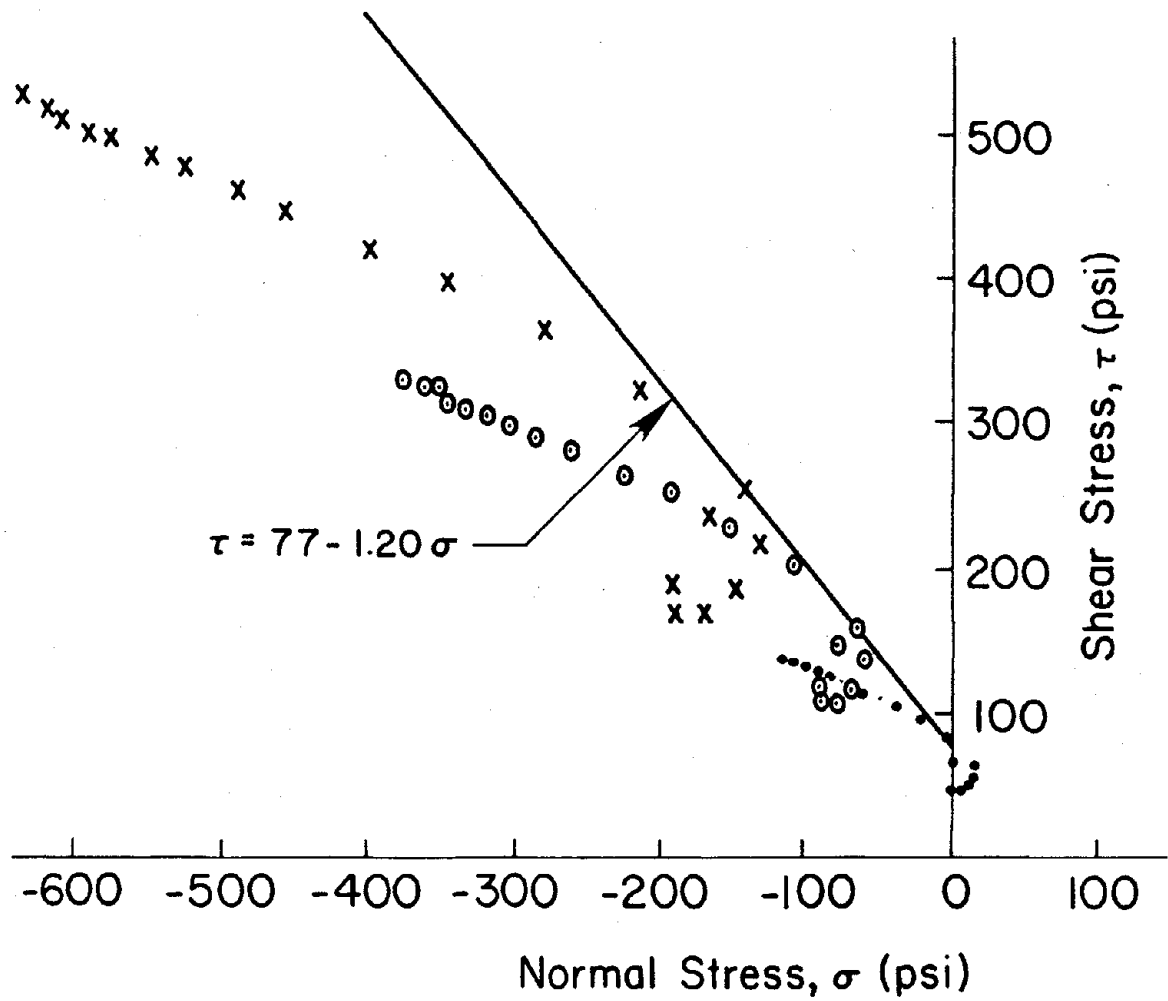
Figure 8.7 Stresses in Hamid's Mortar Joint Specimen from
Finite Element Analysis

Improved Failure Criterion for Concrete Block-Mortar Joints

Shear-Compression in a Joint

The theoretical failure criteria with the shear-compression zone based on the actual stress distributions and loads for the various cases are given by Equations 8.3, 8.4 and 8.7. These equations are of the form

$$\tau = \tau_0 - \mu \sigma \tag{8.8}$$

in which τ_0 is the shear bond strength and μ is the coefficient of shear friction. The magnitudes of these parameters are found to be different in the above equations and are assumed to be dependent upon the elastic modulii of the block and mortar. Using a trial and error procedure, empirical equations have been developed for τ_0 and μ in terms of the material properties which, when used in Equation 8.8, satisfy Equations 8.3, 8.4 and 8.7 very closely, thus yielding a general and improved failure criterion for the concrete block-mortar joints in shear-compression zones. These expressions for τ_0 and μ may be given by

$$\tau_0 = 2E_m/E_{b1} + E_m \times 10^{-2} + 3.974 E_{b1} \times 10^{-3} + 48.36 \tag{8.9}$$

$$\mu = 2.384 E_{b1} \times 10^{-4} + 0.802 \tag{8.10}$$

in which E_m and E_{b1} are the modulii of elasticity of mortar and block in ksi, respectively, and τ_0 is in psi.

Shear-Tension in a Joint

Due to the lack of the sufficient information available in the literature, it is not possible in this case to follow a procedure similar to that used for shear-compression to derive a failure criterion for block-mortar joints in shear-tension. Ali and Page (1) have developed such a failure criterion in which they assume that the tension bond strength, τ_{tb}, is equal to the shear bond strength, τ_0. Results presented

in Reference (81) also show that the tensile bond strength can be taken as equal to the shear bond strength. This is adopted in the failure criterion proposed in this study where it is further assumed that the failure stress varies linearly between the shear bond strength and the tension bond strength. Thus, the complete failure criterion, based on Equations 8.8-8.10 can be proposed as shown in Figure 8.8.

Characteristics of the Proposed Failure Criterion

It should be of interest to compare the magnitude of the shear bond strength given by the proposed Equation 8.9, for E_m equal to E_{b1}, with the ultimate beam shear stress computed by the ACI Code (106) for a specific value of the concrete strength f'_c. The ultimate shear stress τ_f, in psi in concrete at failure is given by $\tau_f = 2 \sqrt{f'_c}$. The ACI Code specifies the modulus of the normal weight concrete in psi as

$$E_c = 57,000 \sqrt{f'_c}. \tag{8.11}$$

Substituting for $\sqrt{f'_c}$ from the second expression into the first gives an expression for the failure shear stress of concrete in terms of its modulus as

$$\tau_f = E_c/28,500. \tag{8.12}$$

The value of τ_0 and τ_f, given by Equations 8.9 and 8.12, respectively, are compared for the special case when $f'_c = 4,000$ psi (i.e., $E_c = 3,640,000$ psi), and $E_m = E_{b1} = E_c$. The value of τ_f calculated using Equation 8.12 is approximately equal to 130 psi, whereas τ_0 from Equation 8.9 equals 101 psi. These results seem justifiable based on physical grounds since the shear bond strength in a joint represents the ultimate shear stress value at the interface of two materials which should be less than the corresponding ultimate shear stress in the absence of the interface.
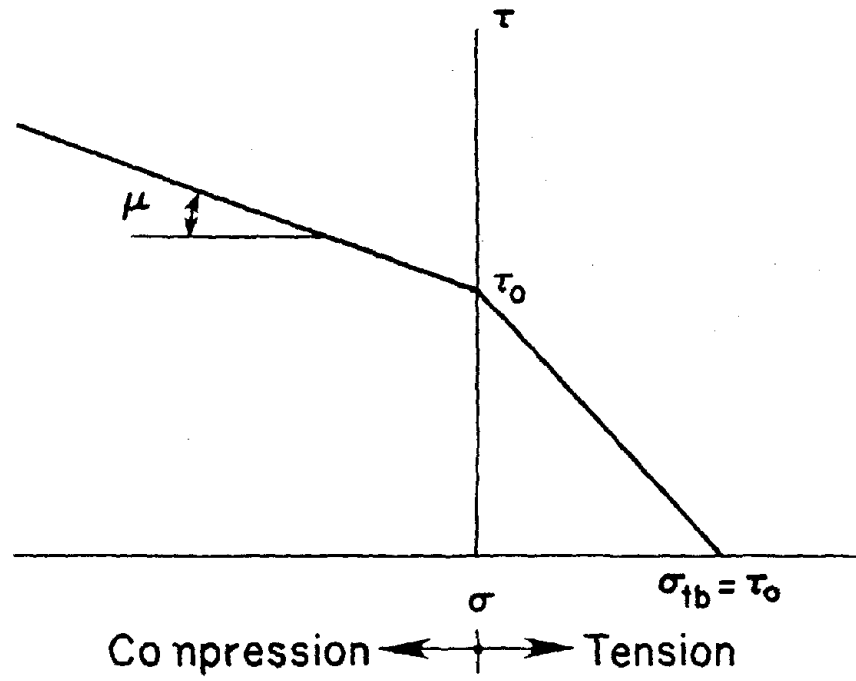
Figure 8.8 Proposed Failure Criterion of a Mortar Joint in Compression and Tension Regions

The values of the elastic modulii used in the finite element analyses

of the specimens to develop failure Equations 8.3, 8.4, and 8.7 are sub-

stituted into the empirical Equations 8.9, and 8.10 to compute the values

of τ_0 and μ which through Equation 8.8 yield

$$\tau = 56.6-0.869 \ \sigma, \tag{8.13}$$

$$\tau = 64.4-0.869 \ \sigma \ \text{and} \tag{8.14}$$

$$\tau = 76.9-1.20 \ \sigma. \tag{8.15}$$

These expressions are almost identical to Equations 8.3, 8.4, and 8.7,

respectively, thus, providing the validity of the empirical equations

with the experimental data.

Equations 8.8 - 8.10 are also calculated for some typical values of

the mortar modulii and ratios of E_m/E_{bl} in order to estimate dependence

of the failure criterion on the modulii. These results are given below.

If $E_m/E_{bl} = 1$, $E_m = 3,000$ ksi (i.e., $E_{bl}=3,000$ ksi), then

$$\tau = 81-1.51 \ \sigma. \tag{8.16}$$

If $E_m/E_{bl} = 1$, $E_m = 300$ ksi (i.e., $E_{bl} = 300$ ksi), then

$$\tau = 54-0.86 \ \sigma. \tag{8.17}$$

If $E_m/E_{bl} = 1$, $E_m = 800$ ksi (i.e., $E_{bl} = 800$ ksi), then

$$\tau = 61-1.05 \ \sigma. \tag{8.18}$$

If $E_m/E_{bl} = 2$, $E_m =3,000$ ksi (i.e., $E_{bl} =1,500$ ksi), then

$$\tau = 88-1.15 \ \sigma. \tag{8.19}$$

If $E_m/E_{bl} = 2$, $E_m = 800$ ksi (i.e., $E_{bl} = 400$ ksi), then

$$\tau = 62-0.89 \ \sigma. \tag{8.20}$$

A thorough study of Equations 8.8-8.10 and 8.16-8.20 reveals that, within

the practical range of values for the elastic modulii of mortar and block,

the shear bond strength increases with the modulus. However, this de-

pendence is rather weak. A four fold increase in the modulus of mortar

(for $E_m/E_{bl} = 1$) yields a predicted increase in the shear bond strength of only 33%.

The empirical Equation 8.10 that defines the coefficient of shear friction, μ, is selected such that μ depends only on E_{bl}. This selection is based on the experimentally determined failure criteria of Hegemier for the bed joints and head joints given in Equations 8.3 and 8.4, respectively. The coefficients of σ in these equations (which represent the coefficient of shear friction, μ) are almost identical although the values of E_m are 420 ksi and 877 ksi, respectively. Thus, it can be surmised that μ is dependent only on E_{bl}. Once again, although Equations 8.16-8.20 indicate a linear increase in the value of μ with an increase in E_{bl}, the dependence of μ with E_{bl} is rather weak. As an example, in Equations 8.16 and 8.17, a ten fold increase of E_{bl} increases the value of the coefficient of shear friction, μ, by only 85%.

Failure Analysis Procedure

The techniques in finite element analysis for modelling progressive cracking in brittle materials are well known. The discrete crack can be introduced into the continuum by progressive elimination of the connection between the appropriate nodes of adjacent elements (discrete crack method). Alternatively, the effects of local cracking can be smeared across the width of the elements in the critical region by appropriate modification of their stiffness characteristics. Both the methods have advantages and disadvantages depending on the type of problem being analyzed. For overall load deflection behavior, the smeared cracking method is found to render best results. In this investigation, cracking of the block-collar joint interface is modelled using the smeared cracking technique. The failure analysis procedure outlined in

Reference (2) and (100) has been appropriately modified and adopted in this research.

The displacement finite element formulation is used in the analysis of the composite wall. The analysis is initiated by applying an arbitrary load on the block wythe. The load factor is estimated from the failure criterion developed earlier in this chapter and the element integration point at which failure would initiate due to cracking is determined. In the analysis procedure developed, the loads can be applied incrementally, thus allowing the program to analyze the behavior of masonry walls subjected to in-plane loading from low load levels through to final failure. Linear elastic behavior of the materials is assumed up until failure.

Crack Modelling

The cracking of the interface between the block wythe and the collar joint is modelled by using a Mohr-Coulomb type of failure criterion suggested in this chapter. At present, failure in the interface between the brick wythe and collar joint is not considered. In the failure analysis, for a particular load level all the integration points in each element are checked for possible initial failure or changes in existing state of post failure by comparing the state of stresses with the failure criterion. If no crack is identified, scaling calculations are performed to determine the load level at which further failure develops in the wall. The load vector is modified using the calculated scaling factor. The material constitutive matrix at a failed integration point is modified depending upon the type of failure. A step by step analysis procedure is given at the end of this chapter. Some important steps which are adopted from Reference (100) are described next. In this research, it

is assumed that cracking initiates in the block wythe-collar joint interface and remain there until final failure.

Checking Integration Points for Failure

Previously Uncracked Integration Points

The shear and normal (parallel and perpendicular to the interface, respectively) stresses at each integration point in the joint are determined first. If the normal stress is less than zero (i.e., compressive) at an integration point, then the point is checked for shear-compression failure. In Figure 8.9(a) the failure envelope in the shear-compression region is shown. At any integration point, if the normal and shear stresses are σ and τ, then the failure shear stress τ_f corresponding to σ can be obtained from the expression of the failure envelope given in Equation 8.8. The actual shear stress τ is compared against the failure shear stress τ_f to determine the status of the integration point. The integration point is said to have failed in shear-compression if

$$\tau \geq \tau_f \tag{8.21}$$

$$\text{or } |1 - \tau/\tau_f| \leq \varepsilon \tag{8.22}$$

where ε is a tolerance, set equal to 0.01.

An integration point is checked for shear-tension failure if the normal stress σ at that point in the initial analysis for a particular load level is greater than zero (i.e., tensile). The failure envelope in the shear-tension region is drawn and appropriate equation for the envelope is shown in Figure 8.9(b). The equation is similar to that for the shear- compression failure envelope except for the slope. The equation for the failure envelope is

$$\tau = \tau_0 - (\tau_0/\sigma_{tb}) \, \sigma \tag{8.23}$$

where
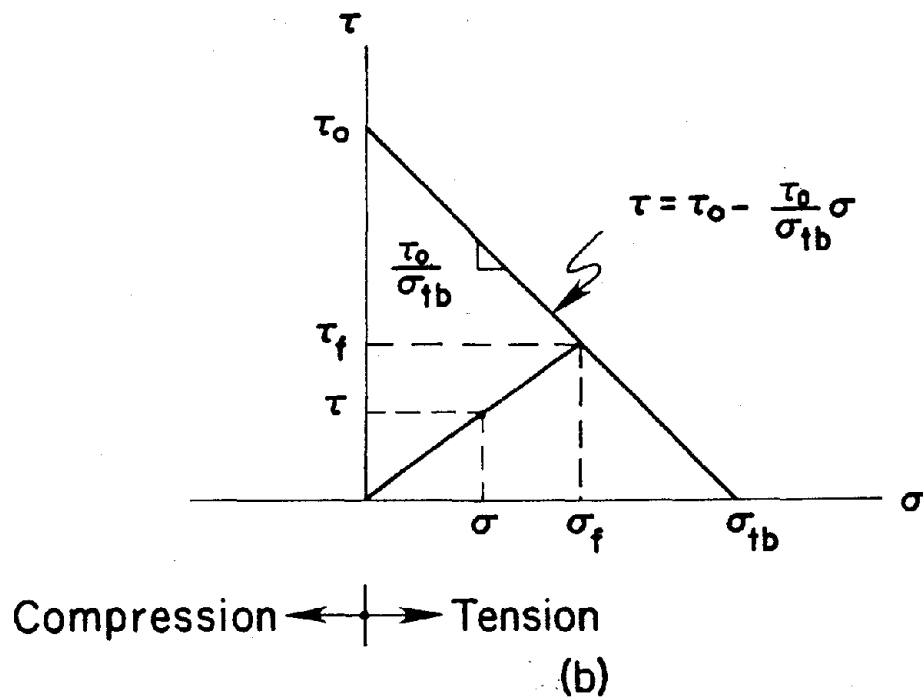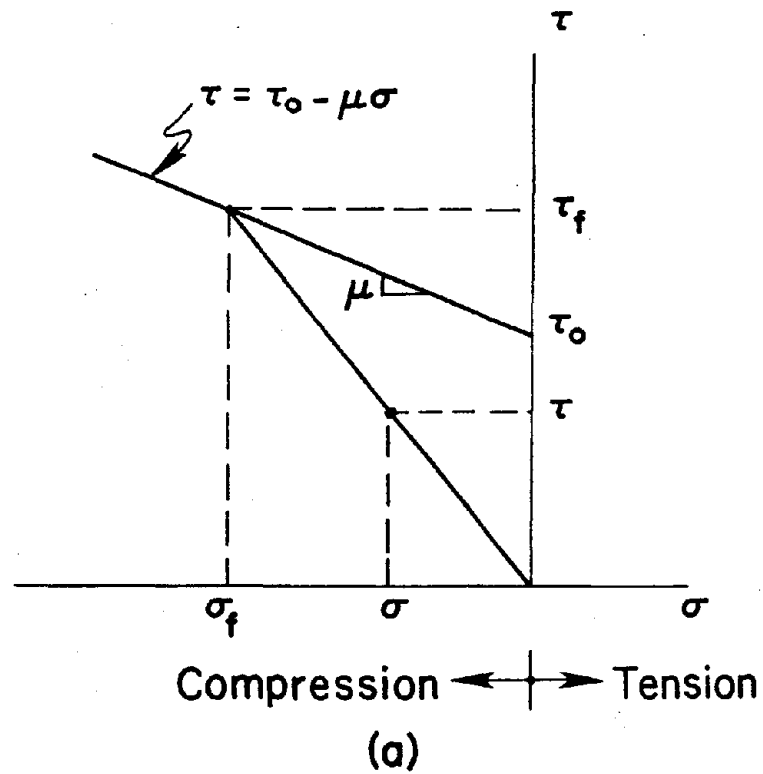
Figure 8.9 Failure Envelopes

σ_{tb} = tensile bond strength, algebraically positive and

σ = normal stress, positive when tensile.

Other symbols have been defined previously. The failure in the shear-tension zone is determined following a procedure similar to that outlined for the shear-compression zone.

Previously Cracked Integration Points

The integration points that have failed at a particular load level may change their status from shear- compression failure to shear-tension failure and vice versa during the subsequent analyses due to the modification of the constitutive matrix, D of the failed integration points.

If the normal stresses at the integration points which have failed previously in shear- compression become tensile in the subsequent analysis, then the status of the integration points are considered to have changed from shear-compression failure to shear-tension failure.

The integration points which have failed in shear-tension or changed from shear-compression to shear-tension are checked to see if the tensile normal stresses at those integration points have changed to compressive in the subsequent analysis. If they are compressive, then the integration points are considered to have changed from shear-tension failure to shear-compression failure.

Scaling Procedure

If the current state of stress of an integration point is τ and σ and if α is the scaling factor by which the current state of stress needs to be multiplied to satisfy the failure criterion, then $\alpha\tau$ and $\alpha\sigma$ must satisfy the expression for failure stresses. Thus,

$$\tau_f = \alpha \ \tau$$

$$\sigma_f = \alpha \ \sigma$$

(8.24)

where τ_f and σ_f are the failure shear and normal stresses.

Shear-Compression Zone

The expression for the failure envelope in the shear-compression zone given in Equation 8.8 must be satisfied by the failure shear and normal stresses. Thus,

$$\tau_f = \tau_0 - \mu \ \sigma_f.$$

(8.25)

Substituting for τ_f and σ_f from Equation 8.24 yields

$$\alpha \ \tau = \tau_0 - \mu \ \alpha \ \sigma.$$

(8.26)

From Equation 8.26 the scaling factor α can be computed and is given by

$$\alpha = \tau_0/(\tau + \mu \ \sigma).$$

(8.27)

τ in this expression is always considered positive and σ is negative when compressive. The above expression is valid for $|\tau/\sigma| > \mu$.

Shear-Tension Zone

The expression for the failure envelope in the shear-tension zone is given in Equation 8.23 and this must be satisfied by the failure shear and normal stresses as

$$\tau_f = \tau_0 - (\tau_0/\sigma_{tb})\sigma_f.$$

(8.28)

Substituting for τ_f and σ_f from Equation 8.24 and rearranging yields

$$\alpha = \tau_0/\{\tau + (\tau_0/\sigma_{tb})\sigma\}$$

(8.29)

where α is the scale factor, τ is always considered as positive and σ is positive when tensile.

Modification of the Constitutive Matrix, D

When an integration point is identified as a failed point, the constitutive matrix for that point is modified depending upon the type of failure.

Uncracked Integration Points.

In two-dimensional analysis, the constitutive matrix for uncracked integration points is given by

$$[D] = \begin{bmatrix} D_{11} & D_{12} & 0 \\ D_{21} & D_{22} & 0 \\ 0 & 0 & D_{33} \end{bmatrix} \qquad (8.30)$$

where for plane strain case, $D_{11} = D_{22} = (1-v)E/\{(1+v)(1-2v)\}$, $D_{12} = D_{21} = Ev/\{(1+v)(1-2v)\}$ and $D_{33} = E/2(1+v)$ and for the plane stress case, $D_{11} = D_{22} = E/(1-v^2)$, $D_{12} = D_{21} = Ev/(1-v^2)$ and $D_{33} = E/2(1+v)$.

Shear-Compression Failure

If the integration point fails due to shear compression, only the shear stiffness is reduced and normal stiffness is assumed to remain the same. The modified D matrix is used until the mode of failure changes from shear-compression to shear-tension. The modified D matrix is given below,

$$[D] = \begin{bmatrix} D_{11} & D_{12} & 0 \\ D_{21} & D_{22} & 0 \\ 0 & 0 & D_{33} \text{xAIF} \end{bmatrix} \qquad (8.31)$$

where

AIF = Aggregate interlock factor.

Shear-Tension Failure

Based on the magnitude of normal and shear stresses when shear-tension failure occurs, the magnitudes of the reduction factors for the elements of the D matrix are computed. These values are used until the failure mode changes to shear-compression. The maximum value of the normal stiffness reduction factor is 1.0 and the maximum value for the shear stiffness reduction factor is equal to the aggregate interlock factor (AIF). A linear variation is assumed between the maximum and minimum values of the normal and shear stiffness reduction factors. This is shown in Figure 8.10. The expressions for the reduction factors as functions of normal stresses can be obtained from Figure 8.10 and are given by

$$\phi = (\phi_1 - 1)\sigma/\sigma_{tb} + 1 \qquad (8.32)$$

and

$$\gamma = (\phi_1 - \gamma_0)\sigma/\sigma_{tb} + \gamma_0$$

where

ϕ = normal stiffness reduction factor,

γ = shear stiffness reduction factor,

$\phi_1 = 0.0001$,

γ_0 = aggregate interlock factor,

σ = actual normal (tensile) stress,

σ_{tb} = tensile bond strength.

The D matrix after modification for shear-tension failure takes the form as

$$[D] = \begin{bmatrix} D_{11}\phi & D_{12}\phi & 0 \\ D_{21}\phi & D_{22} & 0 \\ 0 & 0 & D_{33}\gamma \end{bmatrix} \qquad (8.33)$$

$$\phi = \frac{\phi_1 - 1.0}{\sigma_{tb}} \sigma + 1.0$$

(a)

$$\gamma = \frac{\phi_1 - \gamma_0}{\sigma_{tb}} \sigma + \gamma_0$$
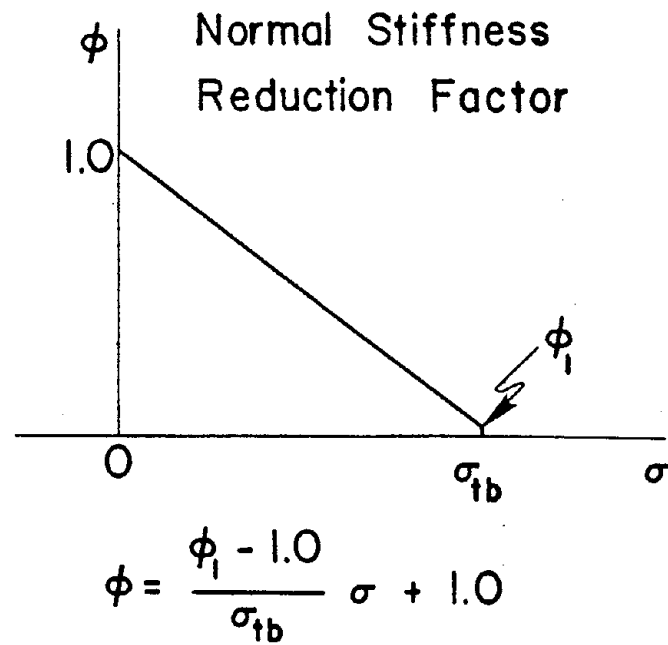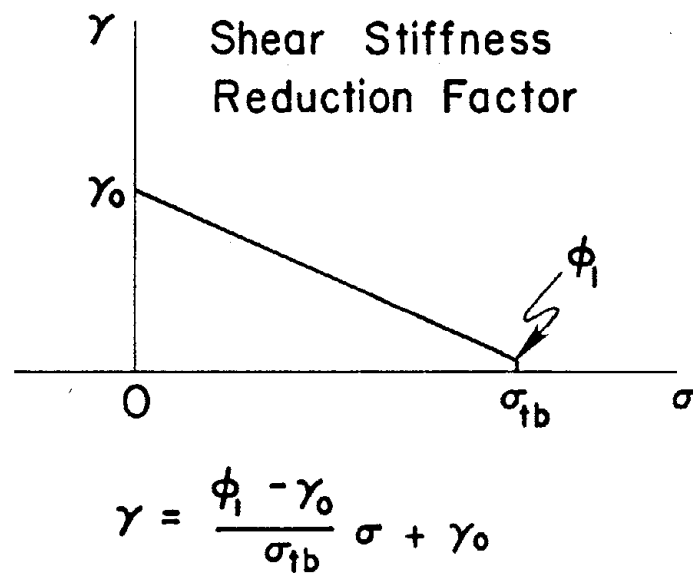
(b)

Figure 8.10   Normal and Shear Stiffness Reduction Factors

Change from Shear-Compression to Shear-Tension Failure

If the status of a failed integration point changes from shear-compression to shear-tension during successive analyses, the elements of the D matrix are modified as is done in the case of shear-tension failure. The factors ϕ and γ are computed based on the current state of normal stress. Equation 8.32 is used to compute the reduction factors ϕ and γ. The modified D matrix is similar to that shown in Equation 8.33.

Change from Shear-Tension to Shear-Compression Failure

The stiffness reduction factors ϕ and γ calculated initially for shear-tension failure are used until normal stress becomes compressive in the subsequent analysis due to the modifications in the D matrices of the failed integration points. If the normal stress changes to compressive, then the D matrix should be modified to take the form shown in Equation 8.31 as in the case of shear- compression failure.

Solution Procedure

Composite masonry walls subjected to in-plane vertical loads lead to a condition of plane strain. Hence, a two-dimensional plane strain finite element analysis procedure may be used to determine the failure in composite masonry walls. The necessary steps for cracking analysis using smeared cracking technique in conjunction with the crack modelling proposed earlier in this section are given below.

Step 1. The analysis is initiated by applying an arbitrary load on the block wythe. Stresses in the block wythe-collar joint interface elements at each integration points are determined. These stresses are compared against the failure stresses.

Step 2. A factor, α, (larger or smaller than one) is computed for each integration point either by Equation 8.27 or by Equation 8.29. The factor from each integration point is compared against the values from other integration points to obtain the smallest value and the corresponding integration point and element number. This yields the scaling factor and the integration point in the element at which failure would initiate due to cracking. All displacements, strains and stresses are scaled using this factor to yield the solution at the initiation of failure.

Step 3. If failure is indicated, the stiffness coefficients appropriate to the failure mode are reduced to a nominal value. This reduction procedure is described in detail in the earlier section under the heading, "Modification of Constitutive Matrix, D". The composite wall under this new state is analyzed once again for the same previously scaled loads to allow stress re-distribution to occur. The stresses at each integration point are checked once again against the failure criterion. If the stresses at any integration point indicate violation of the failure criterion, the D matrix appropriate to the failure mode is modified. This process is continued until no further stress violation occurs at any integration point for the given load level which completes the analysis of the wall at that load.

Step 4. The loads and stresses at the integration points in the wall at the current state of cracking are scaled to compute the scaling factor, as described in step 2, to identify the integration point that would crack next at a new load level. Analyses are carried out as described in step 3 with the modified D matrix for the newly failed integration point at

this load level until no additional stress violations at the integration points take place, thus, completing the solution at this load.

Step 5. The solution technique described above is carried out at successive load levels until enough cracking at the block wythe-collar joint interface has taken place.

Verification of the Proposed Failure Criterion with Experimental Data

The generalized failure criterion developed earlier is verified by its application to two cases of composite wall specimens where the failure loads are known experimentally. The two specimens are modelled by the finite element technique considering plane strain condition. The specimens are assumed to behave linearly. The failure is investigated following the procedure outlined in the previous section. The results of the investigation of the two specimens are presented next.

Specimen of Colville et al.

This specimen, which consisted of two wythes of clay masonry interconnected to a single wythe of concrete block through two 3/8 in collar joints, is shown schematically in Figure 8.11 and is described in detail in Reference (31). From the compressive strengths of the block and brick masonry (using Jefferson bricks and S mortar) given in this paper, the elastic modulii for block masonry, brick masonry and mortar are computed, using ACI 531-79 (104), as 1085, 3180 and 1040 ksi, respectively. It is observed that the failure in the mortar collar joint occurs at the concrete block interface. Consequently, using $E_m = 1040$ and $E_{bl} = 1085$ in Equations 8.9 and 8.10 yield $\tau_0 = 65$ psi and $\mu = 1.06$. a value of 0.1 is assumed for the aggregate interlock factor (AIF).

Figure 8.11   Schematic Test Arrangement of Colville et al.

A finite element analysis of the specimen is performed using these values in which a finite element mesh similar to that shown in Figure 8.3 is utilized for the half specimen. The arbitrarily applied loads are scaled until failure initiates at the concrete block-mortar interface. It is found in these analyses that no additional loads can be applied once the failure at any point on the interface has been initiated. The total load at failure predicted by the finite element analysis using the values of τ_0 and μ given above in the failure criterion is equal to 11,400 lbs. The failure loads determined experimentally for the two tests with failure at the block-mortar interface are 9,410 lbs. and 13,300 lbs. The ratios of the theoretical to experimental failure loads for the two tests are, therefore, 1.20 and 0.86, respectively, which is quite satisfactory.

Specimen Tested at Clemson University

A 48 in x 48 in composite masonry wall specimen with 3/8 in collar joint, shown schematically in Figure 8.12 was tested at Clemson University with loads applied only to the block wythe. The entire top course of the block and the outside cavities of the blocks from top to bottom were grouted. The details of the test procedure along with the compressive strengths of the wall components are available in Reference (79). It was found that the collar joint developed a crack at the block-collar joint interface at a total load of 210 kips. The ultimate failure occured soon thereafter at a total load of 215 kips.

In order to compare the experimental failure load given above with that calculated using the failure criterion given by Equations 8.8-8.10, a finite element analysis of the specimen is carried out. The elastic modulii of the block and brick masonry, and collar joint mortar are calculated, using the compressive strengths given in Reference (79), to yield

Clemson University Test Specimen
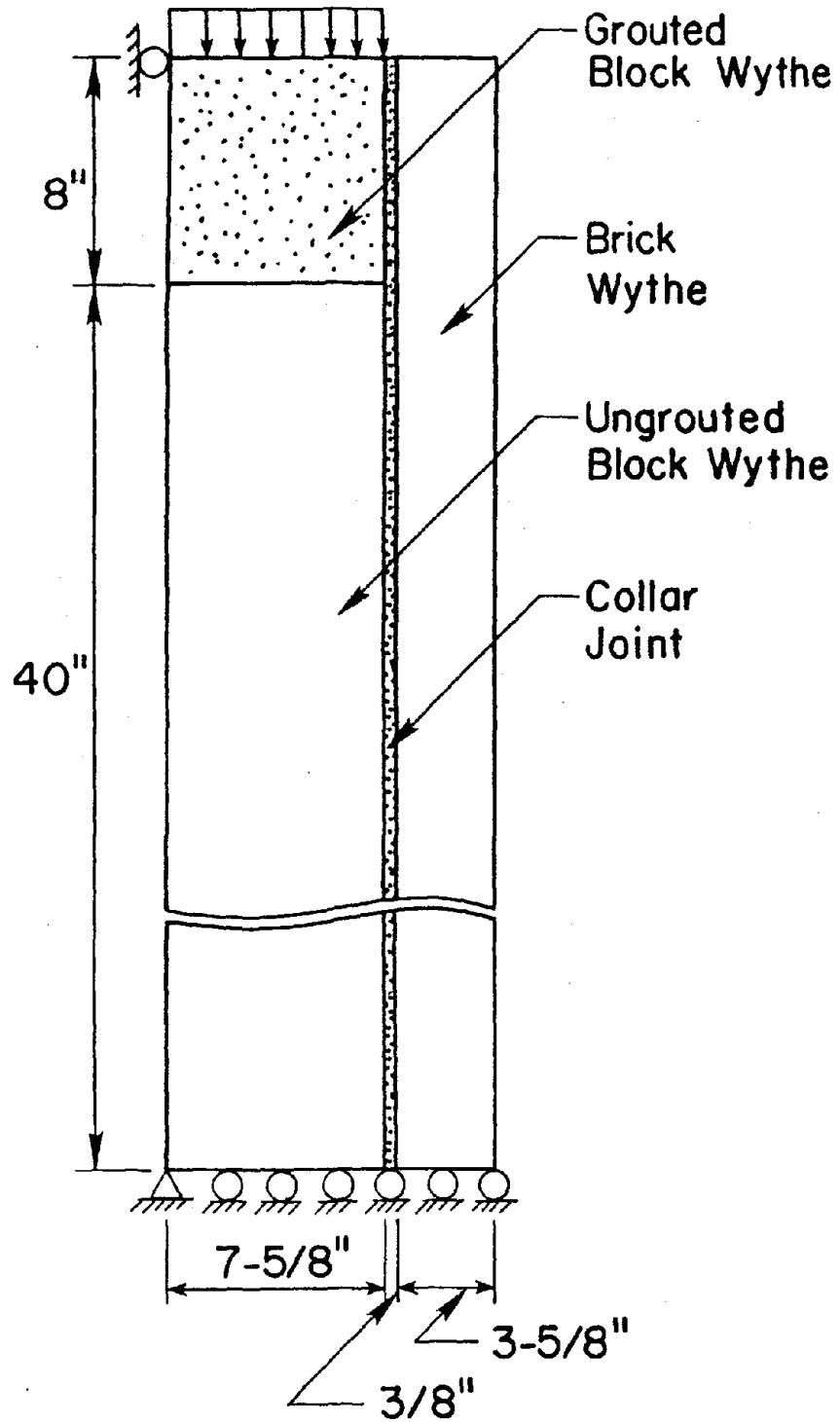
Figure 8.12   Composite Wall Specimen Tested at Clemson University

values of 1,075 ksi, 2,950 ksi, and 2,480 ksi, respectively. The modulus
of elasticity of the grouted block at the top 8 in of the wall is assumed
to be 1,600 ksi. Substitution of E_m = 2,950 and E_{b1} = 1,600 into Equations
8.9 and 8.10 gives τ_0 = 82.6 psi and μ = 1.18. A value of 0.1 is assumed
for the aggregate interlock factor (AIF) in this analysis.

The failure analysis of the cross-section of the specimen shown in
Figure 8.12 is performed, utilizing the load fraction of 0.659 determined
in Chapter VI for a perfectly bonded interface, leads to a predicted
failure load of 192 kips for the entire wall specimen. The ratio of the
theoretical to the experimental failure loads, in this case, is equal to
approximately 0.9 which appears to be quite satisfactory.

Failure Loads in Composite Masonry Walls

It should be of interest to determine the failure loads in composite
walls of various heights using the failure criteria developed and tested
earlier. Composite masonry walls with a 3/8 in slushed collar joint are
analyzed. The failure in these analyses is defined by the generalized
failure criterion developed earlier. Analysis is performed on three
composite walls of different heights.

The failure loads estimated analytically are compared with those
obtained by assuming uniform failure shear stress given in the literature.
In the later case, the block wythe-collar joint interface is assumed to
be the failure plane.

Prediction of Failure Loads by Finite
Element Analysis

Three composite masonry walls with slushed collar joints are ana-
lyzed. In these three walls only the heights are different and their
magnitudes are 10 ft, 15 ft and 20 ft. A representative cross section

consists of an 8 in concrete block wythe connected to a 4 in brick wythe. It is assumed that the external gravity loads act only on the concrete block wythe at the top of the wall. The material properties and the boundary conditions are same in all the three walls. The walls are supported at the bottom and it is assumed that the roof slab provides a lateral support at the top of the wall. The material properties for Colville's specimen (31) made of Jefferson bricks and S mortar are assigned to these walls which lead to the values of the elastic modulii for the block masonry, brick masonry and mortar as 1085, 3180 and 1040 ksi, respectively. Using $E_m = 1040$ and $E_{bl} = 1085$ in Equations 8.9 and 8.10 yield $\tau_0 = 65$ psi and $\mu = 1.06$. A value of 0.1 is assumed for the aggregate interlock factor (AIF).
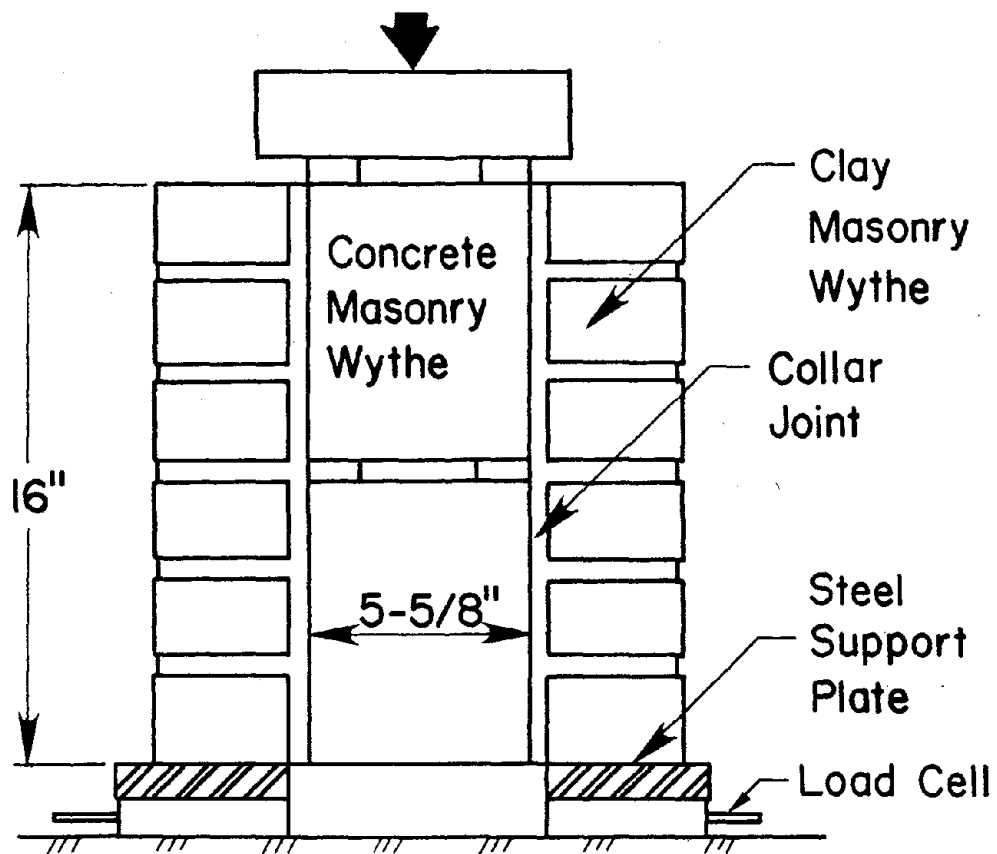
Finite element analysis of the walls are performed under a plane strain condition in which a very fine mesh is provided at the top few inches of each wall. The walls are modelled by quadratic isoparametric elements. The total number of elements and nodal points used in the analyses are 440 and 1405, respectively. In these analyses the block wythe-collar joint interface is assumed to be perfectly bonded together, and since there exists a stress discontinuity at the top of the wall, the results of the top two thin elements at the interface are disregarded. The failure analysis is performed following the procedure outlined earlier. It is observed that the cracking initiates in the third element from the top of the wall (results of the top two elements are neglected) in the collar joint at the block wythe-collar joint interface due to shear-tension at a load level of 1.22 kips per inch length of the wall. After the initial cracking in the wall, the stiffness coefficients of the

top two elements in the interface (results of which are ignored) are re-
duced to a negligible magnitude.

The stiffness coefficients appropriate to the failure mode at the
integration points in the initially failed element are reduced and the
wall is reanalyzed at the same load level. The reduction of the stiffness
coefficients in the failed element does not permit any substantial amount
of vertical load to transfer to the brick wythe. Thus, the initial
cracking load essentially stays within the block wythe and causes a state
of stress in the element (just below the cracked element) similar to that
which was experienced by the previously failed element before cracking.
This causes failure in the second element. In this newly cracked element,
some integration points fail due to shear-tension and other due to
shear-compression. The stiffness coefficients at these integration
points of this newly failed element are reduced. The state of stress in
the previously failed element at each integration point is also examined
after the re-analysis and the stiffness coefficients are again modified
if the state of stress is found to have changed within the element. Be-
cause of reduction in the stiffness of the two failed elements, almost
all of the gravity load travels downward in the block wythe, thus, causing
failure of the next element. This uninhibited failure of one element
after the other continues at essentially the initial cracking load. At
a certain distance from the top of the wall, a small amount of the load
may get transfered to the brick wythe. Due to this re-analysis of the
wall at the initial cracking load may cause less shear as well as normal
stresses in the element of interest. Nevertheless, cracking continues
in new elements at the initial cracking load since a combination of the
normal and shear stresses still lies on the failure surface.

The above cracking phenomenon is observed during the failure analysis of all the three composite masonry walls. The initial cracking load is also found to be the same in all the three different walls. After the initial cracking, the crack in the walls proceeded downwards at the same load level. The analysis is stopped after 60 analyses at which the cracking in the collar joint has extended as far as 7 inches from the top of the wall. The reasons for termination of the analysis are as follows: First, the finite element mesh below 7 inches from the top of the wall is relatively coarse which could produce misleading results. Secondly, the analysis became expensive. For the crack to travel 7 in from the top, 60 analyses were needed for which the required CPU time on VAX 8600 was 2 hours 37 minutes and 39 seconds. One can easily postulate that if the finite element model had a refined mesh for some additional distance from the top of the wall, all the elements in the collar joint at the block wythe-collar joint interface would have cracked without any substantial increase in the value of the applied load of 1.22 k/in length. Thus, the wall would have become unserviceable as a composite masonry wall at this load.

<div align="center">
Failure Loads Based on an Average
Failure Shear Stress
</div>

Several investigators (26,31,65,94) involved in experimental research in the area of composite masonry have suggested average values of failure shear stress for composite masonry walls. These values are derived from laboratory tests of composite masonry specimens subjected to shear loads, in which the shear load at failure is divided by the area of the failure surface (block wythe-collar joint or brick wythe-collar joint interface) to obtain the average failure shear stress. A wide range

of values between 50 to 95 psi for the average failure shear stress is quoted in the literature.

It should be of interest to compare the magnitudes of the failure loads computed by the finite element analyses with those estimated by using the average failure shear stress. Two specimens constructed of Jefferson brick and S mortar tested by Colville et al failed at the block-collar joint interface. The average shear stress at failure in these two specimens were 40.8 and 58.1 psi. The average of these two values is 49.45 psi which may be used to compute the failure loads in the walls. For a 10 ft high wall the failure load computed from this average failure shear stress is 5.93 kips per inch length of wall. For 15 ft and 20 ft walls, the corresponding failure loads are found to be 8.90 and 11.87 kips per inch.

Comparison of Failure Loads

As shown above, the failure loads for 10 ft, 15 ft and 20 ft walls based on an average stress, are 5.93, 8.90 and 11.87 k/in. On the other hand, failure load computed by the finite element analysis is found to be the same for all the three walls and its magnitude is 1.22 kips per inch length of the wall. A comparison of these values indicates that the failure load prediction based on the average stress overestimates the strength of the wall, and the magnitude of this overestimation increases with an increase in the height of the wall. It should be noted here that the failure load based on the average failure shear stress is a linear function of the height of wall. This is unacceptable since the shear stress distribution at the interface along the height of the wall is not uniform. The shear stress is maximum near the top at the point of load application and reduces to almost zero within the top 10-15 inches.

A critical study of the failure loads predicted from the average failure shear stress indicates that this procedure produces unrealistic results. For the walls under consideration, the crushing strength of block masonry is 1085 psi which leads to uniformly distributed ultimate load of 8.26 kips per inch length. This value of block crushing strength is less than the failure loads of 8.90 and 11.87 k/in predicted for 15 ft and 20 ft high walls computed using the average failure shear stress. Thus, the block wythe of these walls will experience a crushing failure before the computed failure loads could be applied. Hence, prediction of failure loads in composite masonry walls using average failure shear stress not only overestimates the strength of the wall but also produces very unrealistic results.

Conclusions

1. It is apparent from the results presented in the previous sections that it may be possible to develop empirical equations that describe the failure criteria of concrete block-mortar joints in terms of the elastic modulii of block masonry and mortar.

2. Equations 8.8-8.10, which define the failure criterion developed in this research , are based upon the results of only two laboratory test programs. In order to obtain more accurate empirical failure relationships, more Mohr-Coulomb type of equations based on additional experimental evidence are needed.

3. It should be kept in mind that important parameters, other than the elastic modulii of the blocks and mortar, such as surface roughness, chemical composition, water content at the time of testing, gradation of the block material, etc., may also play an important role in the joint shear strength.

4. Additional experimental and analytical studies must, therefore, be performed in masonry to develop failure relationships which are very much needed in the development of masonry analysis and design.

5. Failure loads in composite masonry walls of various heights are determined using the failure criterion developed in this research. The failure loads estimated analytically are compared with those obtained by assuming uniform failure shear stress

given in the literature. The later procedure leads to unrealis-
tic failure loads indicating that average shear stress should
not be utilized in determining the shear strength of a composite
masonry wall.

CHAPTER IX

SUMMARY, CONCLUSIONS AND PROPOSED FUTURE WORK

Summary

In this research, it has been attempted to investigate numerically the behavior and failure of composite masonry walls. In composite masonry construction, usually the floor slab rests on the interior block wythe of the composite wall. As a result, the block wythe experiences a significant amount of horizontal and vertical in-plane loads transmitted to it by the floor slab. Failure in composite masonry walls is essentially due to the delamination of the wythes caused by the interface shear stresses. Hence, determination of the correct magnitudes of shear stresses at the interfaces of composite masonry walls is extremely important.

The effects of horizontal and vertical in-plane loads on the behavior of composite masonry walls are investigated using quasi three-dimensional elements.

Shear stresses in a composite masonry wall may develop due to moisture and thermal strains without necessarily any application of external loads. Creep strains under sustained loads also become somewhat important for consideration in the estimation of stresses in a composite wall. The behavior of composite masonry walls subjected to creep strains and temperature variations is studied using two-dimensional finite element models.

In this investigation, a solution procedure using two-dimensional plane strain finite elements is proposed to estimate acceptable stresses

at the interfaces of composite walls. For accurate and economic prediction of the stresses, several types of variable-node-number isoparametric serendipity elements are developed. The locations of optimal stress points within the elements are also determined.

In order to investigate the behavior of the interfaces of composite masonry walls, an interface element is introduced. Strains at various locations are computed by the finite element method using the proposed interface element and without using the interface element. The strains are compared with the experimentally obtained strains to determine the behavior of the interfaces of the composite masonry walls. It is observed that the interfaces in composite masonry walls under realistic boundary conditions behave like perfectly bonded joints, thus, not requiring the use of an interface element. In addition, a procedure using the finite element method for determining stresses in the perfectly bonded joints of composite masonry walls involving stress discontinuities is proposed.

An improved failure criterion (Mohr-Coulomb type) for block wythe-collar joint (mortar) interface is developed. Empirical equations are suggested for obtaining the failure criterion for a specific masonry once the material properties of the masonry units and mortar are known. A finite element procedure for cracking analysis of composite masonry walls is proposed. In addition, failure analyses are carried out for composite walls of various heights utilizing the failure criterion and procedure developed in this research.

Conclusions

The conclusions that can be drawn from the results of this research, described in the preceding chapters may be divided into two parts. The first part is based on the results of the quasi three-dimensional model

which was utilized for walls subjected to both the vertical and horizontal loads. The second part of the conclusions are due to the two-dimensional cross-sectional model which is capable of being subjected to only vertical loads. It can also handle analyses involving thermal, creep and moisture effects.

Conclusions from Quasi Three-dimensional Model

For a single story high wall, subjected to horizontal in-plane loads, the horizontal shear stress in the collar joint at the block wythe- collar joint interface is maximum at the top of the wall and reduces to zero within a distance equal to approximately the width of the loaded wythe.

The vertical shear stress, though much smaller than horizontal shear stress, reduces to zero within the top 15-20 inches. Vertical normal stresses are the largest at the base near the ends of the wall.

The horizontal load transfer from the block wythe to the brick wythe occurs within a distance from the top of the wall which is shorter than the distance within which the vertical load transfer occurs. This phenomenon is due to the smaller horizontal stiffness of the wall compared to its vertical stiffness.

For a two story composite masonry wall, the maximum horizontal shear stress due to in-plane horizontal loads occurs at the roof level. This shear stress reduces to zero at a distance of approximately 10 inches from the top of the wall. The horizontal shear stress at the second floor level, on the other hand, is much smaller.

The shear stress, τ_{xy}, on a horizontal plane in the collar joint is quite significant just below the second floor level. It appears, therefore, that both locations, one at the roof level and the other just below the second floor level are critical for a failure of the collar joint.

The vertical shear stress, τ_{yz}, in the collar joint of a two story wall is smaller than the horizontal shear stress, τ_{xz}, for all loads. Its maximum value due to assumed parabolically distributed vertical loads occurs at the center line of the wall. The corresponding maximum vertical shear stress due to the horizontal loads is much smaller.

The quasi three-dimensional model which is utilized to analyze the composite masonry walls subjected to horizontal loads, predicts higher shear stresses in the collar joint than those predicted by two-dimensional plane strain finite element model (16), and does not take the out-of-plane displacements into account. However, the analysis performed utilizing this model provides sufficient information to understand qualitatively the behavior of the wall subjected to horizontal in-plane loads.

Conclusions Using Two-dimensional Model

All strains increase substantially due to creep during the first 300 days; most of the increase occurs during first month after the load application. The shear stresses in the collar joint remain almost constant with the elapse of time. Normal stresses in the collar joint reduce between 10% and 30% at various times.

The technique presented in this research for determining the stress changes due to creep strains in composite masonry walls can be used for walls of other materials if the specific creep curves for those materials are available.

Normal and shear stresses in the collar joint of composite masonry wall are computed for realistic temperature variations. It is observed that the shear stresses and strains in the collar joint do not undergo any substantial changes due to temperature variations.

The normal stresses in the collar joint can change from a compressive value for the external loads alone to a tensile value for the dead loads and assumed temperature changes. The magnitudes of the change in stress as well as the final tensile normal stress are significant. Hence, it is recommended that vertical reinforcement be provided in the collar joint to resist tensile cracking.

The variable-node-number elements can be used to model the composite masonry walls very efficiently. A very coarse mesh of variable-node-number elements can reproduce the results obtained from a very fine mesh of lower order elements, hence, reducing the cost of analysis considerably.

The interfaces in composite masonry walls behave like perfectly bonded joints. Under realistic boundary conditions, there exists no planes of weakness along the block wythe-collar joint or brick wythe-collar joint interface.

It has been shown that a generalized Mohr-Coulomb type of failure criterion based upon the material properties can be developed for investigating collar joint failure of composite walls. However, the failure criterion for a block-mortar joint developed in this research is based upon the results of only two laboratory test programs. In order to obtain more accurate empirical failure relationships, more Mohr-Coulomb type of equations based on additional experimental evidence are needed.

From the failure loads calculated for composite walls of various heights using the proposed finite element analysis and its comparison with those obtained by assuming uniform failure shear stress in the collar joint, it is shown that the latter method not only overestimates the shear strength of the wall but also produces very unrealistic results.

Accordingly, it is unsafe to design composite walls based on average collar joint shear stresses determined in the laboratory.

Based upon the assumed failure criterion, the uniformly distributed vertical failure load intensity per inch length on the block wythe for the various heights of composite masonry wall is equal to 1.22 k/in. This magnitude of load depends upon the material properties of the wall components. It should be noted that a different failure criterion based on additional experimental data could also yield a different failure load.

Proposed Future Research

From the experience gained so far in estimating analytically the stresses and failure loads in composite masonry walls, it is proposed that future research be conducted using three-dimensional finite elements to estimate the correct stresses and failure loads in the composite masonry walls subjected to horizontal loads due to earthquake and wind loads. In order to perform failure analysis using three-dimensional models, it will be necessary to use a failure criterion based upon the three shear stresses and the associated normal stresses. This type of failure criterion has not been established yet.

In this research, a parabolic temperature profile is assumed across the thickness of the composite masonry wall. The actual temperature profile should be determined and utilized in the analysis technique to estimate more realistically the effects of temperature variations.

It has been shown experimentally and analytically that composite masonry walls fail at a very low load level due to the separation of the wythes when only the inner block wythe is loaded. It is anticipated that the failure loads will be much higher if both the wythes are loaded simultaneously. This should be studied in the future.

The specific tasks that should be executed in the proposed future research are summarized as below. When composite masonry walls are subjected to horizontal and vertical loads simultaneously, failure may occur not only by delamination of the collar joint due to a combined action of the vertical and horizontal shears but also due to possible failure of the horizontal bed joints in the concrete masonry. The possibility of this failure mode is likely to exist in composite walls which are built with hollow concrete blocks and/or which have a minimal amount of vertical reinforcement. Consequently, it is quite important that experimental and analytical investigations be conducted to determine the strength of composite masonry walls subjected to a combination of vertical and horizontal in-plane loads. In this research, a quasi three-dimensional finite element model has been utilized to determine the effects of horizontal and vertical loads on composite masonry walls. The quasi three-dimensional model used in this research predicts higher shear stresses in the collar joint, and does not take the out-of-plane displacements into account. A three-dimensional model must be developed for further investigation of the behavior of composite walls subjected to horizontal loads. This model should be capable of predicting failure of the bed joints in the wythes in addition to delamination of the collar joint.

The exact temperature profile across the thickness of the composite masonry wall should be determined in order to estimate the effects of temperature variations accurately.

A dynamic mesh generation scheme should be developed for two-dimensional failure analysis utilizing the variable-node-number elements. In this scheme, only a small portion near the top of the wall should be modelled by a very fine mesh while the rest of the wall may be modelled

by a very coarse mesh. When a portion of the wall at the top which is modelled by a very fine mesh cracks, that portion of fine mesh should be replace by a coarse mesh and the coarse mesh just below the the cracked portion of the wall should be replaced by a very fine mesh. This process should continue as the crack propagates. The dynamic mesh generation scheme will reduce the failure analysis cost to a great extent.

Mohr-Coulomb type of equations for brick- mortar joints should be determined experimentally in order to obtain empirical failure relation- ships following the procedure suggested in Chapter VIII. More Mohr- Coulomb type of equations for block- mortar joint based on additional experimental evidence should be obtained for improving the empirical failure relationships proposed in Chapter VIII.

The relationship between the failure shear stress and the shear bond strength, the coefficient of friction and the associated normal stress for a block and/or brick-grout interface in composite masonry walls with 2 in collar joint should be develped for utilization in future failure analyses.

Analytical procedures should be developed to predict correct inter- face stresses and failure loads in reinforced masonry walls. Also, a procedure should be developed for dynamic analyses of reinforced compos- ite masonry walls.

APPENDICES

Appendix A

Analytical Solution of a Fully Loaded Brick Wall

For plane strain, in general, stresses can be related to strains by

$$\sigma_x = [E/\{(1+v)(1-2v)\}][(1-v)\varepsilon_x + v\varepsilon_y] \tag{A.1}$$

$$\sigma_y = [E/\{(1+v)(1-2v)\}][(1-v)\varepsilon_y + v\varepsilon_x] \tag{A.2}$$

$$\sigma_z = v(\sigma_x + \sigma_y). \tag{A.3}$$

As there are no deformations along the horizontal direction in the cross section of the wall, strains in this direction are zero, i.e., $\varepsilon_x = 0$. Therefore, the expressions for stresses σ_x and σ_y reduce to

$$\sigma_x = [E/\{(1+v)(1-2v)\}]v\varepsilon_y \tag{A.4}$$

$$\sigma_y = E\varepsilon_y/\{(1+v)(1-2v)\} - Ev\varepsilon_y/\{(1+v)(1-2v)\}. \tag{A.5}$$

Comparing Equation A.4 to Equation A.5 yields

$$\sigma_x = E\varepsilon_y/\{(1+v)(1-2v)\} - \sigma_y. \tag{A.6}$$

Hence, the results of the elastic analysis obtained by the computer program must satisfy this condition.

As the creep analysis is assumed to be within the elastic range, the incremental stresses due to creep, which are calculated from the stress-causing-strain increments $\Delta\varepsilon_x{}^S$ and $\Delta\varepsilon_y{}^S$, are given by

$$\Delta\sigma_x = [E/\{(1+v)(1-2v)\}][(1-v)\Delta\varepsilon_x{}^S + v\Delta\varepsilon_y{}^S] \tag{A.7}$$

$$\Delta\sigma_y = [E/\{(1+v)(1-2v)\}][v\Delta\varepsilon_x{}^S + (1-v)\Delta\varepsilon_y{}^S] \tag{A.8}$$

$$\Delta\sigma_z = v(\Delta\sigma_x + \Delta\sigma_y). \tag{A.9}$$

The stress-causing-strain increments can be expressed as

$$\Delta\varepsilon_x{}^S = \Delta\varepsilon_x - \Delta\varepsilon_x{}^{cr} \tag{A.10}$$

$$\Delta\varepsilon_y{}^S = \Delta\varepsilon_y - \Delta\varepsilon_y{}^{cr} \tag{A.11}$$

where

$\Delta\varepsilon_x$ and $\Delta\varepsilon_y$ = the calculated final creep increments,

$\Delta \varepsilon_x{}^{cr}$ and $\Delta \varepsilon_y{}^{cr}$ = the initial creep strain increments in the x and y directions respectively.

As the wall under consideration is fully loaded and remains loaded at all times, there is no change in the vertical stress, i.e., $\Delta \sigma_y$ in Equation A.8 must be zero, which leads to

$$v \Delta \varepsilon_x{}^S = -(1-v) \Delta \varepsilon_y{}^S. \tag{A.12}$$

In addition, the horizontal strain increment, $\Delta \varepsilon_x$, is also zero, for which Equation A.10 yields

$$\Delta \varepsilon_x{}^S = -\Delta \varepsilon_x{}^{cr}. \tag{A.13}$$

Substituting for $\Delta \varepsilon_y{}^S$ from Equation A.12 into Equation A.7 and simplifying gives

$$\Delta \sigma_x = \{E/(1-v^2)\} \Delta \varepsilon_x{}^S \tag{A.14}$$

which after replacement of $\Delta \varepsilon_x{}^S$ in terms of $\Delta \varepsilon_x{}^{cr}$ from Equation A.13 leads to

$$\Delta \sigma_x = -\{E/(1-v^2)\} \Delta \varepsilon_x{}^{cr}. \tag{A.15}$$

For the specific wall and loads under consideration, the above formulas lead to the following results. The stress intensity in the y-direction is

$$\sigma_y = -0.03125 \text{ ksi.}$$

Considering $\varepsilon_x = 0$ and using Equation A.2, the strain component in the vertical direction for the given problem can be obtained. The magnitude of ε_y is

$$\varepsilon_y = 1.30208 \times 10^{-5}.$$

The stress intensity in x-direction can be calculated by Equation A.4 or Equation A.6 which yields

$$\sigma_x = -0.010416 \text{ ksi.}$$

Also $\sigma_z = v(\sigma_x + \sigma_y)$

$$= -0.0104165 \text{ ksi.}$$

These are the elastic stresses in a fully loaded wall which are also the principle stresses due to the absence of any shear. Substituting these values in Equation 3.8 yields a value for the equivalent stress σ as

$$\sigma = 0.020896 \text{ ksi.}$$

The incremental stress $\Delta\sigma_x$ in the x-direction due to creep for the first time interval can be calculated from Equation A.15 in which $\Delta\varepsilon_x^{cr}$ is the initial creep strain increment for this time interval. The value of $\Delta\varepsilon_x^{cr}$ can be calculated using Equation 3.13.

The first time interval under consideration is 5 days. From Figure 3.2, specific creep strain value for brick wythe for this time interval is 2.8×10^{-5}. The incremental equivalent creep strain for this time interval is given as

$$\Delta\varepsilon^{cr} = 0.020896 \times 2.8 \times 10^{-5}$$

$$= 0.05850 \times 10^{-5}.$$

Using the values for the elastic stresses as well as the incremental equivalent creep strain in Equation 3.13 yields

$$\Delta\varepsilon_x^{cr} = 0.0291 \times 10^{-5}$$

which is utilized in Equation A.15 along with the value of E to give

$$\Delta\sigma_x = -0.062 \times 10^{-2} \text{ psi.}$$

These analytical values of the stresses from the elastic analysis and incremental stresses from the creep analysis are compared with the results obtained from the computer program. These comparisons are given in Table A-I and A-II.

Table A-I. Comparison of Results for Elastic Analysis

Stress (ksi)	Computer Results	Analytical Solution
σ_y	-0.0312498	-0.03125
σ_x	-0.0104116	-0.010416

Table A-II. Comparison of Results for Creep Analysis

Stress (ksi)	Computer Results	Analytical Solution
$\Delta\sigma_y$	-0.93×10^{-9}	0.0
$\Delta\sigma_x$	-0.0622×10^{-2}	-0.062×10^{-2}

Appendix B

Analytical Solution of a Single Element Problem

Analysis Due to External Loads

The stress intensity in the y-direction is given by

$$\sigma_y = 2 \times 1/2 = 1.0 \text{ ksi.} \tag{B.1}$$

Also σ_y for a plane strain case can be obtained

by the following equation:

$$\sigma_y = \frac{E}{(1+v)(1-2v)}\left[v\varepsilon_x + (1-v)\varepsilon_y\right]. \tag{B.2}$$

The strain in x-direction, ε_x is zero, for which Equation B.2 yields

$$\varepsilon_y = 4.16 \times 10^{-4} \text{ in./in.} \tag{B.3}$$

The stress intensity in the x-direction is given by

$$\sigma_x = \frac{E}{(1+v)(1-2v)}\left[(1-v)\varepsilon_x + v\varepsilon_y\right]. \tag{B.4}$$

Considering $\varepsilon_x = 0$, Equation B.4 yields

$$\sigma_x = 0.333 \text{ ksi.} \tag{B.5}$$

Analysis Due to Temperature Gradient

It is assumed that the inside-outside temperatures are 80°, 60°F, for a 20°F lower temperature on the outside than inside. The stress-free temperature is assumed to be 60°F. The temperature at the centroid of the element is 70°F considering a linear variation of temperature from one side to the other side of the specimen. The change in temperature at the centroid of the element is 10°F.

The initial strain can be computed by mutiplying coefficient of thermal expansion with the change in temperature. The initial strains computed are given by

$$\varepsilon_{xi} = \varepsilon_{yi} = 0.0004. \tag{B.6}$$

Equivalent Joint Loads

From Figure B.1,

$$\sigma_x = 2F_x/2 = F_x \tag{B.7}$$

$$\sigma_y = 2F_y/2 = F_y. \tag{B.8}$$

Use of initial strains from Equation B.6 into Equation B.4 in conjunction with Equation B.7 leads to

$$F_x = 1.28 \text{ kips.} \tag{B.9}$$

From the symmetry of the problem,

$$F_y = 1.28 \text{ kips.} \tag{B.10}$$

Resulting Strains

These strains are caused by equivalent joint loads due to initial strains

$$\varepsilon_x = 0$$

$$\sigma_y = 1.28 \times 2/2 = 1.28 \text{ ksi.} \tag{B.11}$$

Utilizing Equation B.11 into Equation B.2 gives

$$\varepsilon_y = 5.33 \times 10^{-4}. \tag{B.12}$$

Stress Causing Strains

The stress causing strains can be obtained by subtracting resulting strains caused by the initial strains from the elastic strains due to external loads.

$$\varepsilon_x = 0-0.0004 = -0.0004 \text{ and} \tag{B.13}$$

$$\varepsilon_y = 5.33 \times 10^{-4} - 4.0 \times 10^{-4} = 1.33 \times 10^{-4}. \tag{B.14}$$

Change in Stresses

Substituting Equations B.13 and B.14 into Equations B.4 and B.2 yields

$$\sigma_x = -0.8536 \text{ ksi.} \tag{B.15}$$

$$\sigma_y = -0.00008 \text{ ksi.} \tag{B.16}$$
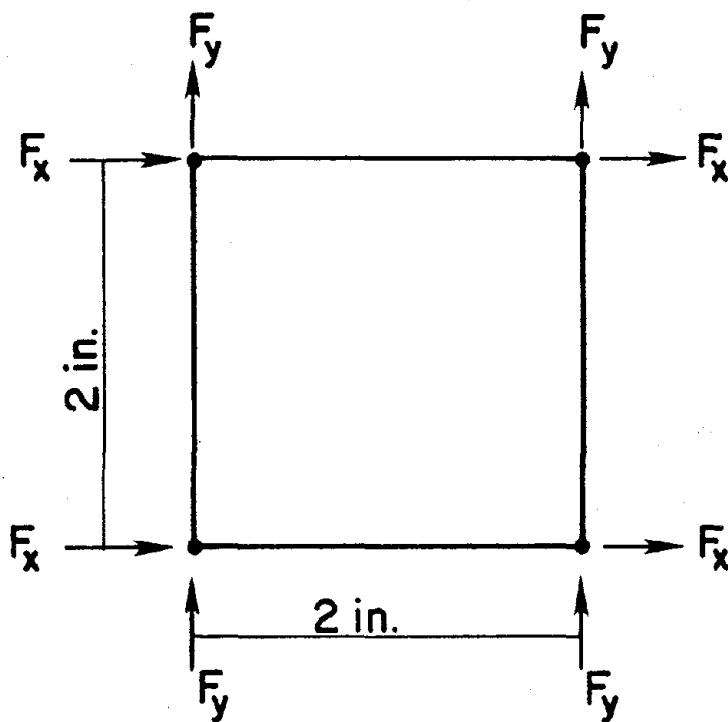
Figure B.1 Joint Loads

Total Strains and Stresses

Total strains are obtained by adding the values of ε_x and ε_y from Equations B.11 and (B.12) to the elastic strains due to external loads, which yields

$$\varepsilon_{xT} = 0.0 \text{ and} \tag{B.17}$$

$$\varepsilon_{yT} = 9.49 \times 10^{-4}. \tag{B.18}$$

Total stresses are obtained by adding the values of σ_x and σ_y from Equations B.15 and B.16 to the elastic stresses due to external loads, which yields

$$\sigma_{xT} = -0.5206 \text{ ksi and} \tag{B.19}$$

$$\sigma_{yT} = +0.99992 \text{ ksi}. \tag{B.20}$$

Table B-I. Comparison of Results for Elastic Analysis

Stresses (ksi) or Strains	Computer Results	Analytical Solution
σ_x	0.3333	0.333
σ_y	1.0	1.0
ε_x	0.0	0.0
ε_y	0.4166×10^{-3}	0.416×10^{-3}

Table B-II. Comparison of Results for Temperature Analysis

Total Stress (ksi) or Total Strains	Computer Results	Analytical Solution
σ_{xT}	-0.520	-0.5206
σ_{yT}	1.0	0.9999
ε_{xT}	0.0	0.0
ε_{yT}	0.95×10^{-3}	0.949×10^{-3}

LITERATURE CITED

1. Ali, S., and Page, A.W., "A Failure Criterion for Mortar Joints
      in Brickwork Subjected to Combined Shear and Tension," Masonry
      International, Vol. 9, Dec. 1986, pp. 43-54.

2. Ali, S., and Page, A.W., "Non-Linear Finite Element Analysis of
      Masonry Subjected to Concentrated Load," Proceedings, Institute
      of Civil Engineers, Part 2, 1987, 83, Dec., pp. 815-832.

3. Anand, S.C., "Shear Stresses in Composite Masonry Walls," Session
      Proceedings, entitled "New Analysis Techniques for Composite
      Masonry," ASCE Structures Congress, Chicago, IL, Sept. 16-18,
      1985, pp. 120-131.

4. Anand, S.C., and Dandawate, B., "Creep Modelling for Composite
      Masonry Walls," Proceedings, 5th ASCE-EMD Specialty Conference,
      University of WY, Laramie, Wyoming, Aug. 1-3, 1984,
      pp.432-437.

5. Anand, S.C., and Dandawate, B., "A Numerical Method to Compute
      Creep Effects in Masonry Walls,"Proceedings, 3rd North American
      Masonry Conference, University of Texas at Arlington, TX, June
      3-5, 1985, pp. 75.1-75.14.

6. Anand, S.C., Dandawate, B., and Brown, R.H., "A Finite Element
      Model for Creep in Composite Masonry," Department of Civil
      Engineering, Clemson University, Clemson, SC, Report No. 20S-
      84, 1984.

7. Anand, S.C., and Gandhi, A., "A Finite Element Model to Compute
      Stresses in Composite Masonry Walls Due to Temperature,
      Moisture, and Creep," Proceedings, 3rd Canadian Masonry Sympo-
      sium '83, University of Alberta, Edmonton, Alberta, June 6-8,
      1983, pp. 34.1-34.20.

8. Anand, S.C., Gandhi, A., and Brown, R.H., "Development of a Finite
      Element Model to Compute Stresses in Composite Masonry due to
      Creep, Moisture and Temperature," Department of Civil
      Engineering, Clemson University, Clemson, SC, Report No. 5S-83,
      1983.

9. Anand, S.C., McCarthy, J., and Brown, R.H., "An Experimental Study
      of the Shear Strength of The Collar Joint in Grouted and
      Slushed Composite Masonry Walls," Department of Civil Enginee-
      ring, Clemson University, Clemson, SC, Report No. 7S-83, 1983.

10. Anand, S.C., and Rahman, M.A., "Creep Modelling for Masonry Under Plane Strain," Proceedings, Ninth Conference on Electronic Computation, University of Alabama at Birmingham, AL, Feb. 23-26, 1986, pp. 629-643.

11. Anand, S.C., and Rahman, M.A., "Temperature and Creep Stresses in Composite Masonry Walls," in 'Advances in Analysis of Structural Masonry, 'Proceedings, ASCE Structures Congress, ed. S.C. Anand, New Orleans, LA, Sept. 15-18, 1986, pp. 111-132

12. Anand, S.C., and Rahman, M.A., "Stresses in Composite Masonry Shear Walls," Proceedings, 4th Canadian Masonry Symposium, University of New Brunswick, Fredicton, B.C., Canada, June 2-4, 1986, pp. 107-121.

13. Anand, S.C., and Stevens, D.J.,"Shear Stresses in Composite Masonry Walls Using 2D Model," Proceedings, 3rd North American Masonry Conference, University of Texas at Arlington, TX, June 3-5, 1985, pp.41.1-41.15.

14. Anand, S.C. and Stevens, D.J., "A Simple Model for Shear Cracking and Failure in Composite Masonry," Proceedings, 6th international Congress on Fracture, New Delhi, India, Dec. 4-10, 1984, 2915-2922.

15. Anand, S.C., and Stevens, D.J., "Computer-Aided Failure Analysis of Composite Concrete Block-Brick Masonry," Proceedings, International Conference on Computer-Aided Analysis and Design of Concrete Structures, Split, Yugoslavia, Sept. 17-21, 1984, pp. 649-661.

16. Anand, S.C., Stevens, D.J., and Brown, R.H., "Development and Application of the Finite Element Method to the Modelling of Composite Masonry Walls" Department of Civil Engineering, Clemson University, Clemson, SC, Report No. 4S-83, 1983.

17. Anand, S.C., and Yalamanchili, K.K., "Evaluation of Loads at Cracking in Collar Joints of Composite Masonry Walls," Proceedings, 4th North American Masonry Conference, University of California at Los Angeles, CA, August 16-19, 1987, pp. 15.1-15.17.

18. Anand, S.C., and Yalamanchili, K.K., "A Quasi Three-dimensional Failure Analysis of Composite Masonry Walls Subjected to Seismic Loads," Proceedings, 8th International Brick/Block Masonry Conference, Dublin, Ireland, Sept. 19-21, 1988, pp. 1205-1216.

19. Anand, S.C., and Young, D.T., "A Finite Element Model for Composite Masonry, "Journal of the Structural Division, ASCE, Vol. 108, No. ST12, 1982, pp. 2637-2648.

20. Anand, S.C., Young, D.T., and Stevens, D.T., "A Model to Predict Shearing Stresses Between Wythes in Composite Masonry Walls due to Differential Movement," Proceedings, 2nd North American Masonry Conference, University of Maryland, College Park, MD, August 9-11, 1982, pp. 7.1-7.16.

21. Arya, S.K., and Hegemier, G.A., "A Finite Element Method for interface Problems with Application to Concrete Masonry," Journal of the Structural Division, ASCE, Vol. 108, No. ST2, Feb. 1982, pp. 327-342.

22. Barlow, J., "Optimal Stress Locations in Finite Element Models," International Journal for Numerical Methods in Engineering, Vol. 10, 1976, pp. 243-251.

23. Bathe, K.J., Finite Element Procedures in Engineering Analysis, Prentice-Hall, Inc., 1982.

24. Bazant, Z.P., "Mathematical Models for Creep and Shrinkage of Concrete," in Creep and Shrinkage of Concrete Structures, Eds. Bazant, Z.P., and Whittman, F.H., John Wiley & Sons, 1982, pp. 312-315.

25. Beer, G., "An Isoparametric Joint/Interface Element for Finite Element Analysis," International Journal for Numerical Methods in Engineering, Vol. 21, 1985, pp. 585-600.

26. Brown, R.H., and Cousins, T.E., "Shear Strength of Slushed Composite Masonry Collar Joints," Proceedings, 3rd Canadian Masonry Symposium '83, University of Alberta, Edmonton, June 6-8, 1983, pp. 38.1-38.16.

27. Buragohain, D.N., and Shah, V.L., "Curved Isoparametric Interface Surface Element," Technical notes, Journal of the Structural Division, ASCE, Vol. 104, No. ST1, January, 1978, pp. 205-209.

28. Bushnell, D., "A Strategy for the Solution of Problems Involving Large Deflections, Plasticity and Creep," International Journal for Numerical Methods in Engineering, Vol. 11, 1977, pp. 683-708.

29. Chan, H.C., and Cheung, Y.K., "Analysis of Shear Walls Using Higher Order Finite Elements," Building and Environment, Vol. 14, 1979, pp. 217-224.

30. Cheung, Y.K., and Chen, H.C., "Generation of a Series of High Order Rectangular Plane Stress Elements," Proceedings, Seventh Canadian Congress of Applied Mechanics, Vol. 2, Sherbrooke, May 1979, pp. 889-900A.

31. Colville, J., Matty, S., and Wolde-Tinsae, A., "Shear Capacity of Mortared Collar Joints," Proceedings, 4th North American Masonry Conference, University of California at Los Angeles, CA, August 1987, pp. 60.1-60.15.

32. Desai, C.S., "Finite Element Method for Analysis and Design of Piles," _Misc. Paper S-76-21, U.S. Army Engineer Waterways Experiment Station_, Vicksburg, MS, October, 1976.

33. Desai, C.S., "Behavior of Interfaces Between Structural and Geologic Media," _International Conference on Recent Advances in Geotechnical Earthquake Engineering and Soil Dynamics_, St. Louis, April 26- May 3, 1981, pp. 619-638.

34. Desai, C.S., Zaman, M.M., Lightner, J.G., and Siriwardane, H.J., "Thin-Layer Element for Interfaces and Joints," _International Journal for Numerical and Analytical Methods in Geomechanics_, Vol. 8, 1984, pp. 19-43.

35. Dilger, W.H., "Methods of Structural Creep Analysis," Eds. Bazant, Z.P.,and Wittman, F.H., John Wiley & Sons, 1982, pp. 184-192.

36. Dyson, B.F., "A Unifying View of the Kinematics of Creep Cavity Growth," in _Creep and Fracture of Engineering Materials and Structures_, Editors, Wilshire, B., and Owen, D.R.J., Pineridge Press, Swansea, UK, 1981, pp. 235-247.

37. Gale, J.E.,Taylor, R.L., Witherspoon, P.A., and Ayatollahi, M.S., "Flow in Rocks with Deformable Fractures," _Finite Element Methods in Flow Problems_, Eds. Oden, J.T., Zienkiewicz, O.C., Gallagher, R.H., and Taylor, D., University of Alabama at Huntsville Press, Huntsville, Alabama, 1974, pp. 583-598.

38. Ghaboussi, J., Wilson, E.L., and Isenberg, J., "Finite Element for Rock Joints and Interfaces," _Journal of the Soil Mechanics and Foundations Division, ASCE_, Vol. 99, No. SM10, October, 1973, pp. 833-848.

39. Glanville, J.I., and Kobak, S.,"The Structural Implications of Some Thermal Effects in High Rise Masonry Buildings," _Proceedings, Second Canadian Masonry Symposium_, Ottawa, Canada, June 9-11, 1980, pp. 493-503.

40. Goodman, R.E., and Dubois, J., "Duplication of Dilatancy in Analysis in Jointed Rocks," _Journal of the Soil Mechanics and Foundations Division, ASCE_, Vol. 98, No. SM4, April, 1972, pp. 399-422.

41. Goodman, R.E., and St. John, C.,"Finite Element Analysis of Discontinuous Rocks," in _Numerical Methods in Geotechnical Engineering_, Eds. Desai, C.S. and Cristian, J.T., McGraw-Hill Book Co., New York, N.Y., 1977, pp. 148-175.

42. Goodman, R.E., Taylor, R.L., and Brekke, T.L., "A Model for the Mechanics of Jointed Rock," _Journal of the Soil Mechanics and Foundations Divisions, ASCE_, Vol. 94, No. SM3, May 1968, pp. 637-659.

43. Greenbaum, G.A., and Rubinstein, M.F., "Creep Analysis of Axisy-
    mmetric Bodies Using Finite Elements," Nuclear Engineering and
    Design, Vol. 7., 1968, pp. 379-397.

44. Grimm, C.T., "Design of Differential Movement in Brick Walls,"
    Journal of the Structural Division, ASCE, Vol. 101, No. ST11,
    November 1975, pp. 2385-2403.

45. Grimm, C.T., "Thermal Strains in Brick Masonry," Proceedings,
    Second North American Masonry Conference, University of
    MD, College Park, Maryland, August 9-11, 1982, pp. 34.1-34.21.

46. Grimm, C.T., and Fowler, D.W., "Differential Movement in Composite
    Load-bearing Masonry Walls," Journal of the Structures Division
    ASCE, Vol. 105, No. ST7, July 1979, pp. 1277-1288.

47. Haggblad, B., and Nordgren, G., "Modelling Nonlinear Soil-Structure
    Interaction Using Interface Elements, Elastic-Plastic Soil
    Elements and Absorbing Infinite Elements," Computers and
    Structures, Vol. 26, No. 1/2, 1987, pp. 307-324.

48. Hamid, A.A., Drysdale, R.G., and Heidebrecht, A.C., "Shear Strength
    of Concrete Masonry Joints," Journal of the Structural Division
    ASCE, Vol. 105, No. ST7, July 1979, pp. 1227-1240.

49. Haque, M.N., Valliapan, S., and Cook, D.J., "Tensile Creep
    Analysis of Concrete Structures," Proceedings, International
    Conference on Finite Element Methods in Engineering, Eds.
    Pulmano, V.A., and Kabalia, A.P., University of New South Wales
    Australia, August 1974, pp. 349-368.

50. Hegemier, G.A., Arya, S.K., Krishnamoorthy,G., Nachbar, W., and
    Furgerson, R., "On the Behavior of Joints in Concrete Masonry,"
    Proceedings, North American Masonry Conference, University of
    Colorado, Boulder, CO, Paper No. 4, August 1978.

51. Herrmann, L.R., "Finite Element Analysis of Contact Problems,"
    Journal of the Engineering Mechanics Division, ASCE, Vol. 104,
    No. EM5, October, 1978, pp. 1043-1057.

52. Heuze, F.E., "Dilatant Effects of Rock Joints," Proceedings, 4th
    Congress of the International Society of Rock Mechanics,
    Montreux, Switzerland, Vol. 1, September, 1979, pp. 169-175.

53. Heuze, F.E., and Goodman, R.E., "Finite Element Studies of
    'Piledriver' Tunnels, Including Considerations of Support
    Requirements," University of California, Berkeley, Report to
    U.S. Corps of Engineers, Omaha, NB, Contact DACA 45-71-C0031,
    August, 1971.

54. Heuze, F.E., Goodman, R.E., and Bornstein, A., "Joint Perturbation
    and No-Tension Finite Element Solutions," Rock Mechanics,
    Springer-Verlag, Wien, Austria, Vol. 3, No. 1, 1971, pp. 13-24.

55. Hilber, H.M., and Taylor, R.L., "A finite Element model for Fluid Flow in Systems of Deformable Fractured Rock," SESM Report No. 76-5, University of California, Berkeley, CA, November 1976.

56. Hill, R., The Mathematical Theory of Plasticity, Clarendon Press, NY, 1950.

57. Hinton, E., and Campbell, J.S., "Local and Global Smoothing of Discontinuous Finite Element Functions Using a Least Squares Method," International Journal for Numerical Methods in Engineering, Vol. 8, 1974, pp. 461-480.

58. Hittinger, M., and Goodman, R.E., "JTROCK: A Computer Program for Stress Analysis of Two-Dimensional Discontinuous Rock Masses," Report UCB/GT/78-04, University of California, Berkeley, CA, 1978.

59. Jessop, E.L., "Moisture, Thermal, Elastic and Creep Properties of Masonry: A State-of-the-Art Report," Proceedings, Second Canadian Masonry Symposium, Ottawa, Canada, June 9-11, 1980, pp. 505-520.

60. Katona, M.G., "A Simple Contact-Friction Interface Element with Applications to Buried Culverts," International Journal for Numerical and Analytical Methods in Geomechanics, Vol. 7, 1983, 1983, pp. 371-384.

61. Lenczner, D., Elements of Loadbearing Brickwork, Pergamon Press, New York, 1972.

62. Lenczner, D., "Design of Brick Masonry for Elastic and Creep Movements," Proceedings, Second Canadian Masonry Symposium, Ottawa, Canada, June 9-11, 1980, pp. 303-316.

63. Lenczner, D., and Salahuddin, T., "Creep and Moisture Movements in Masonry Piers and Walls," Proceedings, First Canadian Masonry Symposium, University of Calgary, Canada, 1976, pp. 72-86.

64. Mahtab, M.A., "Three-Dimensional Finite Element Analysis of Jointed Rock Slopes," Thesis presented to the University of California at Barkeley, CA, in 1970, in partial fulfilment of the requirements for the Doctor of Philosophy.

65. McCarthy, J.A., Brown, R.H., and Cousins, T.E., "An Experimental Study of the Shear Strength of the Collar Joint in Grouted and Slushed Composite Masonry Walls," Proceedings, 3rd North American Masonry Conference, University of Texas at Arlington, Arlington, TX, June 3-5, 1985, pp. 39.1-39.16.

66. Mehlhorn, G., and Keuser, M., "Isoparametric Contact Elements for Analysis of Reinforced Concrete Structures," in Finite Element Analysis of Reinforced Concrete Structures, Proceedings of the Seminar Sponsored by NSF and Japan Society for the Promotion of Science, Tokyo, Japan, 1985.

67. Neville, A.M., and Meyers, B.L., "Creep of Concrete: Influencing Factors and Predictions," _Proceedings, Symposium on Creep of Concrete_, ACI, Houston, TX, 1964, pp. 15-28.

68. Ngo, D., "A Network Topological Approach to the Finite Element Analysis of Progressive Crack Growth in Concrete Members," SESM Report No. 75-6, _University of California, Barkeley_, CA, June, 1975.

69. Nickell, R.E., "Thermal Stresses and Creep," in _Structural Mechanics Computer Programs_, ed. Pilkey, W.,Saczalski, K., and Schaeffer, H., University Press of Virginia, 1974, pp. 103-122.

70. Noorishad, J., "A Method for Coupled Stress and Flow Analysis of Fractured Rock Masses," _Thesis Presented to the University of California at Berkeley_, CA, in 1971, in partial fulfilment of the requirement for the degree of Doctor of Philosophy.

71. Page, A.W., "Finite Element Model for Masonry," _Journal of the Structural Division, ASCE_, Vol.104, No. ST8, 1978, pp. 1267-1285.

72. Pande, G.N., and Sharma, K.G., "On Joint/Interface Elements and Associated Problems of Numerical Illconditioning," Short Communication, _International Journal for Numerical and Analytical Methods in Geomechanics_, Vol. 3, 1979, pp. 293-300.

73. Plummer, H.C.,"_Brick and Tile Engineering_", Brick Institute of America, Third Edition, June 1977.

74. Porter, M., Ahmed, M., and Wolde-Tinsae, A., "Preliminary Work on Reinforced Composite Masonry Shear Walls," _Proceedings, 3rd Canadian Masonry Symposium '83_, University of Alberta, Canada, June 6-8, 1983, pp. 15.1-15.12.

75. Porter, M.L., Wolde-Tinsae, A.M., and Ahmed, M.H., "Strength Analysis of Composite Walls," Session Proceedings, entitled "_Advances in Analysis of Structural Masonry_," ASCE Structures Congress, New Orleans, LA, Sept. 15-18, 1985, published by ASCE, New York, pp.94-110.

76. Porter, M.L., Wolde-Tinsae, A.M., and Ahmed, M.H., "Behavior of Composite Brick Walls," _Proceedings, 7th International Brick Masonry Conference_, Melbourne, Australia, Feb. 17-20, 1985, pp. 877-889.

77. Rahman, A.H., and Suter, G.T., "Thermal Stresses in Intersecting Masonry Walls," _Proceedings, Third North American Masonry Conference_, University of Texas at Arlington, TX, June 1985, pp. 37.1-37.14.

78. Rahman, M.A., "Earthquake Effects on Composite Masonry Walls," _Proceedings, 3rd U.S. National Conference on Earthquake Engineering_, Charleston, SC, August 1986.

79. Rao, M., "Experimental Evaluation of Composite Masonry Walls Subjected to Axial and Shear Loads," M.S. Thesis, Clemson University, Clemson, SC, May 1989.

80. de Rouvray, A.L., and Goodman, R.E., "Finite Element Analysis of Crack Initiation in a Block Model Experiment," Rock Mechanics, Springer-Verlag, Wien, Austria, Vol. 4, 1972, pp. 203-223.

81. Sahlin, S., Structural Masonry, Prentice Hall, Englewood Cliff, NJ, 1971

82. Schafer, H., "A Contribution to the Solution of Contact Problems with the Aid of Bond Elements," Composite Methods in Applied Mechanics and Engineering, Vol. 6, 1975, pp. 335-354.

83. Self, M.W., "Design Guidelines for Composite Clay Brick and Concrete Block Masonry. Part I - Composite Masonry Prisms," Department of Civil Engineering, University of Florida, Gainesville, FL, Research Report, April 1983.

84. Sharma, H.D., et al., "Generalization of Sequential Nonlinear Analysis. A Study of Rockfill Dam with Joint Elements," Proceedings, Second International Conference on Numerical Methods in Geomechanics, Blacksburge, VA, Vol. 2, 1976, pp. 662-685.

85. Shrive, N.G., and England, G.L., "Elastic, Creep and Shrinkage Behavior of Masonry," International Journal of Masonry Construction, Vol. 1, No. 3, 1981, pp.103-109.

86. Spalding, F.P., Masonry Structures, John Wiley & Sons, Inc., New York, Second Edition, 1926.

87. St. John, C.M., "Finite Element Analyses of Two and Three-Dimensional Jointed Structures - Computer Programs," Rock Mechanics Research Report No. 13, Imperial College, London, England, 1972.

88. Taylor, R.L., "On Completeness of Shape Functions for Finite Element Analysis," International Journal for Numerical Methods in Engineering, Vol. 4, 1972, pp. 17-22.

89. Tham, L.G., and Cheung, Y.K., "Approximate Analysis of Shear Wall Assemblies with Openings," The Structural Engineer, Vol. 61B, No. 2, 1983, pp. 41-45.

90. Van Dillen, D.E., and Ewing, R.D., "BMINES: A Finite Element Code for Rock Mechanics Applications," Proceedings, 22nd Symposium on Rock Mechanics, MIT Publishing, Cambridge, MA, 1981, pp. 353-358.

91. Warren, D., and Lenczner, D., "A Creep Time Function for Single Leaf Brickwork Walls," International Journal of Masonry Construction, Vol. 2, No. 1, 1981, pp. 13-19.

92. Warren, D., and Lenczner, D., "Measurement of the Creep Strain Distribution in an Axially Loaded Brickwork Wall," Proceedings, Second North American Masonry Conference, University of Maryland, College Park, MD, August 9-11, 1982, pp. 5.1-5.19.

93. Whitcomb, J.D., Raju, I.S., and Goree, J.G.,"Reliability of the Finite Element Method for Calculating Free Edge Stresses in Composite Laminates," Computer and Structures, Vol. 15, No. 1, 1982, pp. 23-37.

94. Williams, R.T., and Geschwindner, L.F., "Shear Stress Across Collar Joints in Composite Masonry Walls," Proceedings, 2nd North American Masonry Conference, University of Maryland, College Park, MD, Aug. 9-11, 1982, pp. 8.1-8.17.

95. Wilson, E.L., "Finite Elements for Foundations, Joints and Fluids," Finite Elements in Geomechanics, ed. Gudehus, G., John Wiley & Sons, 1977, pp. 319-350.

96. Wilson, E.L., Taylor, R.L., Doherty, W.P., and Ghaboussi, J., "Incompatible Displacement Models," Numerical and Computer Methods in Structural Mechanics, ed. Fenves, S.J. et al., Academic Press, Inc., 1973, pp. 43-57.

97. Wintz, III, J.A., and Yorkdale, A.H., "Composite Masonry: Research Needs," Journal of Structural Division, ASCE, Vol. 108, No. ST6 June 1982, pp. 1414-1423.

98. Wolde-Tinsae, A.M., Porter, M.A., and Ahmed, A.H. "Shear Strength of Composite Brick-to-Block Panels," Proceedings, 3rd North American Masonry Conference, University of Texas at Arlington, TX, June 3-5, 1985, pp. 40.1-40.13.

99. Xiurun, G., "Non-Linear Analysis of a Joint Element and Its Application in Rock Engineering," International Journal for Numerical and Analytical Methods in Geomechanics, Vol. 5, 1981, pp. 229-245.

100. Yalamanchili, K.K., "Failure Analysis of Composite Masonry Walls," Ph.D. Dissertation (under preparation), Clemson University, Clemson, SC.

101. Zienkiewicz, O.C., The Finite Element Method in Engineering Science, McGraw-Hill, 3rd Ed., London, 1977.

102. Zienkiewicz, O.C., "Isoparametric and Allied Numerically Integrated Elements - A Review," Numerical and Computer Methods in Structural Mechanics, ed. Fenves, S.J., et al., Academic Press, Inc., 1973, pp. 13-41.

103. Zienkiewicz, O.C., Best, B., Dullage, C., and Stagg, K.G., "Analysis of Non Linear Problems in Rock Mechanics with Particular Reference to Jointed Rock Systems," _Proceedings, 2nd Congress of the International Society for Rock Mechanics_, Belgrade, Vol. 3, 1970, pp. 501-509.

104. Zienkiewicz, O.C., Watson, M., and King, I.P., "A Numerical Method for Viscoelastic Stress Analysis," _International Journal of Mechanical Sciences_, Vol. 10, 1968, pp. 807-827.

105. "Building Code Requirements for Concrete Masonry Structures," ACI 531-79 (Revised 1983), in ACI Manual of Concrete Practice, Part 5, 1985, _American Concrete Institute_, Detroit, MI.

106. "Building Code Requirements for Reinforced Concrete," (ACI 318-83), _American Concrete Institute_, Detroit, MI.

107. "Minimum Design Loads for Buildings and Other Structures," ANSI A58.1-1982, _American National Standards Institute Inc._, New York, NY.

108. "Recommended Practice for Engineered Brick Masonry," _Brick Institute of America_, McLean, VA, 1975.